



The Abdus Salam
International Centre for Theoretical Physics



2139-22b

**School on Synchrotron and Free-Electron-Laser Sources and their
Multidisciplinary Applications**

26 April - 7 May, 2010

**Surface, Interface, and Materials Studies Using Photoelectron Spectroscopy,
Diffraction, and Holography
(Part 3)**

Charles S. Fadley

*Lawrence Berkeley National Laboratory
USA*

Outline

Surface, interface, and nanoscience—short introduction

Some surface concepts and techniques→photoemission

Synchrotron radiation: experimental aspects

Electronic structure—a brief review

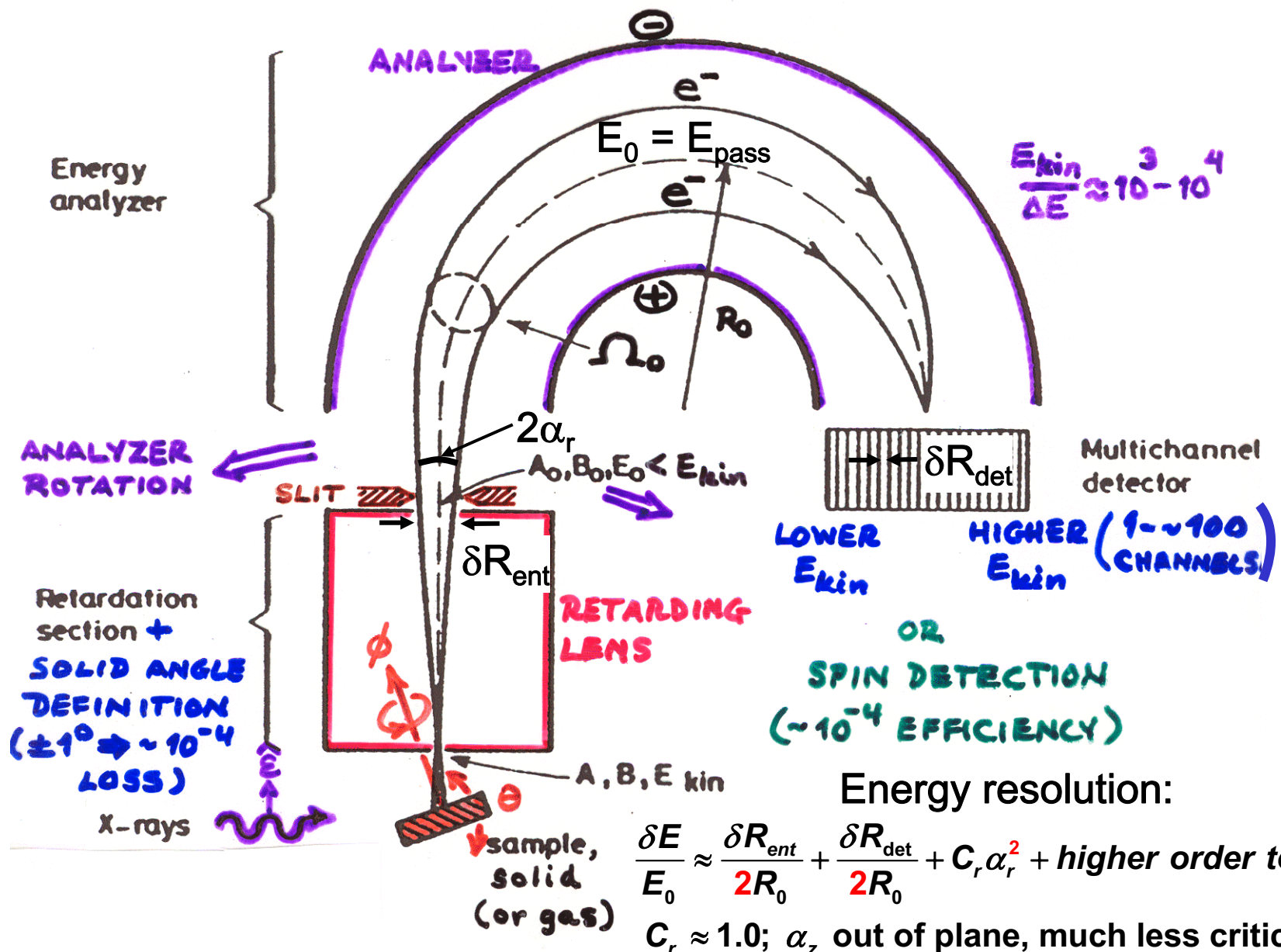
**The basic synchrotron radiation techniques:
more experimental and theoretical details**

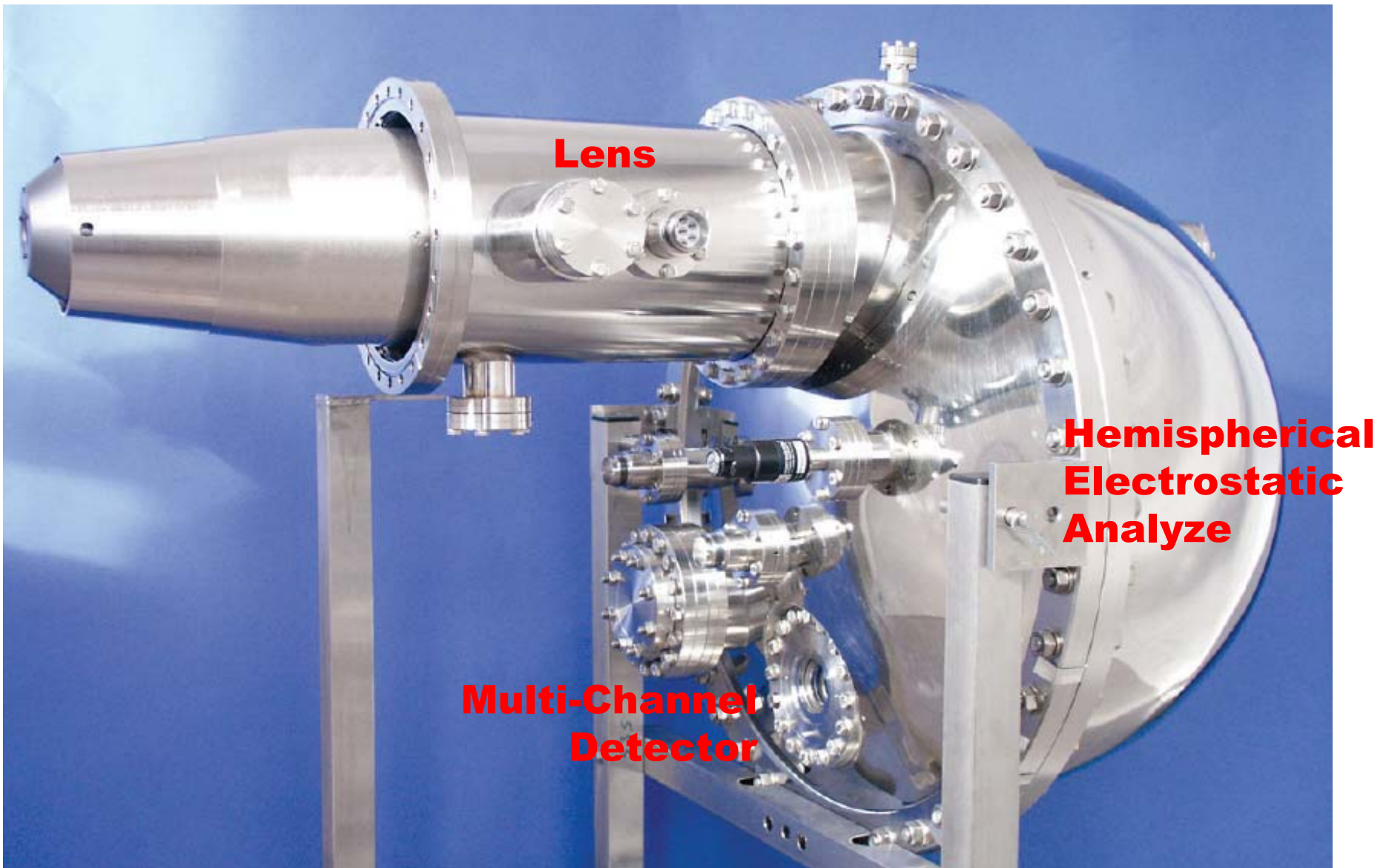
Valence-level photoemission

Core-level photoemission

**Photoemission with high ambient pressure
around the sample**

Electron Spectroscopy—A typical configuration

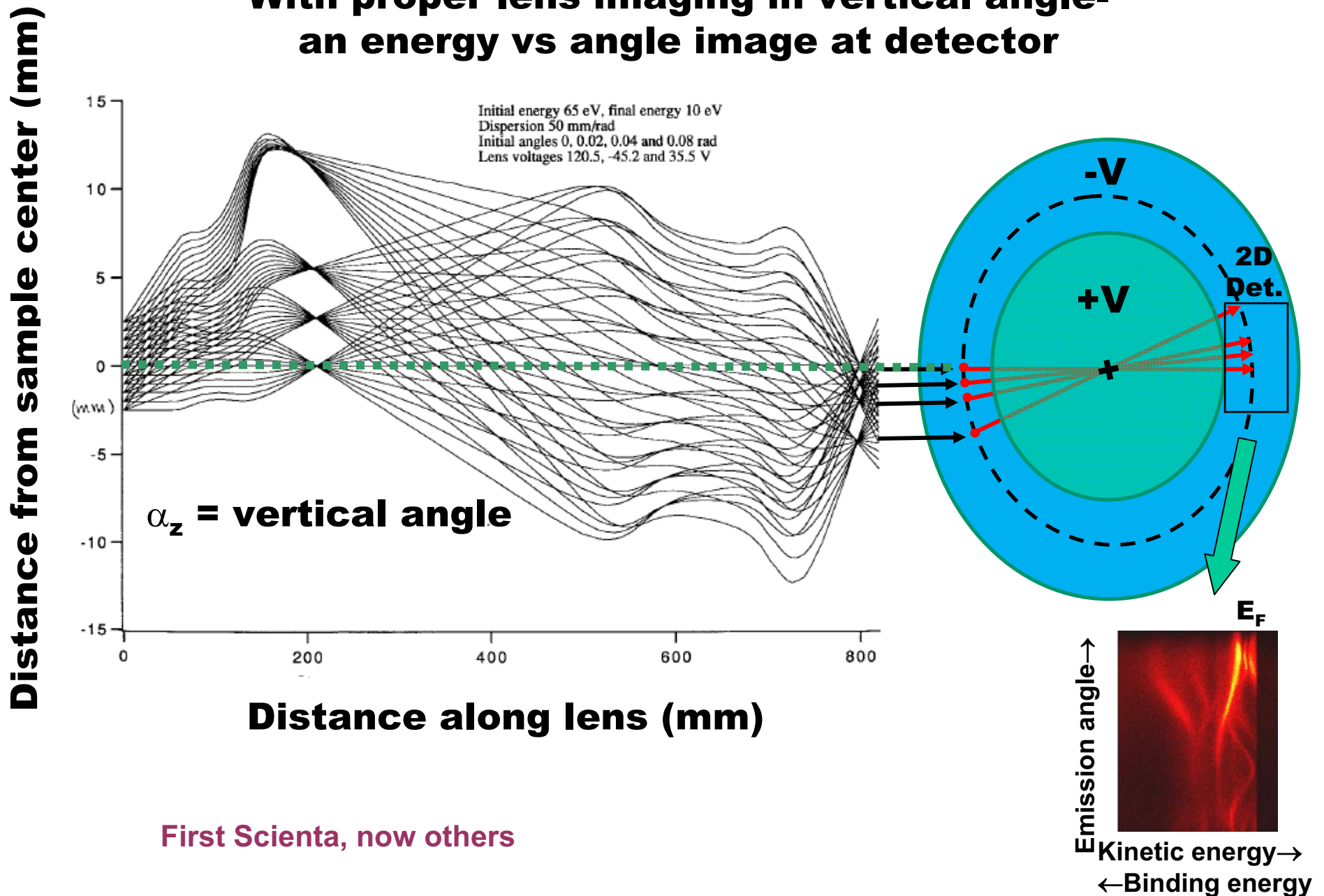




Nilsson et al., Journal of Electron
Spectroscopy and Related Phenomena 70
(1994) 117-128

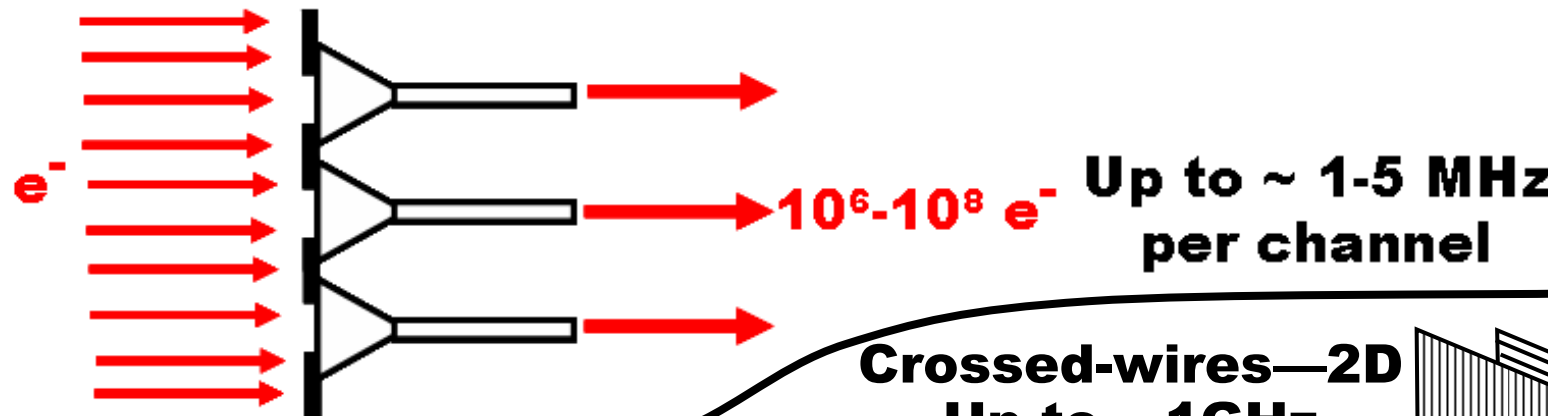
**The Scienta R4000
(plus SPECS, MBS)**

With proper lens imaging in vertical angle- an energy vs angle image at detector

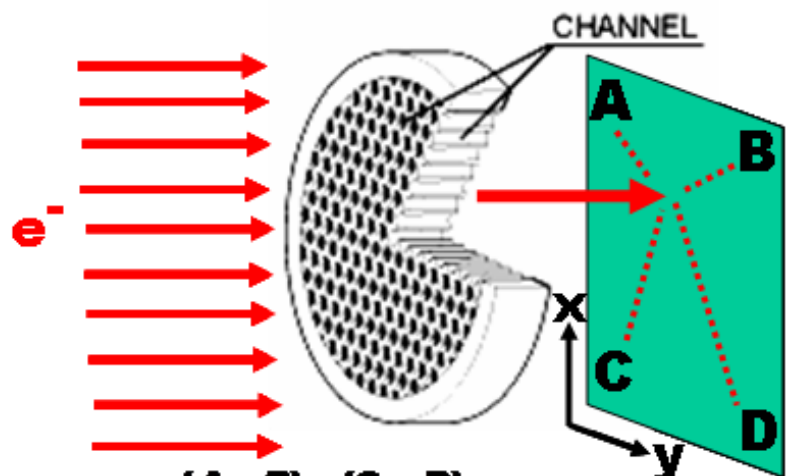


MULTICHANNEL DETECTION GEOMETRIES

Multiple channeltrons: brute force



Microchannel plates (MCPs) and



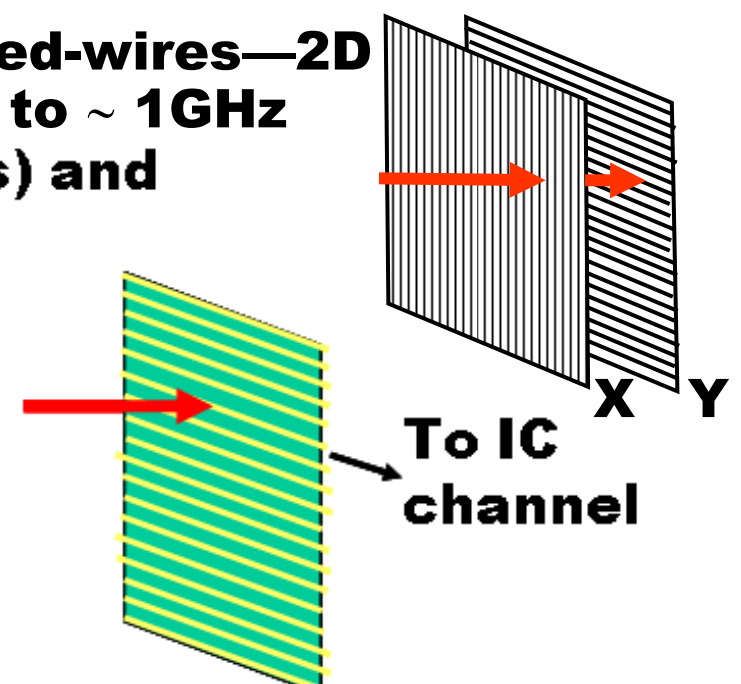
$$x = \frac{(A+B)-(C+D)}{A+B+C+D}$$

$$y = \frac{(B+D)-(A+C)}{A+B+C+D}$$

Resistive

Anode—2D:
Up to ~1 MHz

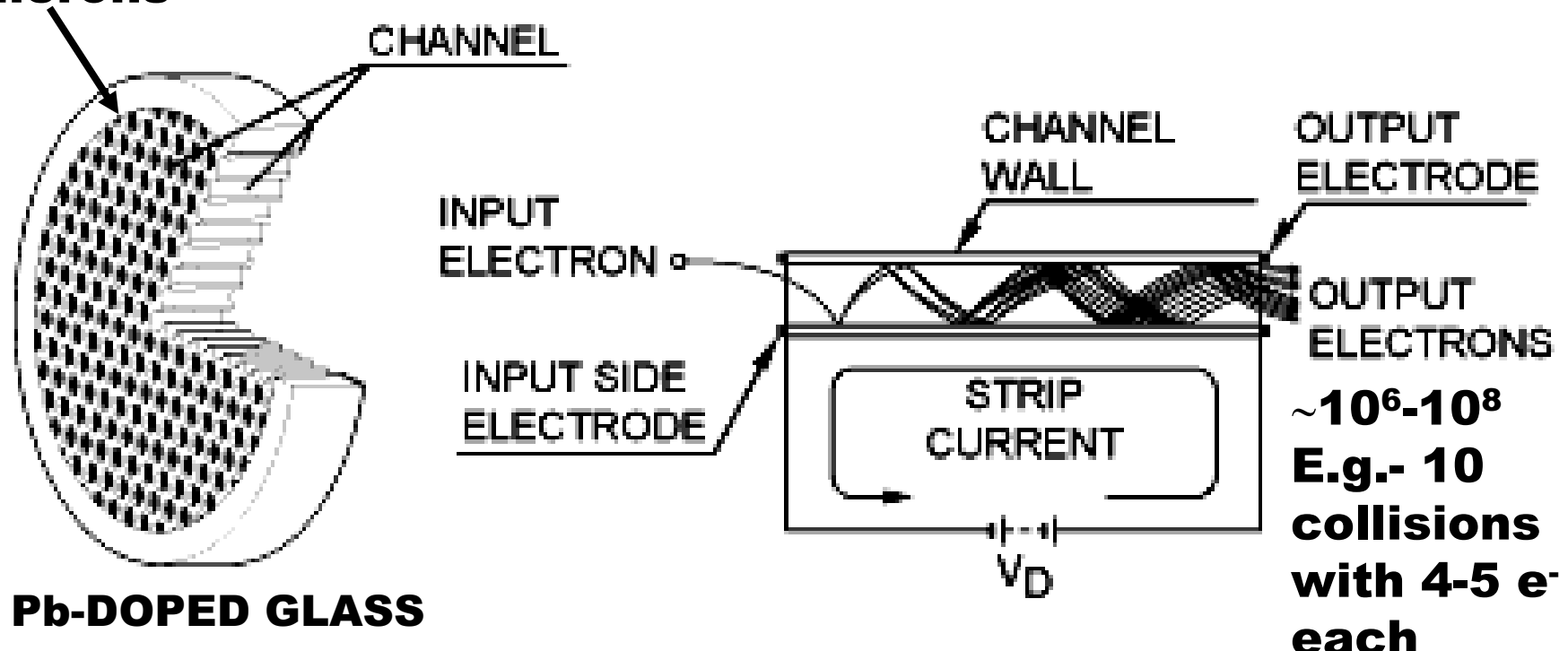
Crossed-wires—2D
Up to ~ 1GHz



Individual Collectors—1D
(Elettra and the ALS):
Up to ~ 1GHz

The Microchannel Plate Electron (and Photon) Multiplier

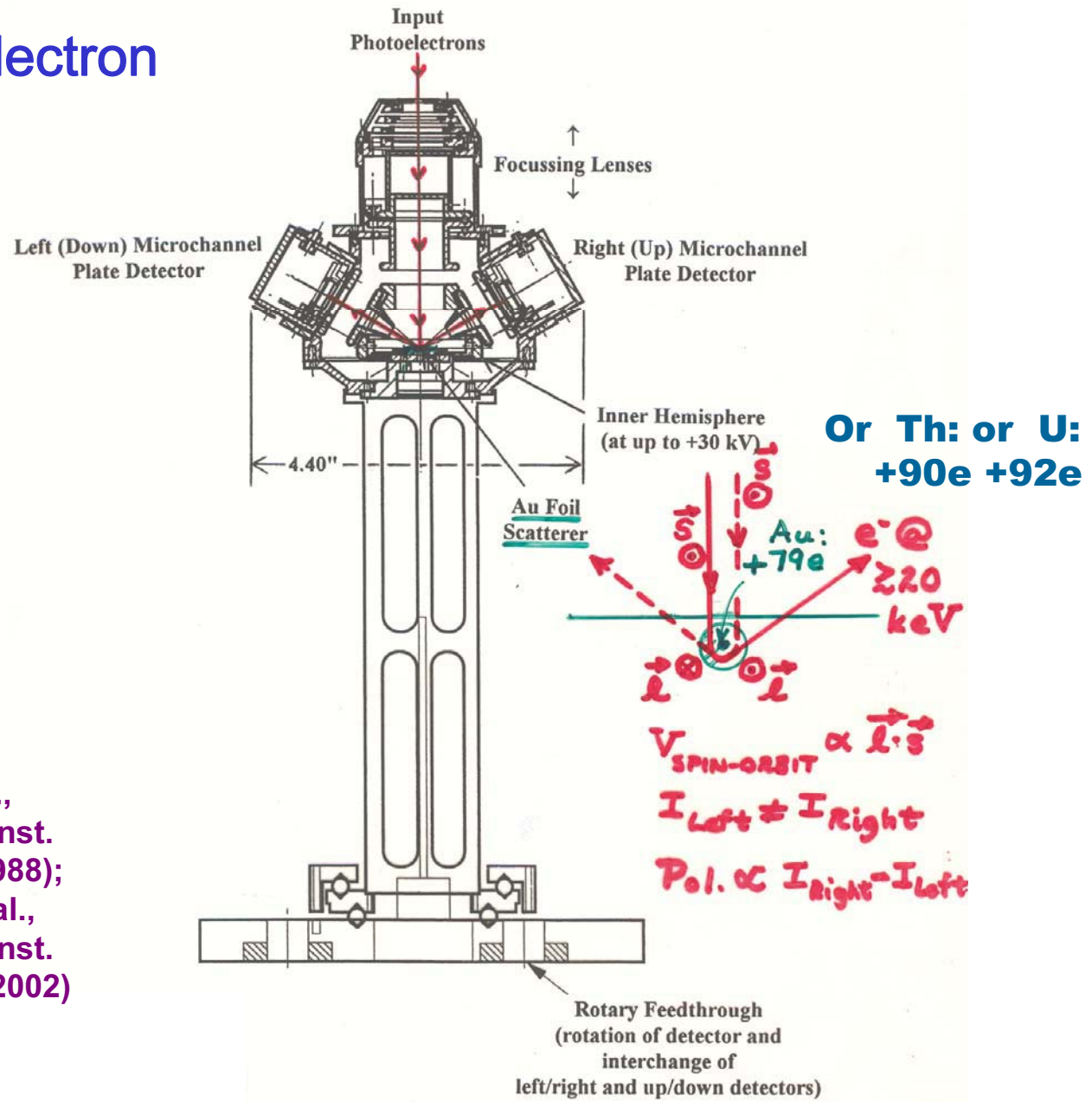
**Diam.
Down to 5
microns**



MICROMOTT DETECTOR
(LBNL/Florida State Univ./UC Davis)

The MicroMott Electron Spin Detector

Tang et al.,
Rev. Sci. Inst.
59, 504 (1988);
Huang et al.,
Rev. Sci. Inst.
73, 3778 (2002)



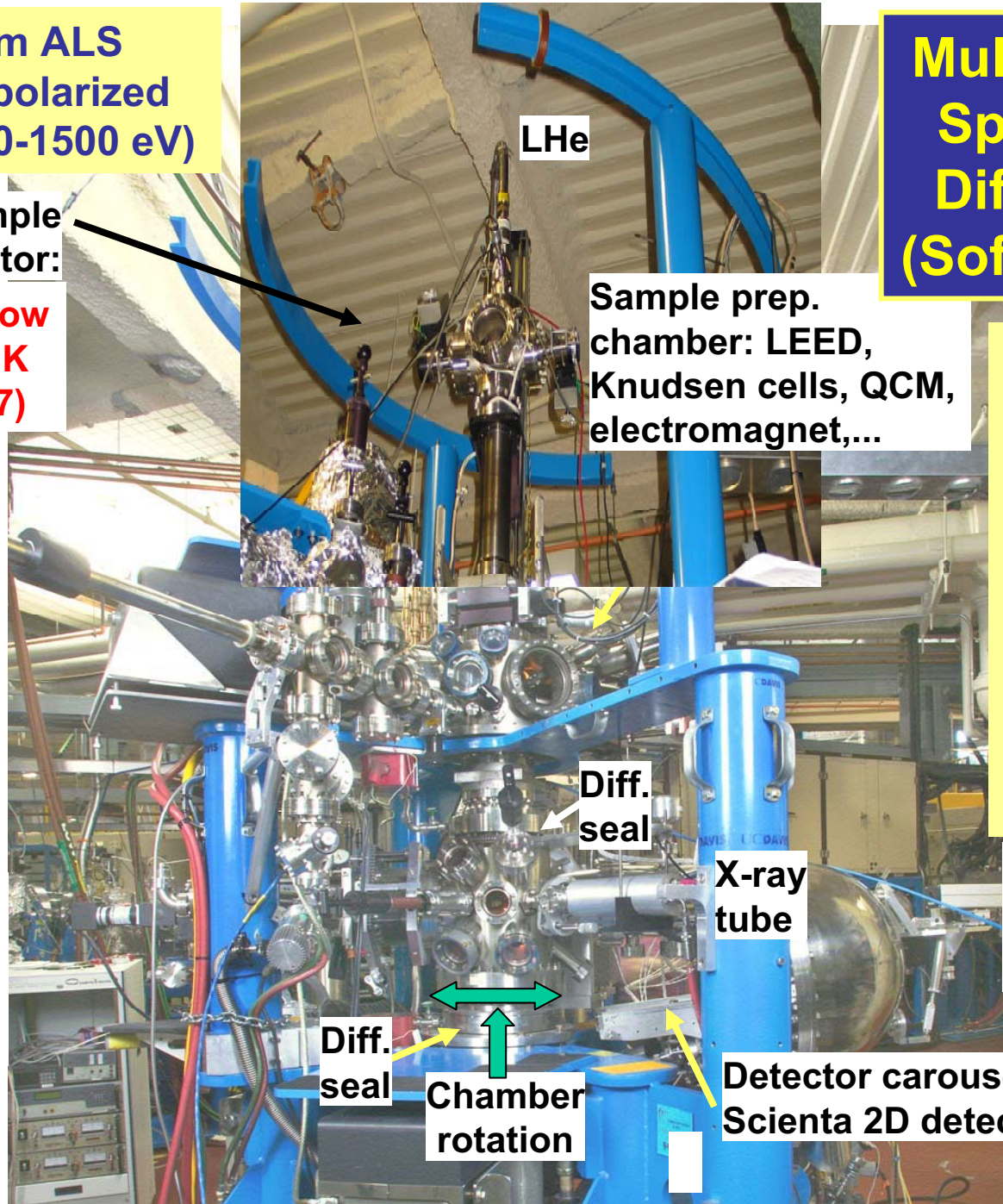
Light from ALS
elliptically polarized
undulator (80-1500 eV)

5-axis sample
manipulator:

New ultralow
temp, ~6 K
(June '07)

Loadlock
for sample
introduction

Soft x-ray
spectrometer:
Scienta
XES 300



Multi-Technique Spectrometer/ Diffractometer (Soft X-Ray/XUV)

Permits using all
relevant soft x-ray
spectroscopies
on a single
sample: PS, PD,
PH; XAS (e⁻ or
photon
detection),
XES/REXS/RIXS,
with MCD, MLD

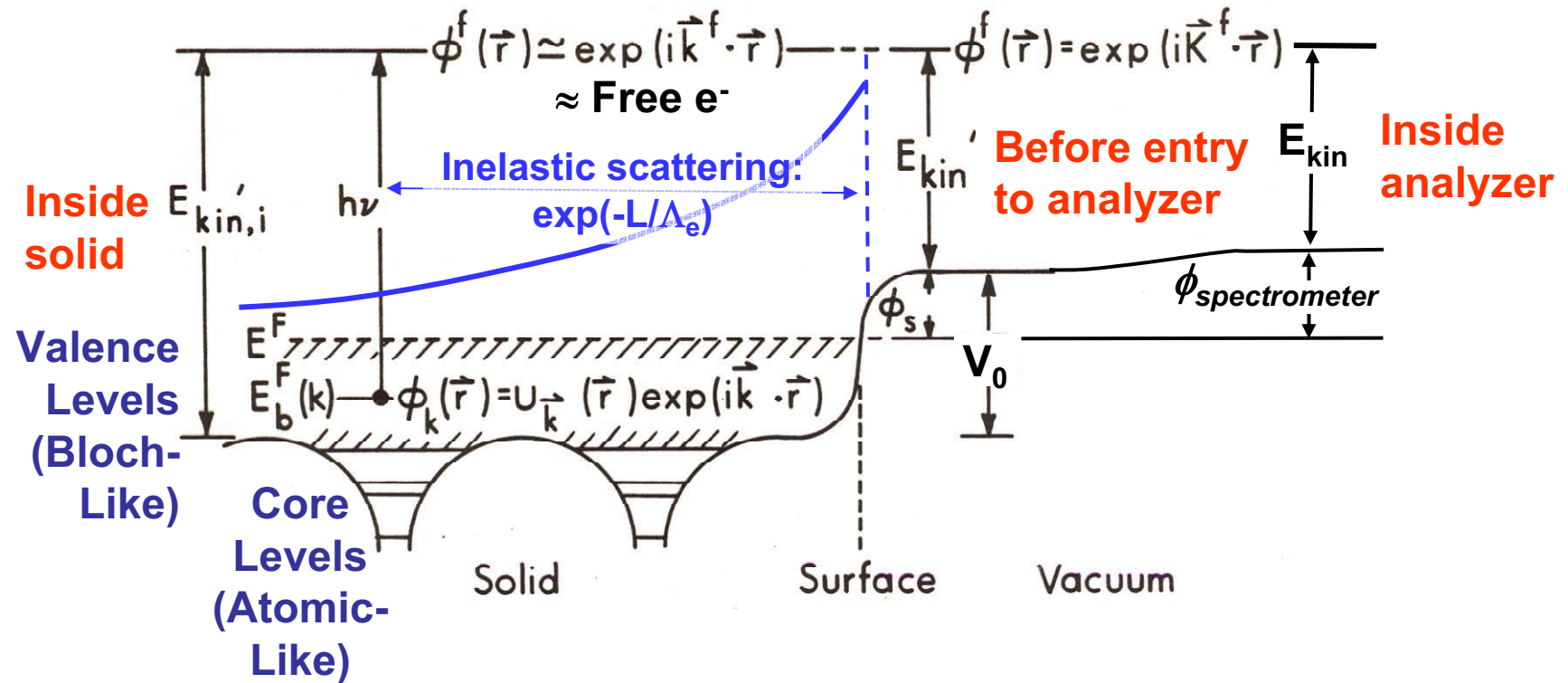
Electron
spectrometer:
Scienta SES "2002"

Detector carousel:
Scienta 2D detection—ARPES

Basic energetics

$$h\nu = E_{binding}^{Vacuum} + E_{kinetic} = E_{binding}^{Fermi} + \varphi_{spectrometer} + E_{kinetic}$$

One-Electron Picture of Photoemission from a Surface



Measuring Electron Binding Energies

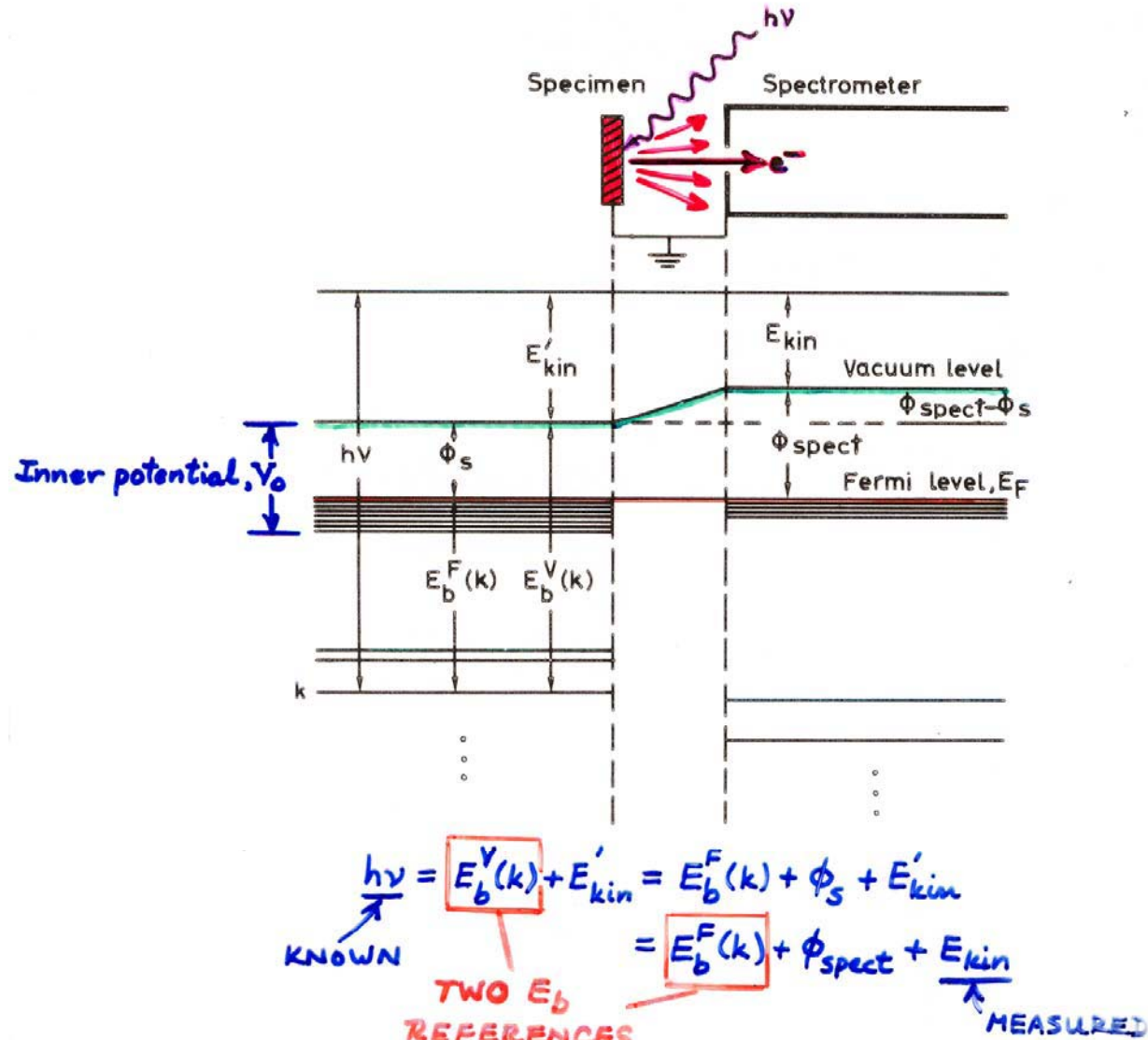
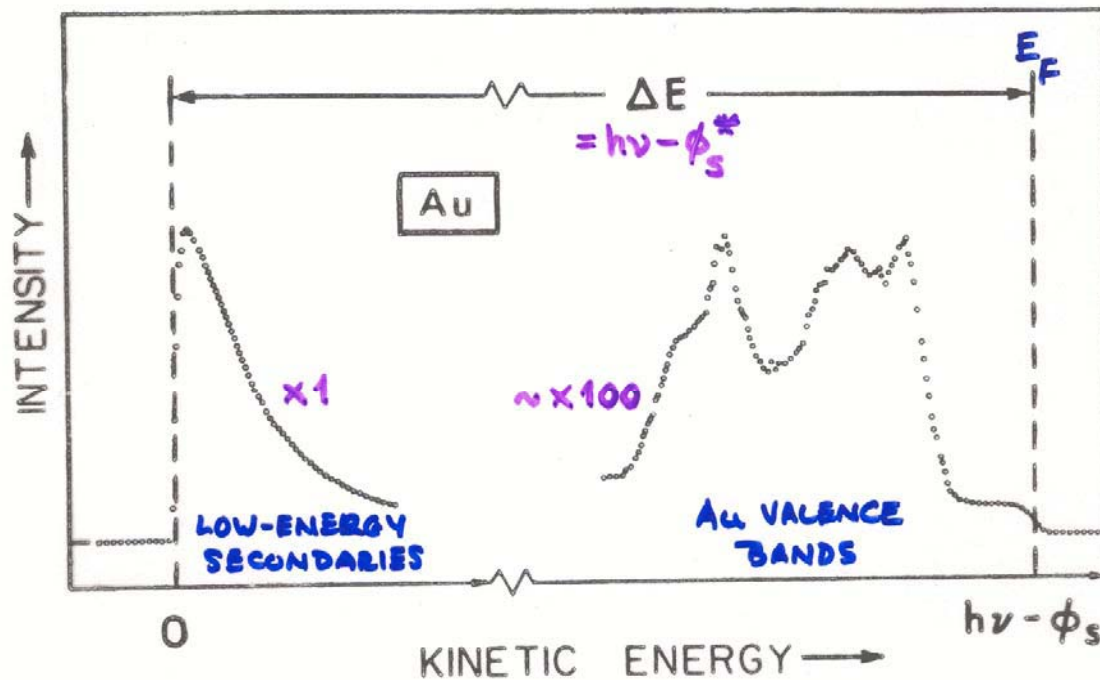


Figure 3 -- Energy level diagram for a metallic specimen in electrical equilibrium with an electron spectrometer. The closely spaced levels near the Fermi level E_F represent the filled portions of the valence bands in specimen and spectrometer. The deeper levels are core levels. An analogous diagram also applies to semiconducting or insulating specimens, with the only difference being that E_F lies somewhere between the filled valence bands and the empty conduction bands above.



* PROVIDED $\phi_s > \phi_{\text{spect}}$ OR,
 IF $\phi_s < \phi_{\text{spect}}$, SAMPLE
 BIASSSED NEGATIVELY BY
 $V_{\text{BIAS}} > \phi_{\text{spect}} - \phi_s$
 (-)

Figure 4 -- Full XPS spectral scan for a polycrystalline Au specimen, showing both the cutoff of the secondary electron peak at zero kinetic energy and the high-energy cutoff for emission from levels at the metal Fermi level. The measureable distance ΔE thus equals $h\nu - \phi_s$, provided that suitable specimen biasing has been utilized. For this case, $h\nu$ was 1253.6 eV and ϕ_s was 5.1 eV. (From Baer, reference 56).

1 H -	Work functions of the Elements [eV]																	2 He -							
Low																									
3 Li 2.4	4 Be 1.5	After L. Ley and M. Cardona, “Photoemission in Solids”, Springer 1979																							
11 Na 2.35	12 Mg 3.6	13 Al 4.25	14 Si 4.8	15 P -	16 S -	17 Cl -	18 Ar -	19 K 2.2	20 Ca 2.8	21 Sc 3.3	22 Ti 3.95	23 V 4.1	24 Cr 4.6	25 Mn 3.8	26 Fe 4.3	27 Co 4.4	28 Ni 4.5	29 Cu 4.4	30 Zn 4.2	31 Ga 4.0	32 Ge 4.8	33 As 5.1	34 Se 4.7	35 Br -	36 Kr -
37 Rb 2.2	38 Sr 2.35	39 Y 3.3	40 Zr 3.9	41 Nb 4.0	42 Mo 4.3	43 Tc -	44 Ru 4.6	45 Rh 4.75	46 Pd 4.8	47 Ag 4.3	48 Cd 4.1	49 In 3.8	50 Sn 4.4	51 Sb 4.1	52 Te 4.7	53 I -	54 Xe -								
55 Cs 1.8	56 Ba 2.5	57 La 3.3	72 Hf 3.5	73 Ta 4.1	74 W 4.5	75 Re 5.0	76 Os 4.7	77 Ir 5.3	78 Pt 5.3	79 Au 4.3	80 Hg 4.5	81 Tl 3.7	82 Pb 4.0	83 Bi 4.4	84 Po -	85 At -	86 Rn -								
87 Fr -	88 Ra -	89 Ac -	High																						
			58 Ce 2.7	59 Pr -	60 Nd -	61 Pm -	62 Sm -	63 Eu -	64 Gd -	65 Tb -	66 Dy -	67 Ho -	68 Er -	69 Tm -	70 Yb -	71 Lu -									
			90 Th 3.3	91 Pa -	92 U 3.3	93 Np -	94 Pu -	95 Am -	96 Cm -	97 Bk -	98 Cf -	99 Es -	100 Fm -	101 Md -	102 No -	103 Lr -									

Electron Work Functions of the Elements

From the CRC-Handbook, 73rd edition (1993)

Element	Surface crystallographic orientation	Work function (eV)
Ag	polycrystalline (100) 4.64 (110) 4.52 (111) 4.74	4.26 ←
Al	polycrystalline (100) 4.41 (110) 4.06 (111) 4.24	4.28 ←
As		3.75
Au	polycrystalline (100) 5.47 (110) 5.37 (111) 5.31	5.1 ←
B		4.45
Ba		2.7
Be		4.98
Bi		4.22
C		5.0

Depends
on surface
orientation

Measuring Electron Binding Energies: Charging Effects For Insulators

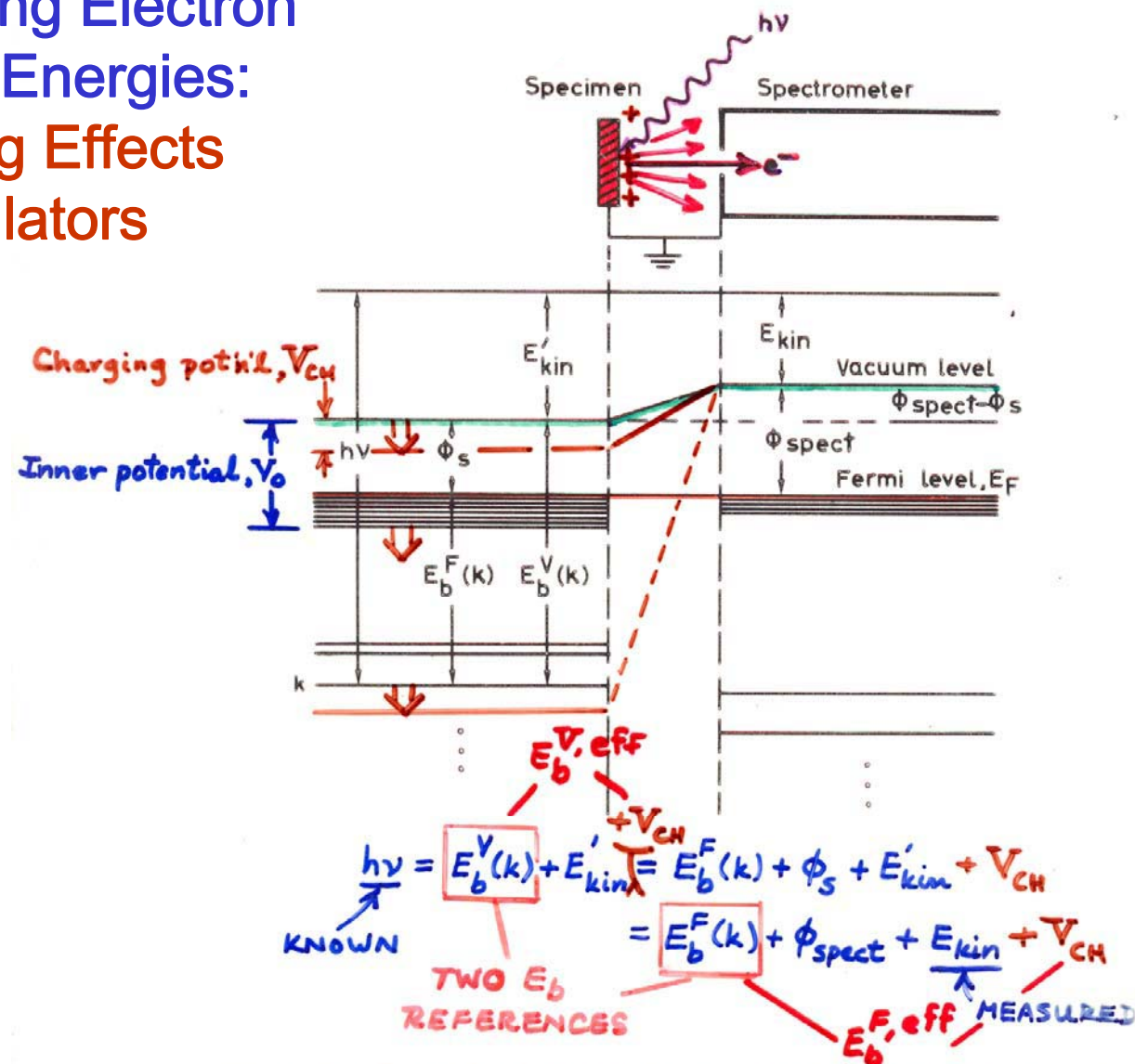
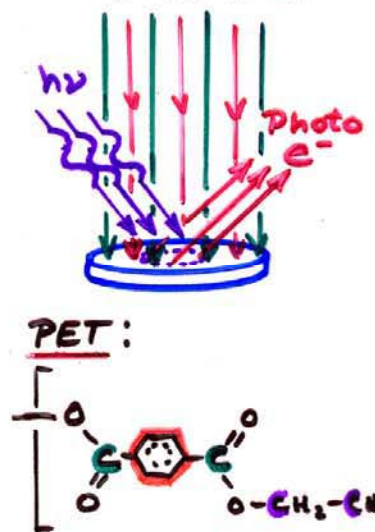


Figure 3 -- Energy level diagram for a metallic specimen in electrical equilibrium with an electron spectrometer. The closely spaced levels near the Fermi level E_F represent the filled portions of the valence bands in specimen and spectrometer. The deeper levels are core levels. An analogous diagram also applies to semiconducting or insulating specimens, with the only difference being that E_F lies somewhere between the filled valence bands and the empty conduction bands above.

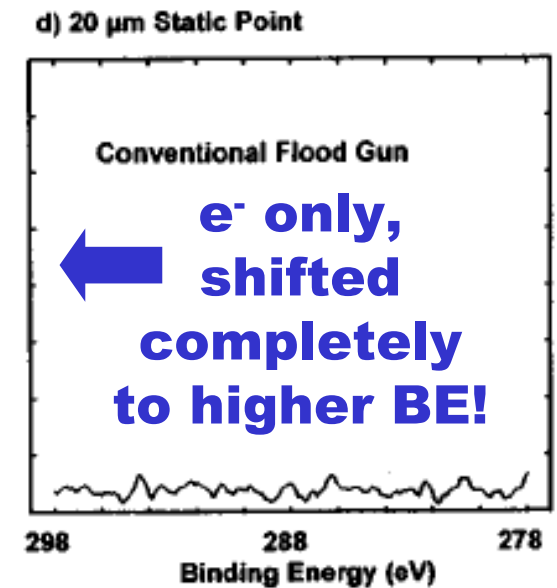
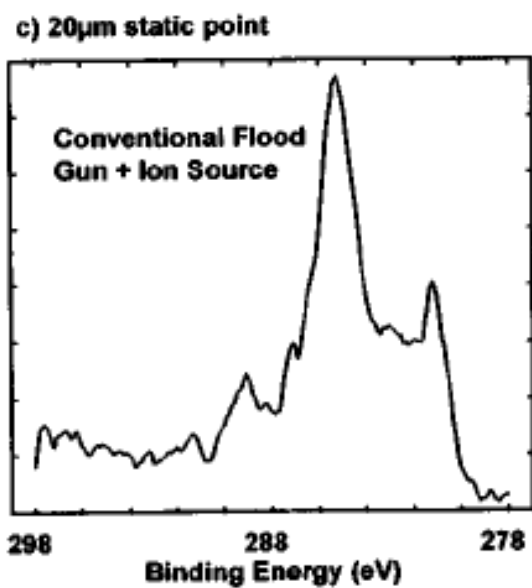
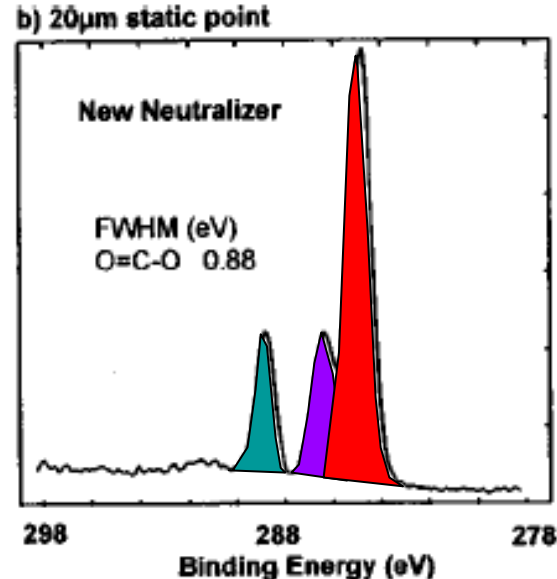
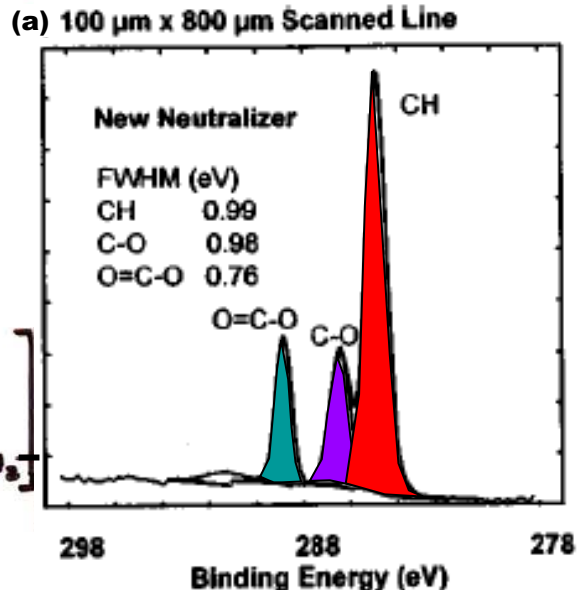
“Basic Concepts of XPS”

Figure 3

Flood e^- : $\frac{1}{2}$ eV
 Ar^+ : 5-10 eV



BEST CURRENT SOLUTION TO AN OLD PROBLEM: CHARGING IN INSULATORS

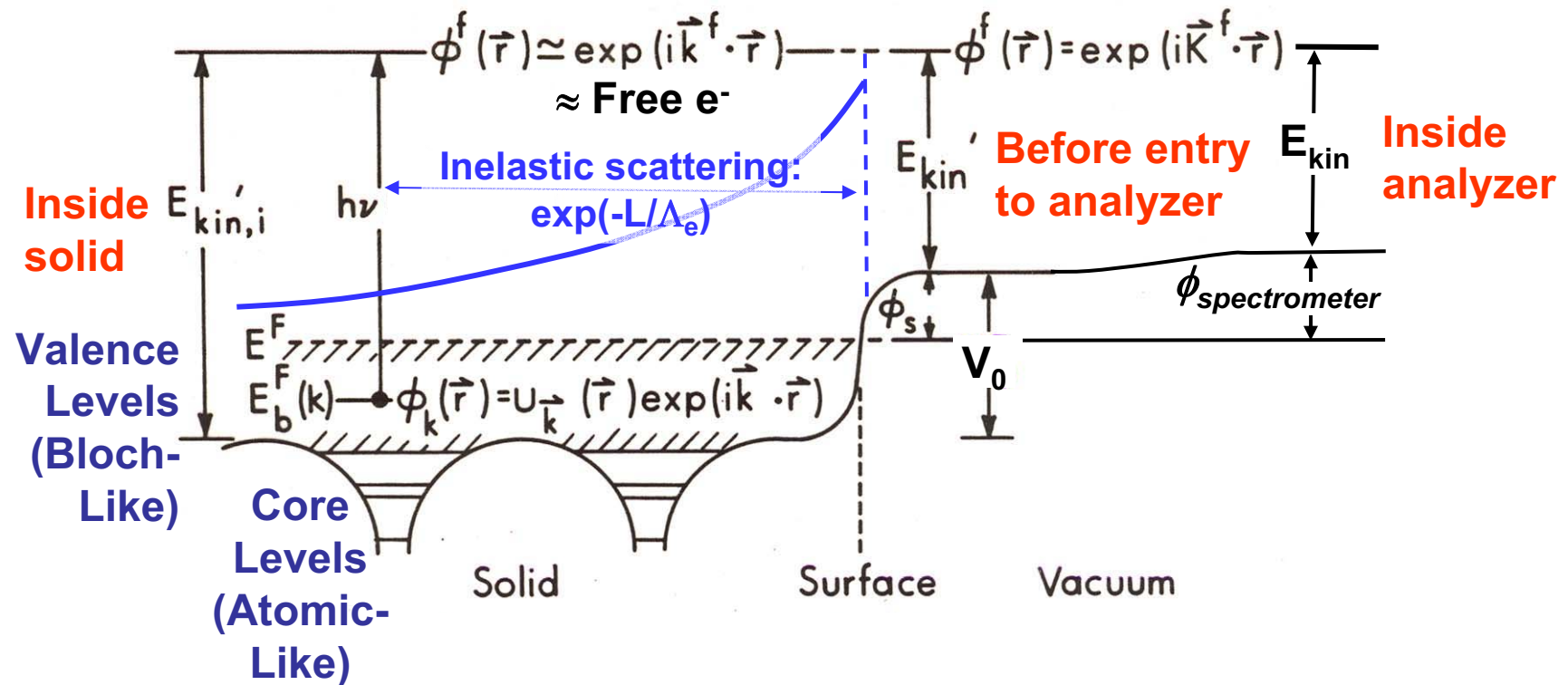


P. LARSON,
M. KELLY,
J. VAC.
SCI. TECH.
16,3483
('98)'

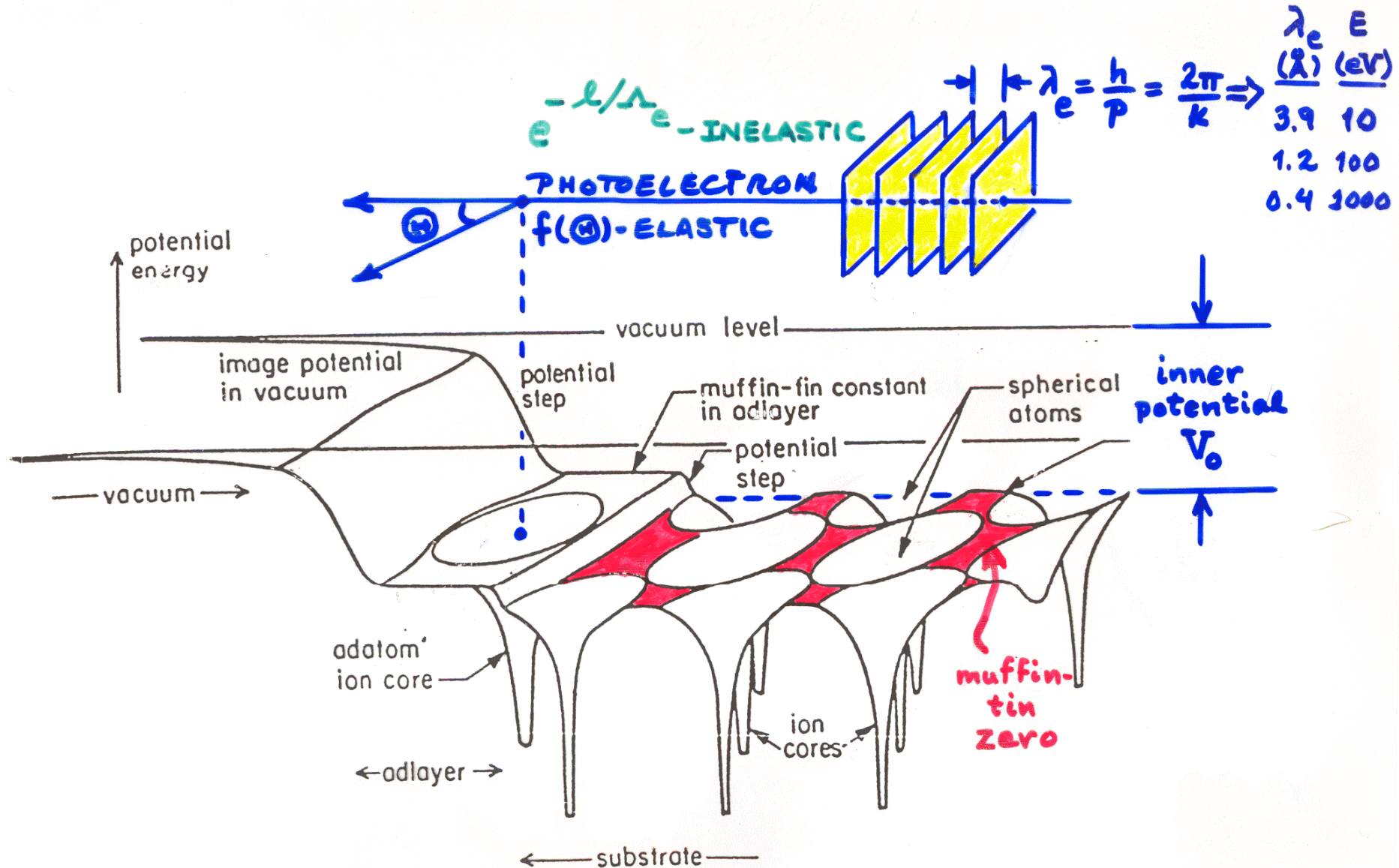
Basic Energetics of Photoelectron Emission

$$h\nu = E_{binding}^{Vacuum} + E_{kinetic} = E_{binding}^{Fermi} + \varphi_{spectrometer} + E_{kinetic}$$

One-Electron Picture of Photoemission from a Surface



One-Electron Picture of Photoemission from a Surface—3D



CALCULATION OF V_0 FOR AN IDEAL FREE-ELECTRON METAL

Fig. 4.2. Electron density profile at a jellium surface for two choices of the background density, r_s (Lang & Kohn, 1970).

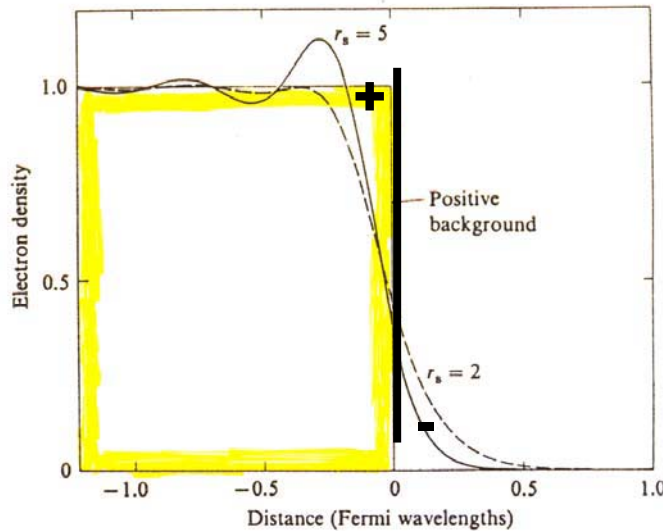
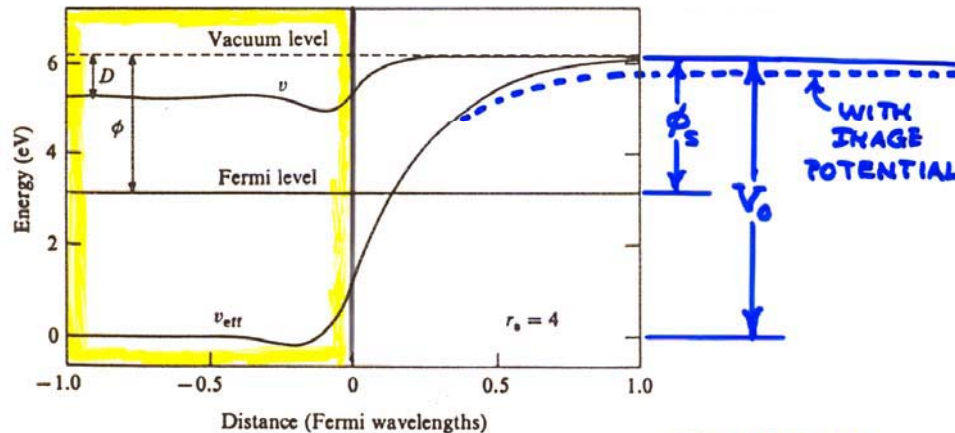
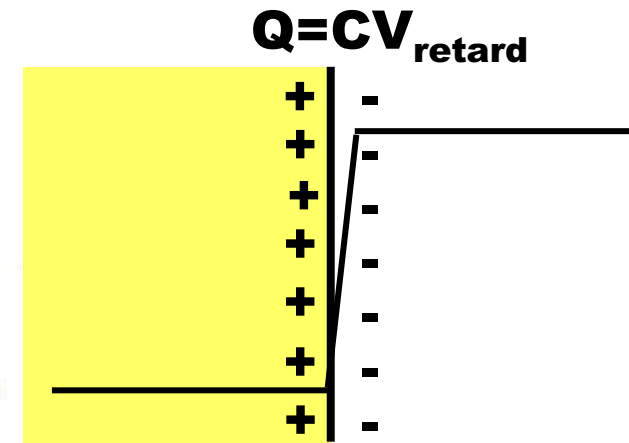
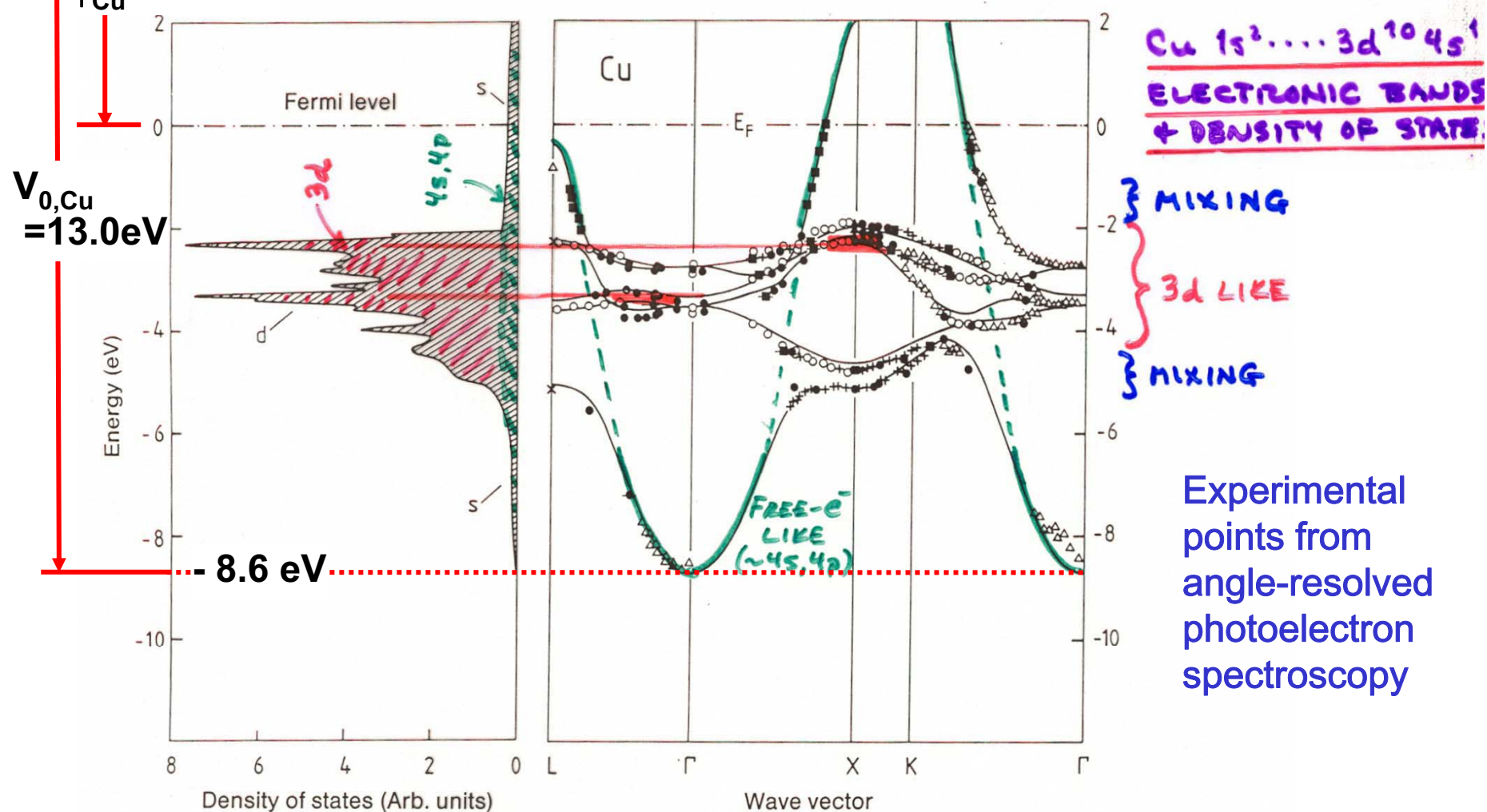


Fig. 4.3. Electrostatic potential, $v(z)$, and total effective one-electron potential, $v_{\text{eff}}(z)$, near a jellium surface (Lang & Kohn, 1970).



ZANGWILL,
"SURFACE
PHYSICS"

Vacuum level-
The electronic structure of a transition metal—fcc Cu



Experimental
points from
angle-resolved
photoelectron
spectroscopy

Fig. 7.12. Bandstructure $E(k)$ for copper along directions of high crystal symmetry (right). The experimental data were measured by various authors and were presented collectively by Courths and Hüfner [7.4]. The full lines showing the calculated energy bands and the density of states (left) are from [7.5]. The experimental data agree very well, not only among themselves, but also with the calculation

Outline

Surface, interface, and nanoscience—short introduction

Some surface concepts and techniques→photoemission

Synchrotron radiation: experimental aspects

Electronic structure—a brief review

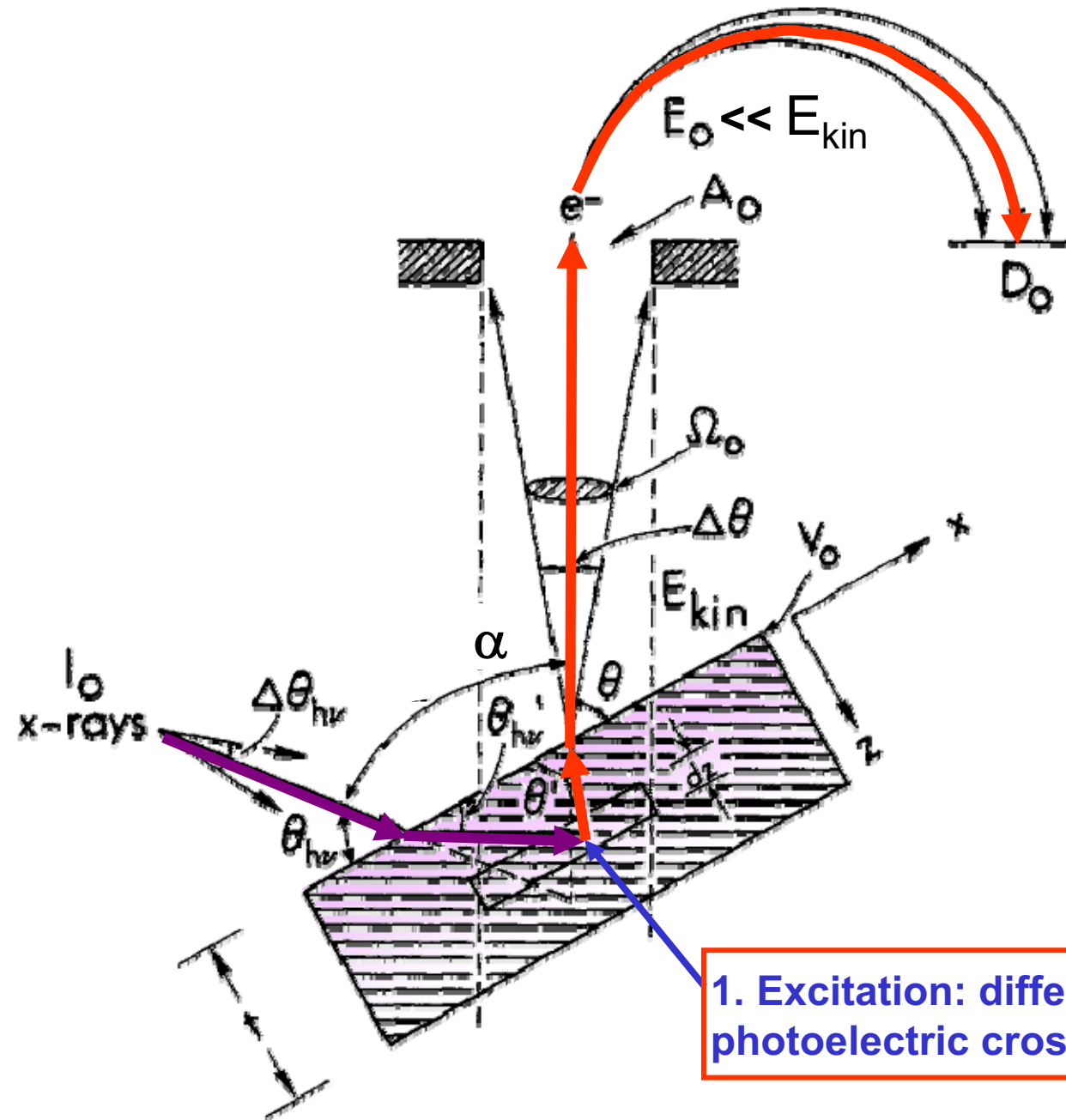
**The basic synchrotron radiation techniques:
more experimental and theoretical details**

Valence-level photoemission

**Core-level photoemission:
peak intensities and surface analysis**

**Photoemission with high ambient pressure
around the sample**

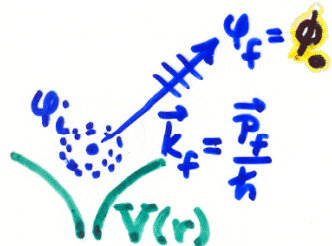
PHOTOELECTRON INTENSITIES—THE 3-STEP MODEL



PHOTOELECTRON EMISSION - BASIC MATRIX ELEMENTS + SELECTION RULES:

• ATOMIC-LIKE (LOCALIZED) STATES \Rightarrow CORE:

$$\Psi_i(\vec{r}) = \Psi_{n_i l_i m_i}(r, \theta, \phi) = R_{n_i l_i}(r) Y_{l_i m_i}(\theta, \phi) \quad \begin{cases} \alpha(\sigma) = m_{si} = +\frac{1}{2} = \uparrow \\ \beta(\sigma) = m_{si} = -\frac{1}{2} = \downarrow \end{cases}$$



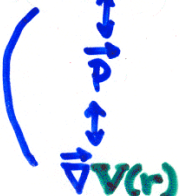
$$\Psi_f(\vec{r}, \vec{k}_f) = \Psi_{E_f}(\vec{r}, \vec{k}_f) \quad \begin{cases} \alpha(\sigma) \\ \beta(\sigma) \end{cases}$$

$$= 4\pi \sum_{l_f, m_f} i^{l_f} e^{-i\delta_{l_f}} Y_{l_f m_f}^*(\theta, \phi) Y_{l_f m_f}(\theta, \phi) R_{E_f l_f}(r) \quad \begin{cases} \alpha(\sigma) \\ \beta(\sigma) \end{cases}$$

PHASE SHIFT OF l_f WAVE IN $V(r)$

DIPOLE APPROX.: INT. $\propto | \langle \Psi_f | \hat{\epsilon} \cdot \vec{r} | \Psi_i \rangle |^2 = | \hat{\epsilon} \langle \Psi_f | \vec{r} | \Psi_i \rangle |^2 \Rightarrow$

EQUIVALENT
WITHIN CONSTANT
FACTOR



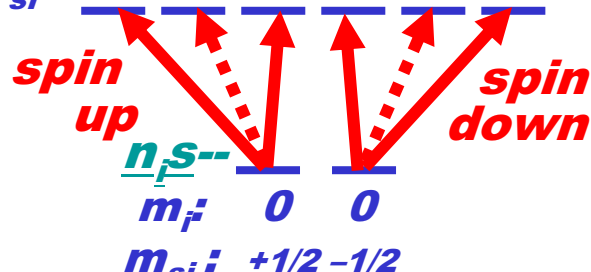
- $\Delta l = l_f - l_i = \pm 1$
- TWO CHANNELS
- $\Delta m = m_f - m_i = 0, \pm 1$
- LINEAR POLARIZ.
- $\Delta m = \pm 1$, CIRCULAR POLARIZATION

$$\Delta m_s = m_{sf} - m_{si} = 0 !$$

$E_f p--$

$$m_f: +1 \quad 0 \quad -1 \quad +1 \quad 0 \quad -1$$

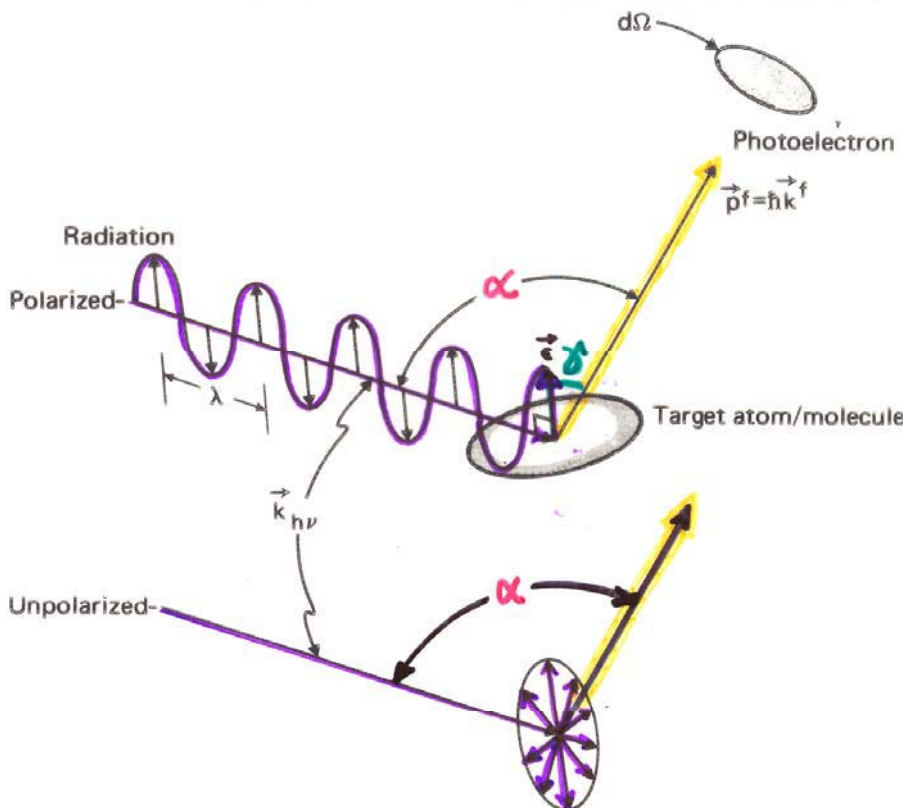
$$m_{sf}: +1/2 \quad +1/2 \quad +1/2 \quad -1/2 \quad -1/2 \quad -1/2$$



FOR A GIVEN $n_i l_i m_i m_{si}$: SUM OVER DEGENERATE INITIAL STATES $m_i m_{si}$ AND AVERAGE OVER FINAL STATES $E_f l_f m_f m_{sf}$ ACCESSED FROM EACH m_i TO YIELD DIFFERENTIAL SUBSHELL PHOTOELECTRIC CROSS SECTION :

$$d\sigma_{n_i l_i} / d\Omega$$

\propto PROBABILITY PER UNIT SOLID ANGLE OF EXCITING ONE ELECTRON FROM SUBSHELL $n_i l_i$ INTO THE DIRECTION k_f



FOR ATOMIC-LIKE EMISSION:

LIN.
POLARIZED: $\frac{d\sigma_{nl}(E_f)}{d\Omega} = \frac{\sigma_{nl}(E_f)}{4\pi} \left[1 + \beta_{nl}(E_f) \left(\frac{3}{2} \cos^2 \gamma - \frac{1}{2} \right) \right] \propto P_2(\cos \gamma) = \frac{1}{2} (3 \cos^2 \gamma - 1)$

UNPOLARIZED: $\frac{d\sigma_{nl}(E_f)}{d\Omega} = \frac{\sigma_{nl}(E_f)}{4\pi} \left[1 + \frac{1}{2} \beta_{nl}(E_f) \left(\frac{3}{2} \sin^2 \alpha - 1 \right) \right] \propto P_2(\cos \theta) = \frac{1}{2} (3 \cos^2 \theta - 1)$

Figure 7 -- General geometry for defining the differential cross section $d\sigma/d\Omega$, showing both polarized and unpolarized incident radiation. The polarization vector \hat{e} is parallel to the electric field \vec{E} of the radiation. In order for the dipole approximation to be valid, the radiation wave length λ should be much larger than typical target dimensions (that is, the opposite of what is shown here).

WITH:

σ_{nl} = TOTAL CROSS SECTION

β_{nl} = ASYMMETRY PARAMETER

σ_{nl}, β_{nl} TABULATIONS IN: GOLDBERG ET AL., J. ELECT. SPECT. & YEH, LINDAU, AT. NUC. DATA 22, 1 (1957) & 21, 285 ('91)

$P_2(\cos x) = 0$ when $x = 54.7^\circ$,
the "magic angle"

TOTAL SUBSHELL CROSS SECTION: $\int \frac{d\sigma_{nl}}{d\Omega} d\Omega =$

$$\sigma_{nl}(E^f) = \frac{4\pi\alpha_0\alpha_0^2}{3} (h\nu)[lR_{l-1}^2(E^f) + (l+1)R_{l+1}^2(E^f)]$$

= SUM OVER ALL m_J, m_S IN SUBSHELL nl

RADIAL MATRIX ELEMENTS TO $l\pm 1$ CHANNELS:

$$R_{l\pm 1}(E^f) = \int_0^\infty R_{nl}(r)r R_{E^f, l\pm 1}(r)r^2 dr = \int_0^\infty P_{nl}(r)r P_{E^f, l\pm 1}(r) dr$$

DIFFERENTIAL CROSS SECTION: UNPOLARIZED

$$\frac{d\sigma_{nl}}{d\Omega}(E^f) = \frac{\sigma_{nl}}{4\pi} [1 - \frac{1}{2}\beta_{nl}(E^f)P_2(\cos \alpha)]$$

$$= \frac{\sigma_{nl}}{4\pi} [1 + \frac{1}{2}\beta_{nl}(E^f)(\frac{3}{2}\sin^2 \alpha - 1)]$$

$$= A + B \sin^2 \alpha$$

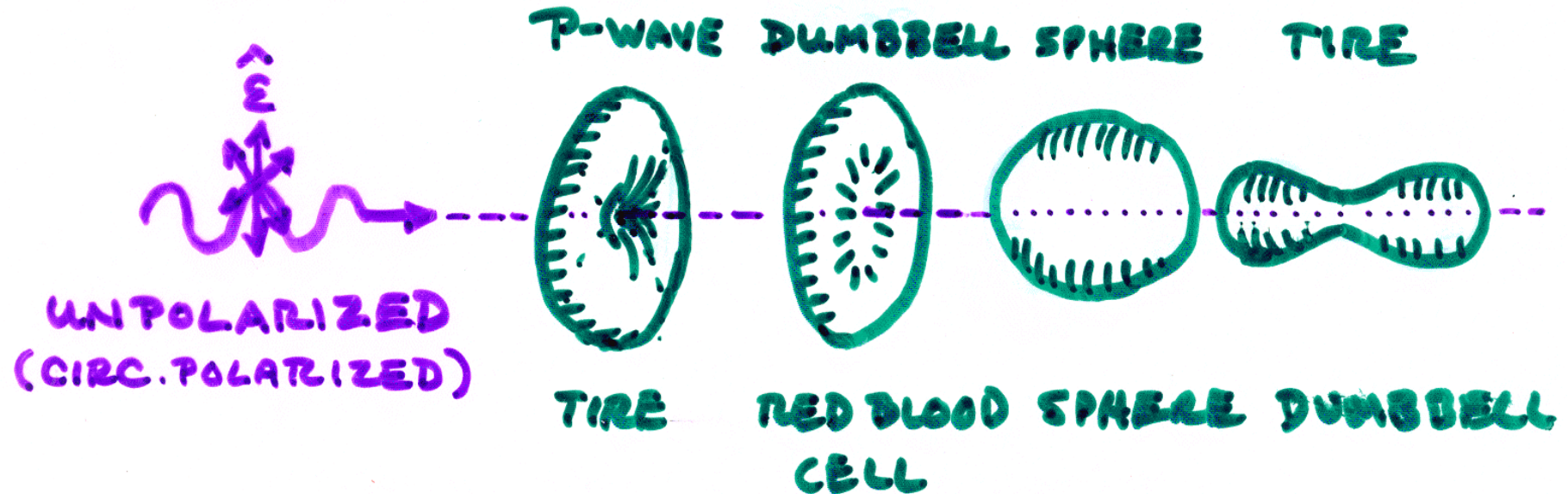
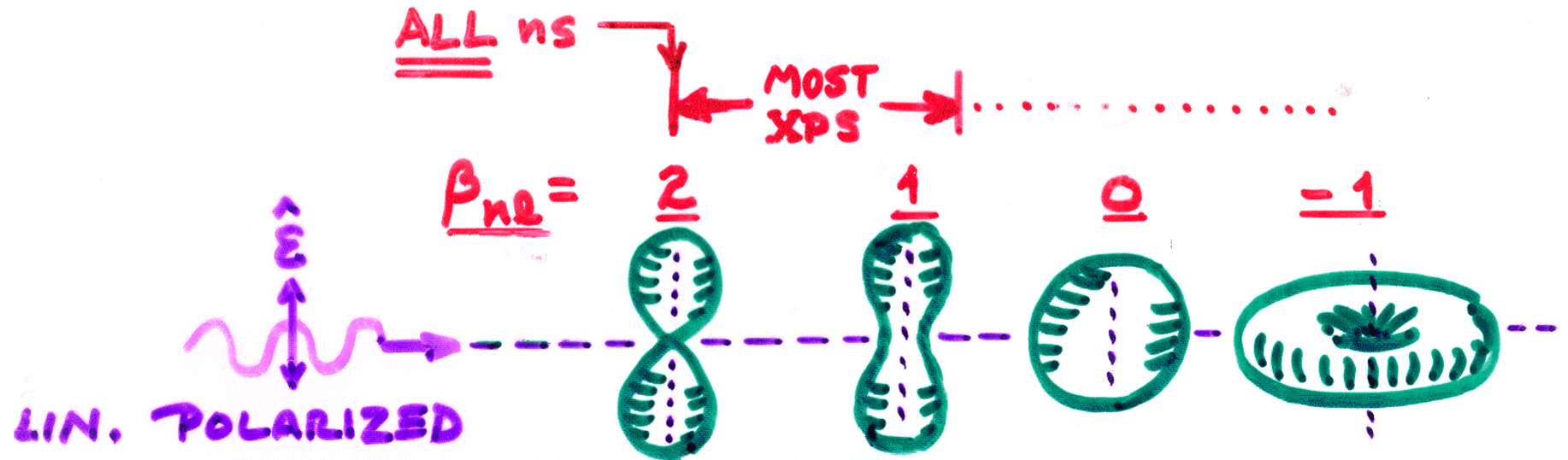
ASYMMETRY PARAMETER:

TERM FOR
 $l\pm 1$ INTERFERENCE

$$\beta_{nl}(E^f) = \frac{\{l(l-1)R_{l-1}^2(E^f) + (l+1)(l+2)R_{l+1}^2(E^f)\}}{(2l+1)[lR_{l-1}^2(E^f) + (l+1)R_{l+1}^2(E^f)]}$$

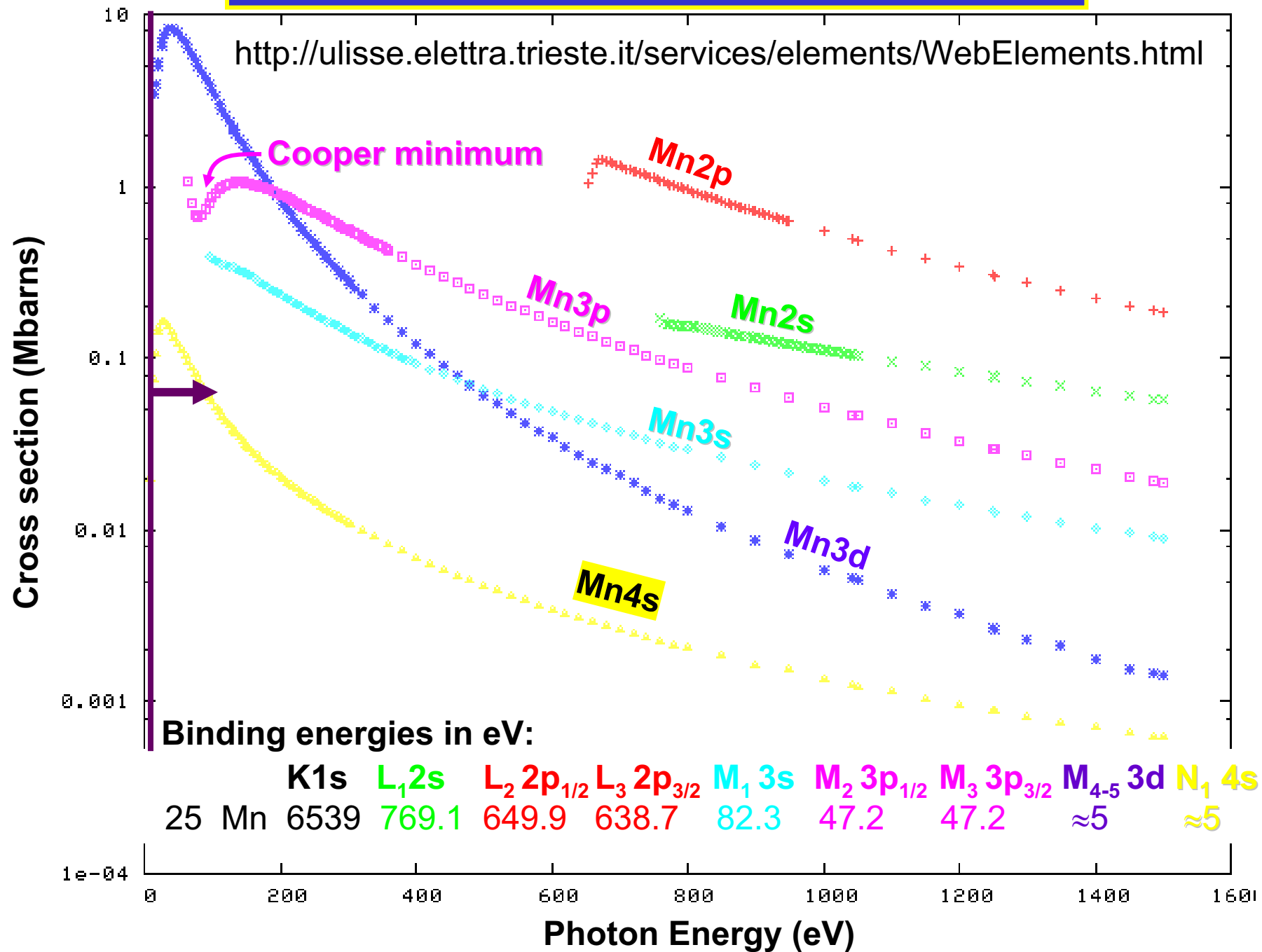
$\underbrace{- 6l(l+1)R_{l+1}(E^f)R_{l-1}(E^f) \cos [\delta_{l+1}(E^f) - \delta_{l-1}(E^f)]}_{\text{TERM FOR } l\pm 1 \text{ INTERFERENCE}}$

$\delta_{l\pm 1}(E^f)$ = CONTINUUM ORBITAL PHASE SHIFTS
IN ATOMIC POTENTIAL $V(r)$



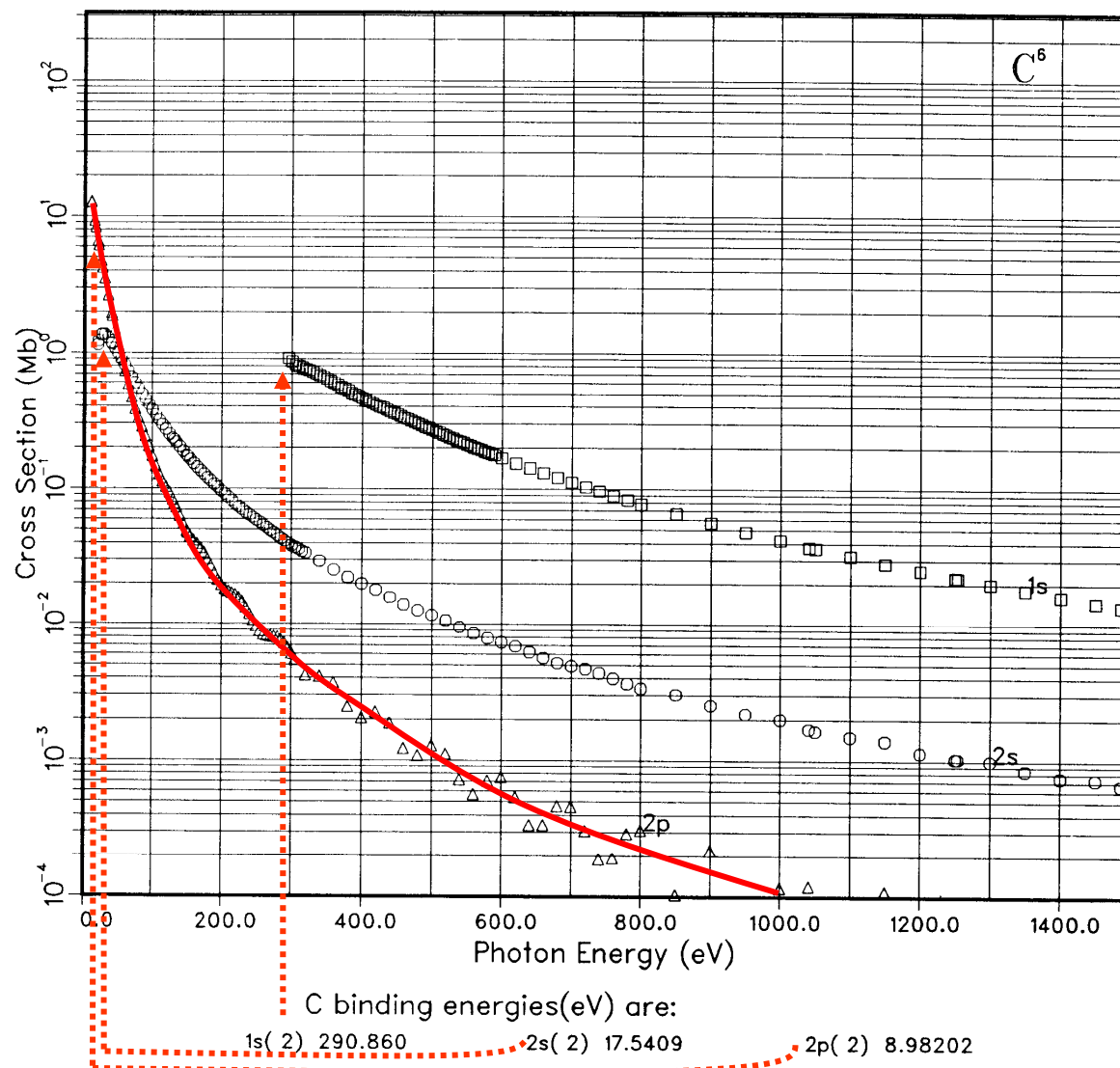
RANGE OF SHAPES OF $\frac{d\sigma}{d\Omega}$

PHOTOELECTRIC CROSS SECTIONS FOR Mn



GRAPH I. Atomic Subshell Photoionization Cross Sections for 0–1500 eV, $1 \leq Z \leq 103$
See page 6 for Explanation of Graphs

PHOTOELECTRIC CROSS SECTIONS FOR C



Plus other Examples from Yeh and Lindau in Sec. 1.5 of X-Ray Data Booklet, and plots for all elements at: <http://ulisse.elettra.trieste.it/elements/WebElements.html>

WebCrossSections - Microsoft Internet Explorer

File Edit View Favorites Tools Help

Back Forward Stop Home Search Favorites Media Mail My Yahoo! Games Yahoo! Personals LAUNCH Sign In

Address http://ulisse.elettra.trieste.it/elements/WebElements.html

Search Web Mail My Yahoo! Games Yahoo! Personals LAUNCH Sign In

Media

Today

Music William New F Kanye D12 G-Unit

Movie Spider Harry Prison Shrek The D King A

Music

Movie

Radio

Internet

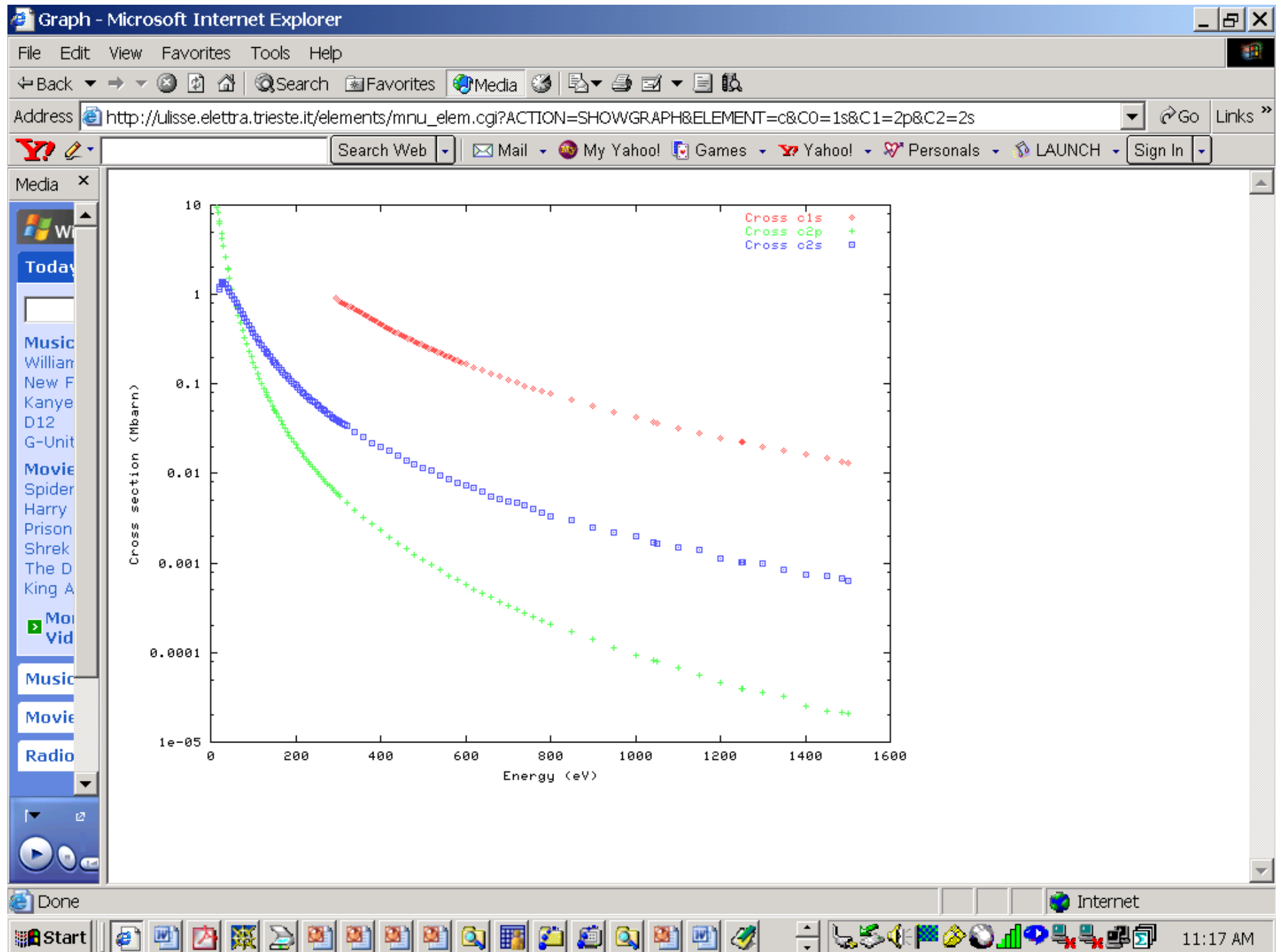
Atomic Calculation of Photoionization Cross-Sections and Asymmetry Parameters

This periodic table interface was developed to easily access the calculated atomic cross sections for photoionization and the related asymmetry parameters. The data are taken from: J.J. Yeh, *Atomic Calculation of Photoionization Cross-Sections and Asymmetry Parameters*, Gordon and Breach Science Publishers, Langhorne, PE (USA), 1993 and from J.J. Yeh and I.Lindau, *Atomic Data and Nuclear Data Tables*, 32, 1-155 (1985). The data shown here are those calculated in the dipole length approximation.

This is a beta version: [comments](#) are welcome.

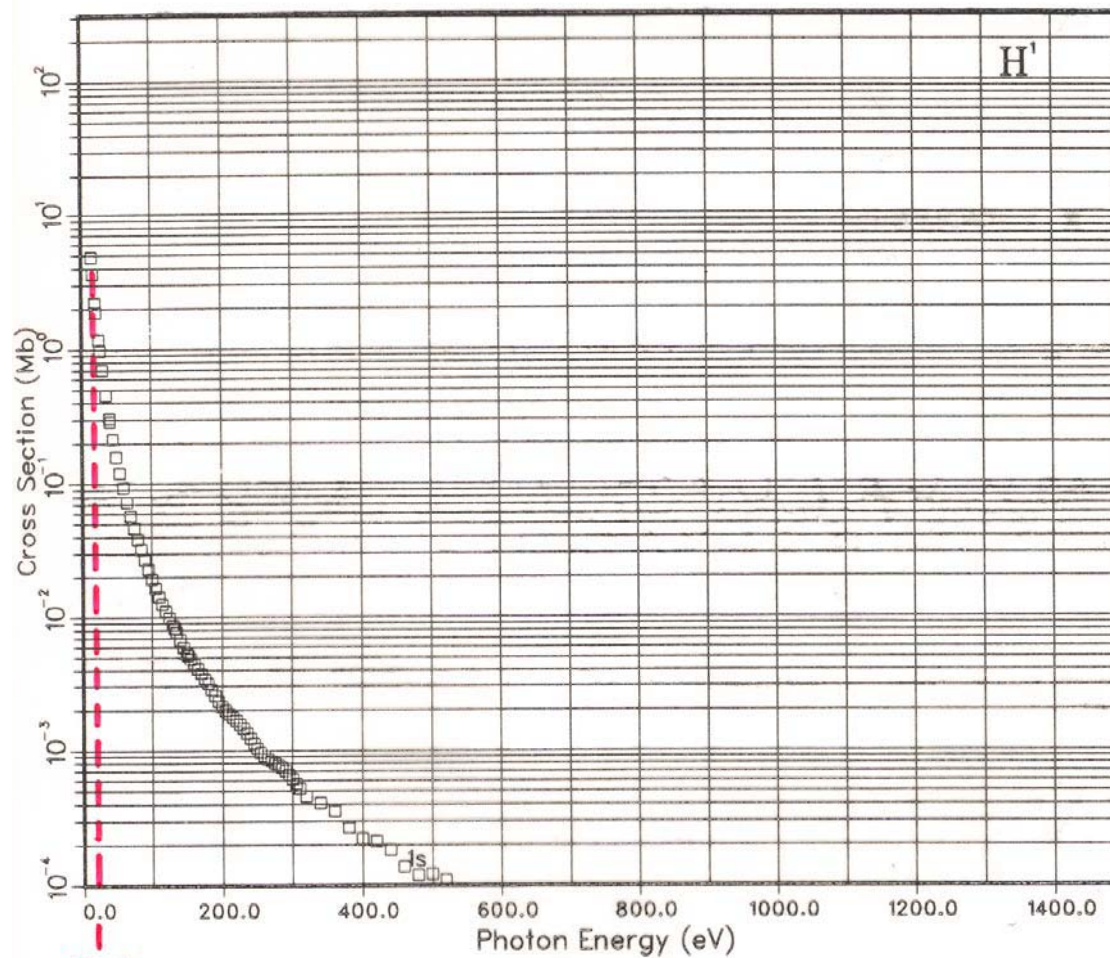
Group	1	2	3	4	5	6	7	8	9	10	11	12	13	14	15	16	17	18
	1A	2A	3B	4B	5B	6B	7B		8B		1B	2B	3A	4A	5A	6A	7A	8A

Period	1	2	3	4	5	6	7	8	9	10	11	12	13	14	15	16	17	18
1	H																	He
2	Li	Be																Ne
3	Na	Mg																Ar
4	K	Ca	Sc	Ti	V	Cr	Mn	Fe	Co	Ni	Cu	Zn	Ga	Ge	As	Se	Br	Kr
	27	29	20	40	41	42	42	44	45	46	47	49	40	50	51	52	54	



GRAPH I. Atomic Subshell Photoionization Cross Sections for 0–1500 eV, $1 \leq Z \leq 103$
See page 6 for Explanation of Graphs

PHOTOELECTRIC CROSS SECTIONS FOR H

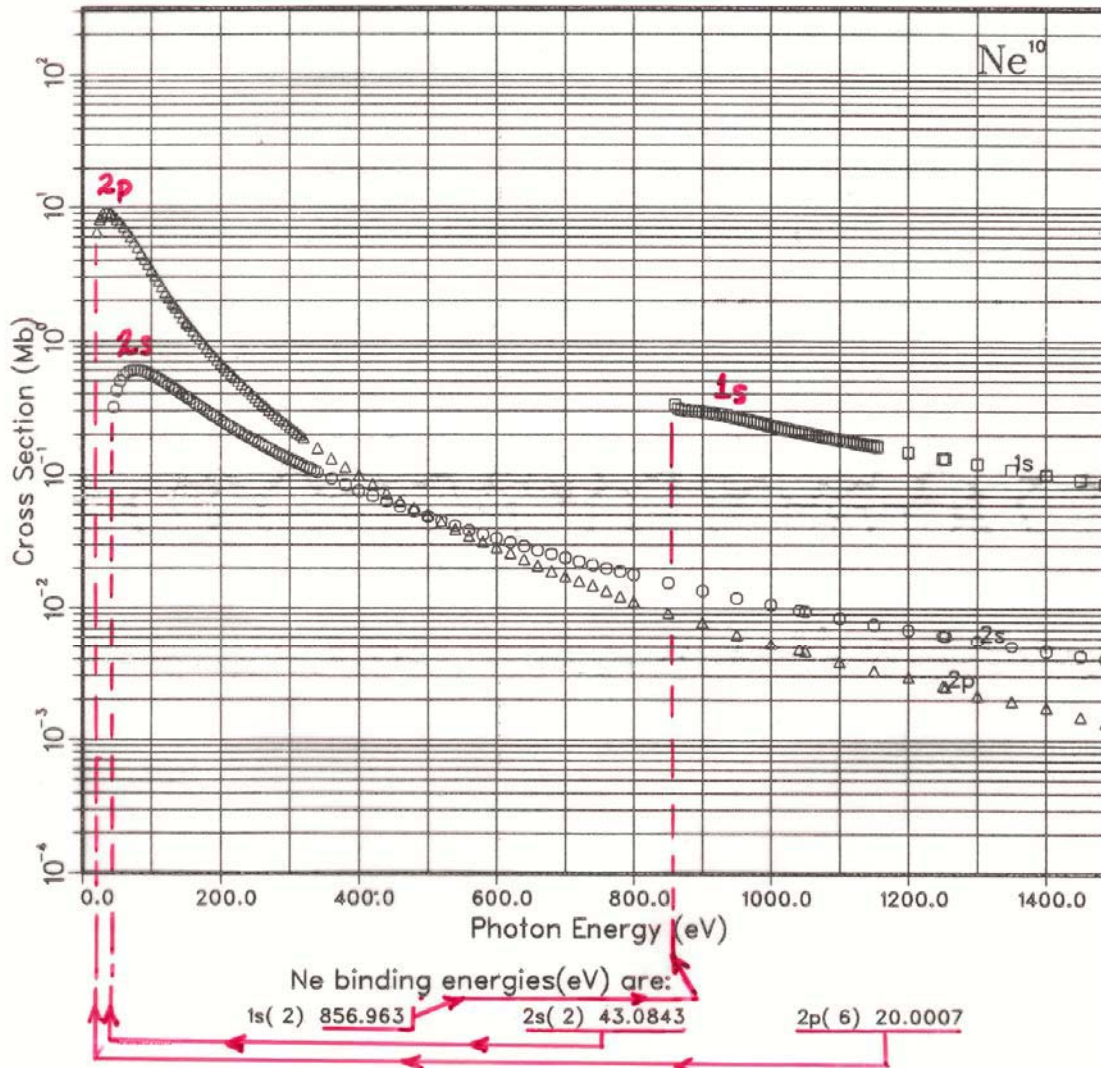


13.6
eV
= THRESHOLD
FOR
 e^- EMISSION

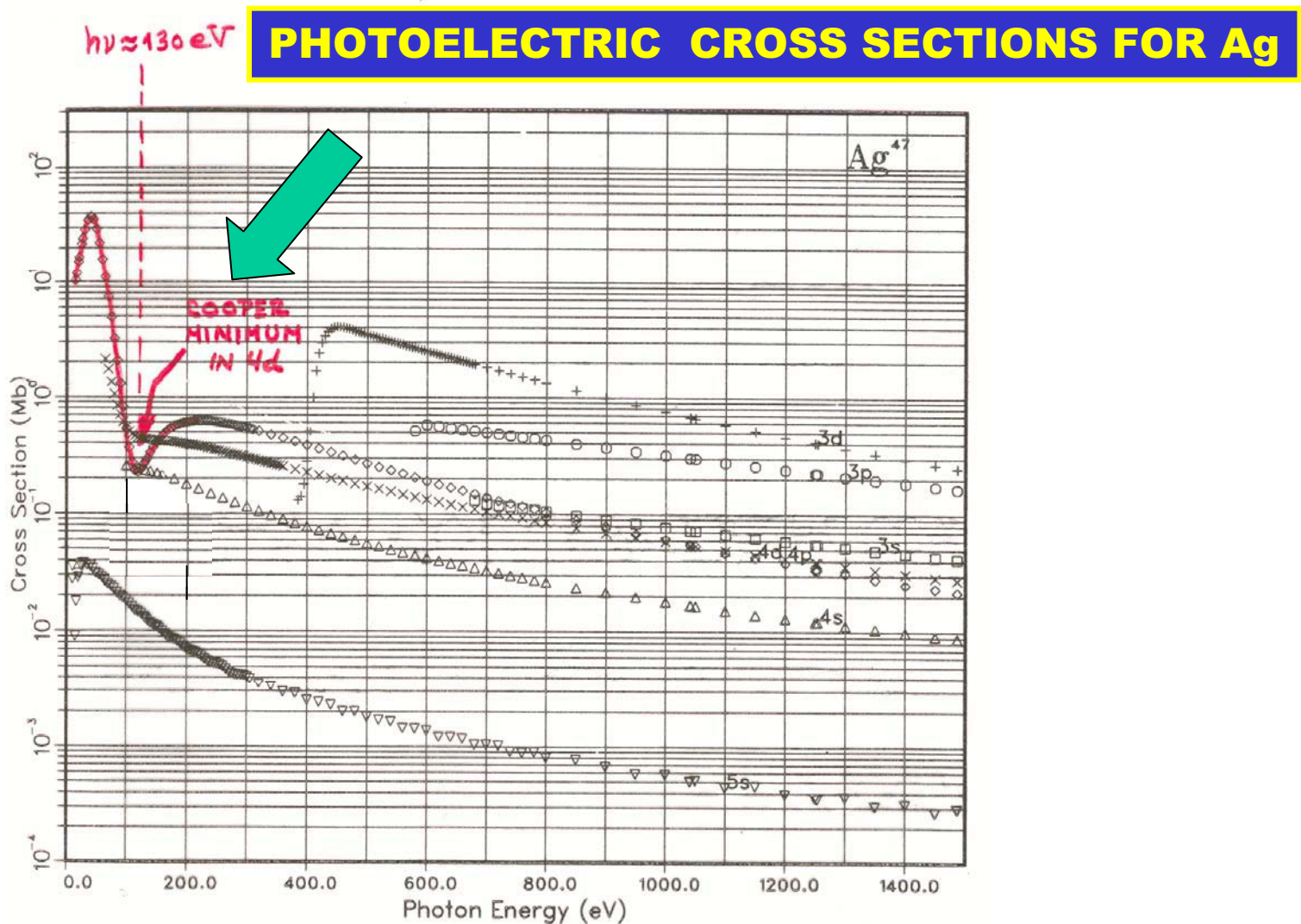
H binding energies(eV) are:
 $1s(1) 13.6050$

GRAPH I. Atomic Subshell Photoionization Cross Sections for 0–1500 eV, $1 \leq Z \leq 103$
See page 6 for Explanation of Graphs

PHOTOELECTRIC CROSS SECTIONS FOR Ne



GRAPH I. Atomic Subshell Photoionization Cross Sections for 0–1500 eV, $1 \leq Z \leq 103$
 See page 6 for Explanation of Graphs



Ag binding energies(eV) are:

1s(2) 24693.5	2s(2) 3591.17	2p(6) 3352.94
3s(2) 665.102	3p(6) 567.203	4s(2) 94.2146
3d(10) 384.360	4p(6) 62.9041	4d(10) 12.6499
5s(1) 6.42700		

COOPER MINIMUM IN Ag 4d (Z = 47) CROSS SECTION : Expt. & Theory

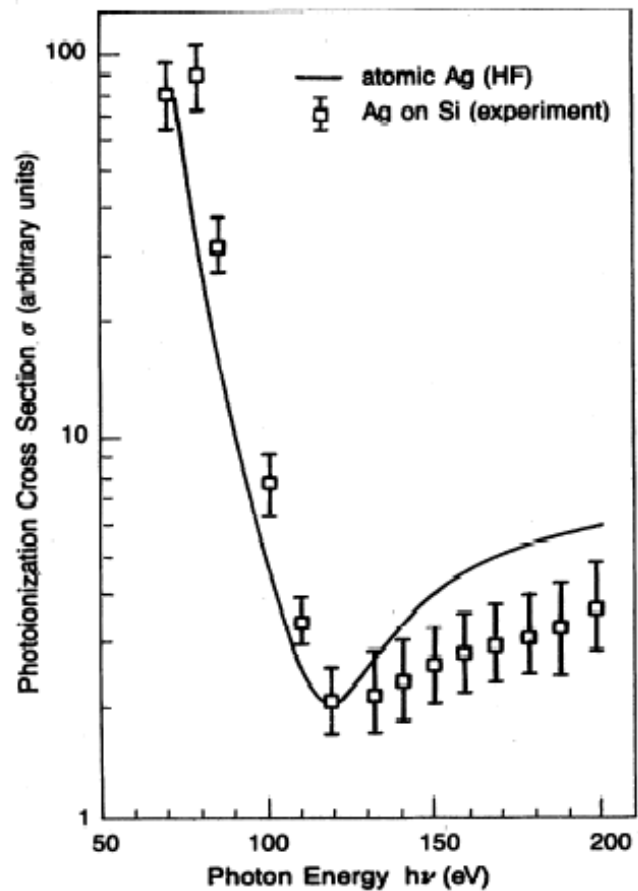


FIG. 5. Partial photoionization cross section for 4d electrons of Ag in logarithmic scale. Our experimental data for the Ag/Si interface (squares) are compared with the Hartree-Fock results for atomic Ag by Yeh and Lindau (solid line). Note that our experimental data are normalized at the minimum to the theoretical value.

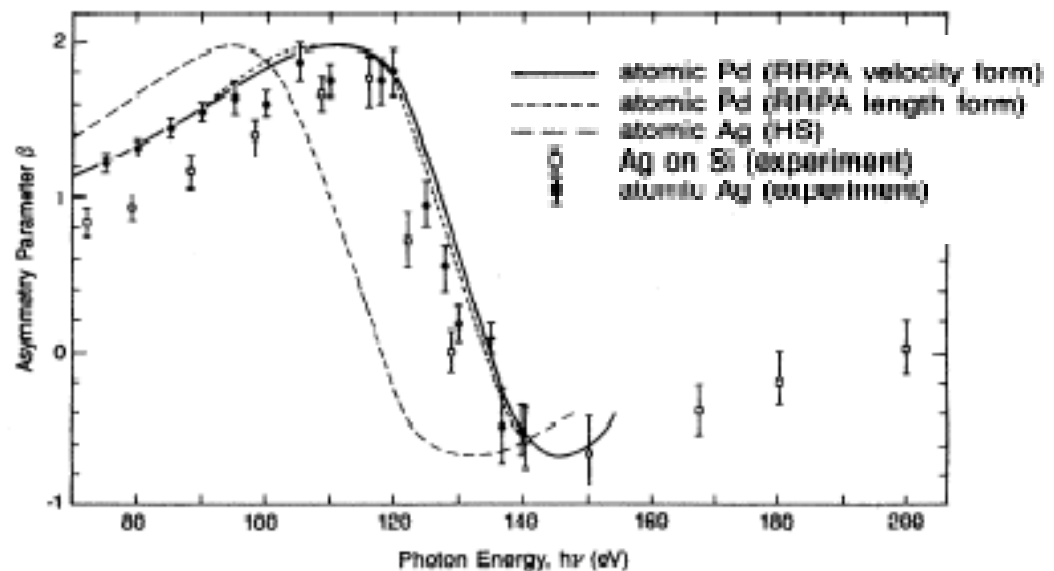
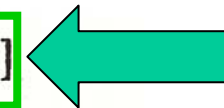


FIG. 6. Asymmetry parameter for 4d electrons of Ag. Our experimental data for the Ag/Si interface (squares) are compared with the data for atomic Ag (circles), the RRPA prediction for atomic Pd by Radojevic and Johnson (solid line, velocity form; short-dashed line, length form), and the HS calculations for atomic Ag by Manson (long-dashed line).

TOTAL SUBSHELL CROSS SECTION: $\int \frac{d\sigma_{nl}}{d\Omega} d\Omega =$

$$\sigma_{nl}(E^f) = \frac{4\pi\alpha_0\alpha_0^2}{3} (hv) [lR_{l-1}^2(E^f) + (l+1)R_{l+1}^2(E^f)]$$

= SUM OVER ALL m_l, m_s IN SUBSHELL nl



RADIAL MATRIX ELEMENTS TO $l\pm 1$ CHANNELS:

$$R_{l\pm 1}(E^f) = \int_0^\infty R_{nl}(r) r R_{E^f, l\pm 1}(r) r^2 dr = \int_0^\infty P_{nl}(r) r P_{E^f, l\pm 1}(r) dr$$

DIFFERENTIAL CROSS SECTION: UNPOLARIZED

$$\frac{d\sigma_{nl}}{d\Omega}(E^f) = \frac{\sigma_{nl}}{4\pi} [1 - \frac{1}{2}\beta_{nl}(E^f)P_2(\cos \alpha)]$$

$$= \frac{\sigma_{nl}}{4\pi} [1 + \frac{1}{2}\beta_{nl}(E^f)(\frac{3}{2}\sin^2 \alpha - 1)]$$

$$= A + B \sin^2 \alpha$$

ASYMMETRY PARAMETER:

TERM FOR
 $l\pm 1$ INTERFERENCE

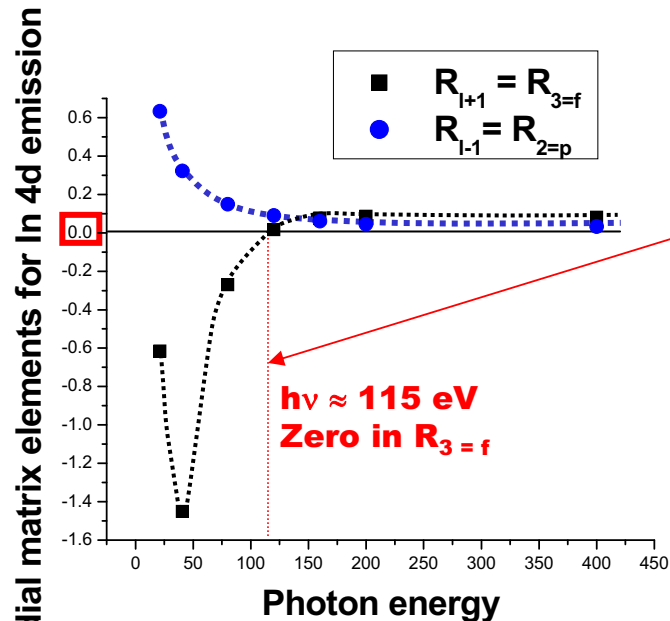
$$\beta_{nl}(E^f) = \frac{l(l-1)R_{l-1}^2(E^f) + (l+1)(l+2)R_{l+1}^2(E^f)}{(2l+1)[lR_{l-1}^2(E^f) + (l+1)R_{l+1}^2(E^f)]}$$

$\delta_{l\pm 1}(E^f)$ = CONTINUUM ORBITAL PHASE SHIFTS
IN ATOMIC POTENTIAL $V(r)$

COOPER MINIMUM IN In 4d (Z = 49)

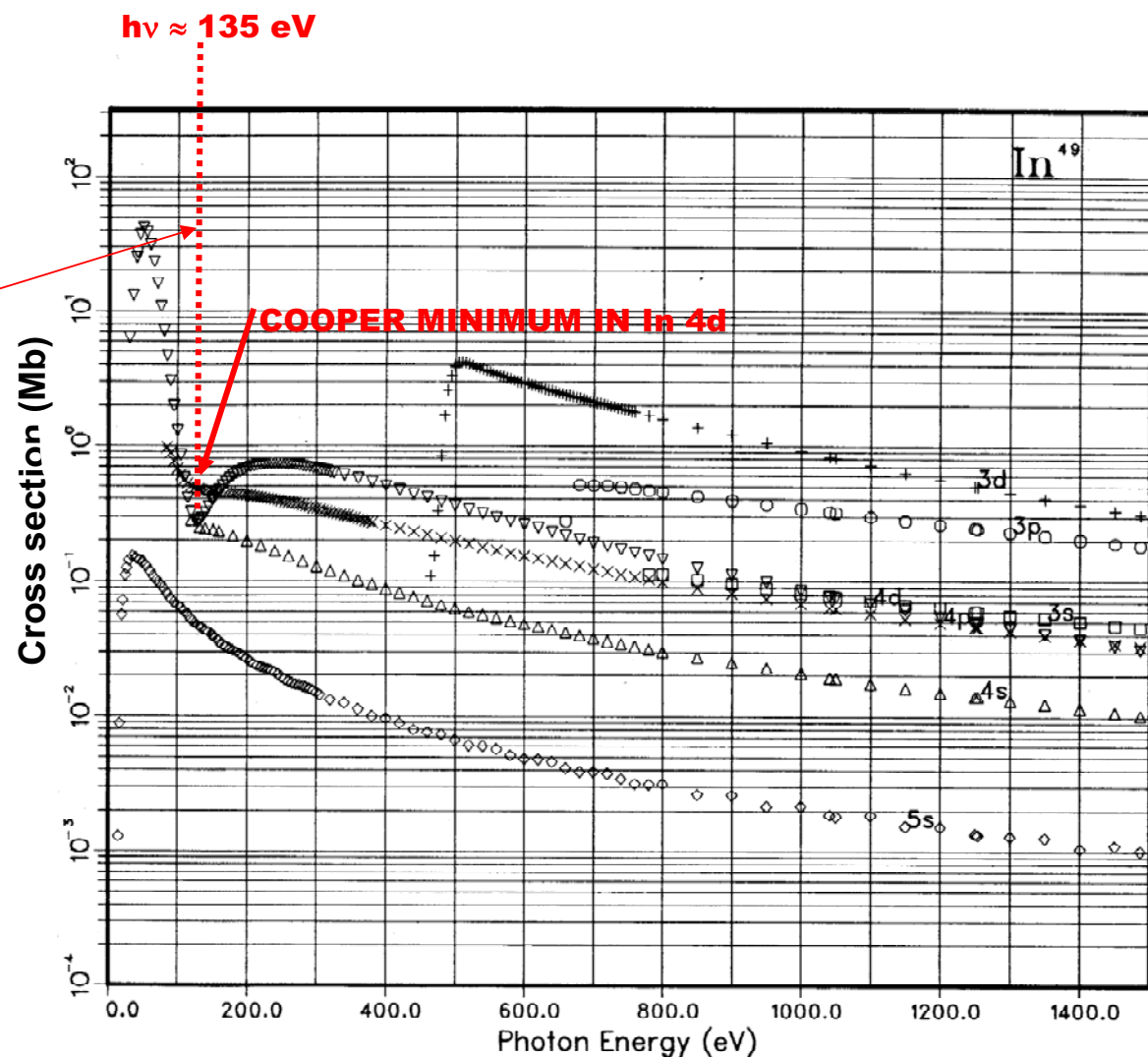
CROSS SECTION—Radial Matrix

Element Variation



Goldberg, Kono, Fadley
J. Elect. Spect. 21, 285 ('81)

GRAPH I. Atomic Subshell Photoionization Cross Sections for 0–1500 eV, $1 \leq Z \leq 103$
See page 6 for Explanation of Graphs



In binding energies(eV) are:

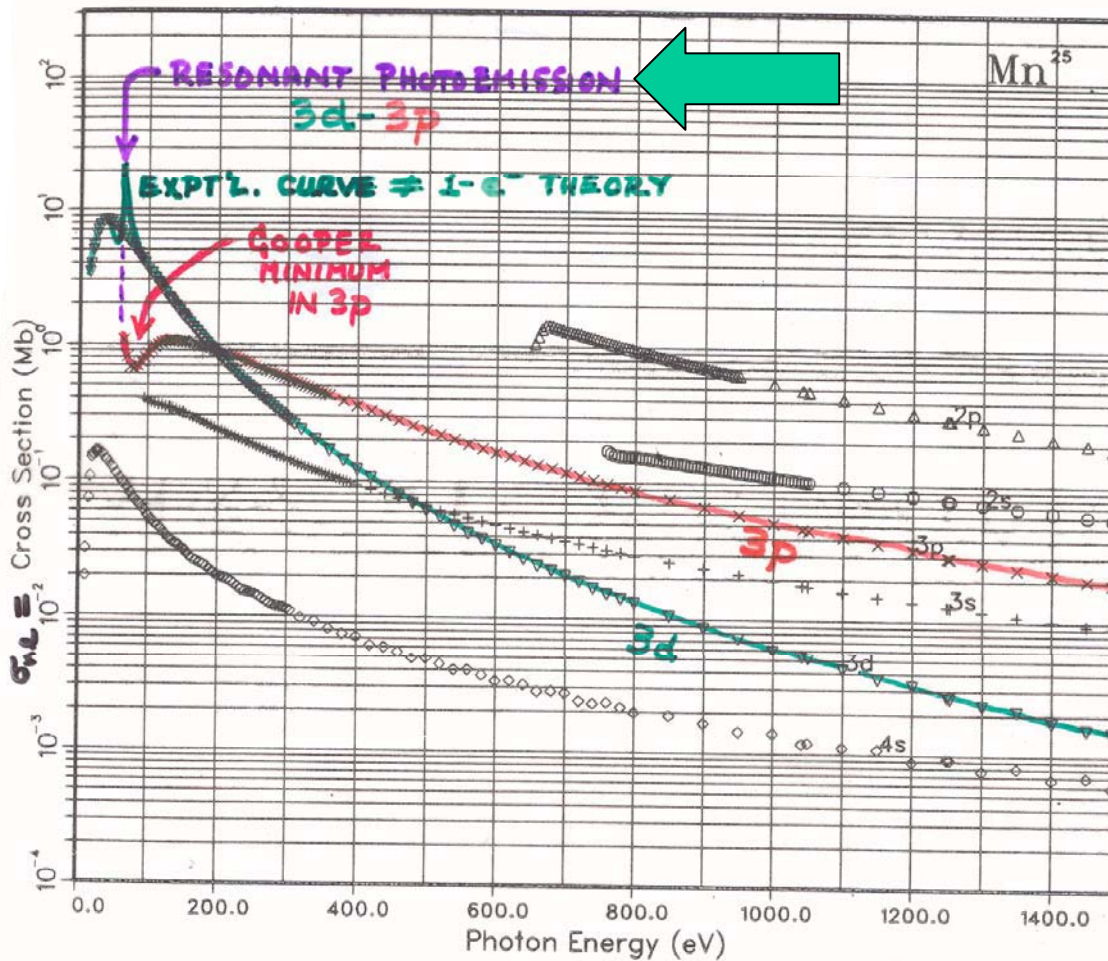
1s(2)	26971.5	2s(2)	3983.01	2p(6)	3731.41
3s(2)	764.232	3p(6)	659.286	4s(2)	118.953
3d(10)	462.909	4p(6)	84.0558	5s(2)	10.1384
4d(10)	26.2168	5p(1)	4.69781		

ATOMIC & NUCLEAR DATA TABLES 32, 45 (1985)

GRAPH I. Atomic Subshell Photoionization Cross Sections for 0-1500 eV, $1 \leq Z \leq 103$

See page 6 for Explanation of Graphs

PHOTOELECTRIC CROSS SECTIONS FOR Mn



Mn binding energies(eV) are:

1s(2) 6455.26

2s(2) 755.155

2p(6) 653.681

3s(2) 90.8814

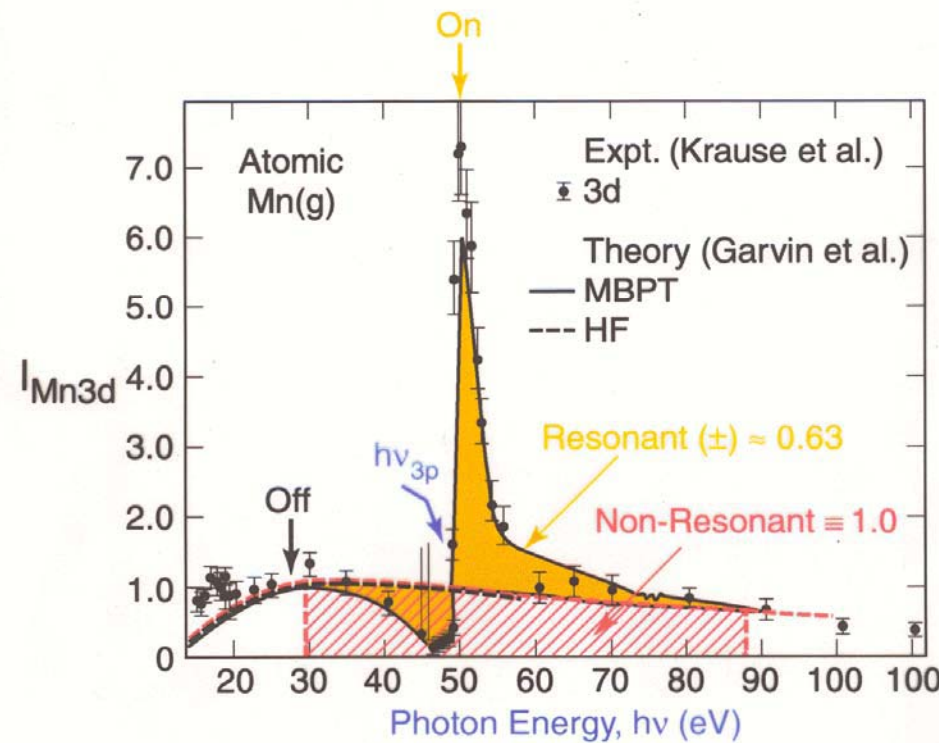
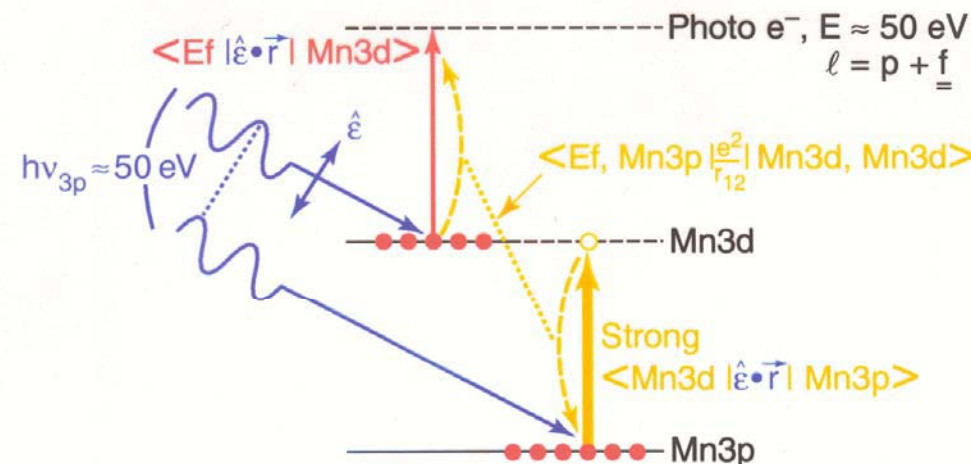
3p(6) 60.9150

4s(2) 7.14671

3d(5) 12.0486

RESONANT PHOTOEMISSION FOR Mn-A MANY-ELECTRON EFFECT

Ex. – Mn atom: Mn3d emission, resonance with Mn3p

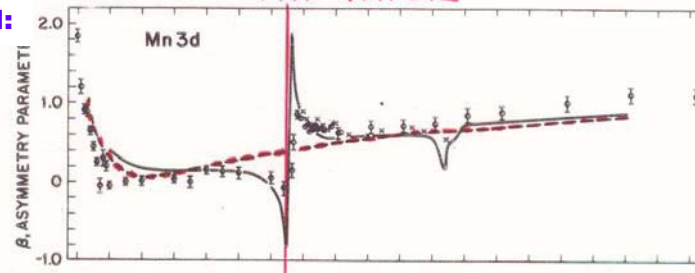


**SINGLE-ATOM
RESONANT
PHOTOEMISSION:**

HOTOELECTRON SPECTROMETRY OF MANGANESE VAPOR . . .

1315

β_{3d}



σ_{3d}

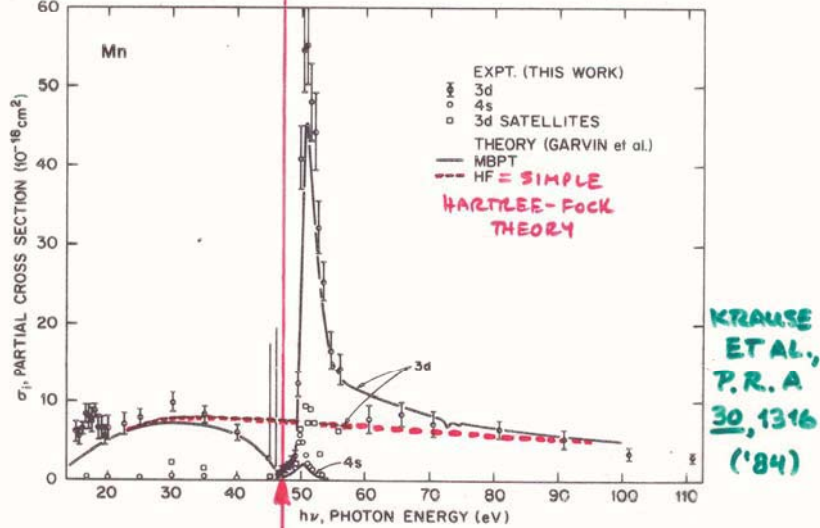
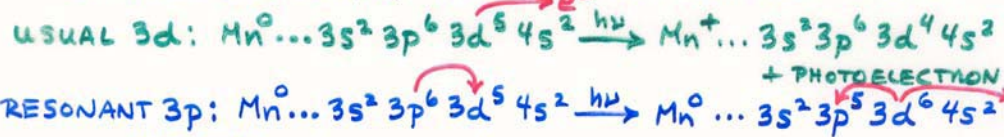


FIG. 2. Angular distribution parameter β of 3d photoelectrons (upper panel) and partial cross sections of 4s, 3d and satellite peaks (lower panel). Crosses (\times) for β are from Ref. 3, theory from Ref. 6. The resonance near 50 eV is due to the $3p \rightarrow 3d$ excitation into the partially filled 3d subshell of Mn.

$$h\nu = E_b^{\text{V}}(\text{Mn}3p)$$

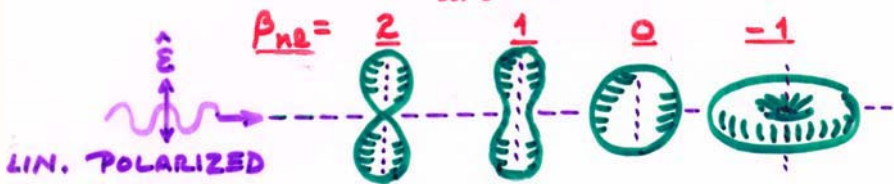
RESONANT PROCESS:

IF $h\nu \approx E_b$ OF $n\ell'$ SUBSHELL INSIDE OF $n\ell$ SUBSHELL OF INTEREST (E.G., $3p$ FOR $3d$), TWO "CHANNELS" COUPLE-



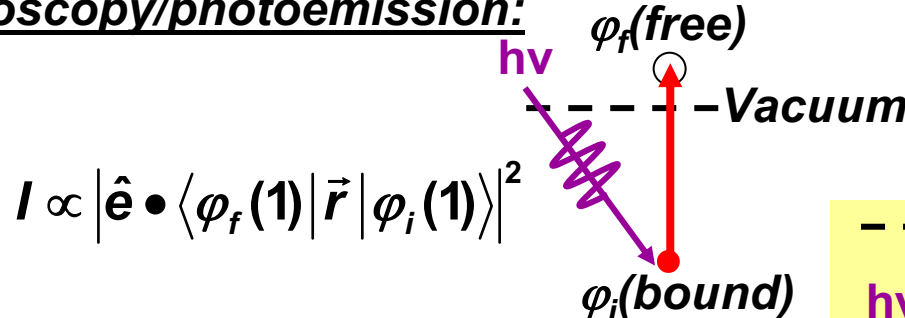
AUTOIONIZATION
 $(\approx$ AUGER) + ELECTRON @ SAME ENERGIES AS PHOTOEJECTION

|| COUPLING MUCH
ENHANCES CROSS
SECTION ||



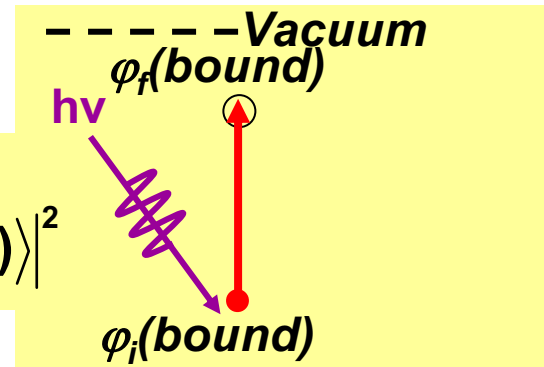
MATRIX ELEMENTS IN THE SOFT X-RAY SPECTROSCOPIES: DIPOLE LIMIT

- **Photoelectron spectroscopy/photoemission:**



- ### **• Near-edge x-ray absorption:**

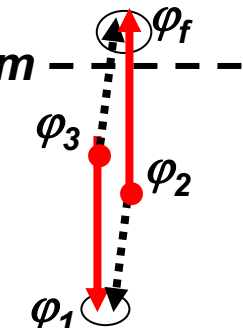
$$I \propto |\hat{\mathbf{e}} \bullet \langle \varphi_f(\mathbf{1}) | \vec{r} | \varphi_i(\mathbf{1}) \rangle|^2$$



- **Auger electron emission:**

$$I \propto \left| \langle \varphi_f(1)\varphi_1(2) | \frac{e^2}{r_{12}} | \varphi_3(1)\varphi_2(2) \rangle - \langle \varphi_1(1)\varphi_f(2) | \frac{e^2}{r_{12}} | \varphi_3(1)\varphi_2(2) \rangle \right|^2$$

Direct **Exchange**



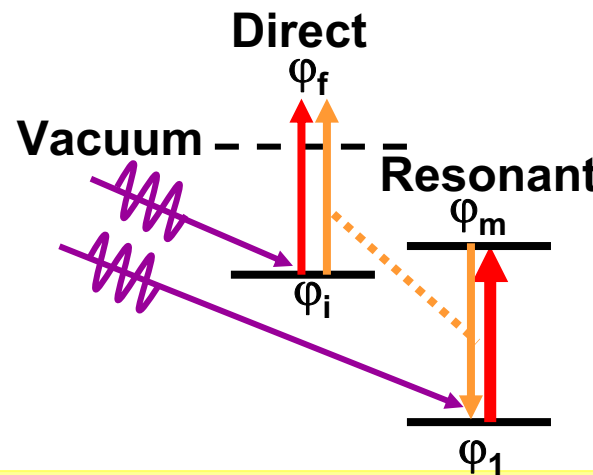
- X-ray emission:

$$I \propto |\hat{\mathbf{e}} \cdot \langle \varphi_f(1) | \vec{r} | \varphi_i(1) \rangle|^2$$

MATRIX ELEMENTS IN THE SOFT X-RAY SPECTROSCOPIES: RESONANT EFFECTS

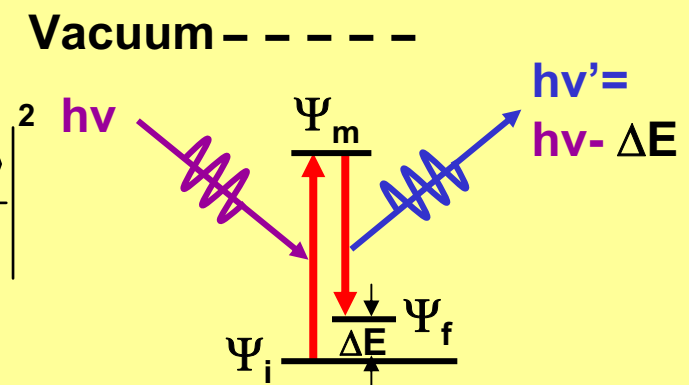
- Resonant photoemission:

$$I \propto \left| \langle \varphi_f(1) | \hat{e} \bullet \vec{r} | \varphi_i(1) \rangle + \sum_m \langle \varphi_f(1) \varphi_1(2) | \frac{e^2}{r_{12}} | \varphi_i(1) \varphi_m(2) \rangle \langle \varphi_m(1) | \hat{e} \bullet \vec{r} | \varphi_1(1) \rangle \right|^2 \times \delta(h\nu - (E_m - E_1))$$



- Resonant inelastic x-ray scattering:

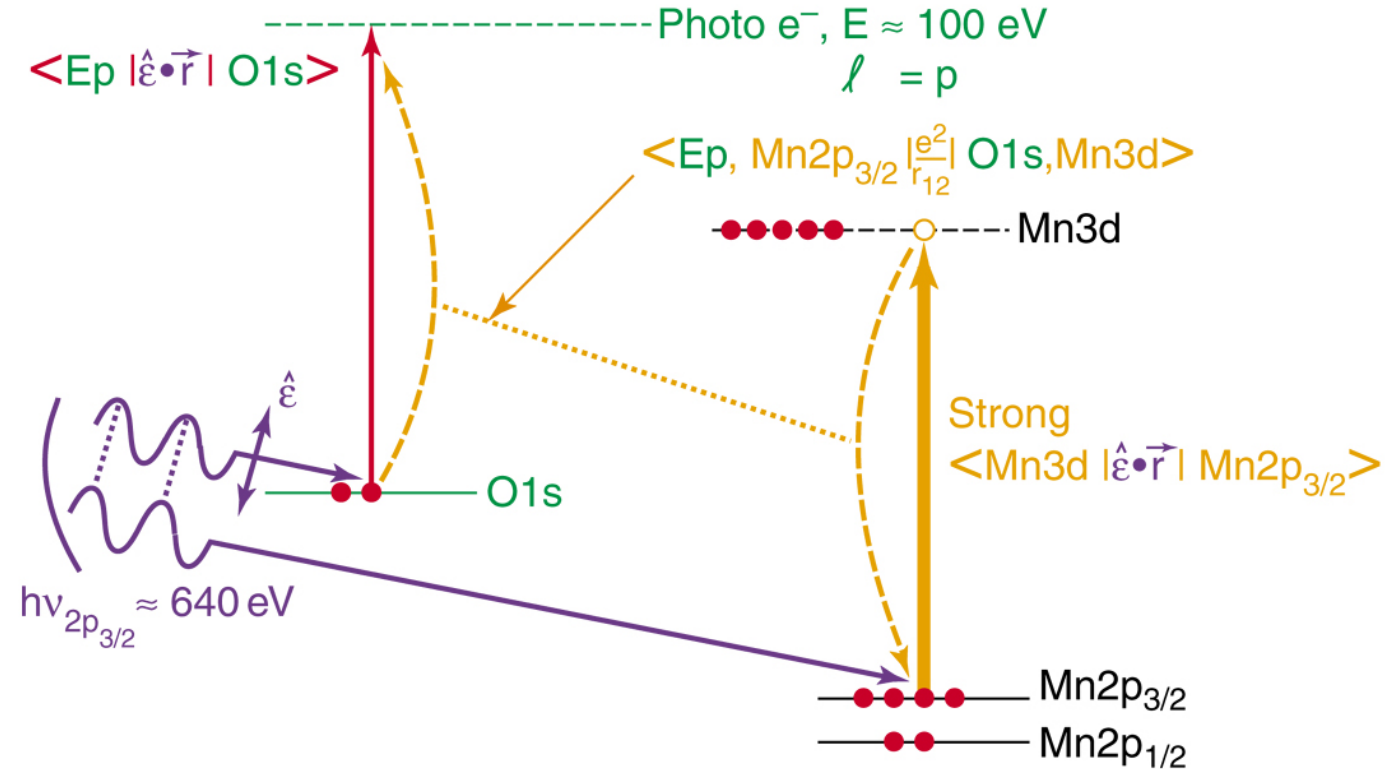
$$I \propto \sum_f \left| \sum_m \frac{\langle \Psi_f(N) | \hat{e} \bullet \vec{r} | \Psi_m(N) \rangle \langle \Psi_m(N) | \hat{e} \bullet \vec{r} | \Psi_i(N) \rangle}{h\nu + E_i(N) - E_m(N) - i\Gamma} \right|^2 \times \delta(h\nu - (E_m(N) - E_i(N)))$$



Multi-Atom Resonant Photoemission

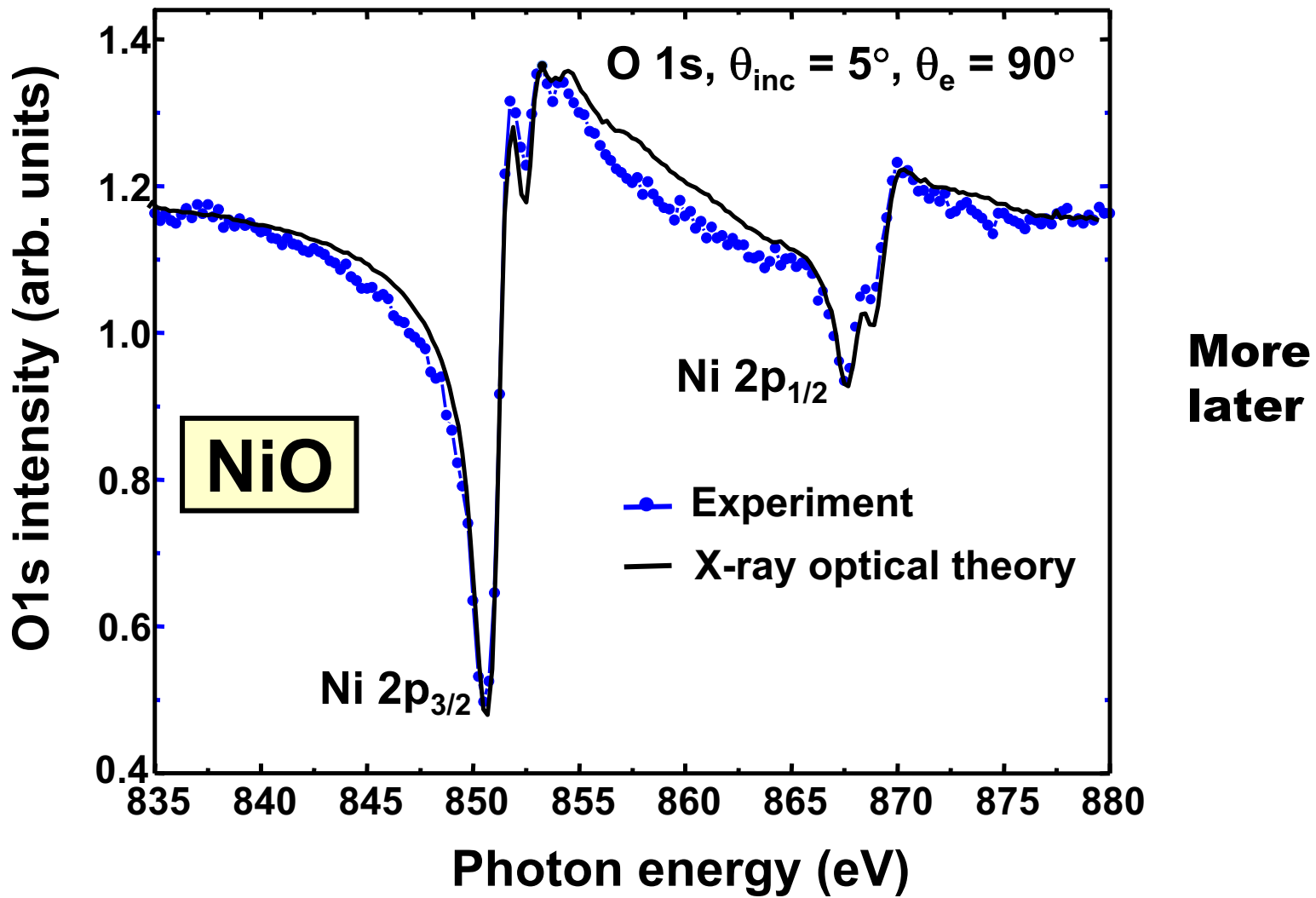
*Microscopic
Q.M. picture*

Ex. – MnO(001): O1s emission, resonance with Mn2p_{3/2}



Kay et al.,
Science 281, 679 ('98);
Corrected picture in
PRB 61, 5119 ('01) ←

Multi-Atom Resonant Photoemission— O 1s emission from NiO(001)

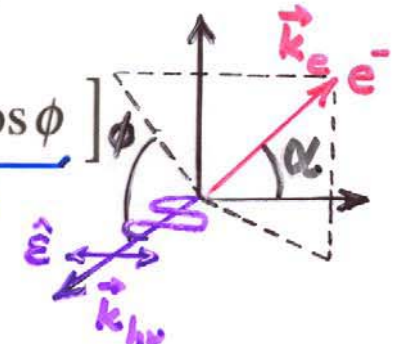


Mannella et al., to be published

Effects beyond the dipole approximation

The differential cross section for photoionization of randomly oriented target atoms by 100% linearly polarized photons has the form:

$$\frac{d\sigma}{d\Omega} = \left(\frac{\sigma}{4\pi} \right) \left[1 + \underbrace{\beta P_2(\cos \alpha)}_{\text{DIPOLE}} + \underbrace{(\delta + \gamma \cos^2 \alpha) \sin \alpha \cos \phi}_{\text{NON-DIPOLE}} \right]$$



with:

$$P_2(\cos \alpha) = \frac{1}{2} (3 \cos^2 \alpha - 1)$$

σ : angle integrated cross section

pole electron anisotropy parameter

β : electron anisotropy parameter

δ : non-dipole electron anisotropy parameter

$$\exp(i \vec{k}_{hv} \cdot \vec{r}) = \underbrace{1}_{\text{DIPOLE}} + \underbrace{i \vec{k}_{hv} \cdot \vec{r} - \frac{1}{2} (\vec{k}_{hv} \cdot \vec{r})^2 + \dots}_{\text{NON-DIPOLE}}$$

Krause et al.
Lindle et al.
Krässig et al.

$k_{hv} = 2\pi/\lambda_{hv} = 0.75 \text{ \AA}^{-1}$ @ 1.49 keV $\rightarrow k_{hv} \cdot [\langle r_{nl} \rangle \approx 1 \text{ \AA}] \approx 0.75$ —Non-dipole imp?
 0.075 \AA^{-1} @ 149 eV $\rightarrow k_{hv} \cdot [\langle r_{nl} \rangle \approx 1 \text{ \AA}] \approx 0.075$ —Dipole ~OK

BEYOND THE DIPOLE APPROXIMATION?
FREE-ATOM DIFFERENTIAL CROSS SECTIONS
 (KRAUSE, PHYS. REV. 177, 151 ('69))

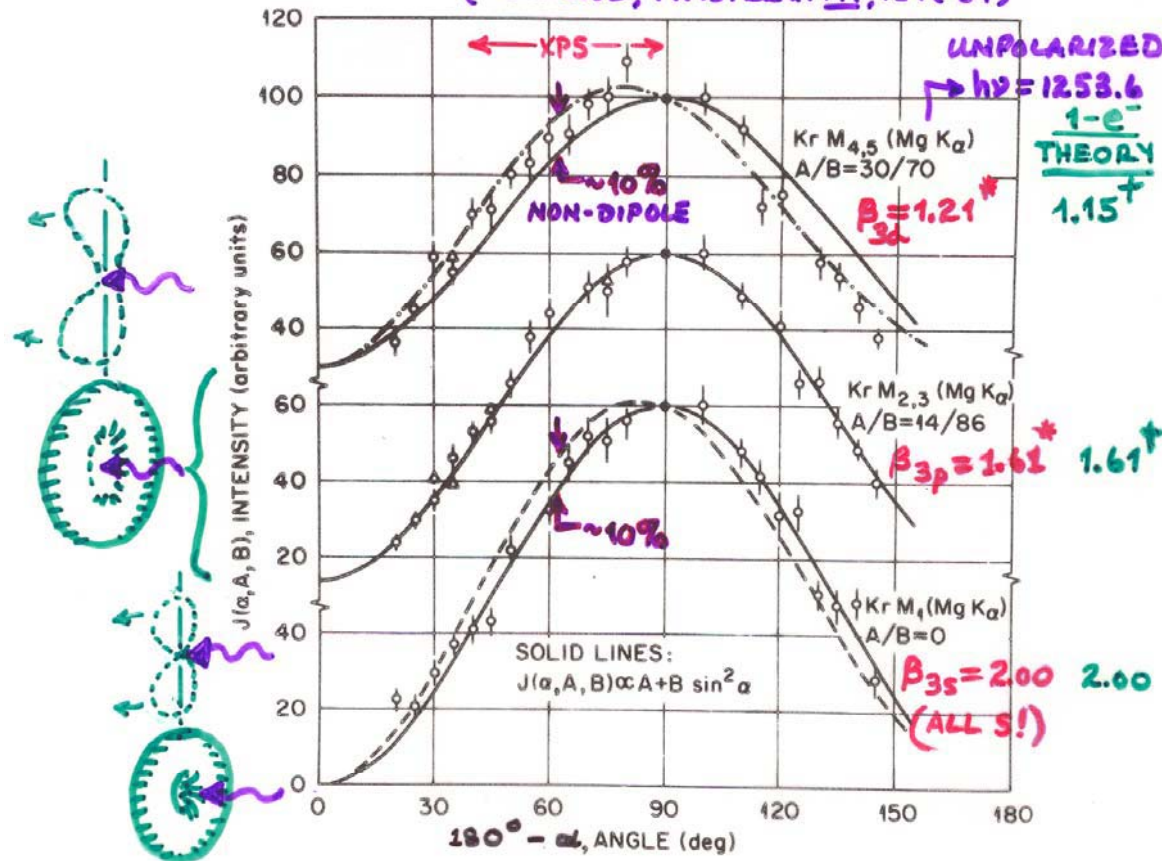


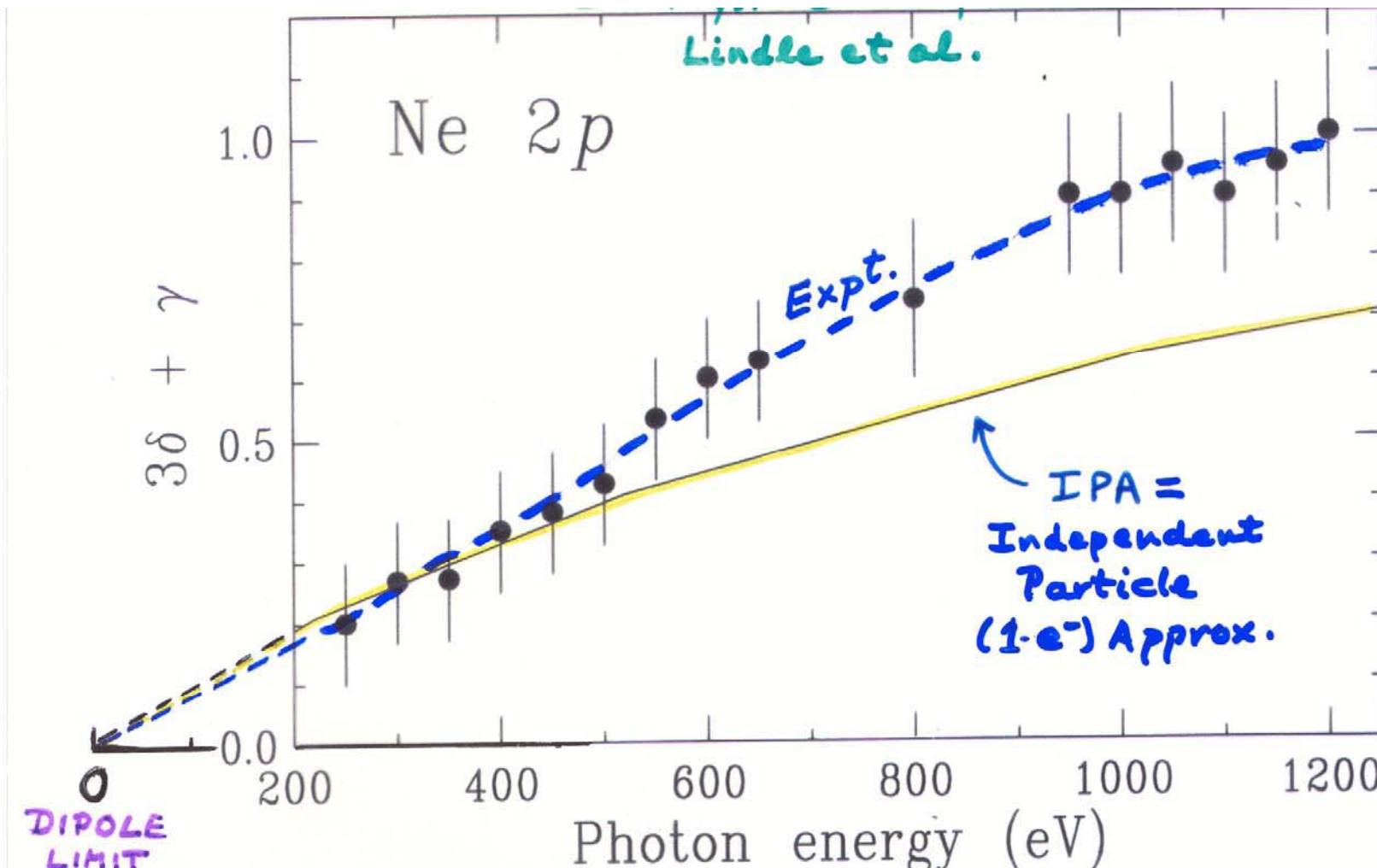
Figure 1J -- Experimental angular distributions of 3s ($= M_1$), 3p ($= M_{2,3}$), and 3d ($= M_{4,5}$) photoelectrons excited from gaseous Kr with MgK α X-rays. The curves represent least-squares fits to the data points of a relationship of the form of Equation (93), in which A and B were treated as empirical constants. (From Krause, reference 142.)

$$\begin{aligned} * \text{ FROM: } \beta_{nl} &= \frac{4B}{(3A+2B)} \\ &= \frac{4}{(3A/B+2)} \end{aligned}$$

NEAR EQ. 93;
 FADLEY, "BASIC
 CONCEPTS OF XPS"

|| + FROM YEH
 & LINDAU
 TABLES "Basic Concepts of XPS"
 Figure 10

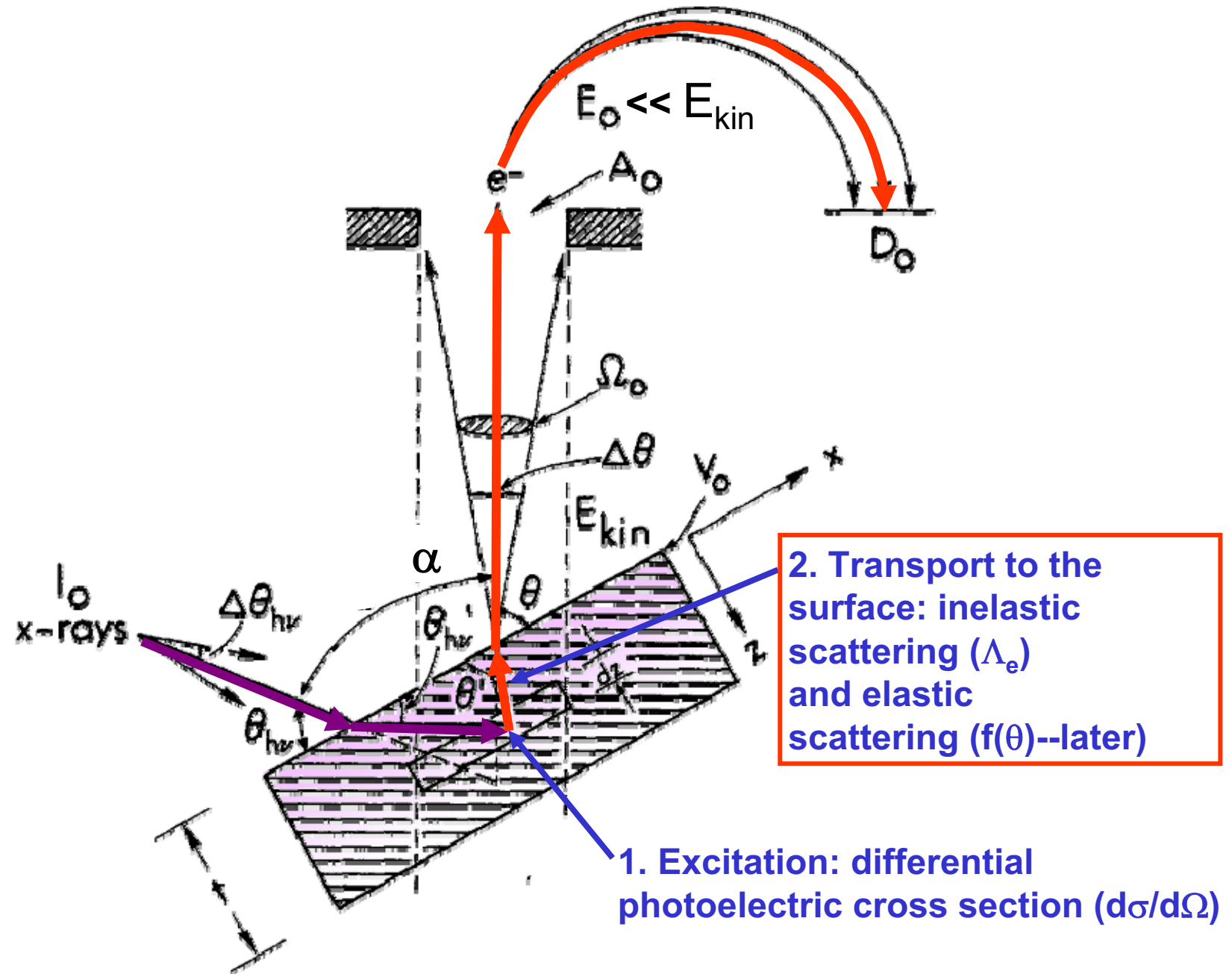
Non-dipole effects in 2p emission from Ne



+ see Phys. Rev. Lett. 78, 4553 ('97): Lindle et al.

" " " 75, 4736 ('95): Krässig et al.

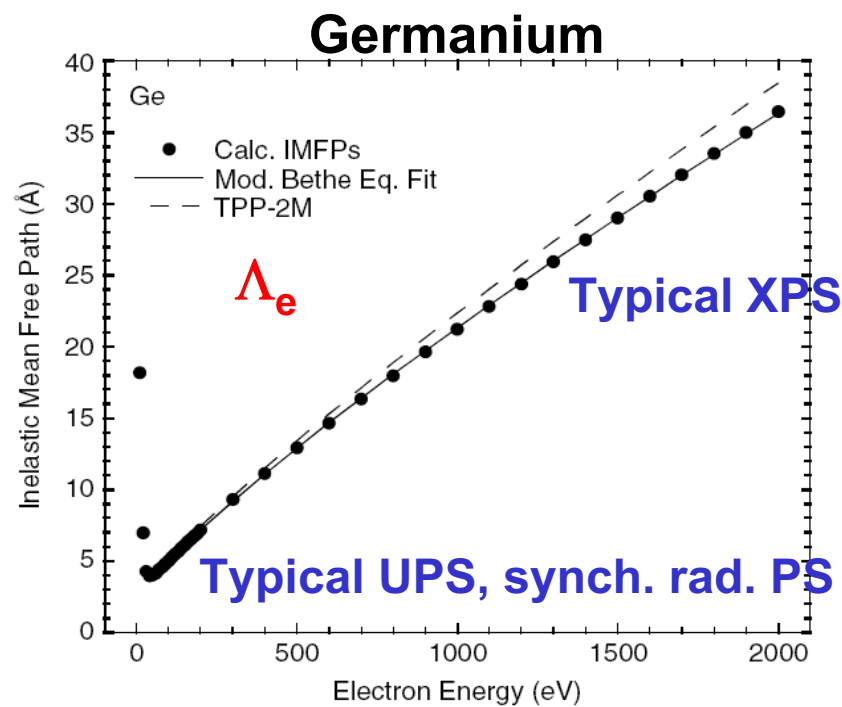
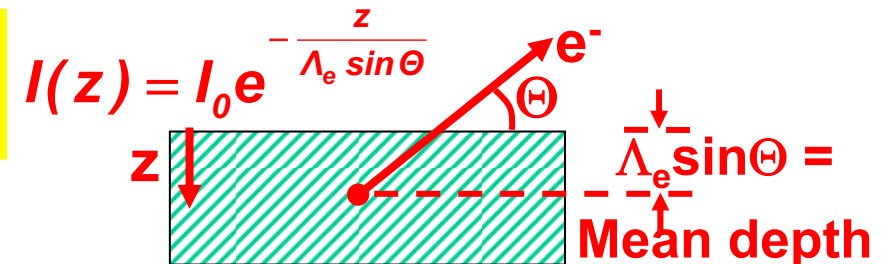
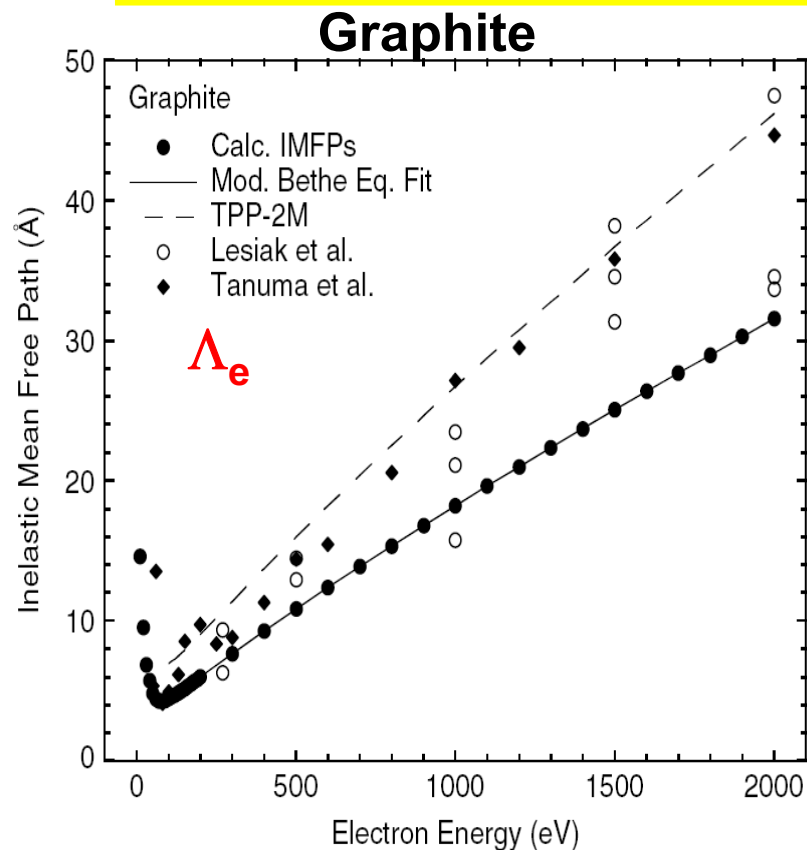
PHOTOELECTRON INTENSITIES—THE 3-STEP MODEL



Electron inelastic attenuation length in solids—the “universal curve”

Photoemission is a surface sensitive experiment

Changing angle:
1st way to vary surface sensitivity



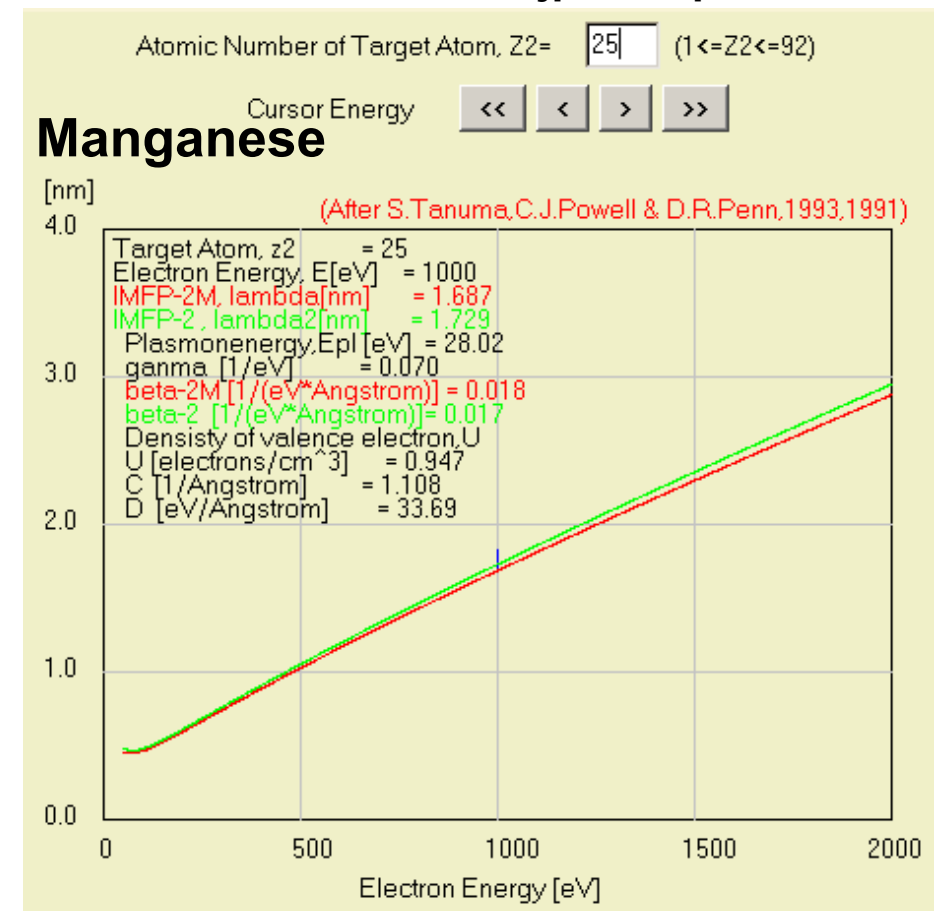
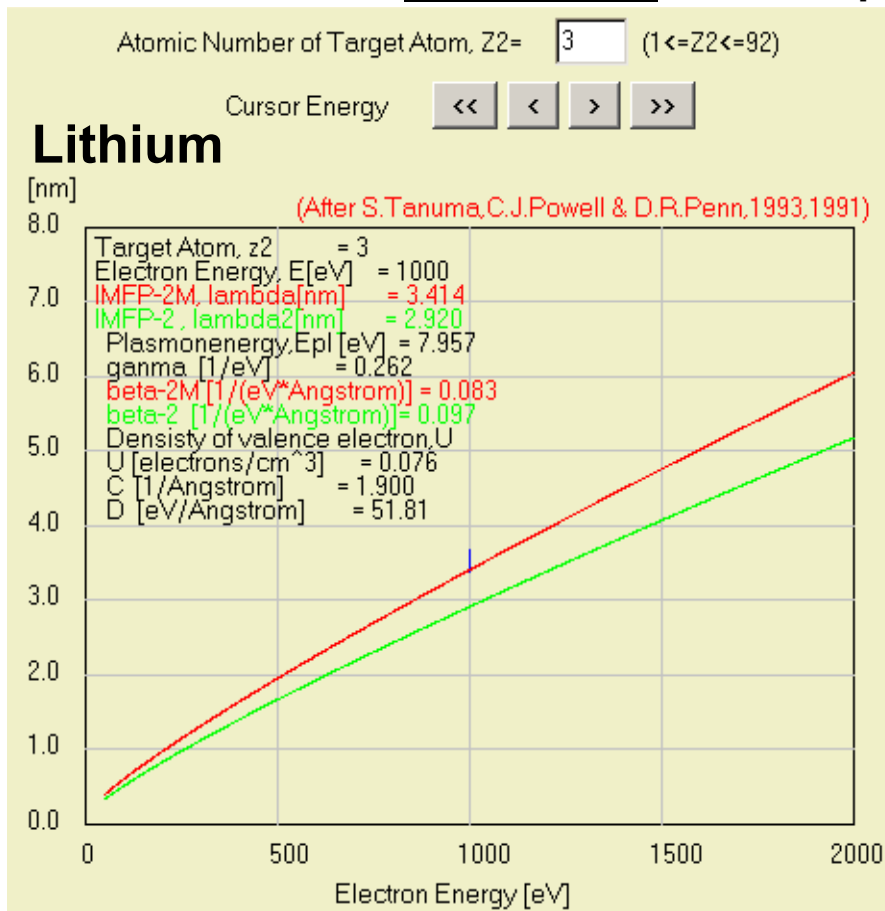
Changing photon energy:
2nd way to vary surface sensitivity

Inelastic mean free paths in solids

Database of experimental and theoretically estimated mean free paths at
<http://www.nist.gov/srd/webguide/nist71/71imfp.htm#elements>

Plus estimation with the **TPP-2M (TPP-2)** formula of Tanuma, Powell, Penn:

Web calculation for elements from: <http://www.ss.teen.setsunan.ac.jp/e-imfp2.html>



Inelastic mean free paths in solids

Estimation from the TPP-2M formula: any compound

$$\Lambda_e \approx \lambda = \frac{E}{E_p^2 [\beta \ln(\gamma E) - (C/E) + (D/E^2)]}$$

where

$$\beta = -0.10 + 0.944/(E_p^2 + E_g^2)^{1/2} + 0.069\rho^{0.1}$$

$$\gamma = 0.191\rho^{-0.50}$$

$$C = 1.97 - 0.91U$$

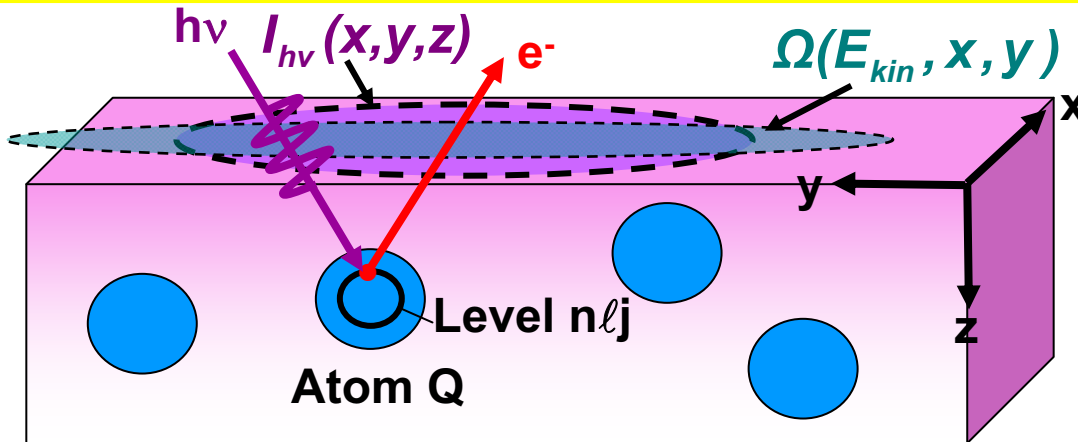
$$D = 53.4 - 20.8U$$

$$U = N_v \rho / M = E_p^2 / 829.4$$

and $E_p = 28.8 (N_v \rho / M)^{1/2}$ is the free-electron plasmon energy (in eV), ρ is the density (in g cm⁻³), N_v is the number of valence electrons per atom (for an element) or molecule (for a compound), M is the atomic or molecular weight, and E_g is the bandgap energy (in eV). These equations are collectively known as the **TPP-2M** equation.

Tanuma, Powell, Penn, Surf. Interface Anal.
21, 165 (1994)

CORE PHOTOELECTRON INTENSITIES AND COMPOSITION



$$I(Qn\ell j) =$$

$$C \int_0^{\infty} I_{hv}(x,y,z) \rho_Q(x,y,z) \frac{d\sigma_{Qn\ell j}(hv)}{d\Omega} \exp\left[-\frac{z}{\Lambda_e(E_{kin}) \sin \theta}\right] \Omega(E_{kin}, x, y) dx dy dz$$

$I_{hv}(x,y,z)$ = x-ray flux

$\rho_Q(x,y,z)$ = density of atoms Q → quantitative analysis

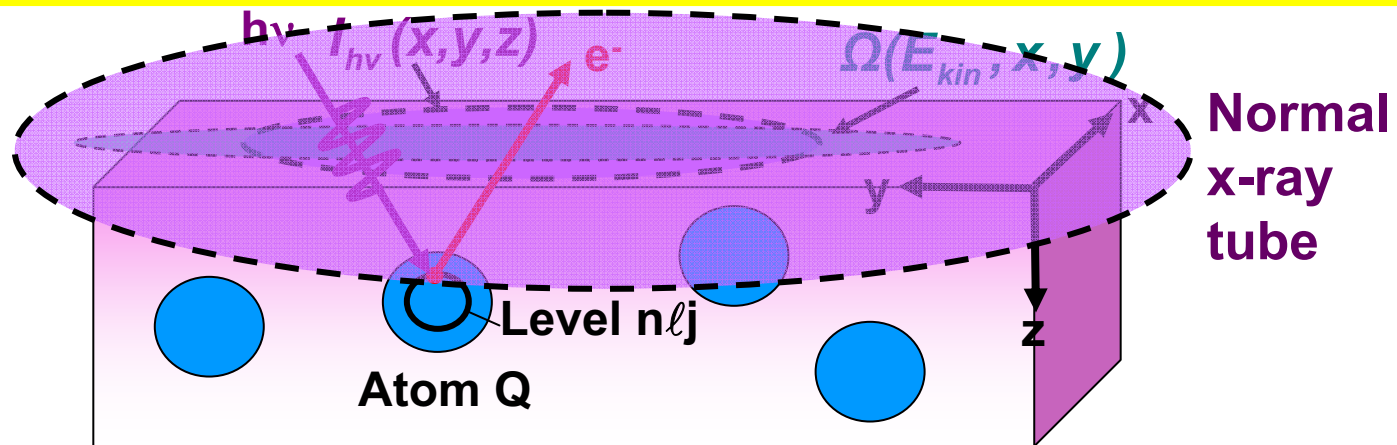
$\frac{d\sigma_{Qn\ell j}(hv)}{d\Omega}$ = energy-dependent differential photoelectric cross section for subshell $Qn\ell j$

$\Lambda_e(E_{kin})$ = energy-dependent inelastic attenuation length

→ Effective Attenuation Length (EAD) → Mean Emission Depth (MED)

$\Omega(E_{kin}, x, y)$ = energy-dependent spectrometer acceptance solid angle

CORE PHOTOELECTRON INTENSITIES AND COMPOSITION



$$I(Qn\ell j) =$$

$$C \int_0^\infty I_{hv}(x,y,z) \rho_Q(x,y,z) \frac{d\sigma_{Qn\ell j}(h\nu)}{d\Omega} \exp\left[-\frac{z}{\Lambda_e(E_{kin}) \sin \theta}\right] \Omega(E_{kin}, x, y) dx dy dz$$

$I_{hv}(x,y,z)$ = x-ray flux

$\rho_Q(x,y,z)$ = density of atoms $Q \rightarrow$ quantitative analysis

$\frac{d\sigma_{Qn\ell j}(h\nu)}{d\Omega}$ = **energy-dependent** differential photoelectric cross section for subshell $Qn\ell j$

$\Lambda_e(E_{kin})$ = **energy-dependent** inelastic attenuation length

→ Effective Attenuation Length (EAD) → Mean Emission Depth (MED)

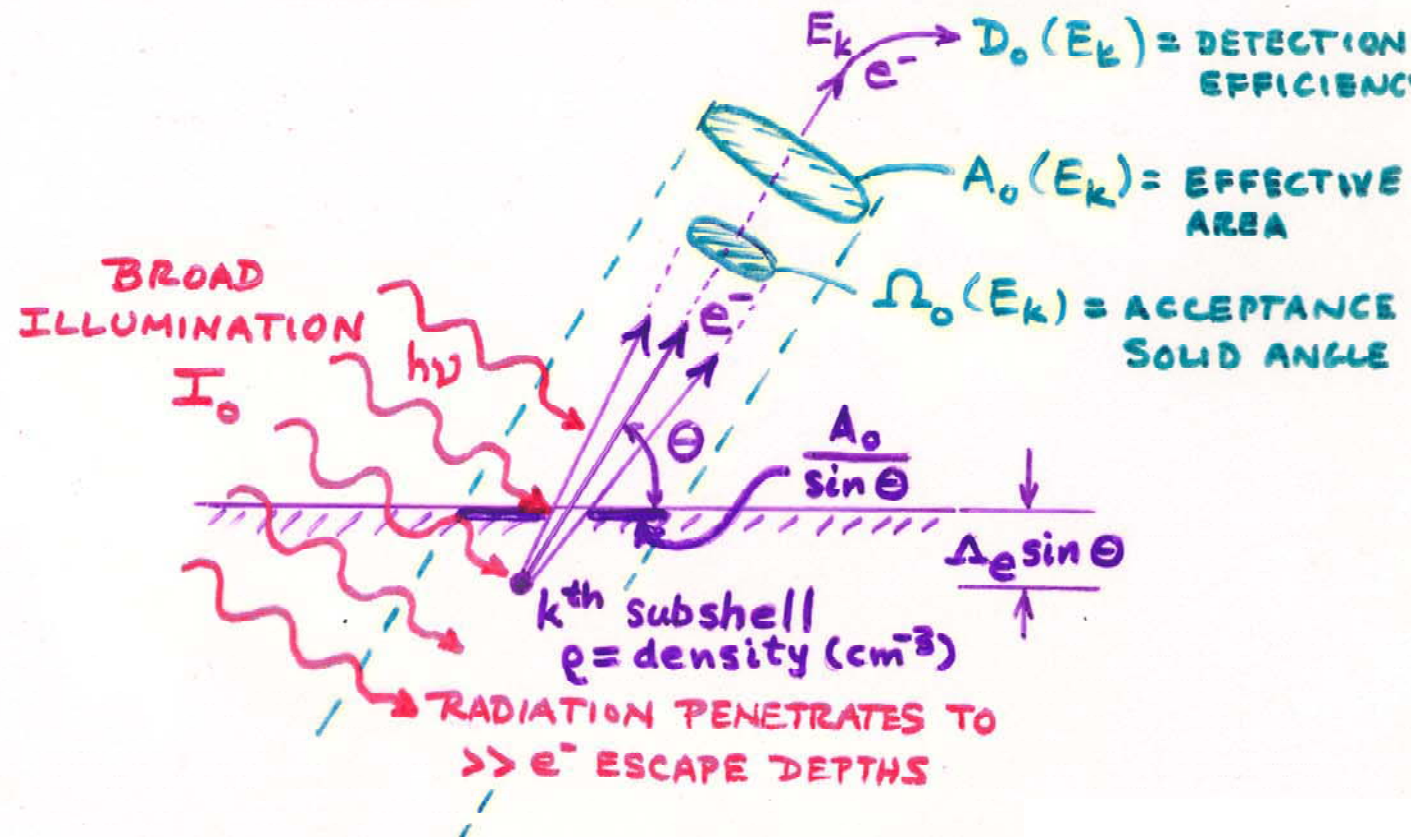
$\Omega(E_{kin}, x, y)$ = **energy-dependent** spectrometer acceptance solid angle

PHOTOELECTRON INTENSITIES FOR SOME USEFUL CASES

(a) Semi-infinite specimen, atomically clean surface, peak k with $E_{\text{kin}} \equiv E_k$:

$$N_k(\theta) = I_0 \Omega_0(E_k) A_0(E_k) D_0(E_k) \rho \frac{d\sigma_k}{d\Omega} \Lambda_e(E_k) \left(\frac{\text{NO}}{\Theta} \right) \text{DEP.} \quad (115)$$

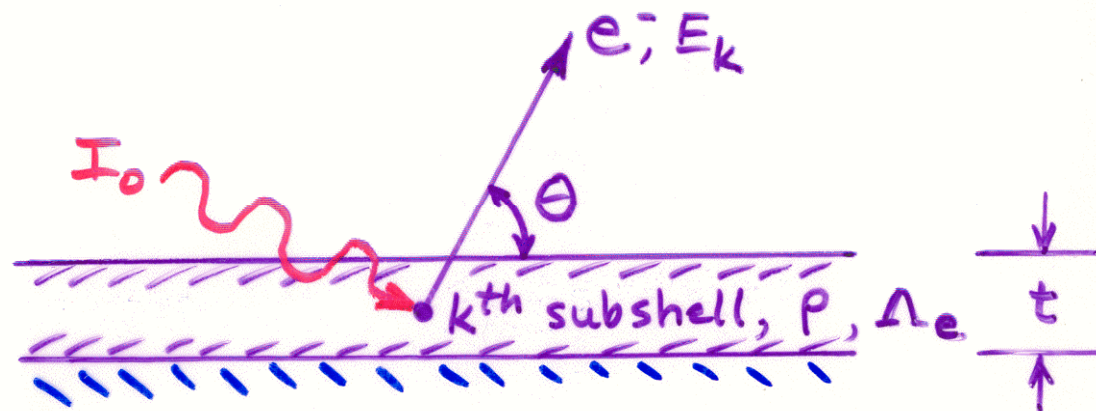
This case corresponds to an optimal measurement on a homogeneous specimen for which no surface contaminant layer is present.



(b) Specimen of thickness t , atomically clean surface, peak k with $E_{\text{kin}} \equiv E_k$:

$$N_k(\theta) = I_0 \Omega_0(E_k) A_0(E_k) D_0(E_k) \rho \frac{d\sigma_k}{d\Omega} \Lambda_e(E_k) \times [1 - \exp(-t/\Lambda_e(E_k) \sin \theta)] \quad (116)$$

Here, the intensity of a peak originating in a specimen of finite thickness is predicted to increase with decreasing θ .



(c) Semi-infinite substrate with uniform overlayer of thickness t -
 Peak k from substrate with $E_{\text{kin}} \equiv E_k$:

$$N_k(\theta) = I_0 \Omega_0(E_k) A_0(E_k) D_0(E_k) \rho \frac{d\sigma_k}{d\Omega} \Lambda_e(E_k) \\ \times \exp(-t/\Lambda_e'(E_k) \sin \theta) \quad (117)$$

Peak l from overlayer with $E_{\text{kin}} \equiv E_l$:

$$N_l(\theta) = I_0 \Omega_0(E_l) A_0(E_l) D_0(E_l) \rho' \frac{d\sigma_l}{d\Omega} \Lambda_e'(E_l) \\ \times [1 - \exp(-t/\Lambda_e'(E_l) \sin \theta)] \quad (118)$$

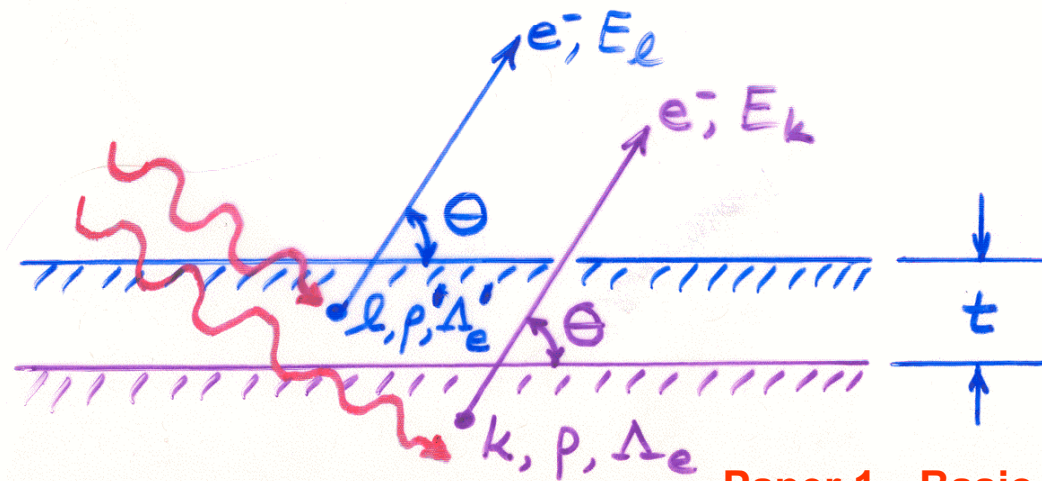
where

$\Lambda_e(E_k)$ = an attenuation length in the substrate

$\Lambda_e'(E_k)$ = an attenuation length in the overlayer

ρ = an atomic density in the substrate

ρ' = an atomic density in the overlayer.



(d) Semi-infinite substrate with a non-attenuating overlayer at fractional monolayer coverage—Peak k from substrate: Eq. (115).

Peak l from overlayer:

$$N_l(\theta) = I_0 \Omega_0(E_l) A_0(E_l) D_0(E_l) s' (\frac{d\sigma_l}{d\Omega}) (\sin \theta)^{-1} \quad (120a)$$

Overlayer/substrate ratio:

$$\begin{aligned} \frac{N_l(\theta)}{N_k(\theta)} &= \frac{\Omega_0(E_l) A_0(E_l) D_0(E_l) s' (\frac{d\sigma_l}{d\Omega})}{\Omega_0(E_k) A_0(E_k) D_0(E_k) s (\frac{d\sigma_k}{d\Omega}) (\Lambda_e(E_k) \sin \theta / d)} \\ &= \left[\frac{s'}{s} \right] \cdot \frac{D_0(E_l) \Omega_0(E_l) A_0(E_l) (\frac{d\sigma_l}{d\Omega}) d}{D_0(E_k) \Omega_0(E_k) A_0(E_k) (\frac{d\sigma_k}{d\Omega}) \Lambda_e \sin \theta} \end{aligned} \quad (120b)$$

with

s' = the mean surface density of atoms in which peak l originates in cm^{-2}

s = the mean surface density of substrate atoms in $\text{cm}^{-2} \equiv \rho_s$

s'/s = the fractional monolayer coverage of the atomic species in which peak l originates

d = the mean separation between layers of density s in the substrate (calculable from s/ρ).

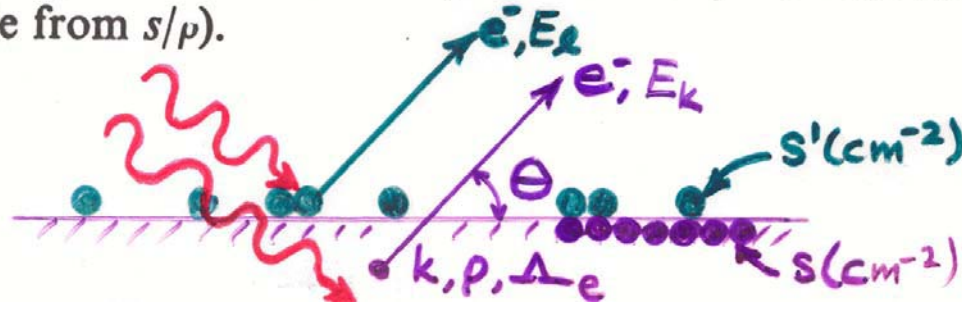


Table 4 Density and atomic concentration

The data are given at atmospheric pressure and room temperature, or at the stated temperature in deg K. (Crystal modifications as for Table 3.)

H	4K	0.088													He	2K	0.205 (at 37 atm)	
Li	78K	Be	0.542	1.82	4.700	12.1	3.023	2.22										
Na	5K	Mg	1.013	1.74	2.652	4.30	3.659	3.20										
K	5K	Ca	0.910	1.53	2.99	4.51	6.09	7.19	7.47	7.87	8.9	8.91	8.93	7.13	Al	Si	P	
Rb	5K	Sr	1.629	2.58	4.48	6.51	8.58	10.22	11.50	12.36	12.42	12.00	10.50	8.65	C	N	O	
Cs	5K	Ba	1.997	3.59	6.17	13.20	16.66	19.25	21.03	22.58	22.55	21.47	19.28	14.26	F	Ne	4K	
Fr	Ra	Ac	—	—	10.07	Ce	Pr	Nd	Pm	Sm	Eu	Gd	Tb	Dy	Ho	Er	Tm	
					2.66	6.77	6.78	7.00	—	7.54	5.25	7.89	8.27	8.53	8.80	9.04	9.32	6.97
					3.76	2.91	2.92	2.93	—	3.03	2.04	3.02	3.22	3.17	3.22	3.26	3.32	3.02
						3.65	3.63	3.66		3.59	3.96	3.58	3.52	3.51	3.49	3.47	3.54	3.88
						Th	Pa	U	Np	Pu	Am	Cm	Bk	Cf	Es	Fm	Md	No
						11.72	15.37	19.05	20.45	19.81	11.87	—	—	—	—	—	—	—
						3.04	4.01	4.80	5.20	4.26	2.96	—	—	—	—	—	—	—
						3.60	3.21	2.75	2.62	3.1	3.61							

$$\text{Atomic radius} = r_{\text{MT}} = 0.5 \text{ n-n dist.}$$

$$\begin{array}{ccc} \text{Density in g cm}^{-3} (10^3 \text{kg m}^{-3}) & & \\ \text{Concentration in } 10^{22} \text{ cm}^{-3} (10^{28} \text{ m}^{-3}) & & \\ \text{Nearest-neighbor distance, in \AA (10}^{-10}\text{m}) & & \end{array}$$

$$\text{Average surface density} = \rho_s = (\rho_v)^{2/3}$$

Surface sensitivity enhancement for grazing exit angles

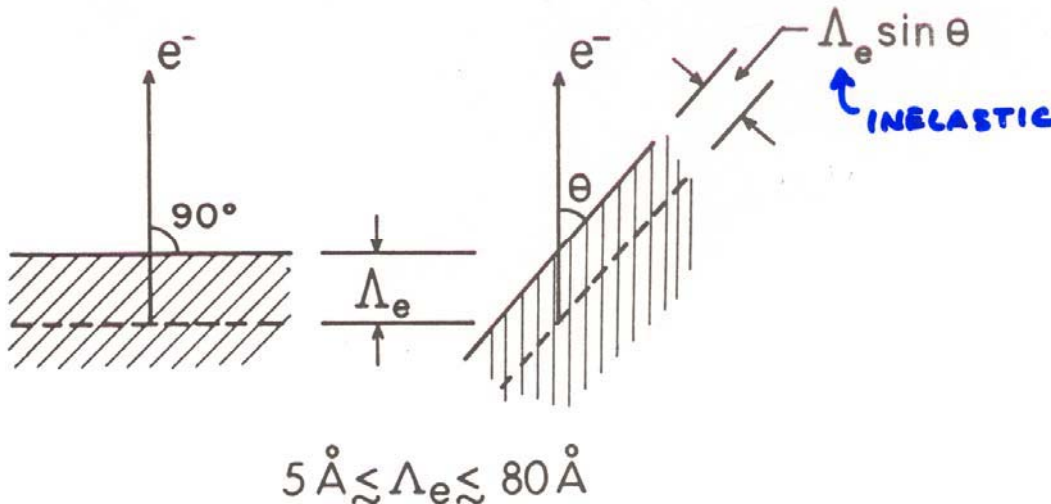
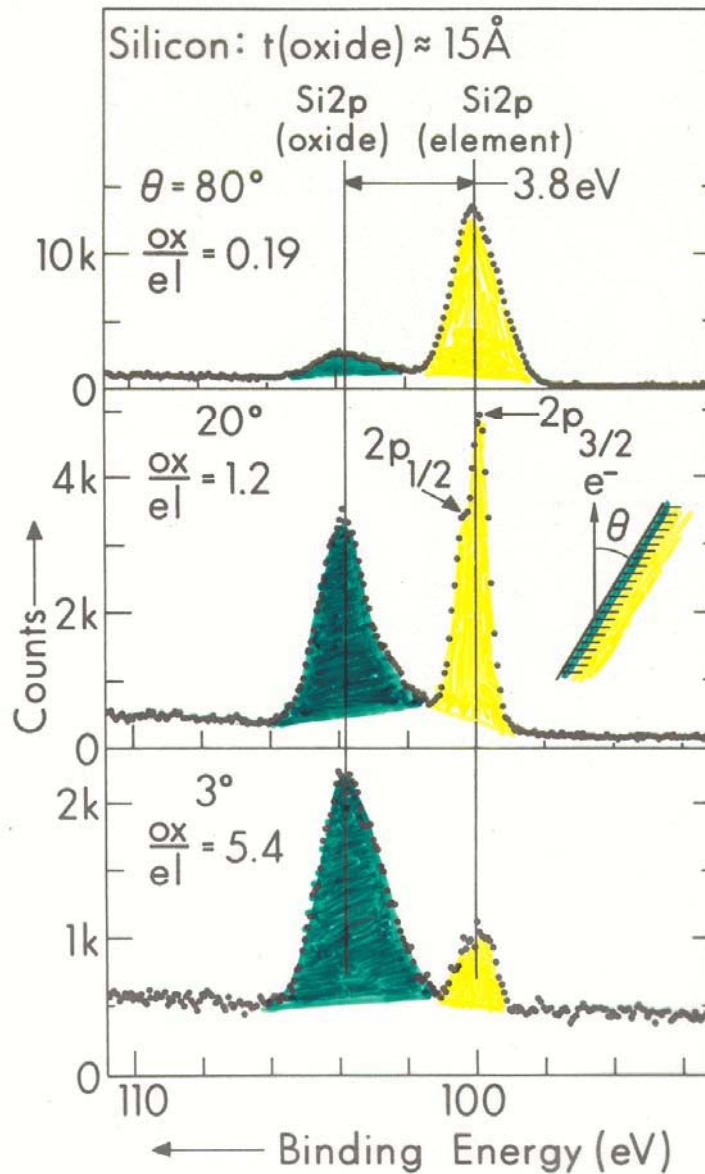


Fig. 5. Illustration of the basic mechanism producing surface sensitivity enhancement for low electron exit angles θ . The average depth for no-loss emission as measured perpendicular to the surface is $\Lambda_e \sin \theta$.

E.g. - $\Lambda_e = 28 \text{ \AA}$ in Au(s) at 1400 eV	θ	Mean Depth	No. layers
"BULK" $\rightarrow 90^\circ$		28 \AA	~ 9
"SURFACE" $\rightarrow 10^\circ$		$\sim 4.4 \text{ \AA}$	~ 1.5

... BUT REFRACTION AT SURFACE AND
ELASTIC SCATTERING CAN REDUCE
SURFACE ENHANCEMENT, ESP. AT LOW $\theta \leq 30^\circ$

Surface sensitivity enhancement for grazing exit angles



Fadley, *Progress in Surface Science*, **16**, 275 ('84)

Fig. 7. $Si2p$ spectra at three electron exit angles for a Si specimen with a 15-Å thick oxide overlayer. Note the complete reversal of the relative intensities of oxide and element between high and low θ . (From Hill et al., ref. (19).)

Surface sensitivity enhancement for grazing exit angles

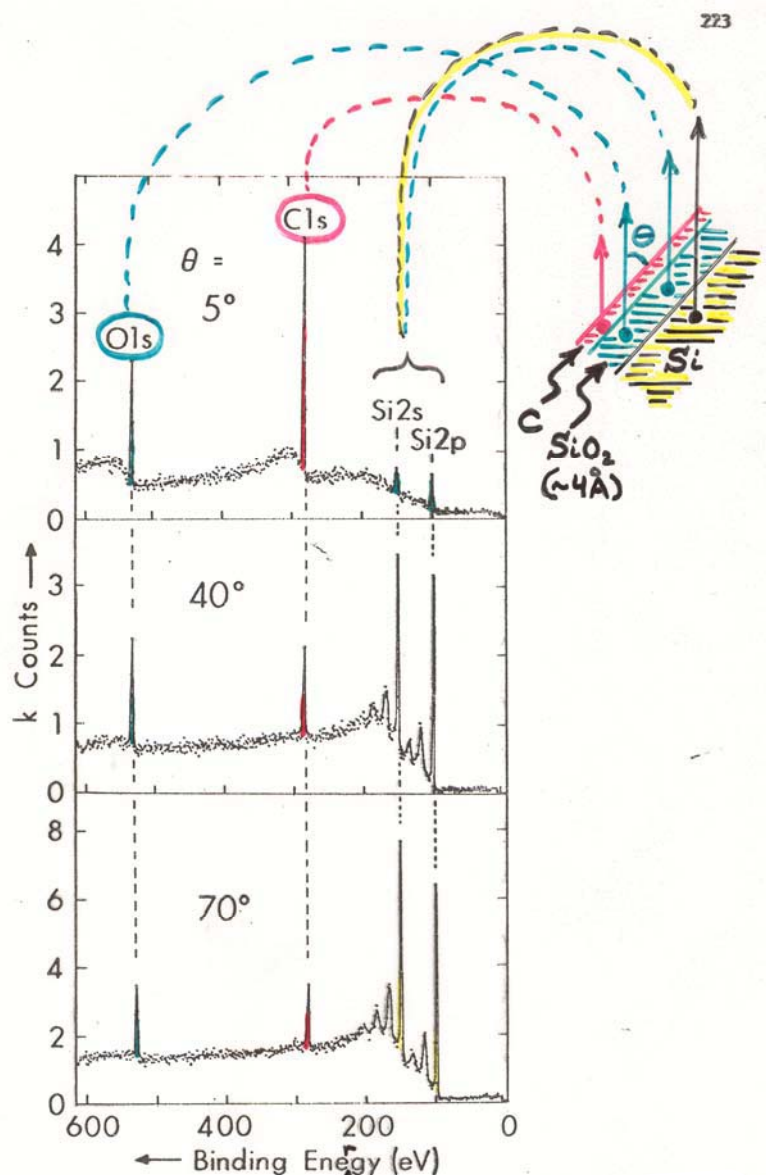
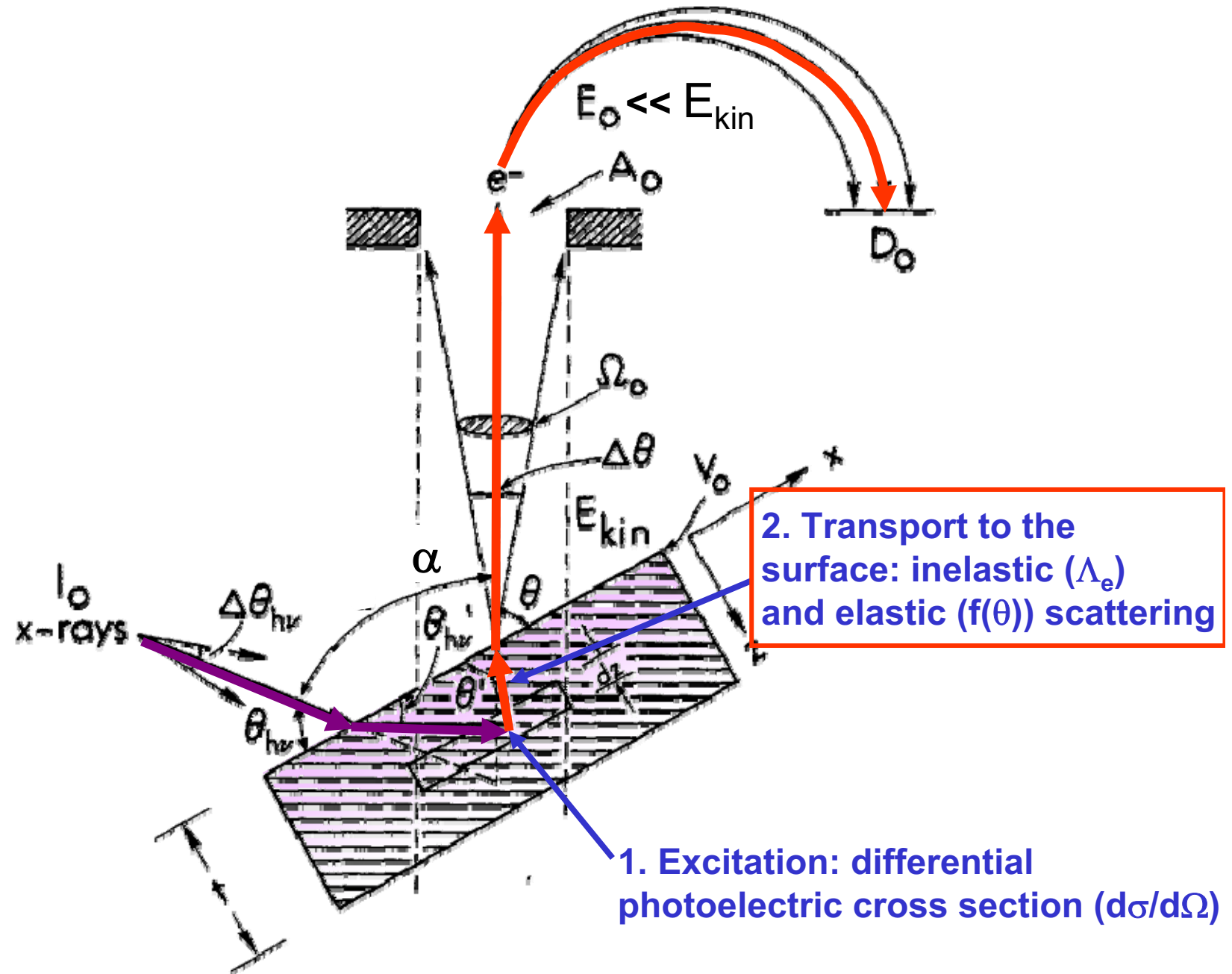


Figure 44 -- Broad-scan core spectra at low and high exit angles for a Si specimen with a thin oxide overlayer ($\sim 4\text{\AA}$) and an outermost carbon contaminant overlayer approximately 1-2 monolayers in thickness. The C1s and O1s signals are markedly enhanced in relative intensity at low θ due to the general effect presented in Figure 43. (From Endley, reference 17.)

PHOTOELECTRON INTENSITIES—THE 3-STEP MODEL



EFFECTS OF ELASTIC SCATTERING ON ANGULAR DISTRIBUTIONS: POLYCRYSTALLINE OR AMORPHOUS SAMPLE

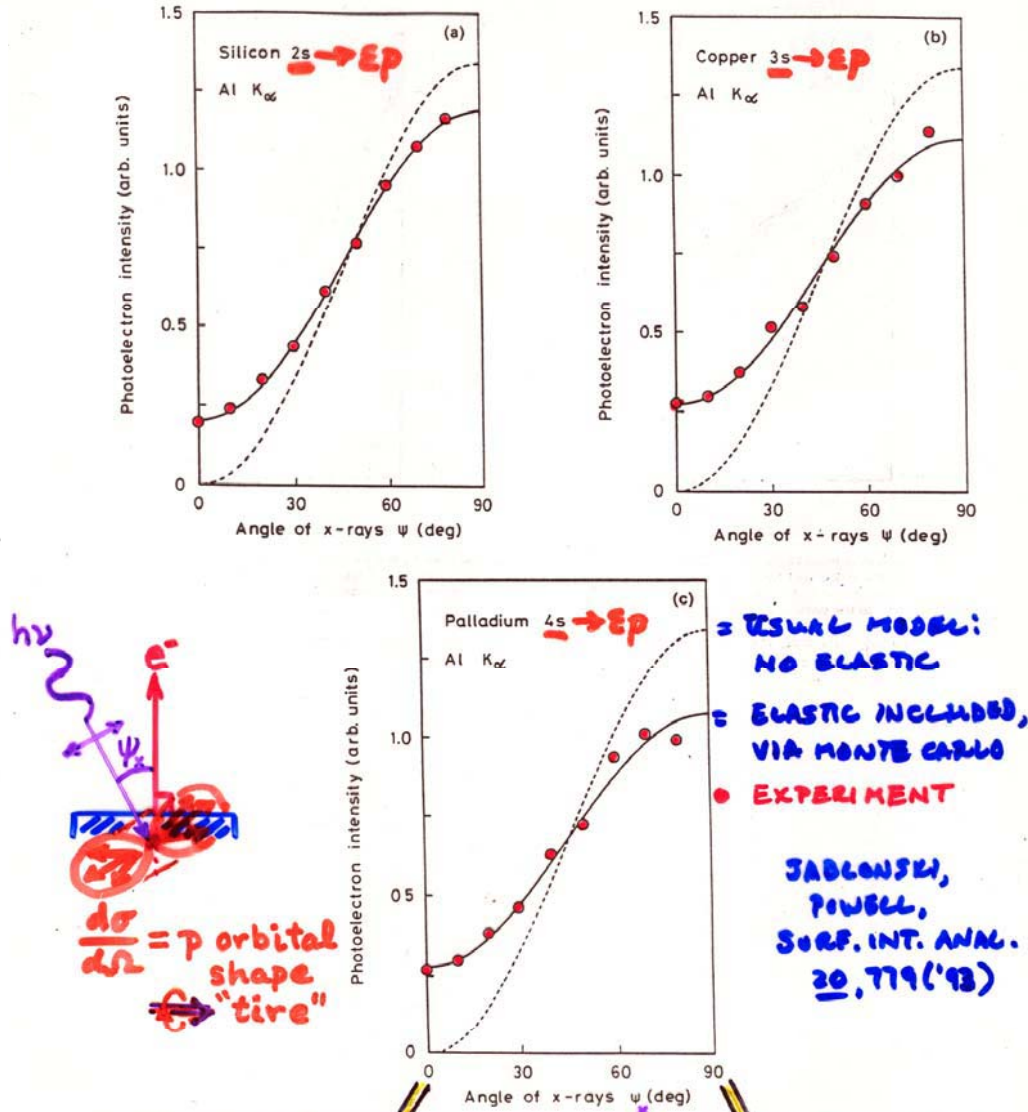
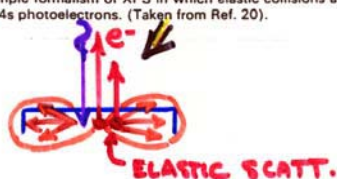
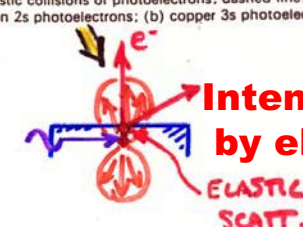


Figure 4. Dependence of the photoelectron intensity emitted normal to the surface on the angle of Al K α x-rays with respect to the direction of analysis. Circles and solid line: Monte Carlo calculations accounting for elastic collisions of photoelectrons; dashed line: result of common simple formalism of XPS in which elastic collisions are neglected. (a) Silicon 2s photoelectrons; (b) copper 3s photoelectrons; (c) palladium 4s photoelectrons. (Taken from Ref. 20).

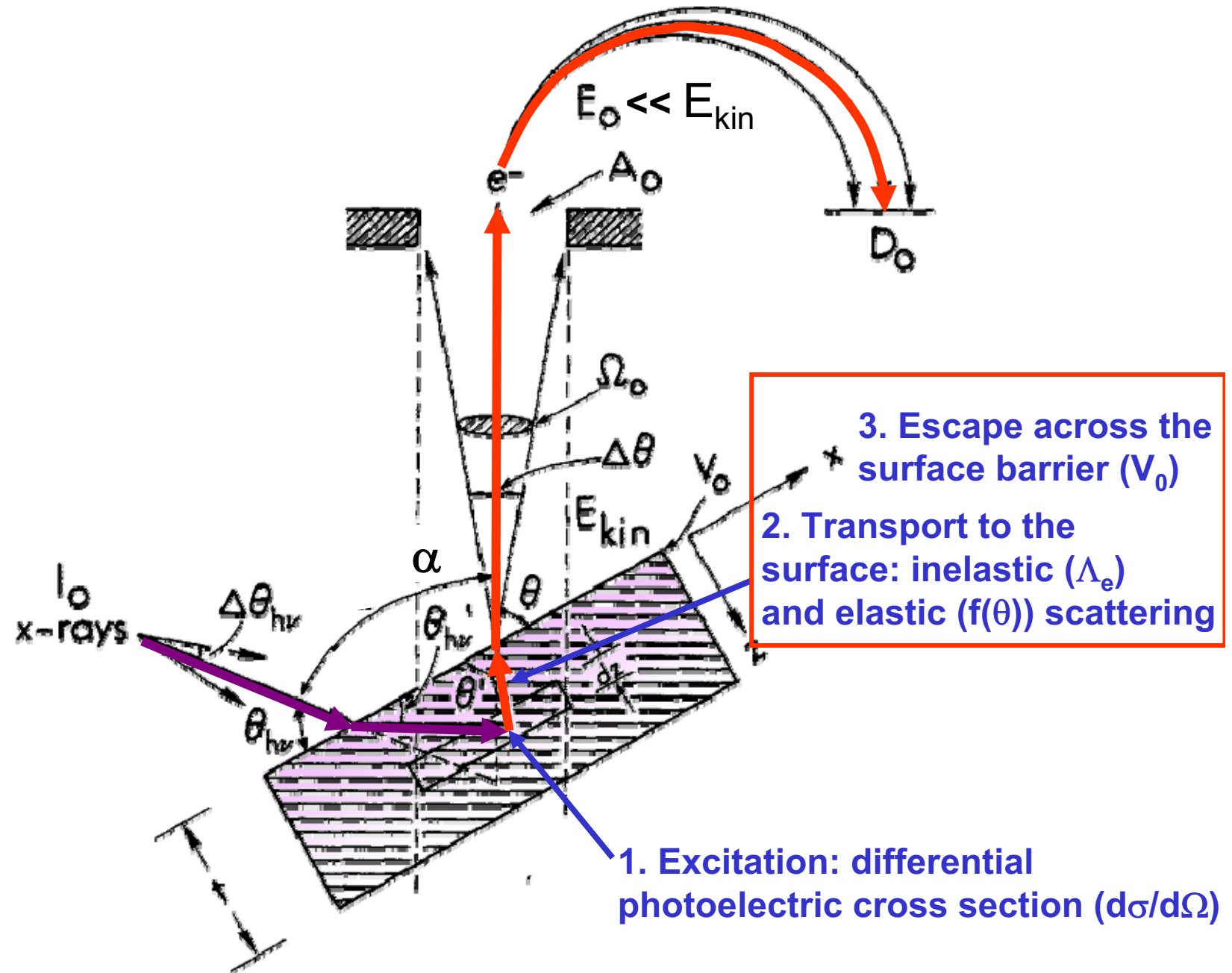
Intensity increased by elastic scattering



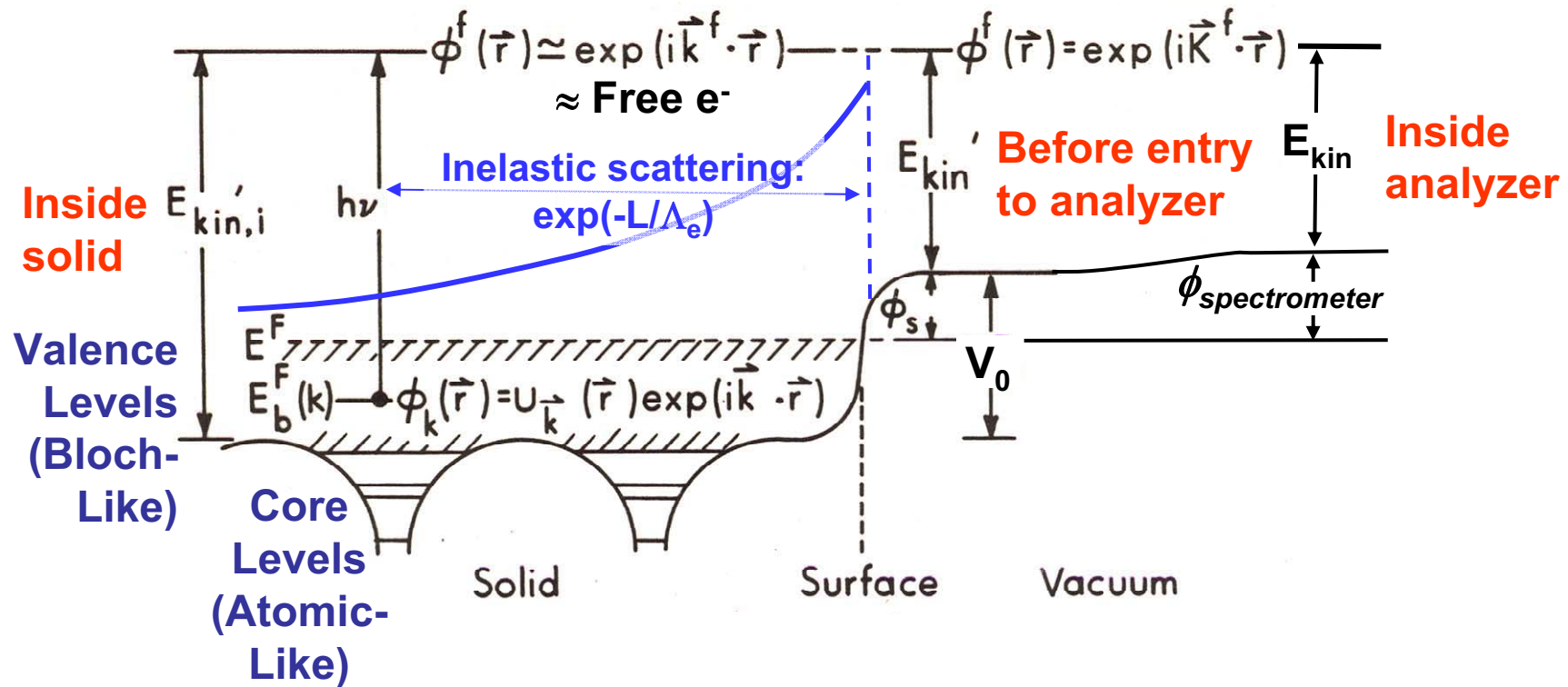
Intensity decreased by elastic scatt.



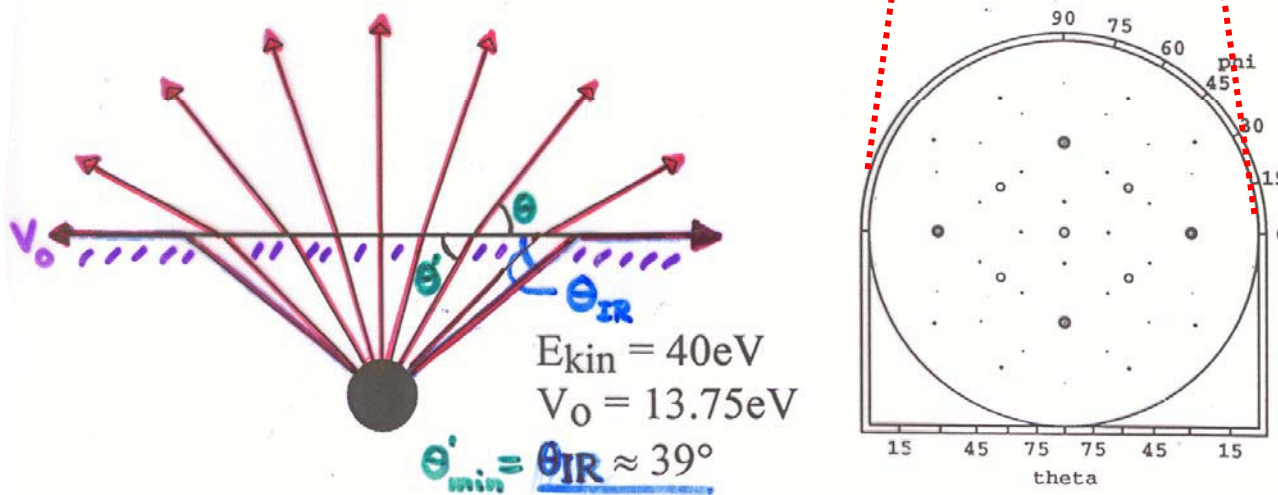
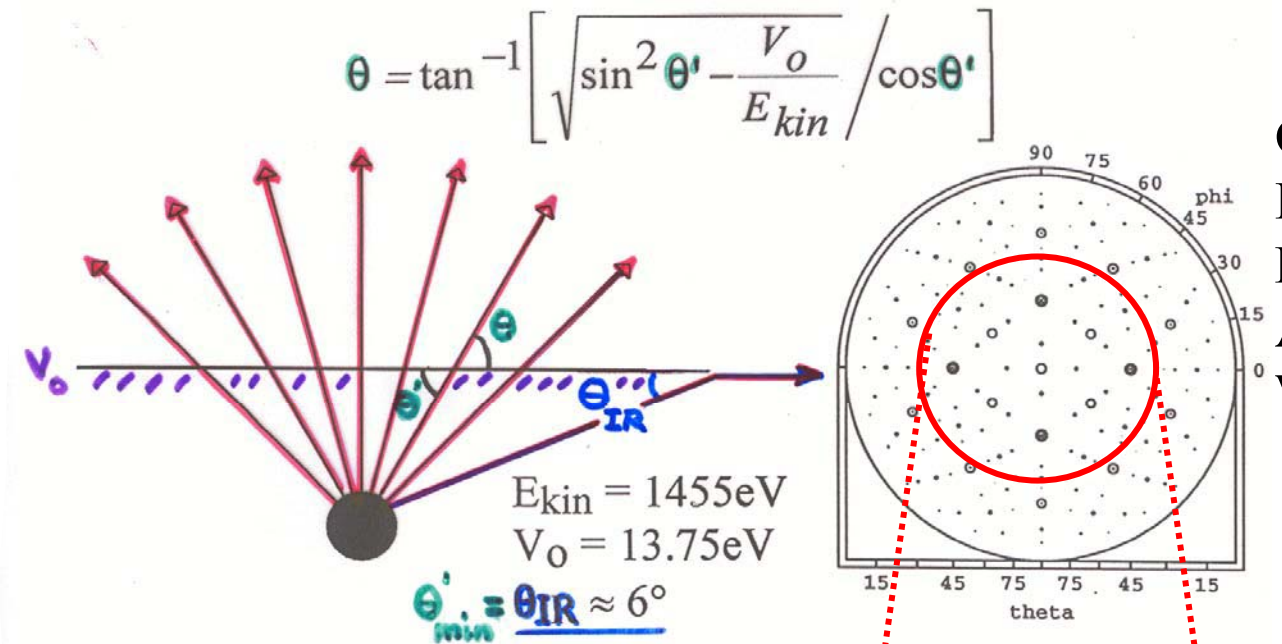
PHOTOELECTRON INTENSITIES—THE 3-STEP MODEL



One-Electron Picture of Photoemission from a Surface



Electron Refraction at the Surface Due to the Inner Potential



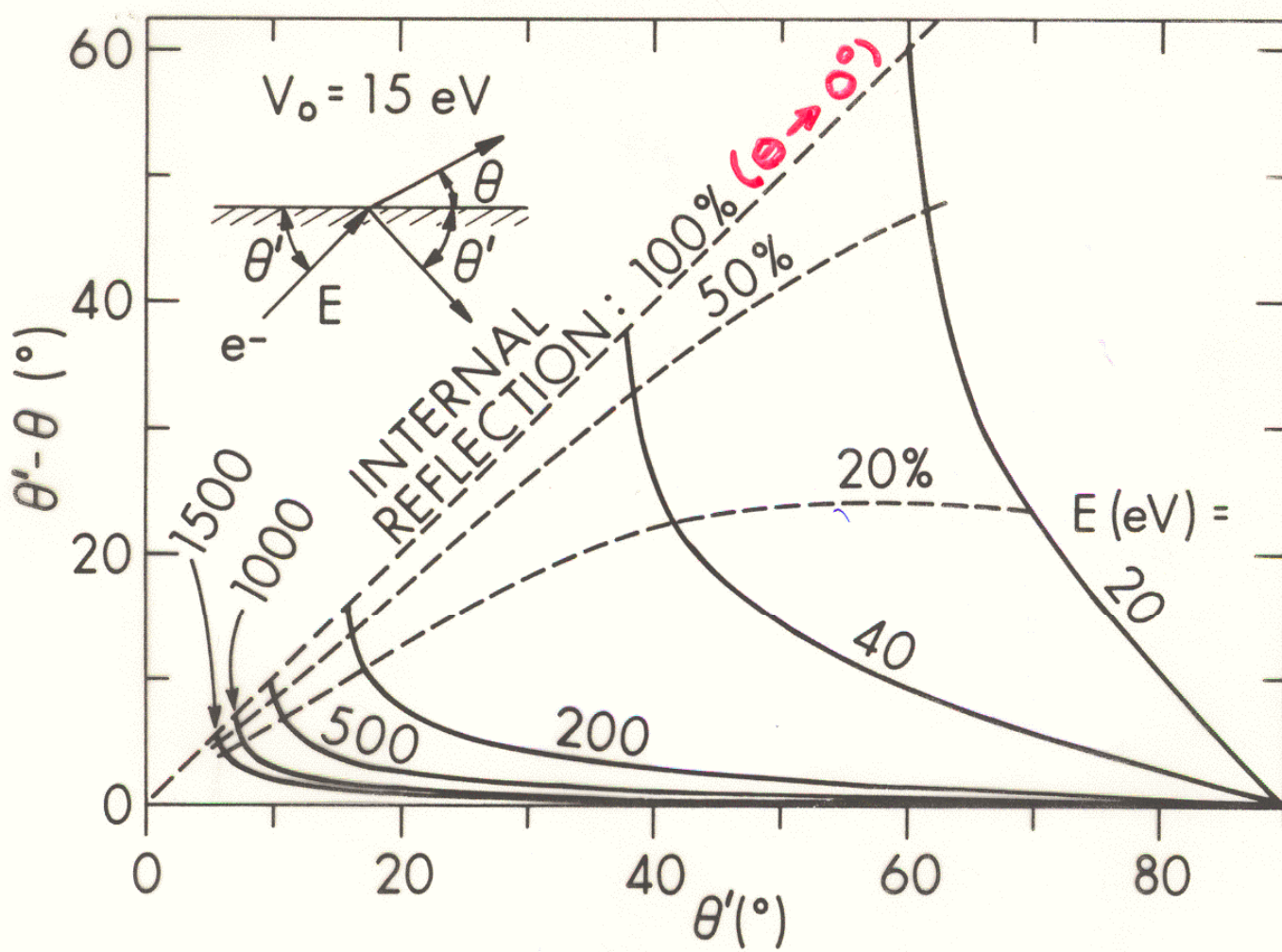


Fig. 14. Calculation of electron refraction effects for different electron kinetic energies and a typical V_0 value of 15 eV. The degree of refraction is indicated by the difference θ' (internal) - θ (external). Contours of equal probability of internal reflection are also shown. (From ref. (5).)

Varying surface sensitivity for lower electron takeoff angles

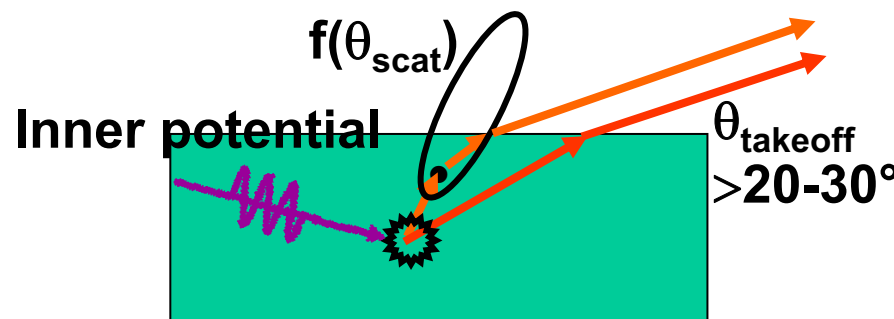
Simplest interpretation:

$$\text{Average emission depth} = \Lambda_{\text{inelastic}} \sin \theta_{\text{takeoff}}$$

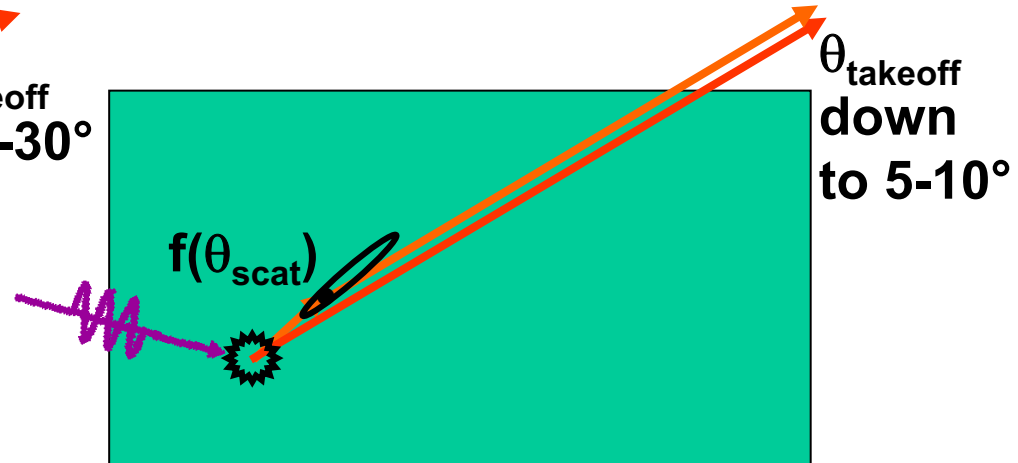
How valid?

$$E_{\text{kin}} \approx 500-1000 \text{ eV}$$

$$E_{\text{kin}} \approx 10,000 \text{ eV}$$



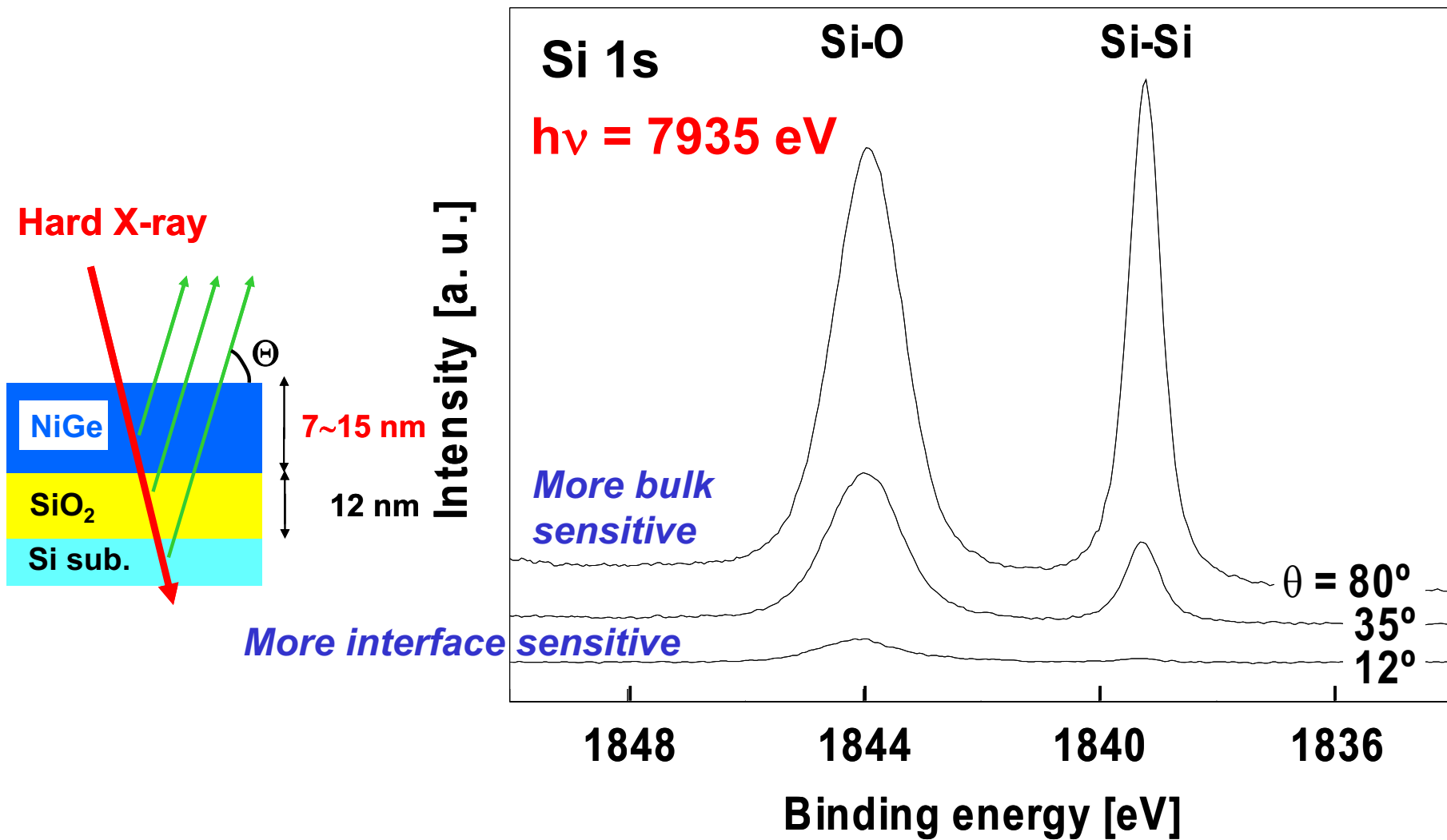
E.g.: A. Jablonski and C. J. Powell,
J. Vac. Sci. Tech. A 21, 274 (2003):
→ Mean Emission Depth (MED)
more relevant than $\Lambda_{\text{inelastic}}$



Simpler analysis
Cleaner bulk & surface distinction

C. J. Powell, W. Werner et al., priv. comm.;
C.S.F., Nucl. Inst. & Meth. A 547, 24 (2005)

Variable takeoff-angle Si 1s photoelectron spectra from NiGe(12-nm)/SiO₂(12-nm)/Si(100)



T. Hattori et al., Int. J. High Speed Electronics 16 (2006) 353
SPring8-Japan

Outline

Surface, interface, and nanoscience—short introduction

Some surface concepts and techniques→photoemission

Synchrotron radiation: experimental aspects

Electronic structure—a brief review

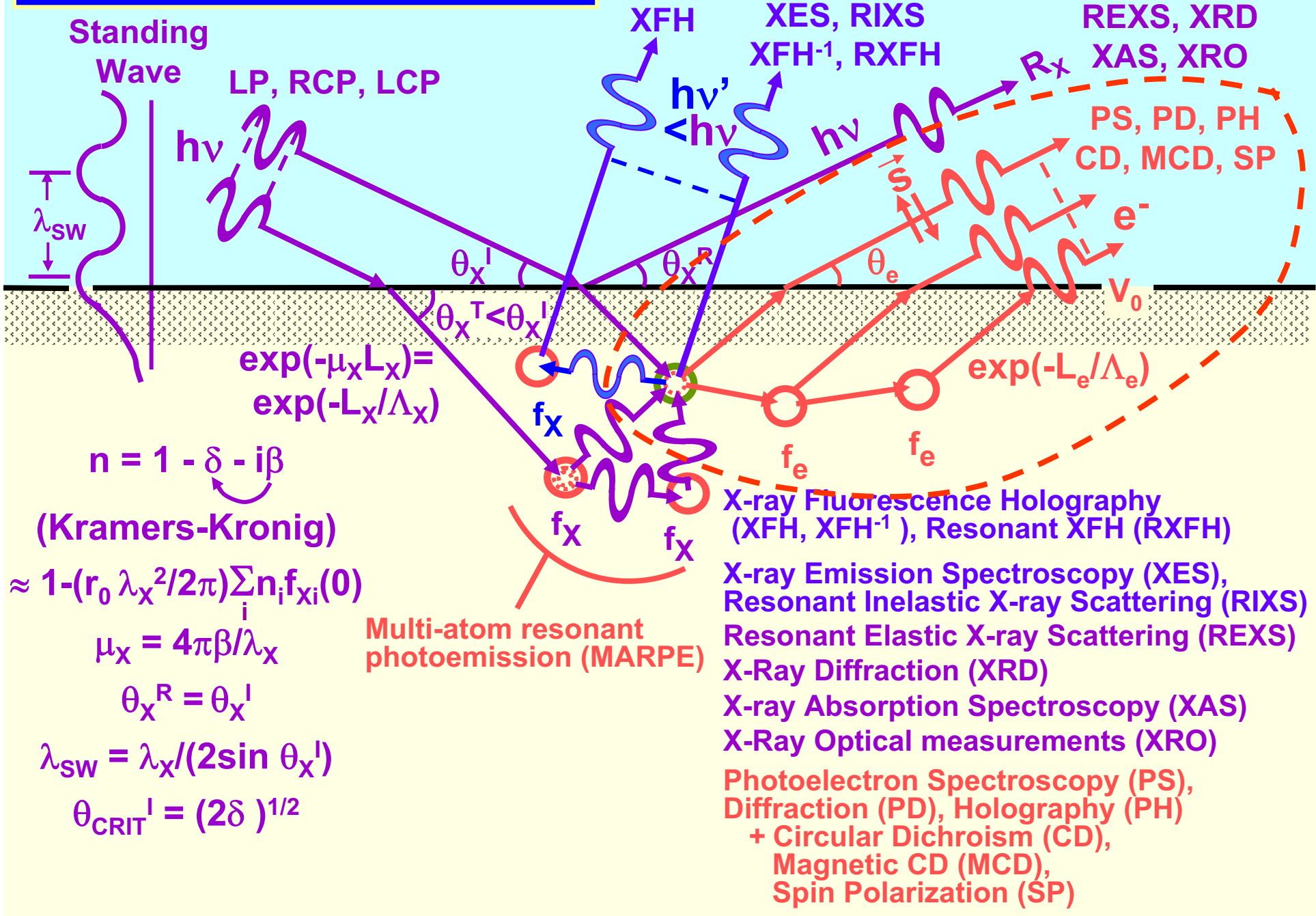
**The basic synchrotron radiation techniques:
more experimental and theoretical details**

Valence-level photoemission

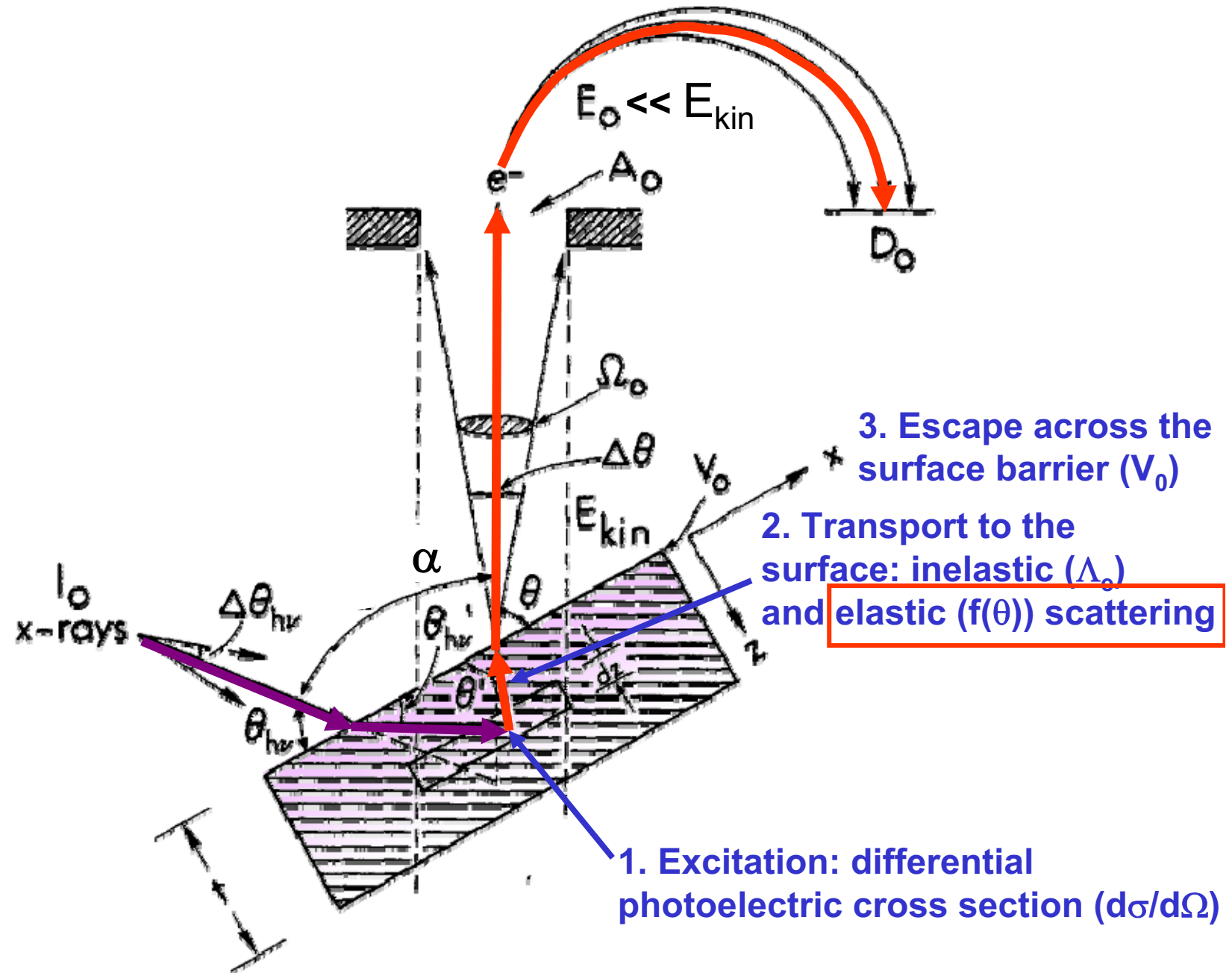
**Core-level photoemission:
photoelectron diffraction**

**Photoemission with high ambient pressure
around the sample**

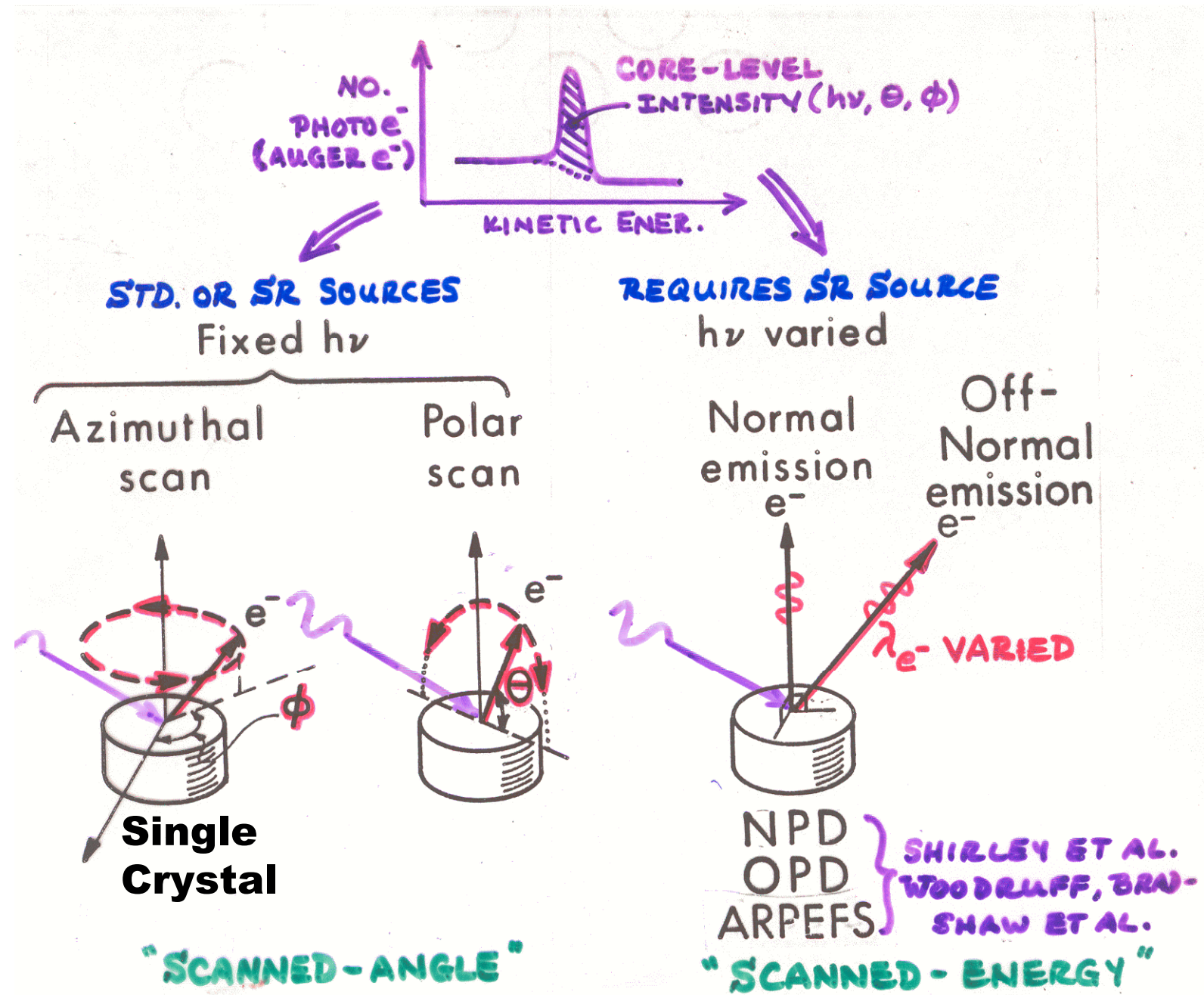
Some basic measurements:



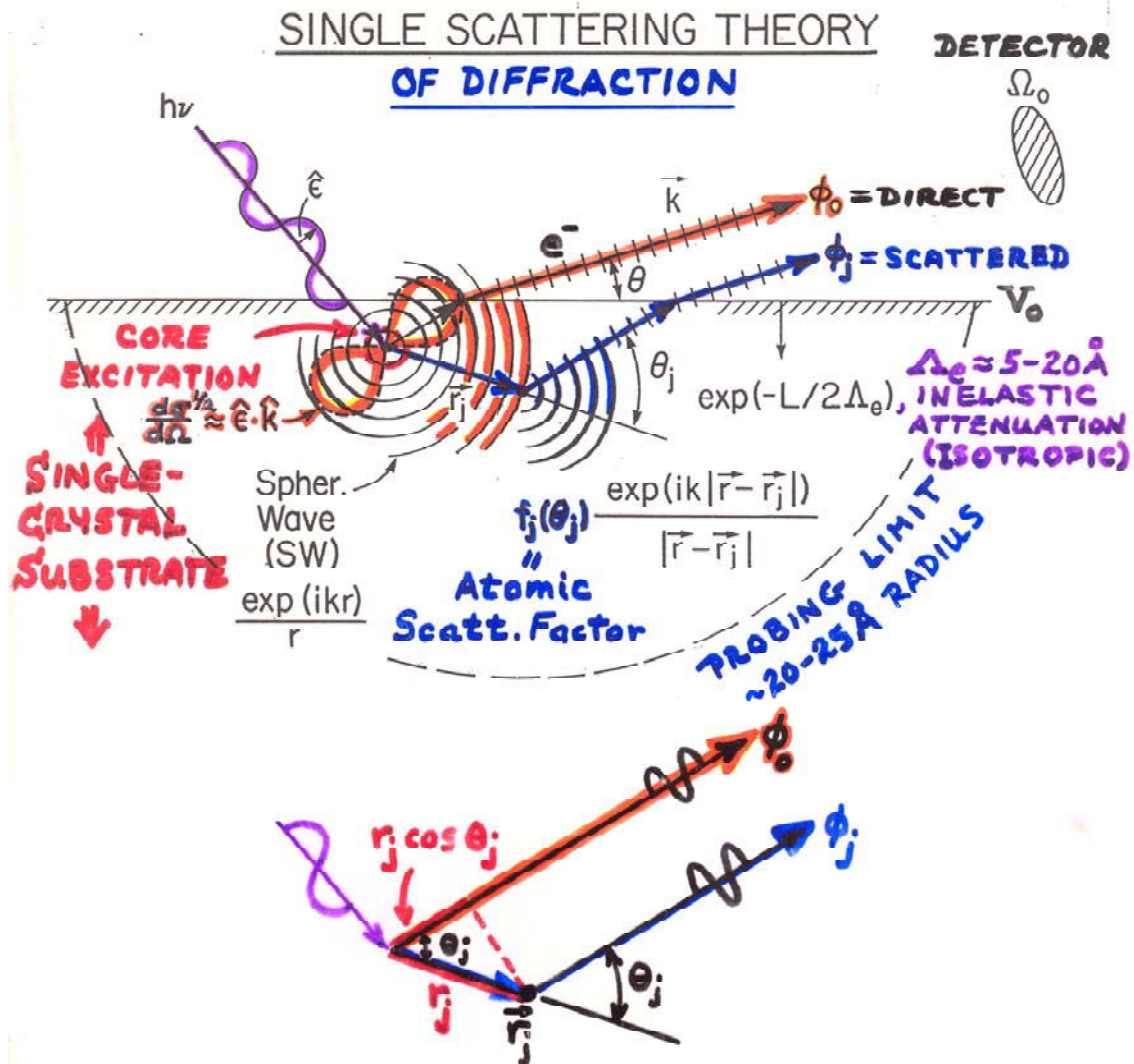
PHOTOELECTRON INTENSITIES—THE 3-STEP MODEL



PHOTOELECTRON DIFFRACTION AND HOLOGRAPHY



**EFFECTS OF
ELASTIC
SCATTERING ON
ANGULAR
DISTRIBUTIONS:
SINGLE-CRYSTAL
SAMPLE →
PHOTOELECTRON
DIFFRACTION
And
PHOTOELECTRON
HOLOGRAPHY**

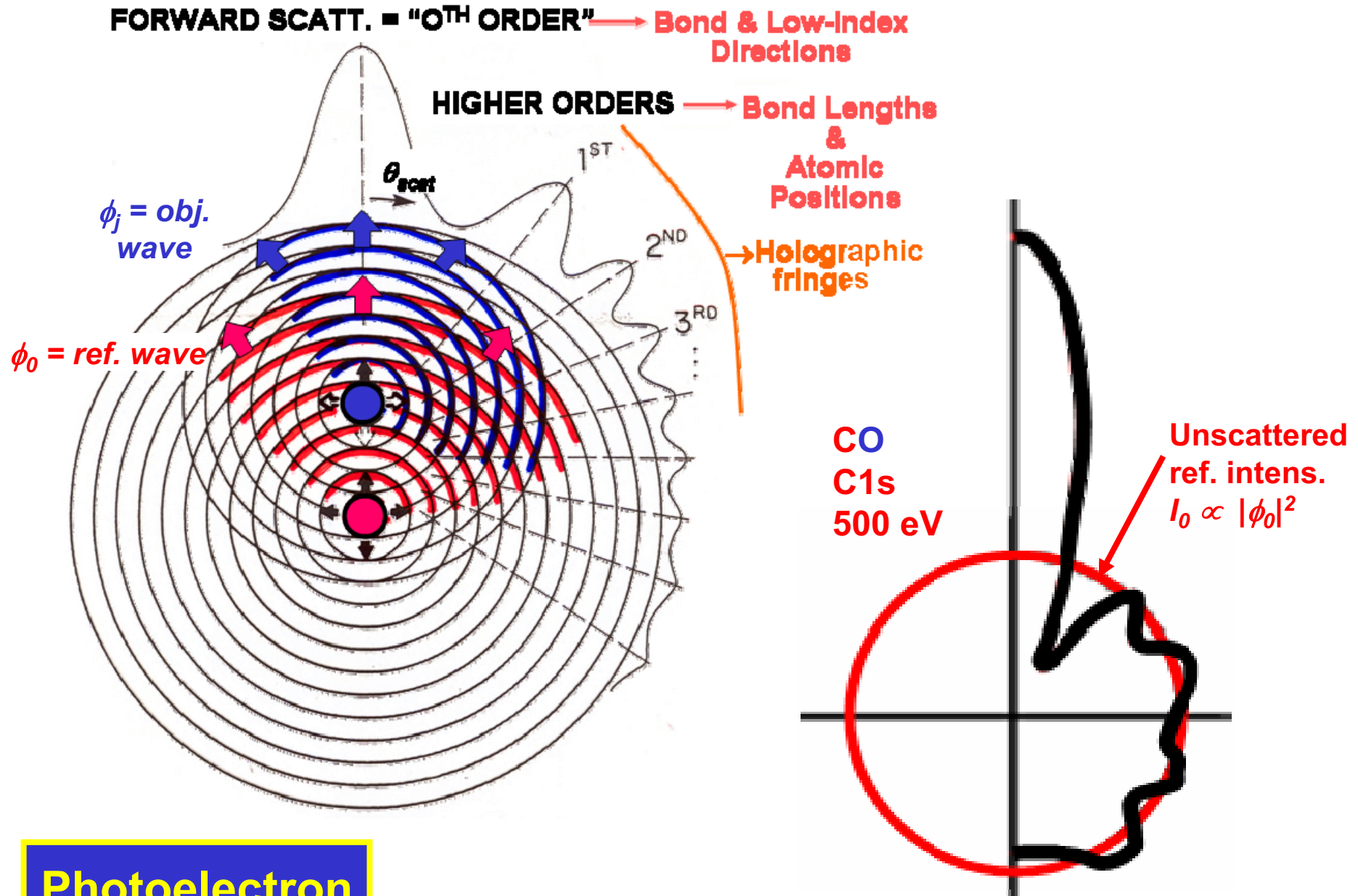


⇒ ALL BOND DISTANCE INFORMATION IN:

$$\text{PATH LENGTH DIFFERENCE} = r_j(1 - \cos \theta_j)$$

$$\therefore \text{PHASE DIFFERENCE} = kr_j(1 - \cos \theta_j) \\ = kr_j - \vec{k} \cdot \vec{r}_j$$

Paper 3
“Study of Surface
Structures...”
Figure 3



Photoelectron
Diffraction

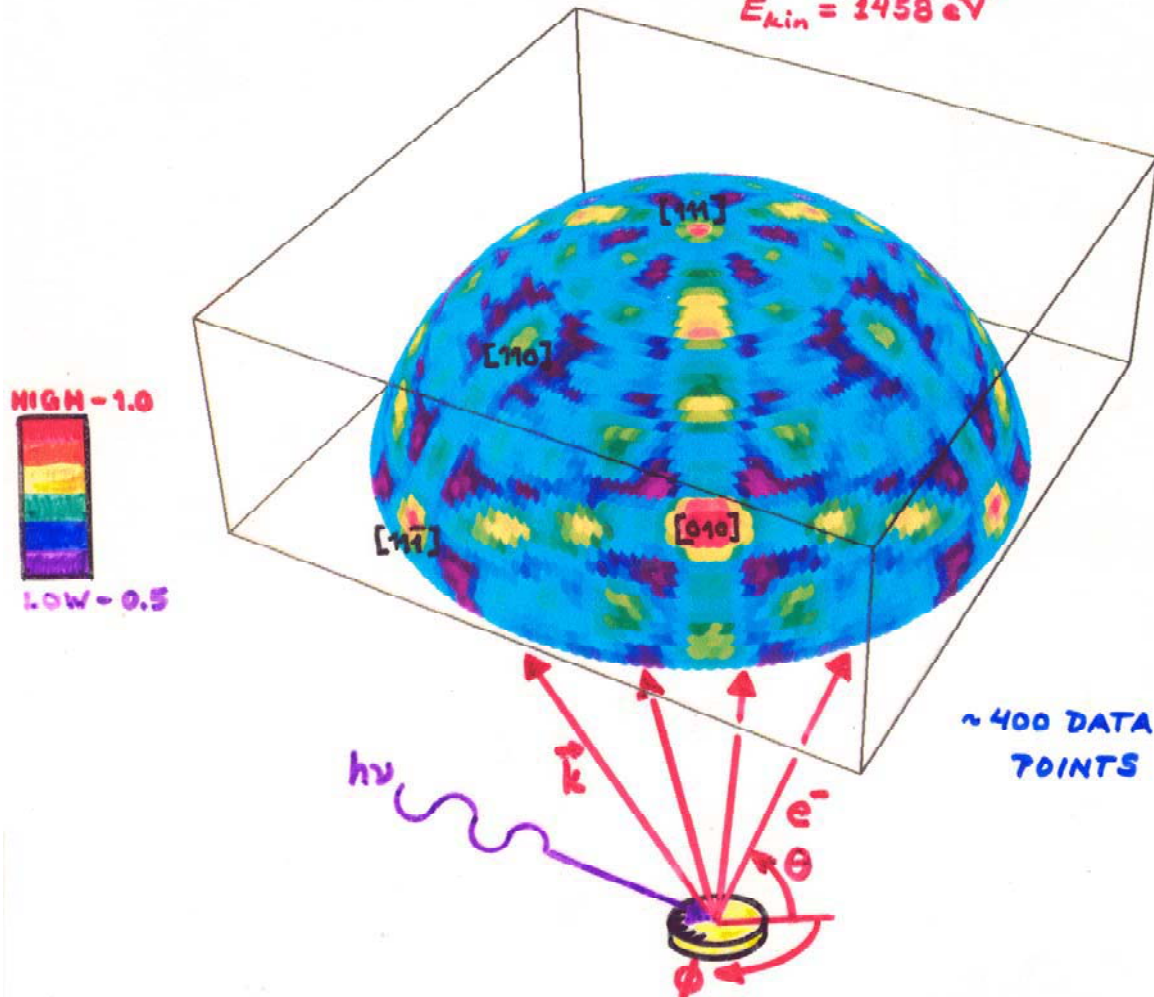
EDAC program: Javier Garcia de Abajo
<http://maxwell.optica.csic.es/software/edac/index.html>

SCANNED-ANGLE PHOTOELECTRON DIFFRACTION

Example:

Ge(111) - Ge3d Photoelectron Hologram

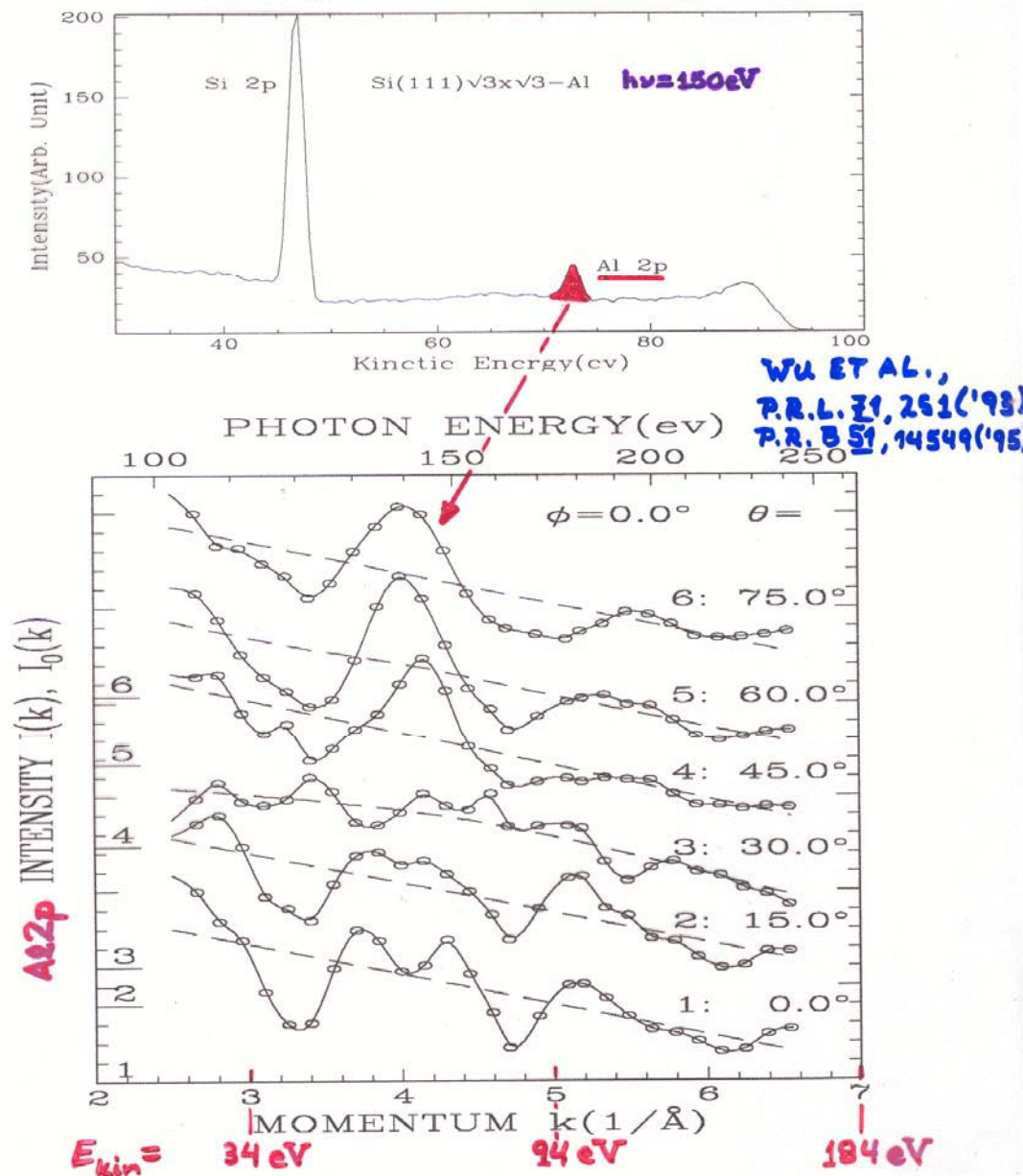
$E_{kin} = 1458 \text{ eV}$



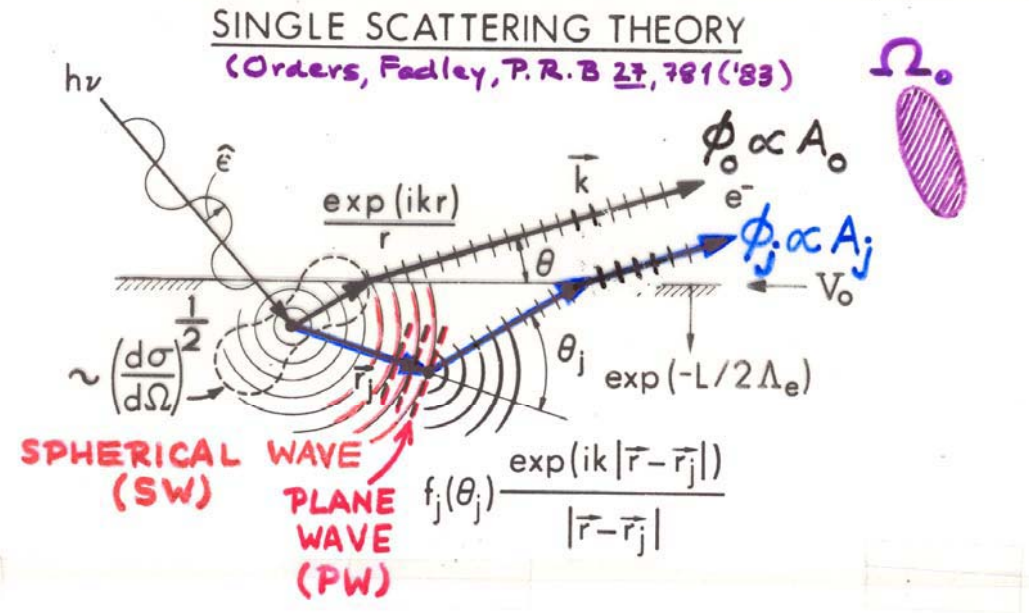
TRAN ET AL.,
SURF. SCI. 281,
270 ('93) +
BUDGE, YNZUNZA

SCANNED-ENERGY PHOTOELECTRON DIFF.
 $(\sqrt{3} \times \sqrt{3})$ Al on Si(111)

* 41 diffraction curves χ taken from Al 2p } ~1100 DATA POINTS
 * $\theta = 0 \sim 70^\circ, \varphi = 0 \sim 60^\circ$



Photoelectron diffraction: Simple single-scattering theory for s-subshell emission



$$\chi(E \text{ or } \vec{k}) \propto \sum_j \frac{F_j(k)}{F_0} \cos \left[kr_j (1 - \cos \theta_j) + \Psi_j(\theta_j, k) \right]$$

Ω
(CLUSTER)
PATH LENGTH
DIFFERENCE
(P.L.D.)
SCATTERING
PHASE SHIFT

$$F_j(k) = (\hat{\epsilon} \cdot \hat{r}_j) \frac{|f_j(\theta_j, k)|}{r_j} W_j(\theta_j, k) \exp(-L_j/2\Lambda_e)$$

ELASTIC e⁻-ATOM SCATTERING
DEBYE-WALLER
INELASTIC e⁻-e⁻ SCATTERING

= amplitude of scattered wave

$$F_0 = (\hat{\epsilon} \cdot \hat{k}) \exp(-L_0/2\Lambda_e)$$

= amplitude of direct wave

“Study of Surface Structures...”

Figure 3

FROM SINGLE-SCATTERING THEORY:

(E.G., P.R.B 22, 6085 ('80); P.R.B 27, 781 ('83))

$$I(\vec{k}) \propto \left| \phi_0 + \sum_j \phi_j \right|^2, \quad \sum_j \text{ ON FINITE CLUSTER},$$

$$\propto |\phi_0|^2 + \sum_j (\phi_0^* \phi_j + \phi_0 \phi_j^*) + \sum_j \sum_{j'} \phi_j^* \phi_{j'}$$

IF $\phi_j \phi_j^*$ SMALL W.R.T $\phi_0^* \phi_j + \phi_0 \phi_j^*$, A NECESSARY CONDITION FOR SIMPLE HOLOGRAPHY:

$$I(\vec{k}) \propto F_0^2 + 2F_0 \sum_j |F_j(\theta_j)| \cos [kr_j(1 - \cos \theta_j) + \Psi_j(\theta_j, k)]$$

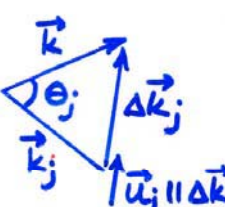
PATH LENGTH SCATTERING
DIFFERENCE PHASE

$$X(\vec{k}) = \frac{I(\vec{k}) - I_0}{I_0^{1/2}} \propto \left\{ \sum_j |F_j(\theta_j)| \cos [kr_j(1 - \cos \theta_j) + \Psi_j(\theta_j, k)] \right\}$$

WITH: $F_0 = (\hat{\epsilon} \cdot \hat{k}) \exp(-L_0/2\Delta_e)$
 $= \text{amplitude of direct wave} = I_0^{1/2}$

$$|F_j(\theta_j)| = (\hat{\epsilon} \cdot \hat{r}_j) \frac{|f_j(\theta_j)|}{r_j} W_j(\theta_j) \exp(-L_j/2\Delta_e)$$

\hat{k}



$$W_j = \exp(-\Delta k_j^2 \bar{u}_j^2)$$

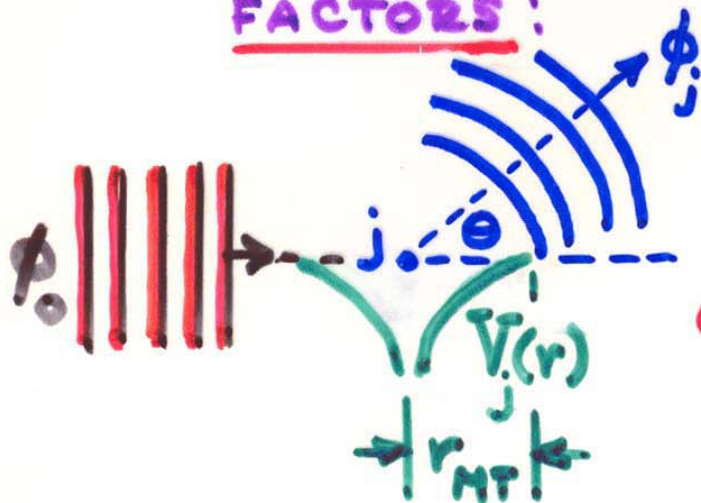
$$= \exp(-2k^2(1 - \cos \theta_j) \bar{u}_j^2)$$

LIKE EXAFS/SEXAFS, BUT THERE:

- ADD CENTRAL ATOM PHASE SHIFT δ_i
- $\Psi_j \Rightarrow \pi$ FOR ALL SCATTERERS
- $\cos \Rightarrow \sin$ IN ANGLE INTEGRATION
- $\hat{\epsilon} \cdot \hat{r}_j / r_j \Rightarrow \hat{\epsilon} \cdot \hat{r}_j / r_j^2$ IN OUT/BACK PATHS

CALCULATION OF e⁻-ATOM SCATTERING

FACTORS :



PLANE-WAVE SCATTERING:

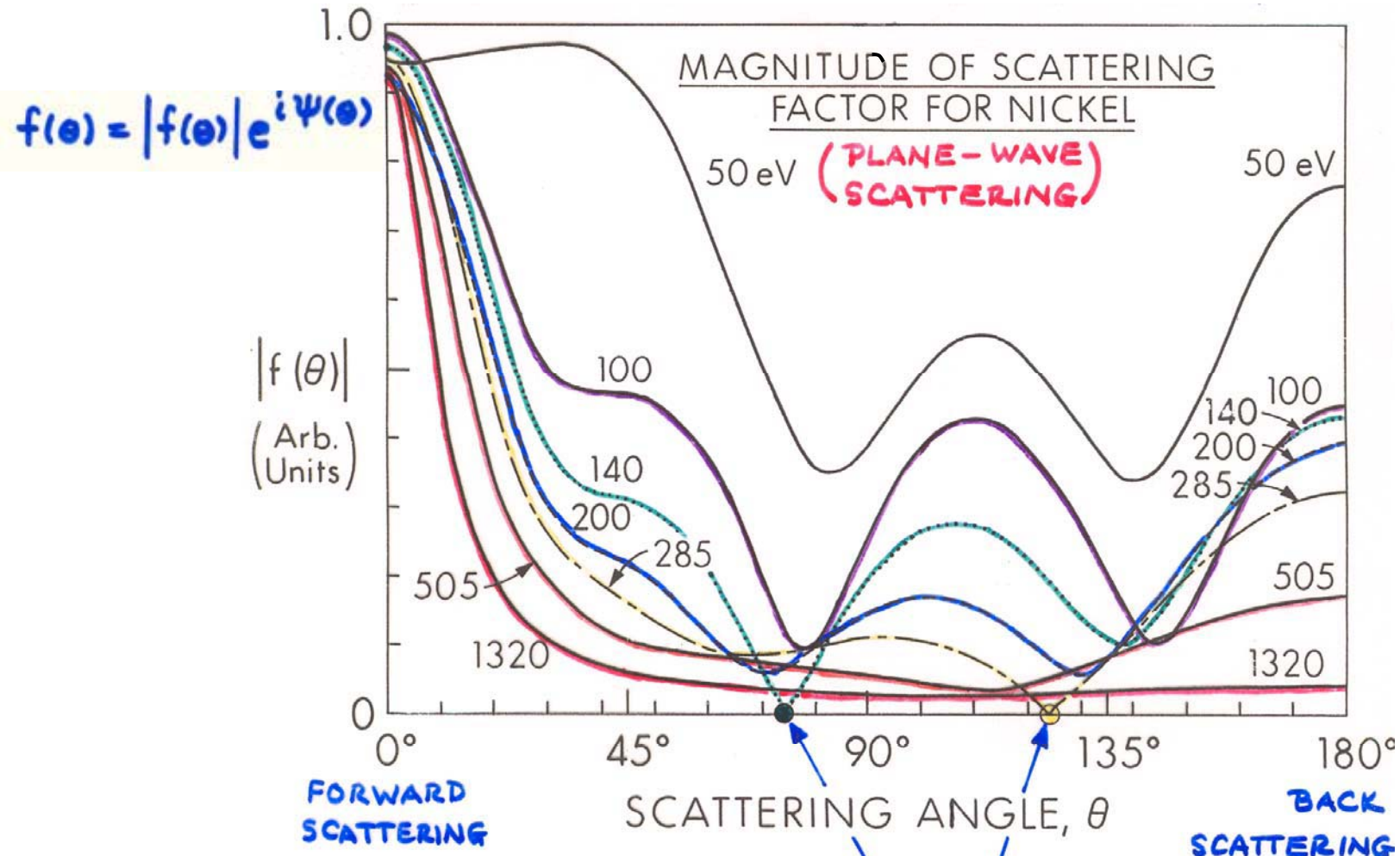
PARTIAL-WAVE METHOD⁺

• $f_j(\theta) = \frac{1}{k} \sum_{l=0}^{l_{\max}} (2l+1) e^{i\delta_l} \sin \delta_l P_l(\cos \theta)$

$$l_{\max} \approx kr_{MT}$$

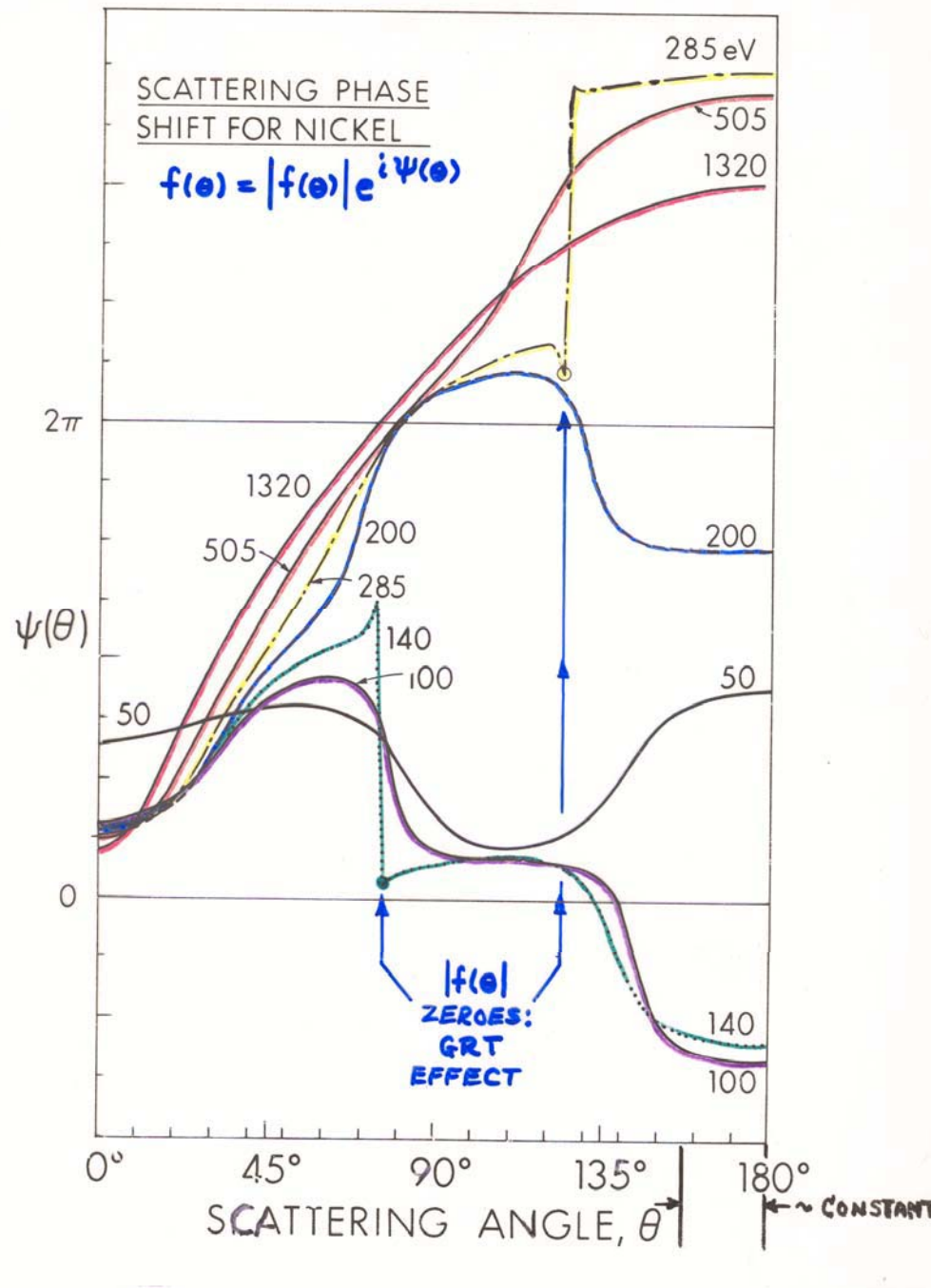
+ ANY TEXTBOOK ON SCATTERING

ENERGY DEPENDENCE OF ELECTRON ELASTIC SCATTERING

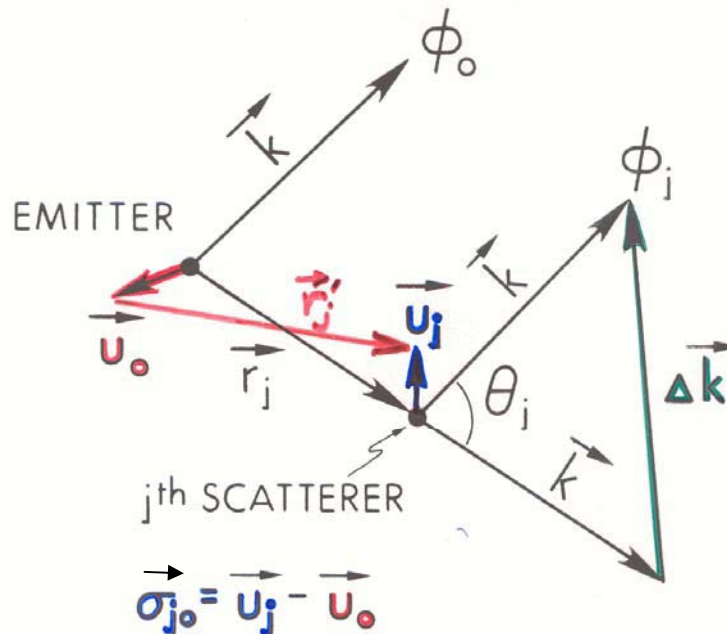


"Study of Surface Structures..."
Figure 2

ENERGY DEPENDENCE OF ELECTRON ELASTIC SCATTERING



Vibrational effects on diffraction



- DW FACTOR = $e^{-\frac{1}{2}(\Delta \vec{k} \cdot \vec{\sigma}_{jo})^2} = e^{-\frac{1}{2} \Delta k^2 \sigma_{jo,||}^2}$

- \vec{U}_j, \vec{U}_o UNCORRELATED:

$$DW = e^{-\frac{1}{2}(\Delta \vec{k} \cdot \vec{u}_j)^2} e^{-\frac{1}{2}(\Delta \vec{k} \cdot \vec{u}_o)^2}$$

- $\vec{U}_j \approx \vec{U}_o$ IN DISTRIBUTION:

$$DW = e^{-\frac{1}{2}(\Delta \vec{k} \cdot \vec{u}_j)^2}$$

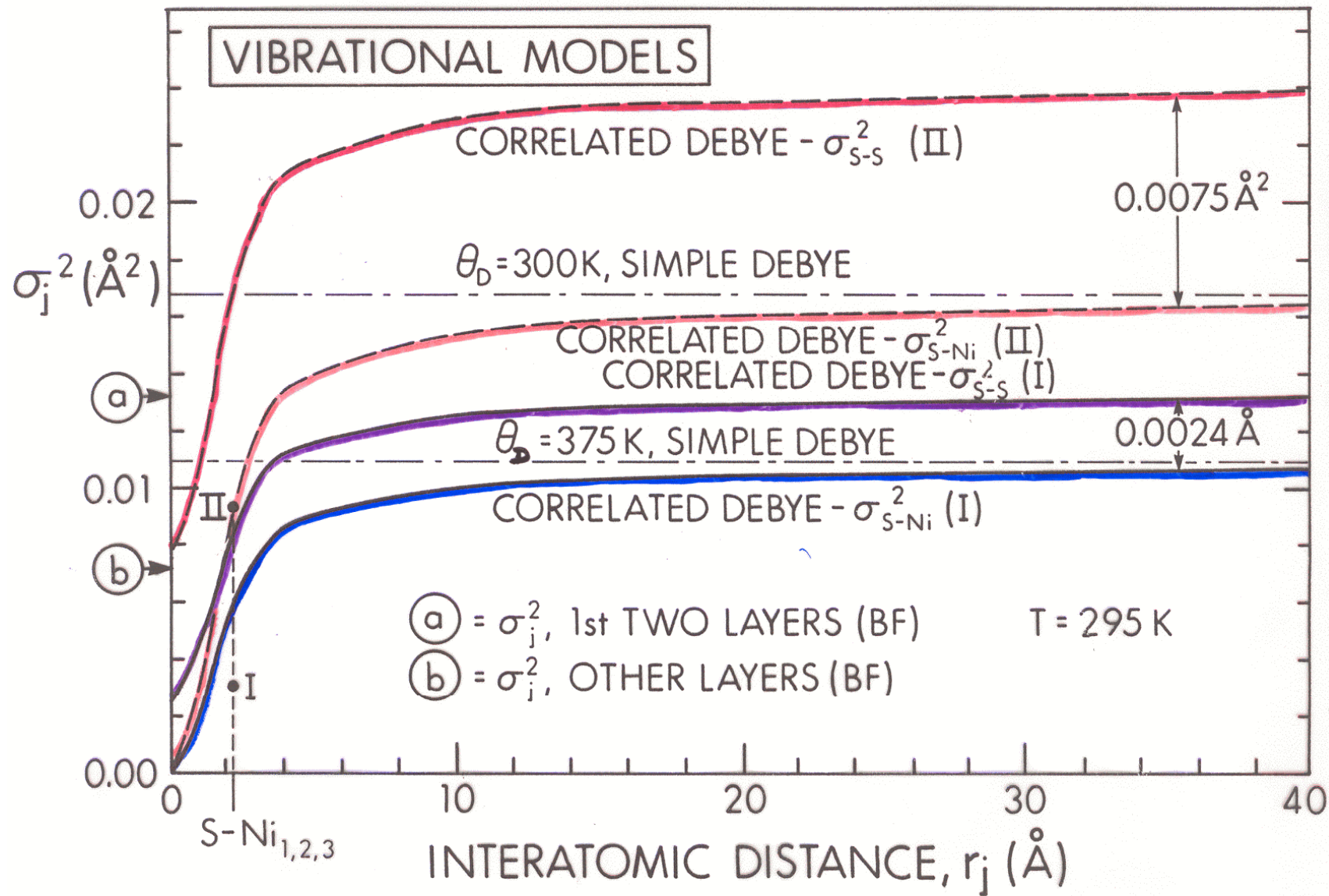
- \vec{U}_j ISOTROPIC:

$$DW = e^{-\Delta k^2 \overline{u_j^2}} = e^{-2k^2(1-\cos\theta_j) \overline{u_j^2}}$$

← USUAL LEVEL

DECREASING
ACCURACY

↓ CORRE-
LATED?



[SAGURTON, BULLOCK, FADLEY, SURF. SCI.
182, 287 (1987)]

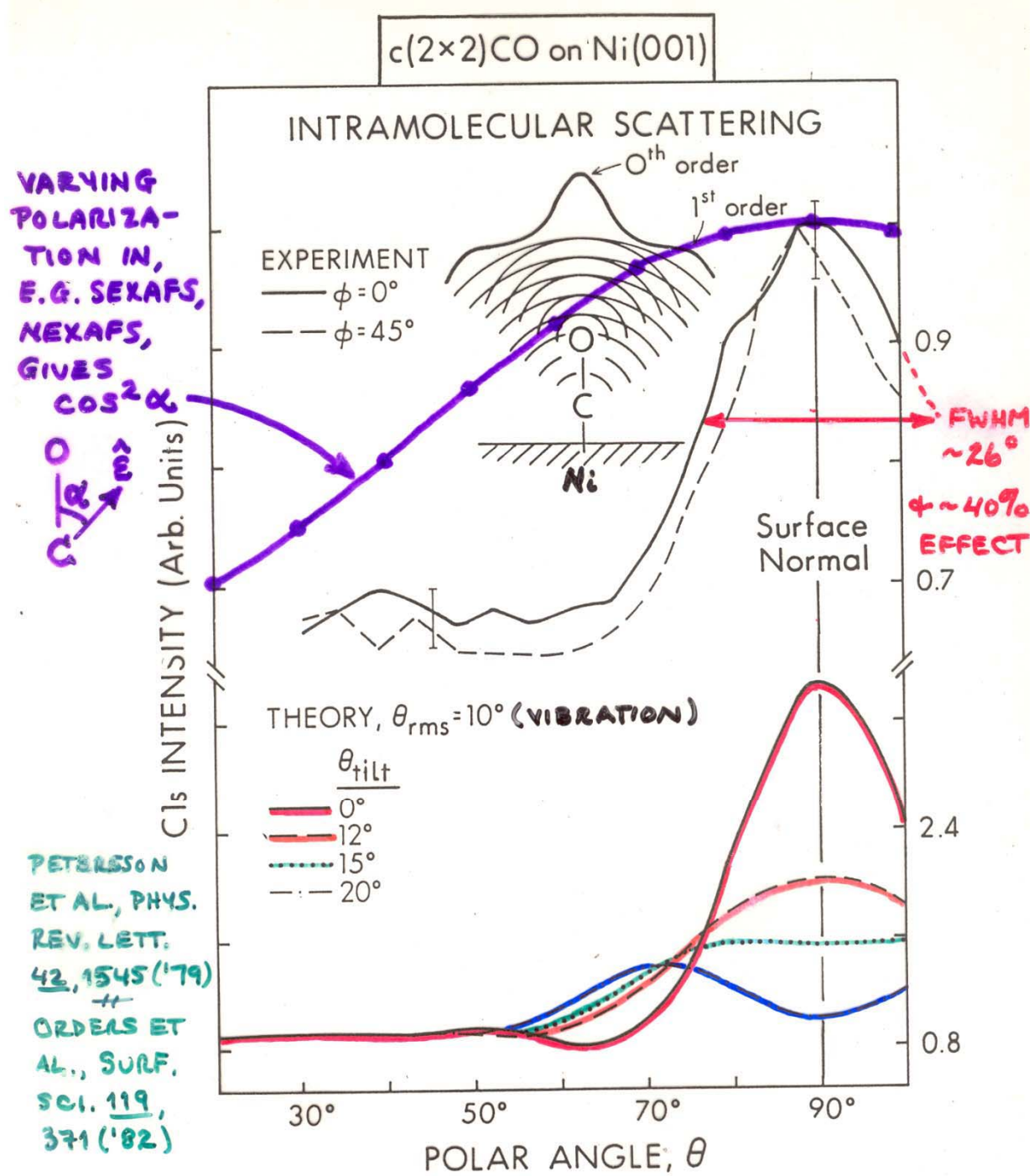
Table 1 Debye temperature and thermal conductivity^a

Li	Be													B	C	N	O	F	Ne
344	1440													2230				75	
0.85	2.00													0.27	1.29				
Na	Mg													Al	Si	P	S	Cl	Ar
158	400	Low temperature limit of θ , in Kelvin												428	645			92	
1.41	1.56	Thermal conductivity at 300 K, in $\text{W cm}^{-1}\text{K}^{-1}$												2.37	1.48				
K	Ca	Sc	Ti	V	Cr	Mn	Fe	Co	Ni	Cu	Zn	Ga	Ge	As	Se	Br	Kr		
91	230	360.	420	380	630	410	470	445	450	343	327	320	374	282	90		72		
1.02		0.16	0.22	0.31	0.94	0.08	0.80	1.00	0.91	4.01	1.16	0.41	0.60	0.50	0.02				
Rb	Sr	Y	Zr	Nb	Mo	Tc	Ru	Rh	Pd	Ag	Cd	In	Sn _w	Sb	Te	I	Xe		
56	147	280	291	275	450		600	480	274	225	209	108	200	211	153		64		
0.58		0.17	0.23	0.54	1.38	0.51	1.17	1.50	0.72	4.29	0.97	0.82	0.67	0.24	0.02				
Cs	Ba	La β	Hf	Ta	W	Re	Os	Ir	Pt	Au	Hg	Tl	Pb	Bi	Po	At	Rn		
38	110	142	252	240	400	430	500	420	240	165	71.9	78.5	105	119					
0.36		0.14	0.23	0.58	1.74	0.48	0.88	1.47	0.72	3.17		0.46	0.35	0.08					
Fr	Ra	Ac	Ce	Pr	Nd	Pm	Sm	Eu	Gd	Tb	Dy	Ho	Er	Tm	Yb	Lu			
									200		210				120	210			
			0.11	0.12	0.16		0.13		0.11	0.11	0.11	0.16	0.14	0.17	0.35	0.16			
			Th	Pa	U	Np	Pu	Am	Cm	Bk	Cf	Es	Fm	Md	No	Lr			
			163		207		0.06	0.07											
			0.54		0.28														

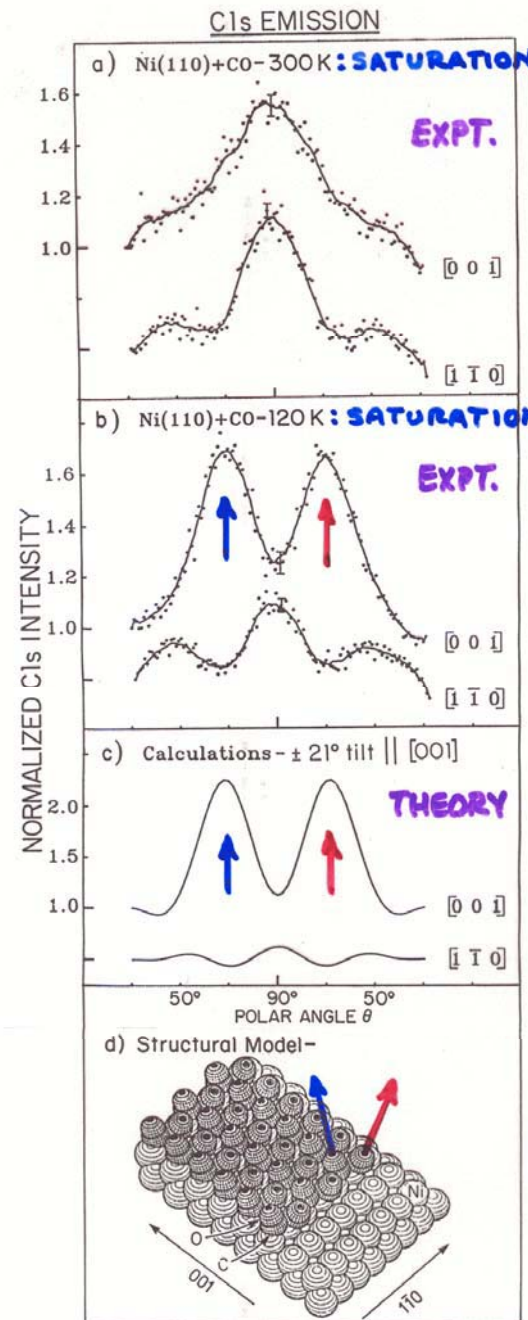
^a Most of the θ values were supplied by N. Pearlman; references are given in the A.I.P. Handbook, 3rd ed; the thermal conductivity values are from R. W. Powell and Y. S. Touloukian, Science 181, 999 (1973).

**Case study:
Determining
the orientation of
an adsorbed
molecule from
photoelectron
diffraction at about
1 keV energy**

Paper 3
“Study of Surface Structures...”
Figure 8

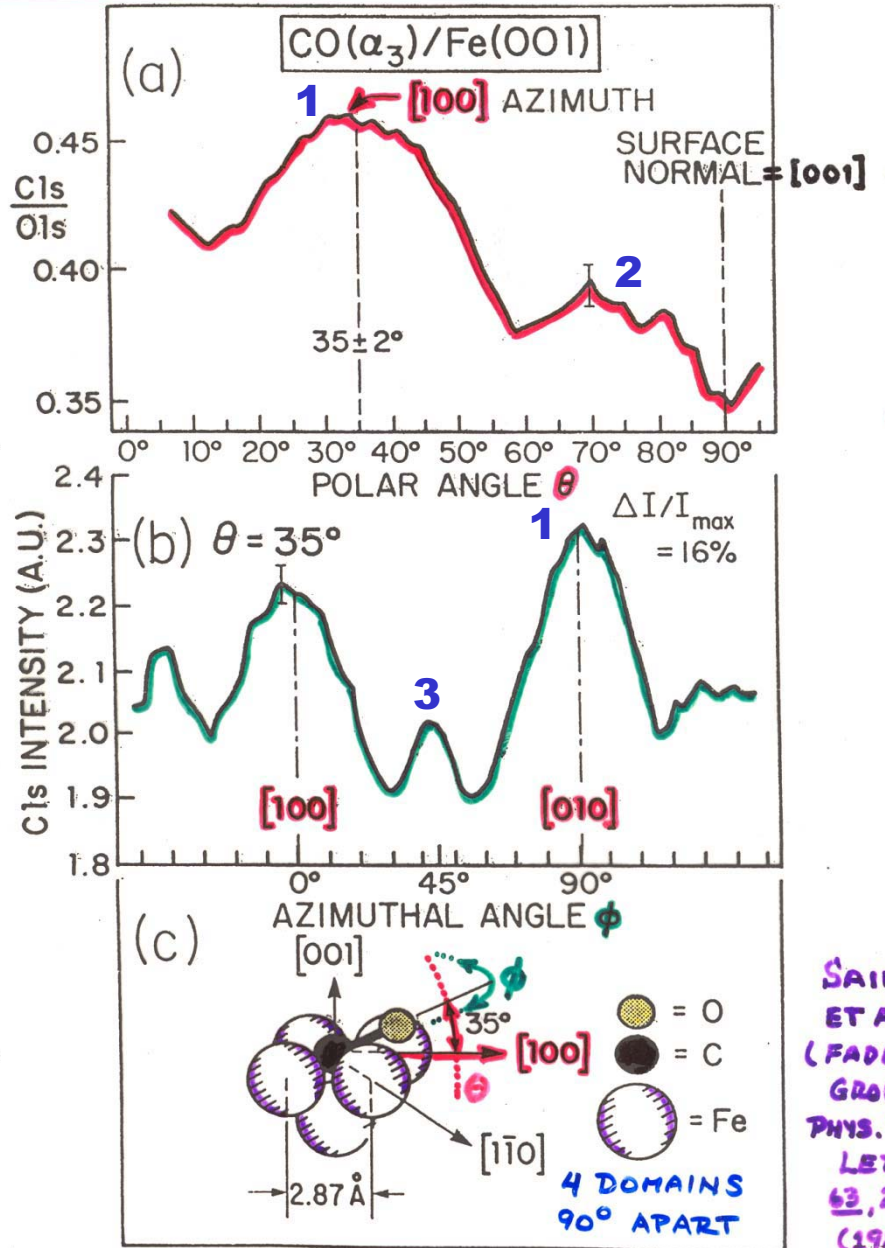


TEMPERATURE-
DEPENDENT
ADSORBATE
ORIENTATION



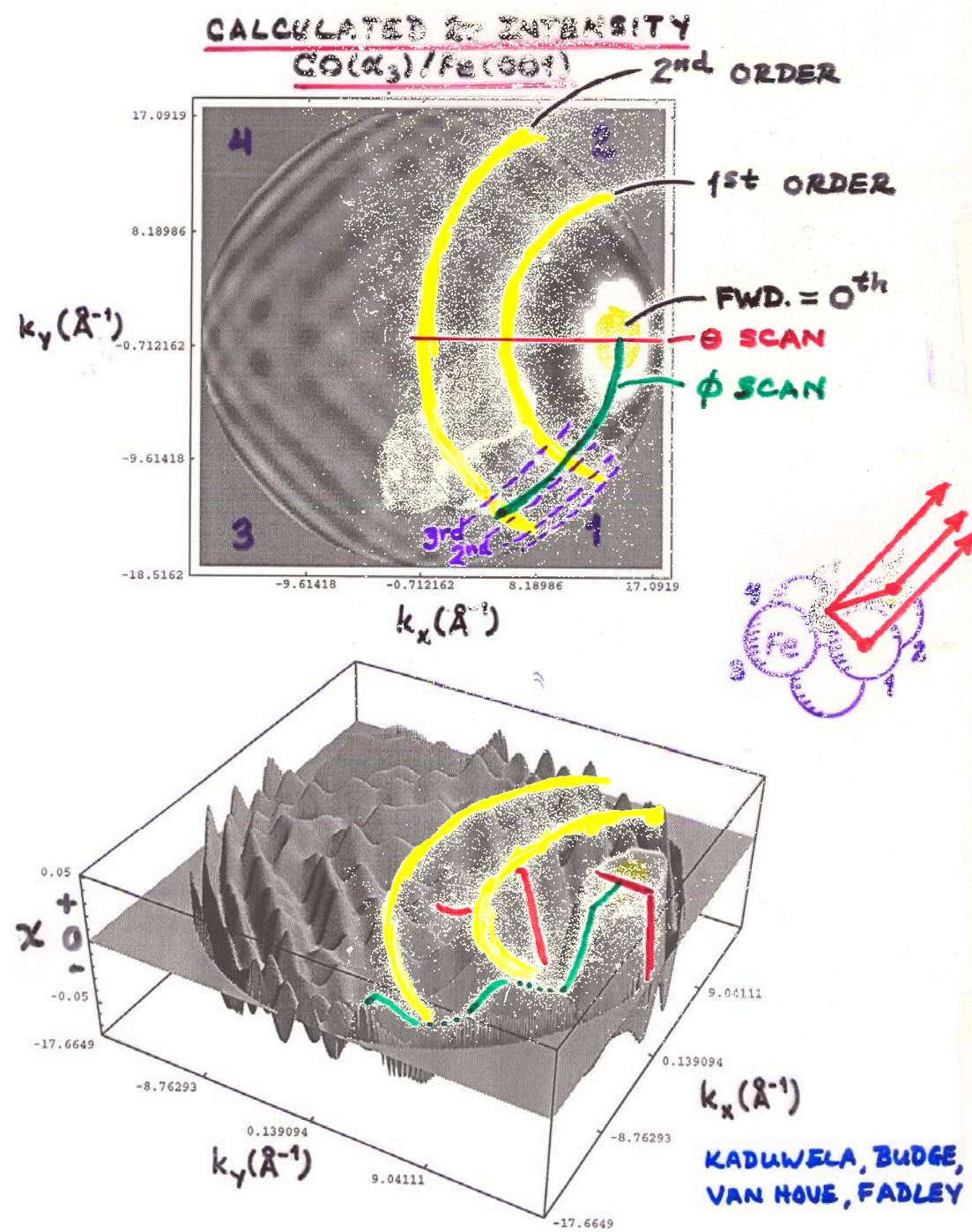
Paper 3
“Study of Surface Structures...”
Figure 12

ORIENTATION OF A HIGHLY TILTED MOLEC. ON SURFACE



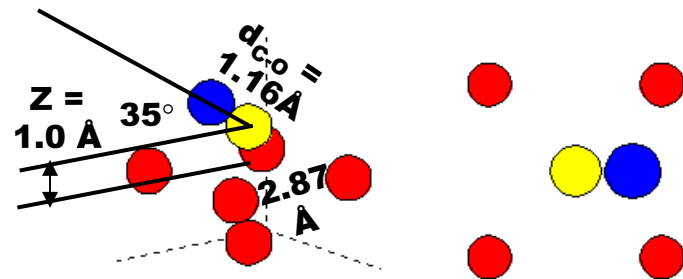
SAIKI
ET AL.
(FADLEY
GROUP)
PHYS. REV.
LETT.
63, 283
(1984)

Paper 3
“Study of Surface Structures...”
Figure 9

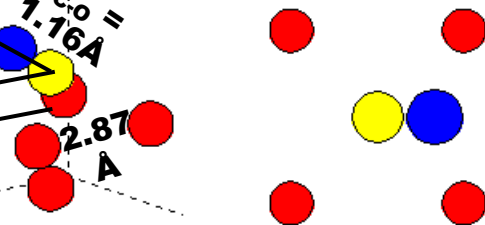


Online calculation of photoelectron diffraction patterns:

7 atoms:



Left: representation of the cluster rocking around a line parallel to the z direction and passing by the emitter (yellow atom). The dashed lines stand for the xyz axes. **Right:** top view of the cluster, where the x/y direction (not plotted) runs along the horizontal/vertical screen direction. Different atomic species have been assigned the colors **O**, **Fe**.



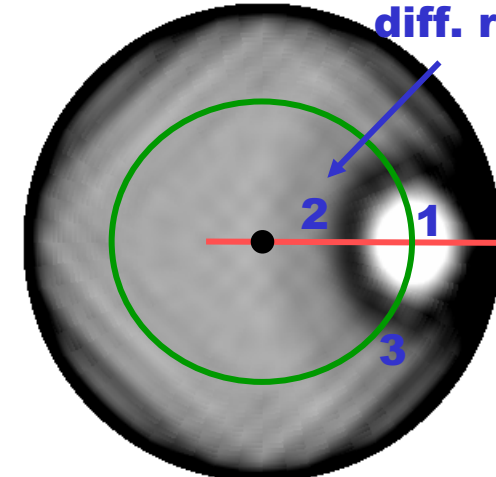
EDAC output for CO/Fe(001)

Click on the figure to download data.

<http://csic.sw.ehu.es/jga/software/edac/a.html>



**Oxygen
1st order
diff. ring**



Polar scan of photoemission intensity (logarithmic scale). White/black regions correspond to high/low intensity. The orientation is the same as in the top-view of the cluster. The distance to the center of the figure is proportional to the polar angle θ . The polar angle range is (0.0, 89.0) (in degrees).

Parameters used in the calculation:

$N=7$ atoms

Iteration order=4

$l_{\max}=25$

$V_0=10.5$ eV

Photoelectron energy=1202 eV

p-polarized light

$z_0=1.435$ Å

Recursion iteration method

**X 4 domains
rotated by 90°**

Electron Diffraction in Atomic Clusters

for Core Level Photoelectron Diffraction Simulations



Created by **F. Javier García de Abajo** (CSIC and DIPC, San Sebastian, Spain)
in collaboration with **M. A. Van Hove** and **C. S. Fadley** (LBNL, Berkeley, and UCD, Davis, California)

This site allows performing on-line photoelectron diffraction calculations. Multiple scattering (MS) of the photoelectron is carried out for a cluster representing a solid or molecule. Select the corresponding parameters and click on the "Calculate" button below to perform the actual calculation and to produce a plot of the calculated data (a separate window pops out to display it). A numerical data table can be downloaded by clicking on the resulting plot. Click on the different parameter names in blue to see fuller explanations. Click on the "Preview Cluster" button to display the currently selected atomic cluster (but without performing a MS calculation) or the button "Download Cluster" to download the currently selected cluster. Notice that the scattering phase shifts and excitation radial matrix elements are calculated internally for each cluster configuration, so that the user does not have to provide them. Please, read the [terms of use](#) and the [restrictions on input parameters](#) before using this site for the first time.

Terms and conditions of use

[Terms of use](#)[Restrictions on input parameters](#)Password:

A password is only necessary for large computation times (click [here](#) for more details). Leave it blank otherwise.

Title (optional):

Cluster definition

The cluster and the list of emitters are defined by a list of commands with the following format (click [here](#) or on the items of this list for further details):

atom symbol $x\ y\ z$ layer symbol $x\ y\ z\ a\ b\ \alpha_1\ \alpha_2$

surface symbol $x\ y\ z\ a$ type emitter $x\ y\ z$

Fill in the text box with these commands according to the cluster specifications that you need. Some examples are provided by clicking [here](#) (you may cut and paste them to this page and modify them further).

```

atom O 0.95 0 1.66
atom C 0 0 1.0
surface Fe 1.435 1.435 0 2.87 bcc100
emitter 0 0 1.0
end

```

The cluster consists of a maximum of atoms. (Warning: a finite number of atoms generally introduces symmetry breaking.)

The size of the cluster is determined by the distance $d_{\max} = \boxed{10}$ Å and the reference point $x_0 = \boxed{0}$ Å, $y_0 = \boxed{0}$ Å, $z_0 = \boxed{0}$ Å.

See [cluster shape](#) for more details.

Plot cluster on output? Yes
 No

Cluster shape: Parabolic
 Spherical

[Preview Cluster*](#)

[Download Cluster*](#)

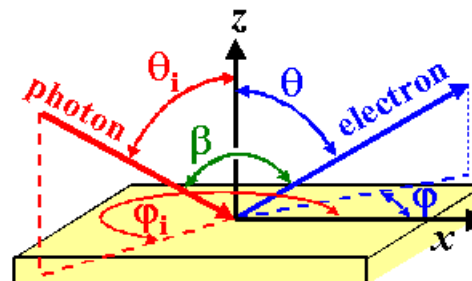
Geometry of beam and analyzer

Incoming beam parameters (see figure)

Polar angle $\theta_i = \boxed{0}$ degrees

Azimuthal angle $\varphi_i = \boxed{0}$ degrees

p-polarization
 s-polarization
 RCP
 LCP



[Schematic representation of the geometry](#)

Mobility of cluster

beam, and sample

(click here for details):

- Only the sample moves with constant $\beta = \boxed{90}$ degrees
- Only the analyzer moves
- Both the sample and the analyzer move

Energy and angle scanning parameters (see figure above)

The following entries will select the range of photoelectron energies and angles of emission.

Energy scans for a given emission angle can be chosen by selecting more than one energy of emission and only one polar angle and one azimuthal angle (the value of each angle is then taken as the lower limit of the selected angular range, and the value of the upper limits are disregarded). In this case, the output is a 1D plot with the photoelectron intensity as a function of photoelectron energy.

Electron energy range: 1 equally-spaced value(s) of the electron energy from 1202 eV to 1202 eV

Polar angle: 50 equally-spaced value(s) of the polar angle θ from 0 degrees to 89 degrees

Azimuthal angle: 61 equally-spaced value(s) of the azimuthal angle ϕ from 0 degrees to 360 degrees

Type of 2D angular Linear scale

Logarithmic scale

Type of azimuthal of polar Cartesian

Polar

Photoelectron detector half-width acceptance angle = 0 degrees. The photoelectron intensities are angle-averaged over a cone with half aperture given by this parameter.

Multiple scattering parameters

Additional solid parameters

Inner potential V_0 = 12.4 eV

Electronic edge z_0 = 1.435 Å

8.1 eV from band struct.
+ work function = 4.3 eV
= 12.4 eV

Inelastic mean free path: either choose a fixed value = 17.8 Å

or (if that last entry is <0) use the TPP-2M formula

with parameters ρ = 7.87 g/cm³, N_v = 8, E_p = 30.57 eV, and E_g = 0 eV

Temperature (K) = 300 and Debye Temperature (K) = 470

Internal code parameters

Maximum orbital quantum number l_{\max} = 25

Scattering order = 4

Iteration method: Jacobi regular MS
 Recursion

Initial core-state quantum numbers

Radial matrix elements:

Automatic: core level (e.g. 1s, 2s, 2p, etc.) = 1s

Manual: l_0 = 0, R_{10+1} = 1.0, δ_{10+1} = 0.0, R_{10-1} = 0.0, δ_{10-1} = 0.0

Table 4 Density and atomic concentration

The data are given at atmospheric pressure and room temperature, or at the stated temperature in deg K. (Crystal modifications as for Table 3.)

H	4K	0.088													He	2K	0.205 (at 37 atm)	
Li	78K	Be	0.542	1.82	4.700	12.1	3.023	2.22										
Na	5K	Mg	1.013	1.74	2.652	4.30	3.659	3.20										
K	5K	Ca	0.910	1.53	2.99	4.51	6.09	7.19	7.47	7.87	8.9	8.91	8.93	7.13	Al	Si	P	
Rb	5K	Sr	1.629	2.58	4.48	6.51	8.58	10.22	11.50	12.36	12.42	12.00	10.50	8.65	C	N	O	
Cs	5K	Ba	1.997	3.59	6.17	13.20	16.66	19.25	21.03	22.58	22.55	21.47	19.28	14.26	F	Ne	4K	
Fr	Ra	Ac	—	—	10.07	Ce	Pr	Nd	Pm	Sm	Eu	Gd	Tb	Dy	Ho	Er	Tm	
					2.66	6.77	6.78	7.00	—	7.54	5.25	7.89	8.27	8.53	8.80	9.04	9.32	6.97
					3.76	2.91	2.92	2.93	—	3.03	2.04	3.02	3.22	3.17	3.22	3.26	3.32	3.02
						3.65	3.63	3.66		3.59	3.96	3.58	3.52	3.51	3.49	3.47	3.54	3.88
						Th	Pa	U	Np	Pu	Am	Cm	Bk	Cf	Es	Fm	Md	No
						11.72	15.37	19.05	20.45	19.81	11.87	—	—	—	—	—	—	—
						3.04	4.01	4.80	5.20	4.26	2.96	—	—	—	—	—	—	—
						3.60	3.21	2.75	2.62	3.1	3.61							

$$\text{Atomic radius} = r_{\text{MT}} = 0.5 \text{ n-n dist.}$$

$$\begin{array}{ccc} \text{Density in g cm}^{-3} (10^3 \text{kg m}^{-3}) & & \\ \text{Concentration in } 10^{22} \text{ cm}^{-3} (10^{28} \text{ m}^{-3}) & & \\ \text{Nearest-neighbor distance, in \AA (10}^{-10}\text{m}) & & \end{array}$$

$$\text{Average surface density} = \rho_s = (\rho_v)^{2/3}$$

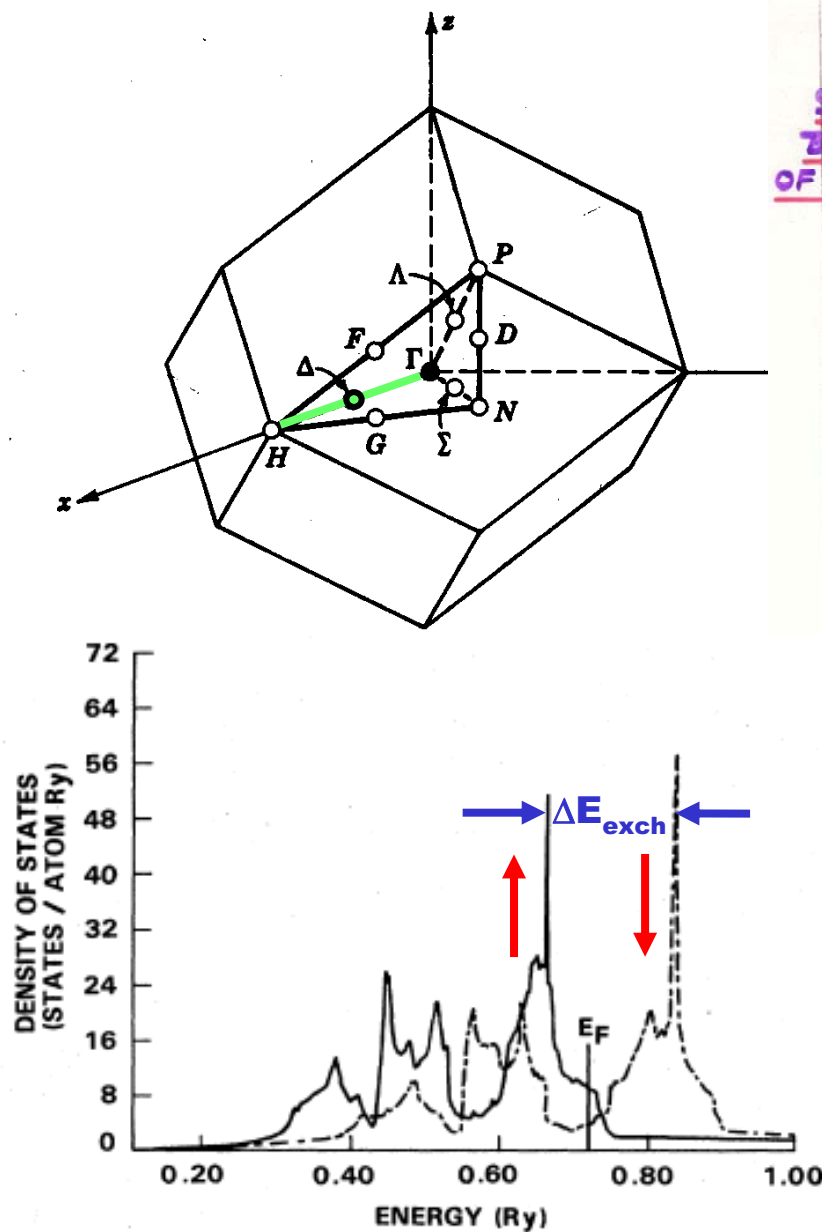
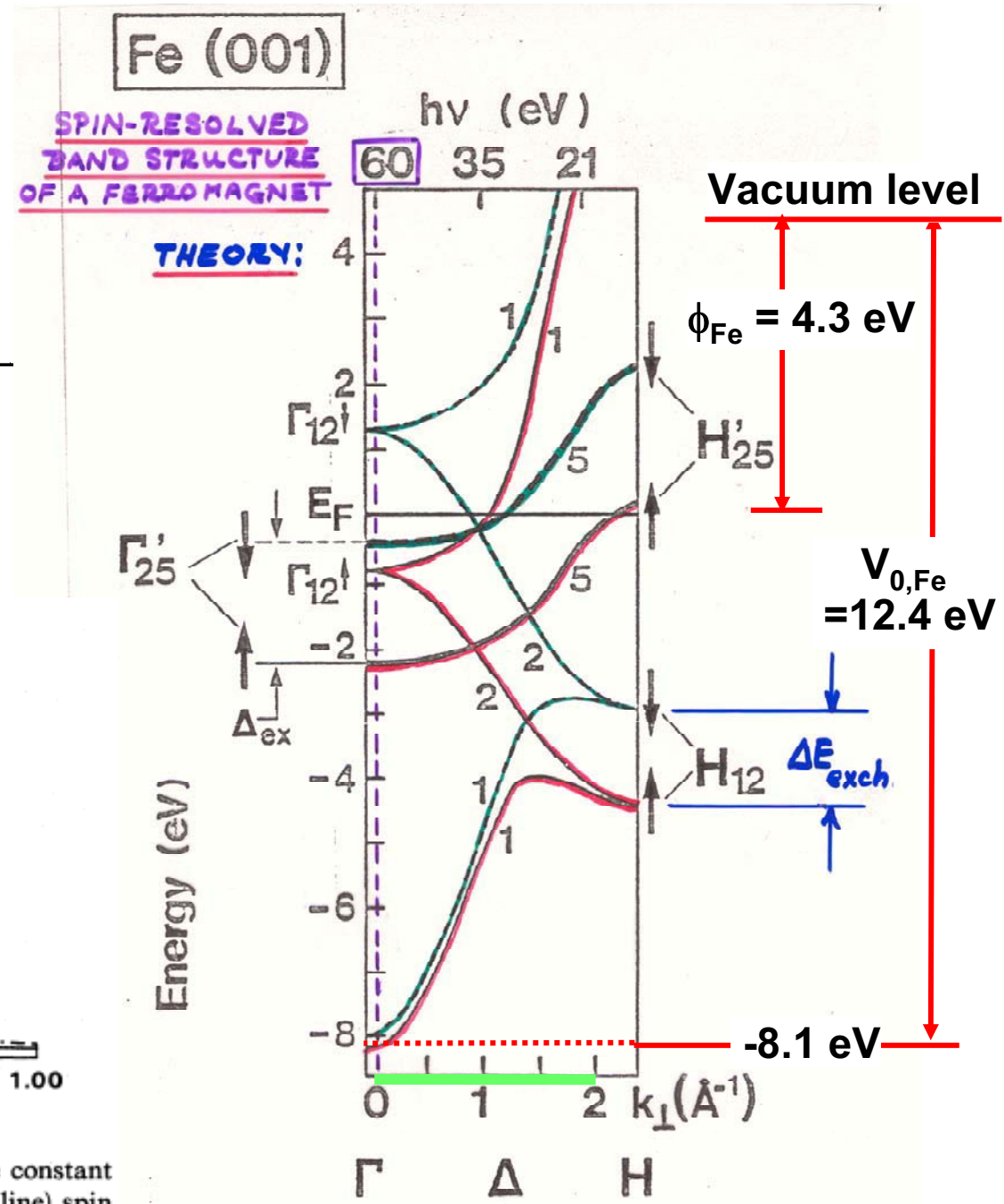


FIG. 4. Density of states at the equilibrium lattice constant of Fe for majority- (solid line) and minority- (broken line) spin states.

Hathaway et al., Phys. Rev. B 31, 7603 ('85)



E. KISKER ET AL., PHYS. REV. B
31, 329 (1985)

Initial core-state quantum numbers

Radial matrix elements:

- Automatic: core level (e.g. 1s, 2s, 2p, etc.) =
- Manual: $l_0 =$, $R_{10+1} =$, $\delta_{10+1} =$, $R_{10-1} =$, $\delta_{10-1} =$

Calculate*

Download Input File**

Reset***

COMPUTATION TIME: the CPU time needed for the calculation using the default cluster and input parameters (use Reset to recover default input) is 1.24 seconds on a Pentium III @ 733 MHz. This gives a time scale to estimate the computation time for other input parameters, keeping in mind that it scales like $\sim (n_{\text{scat}} - 1) N^2 (l_{\text{max}} + 1)^3$, where N is the number of atoms in the cluster and n_{scat} is the scattering order. For reference, the default values are $N=48$, $l_{\text{max}}=6$, and $n_{\text{scat}}=2$, for which the above number is $7.9 \cdot 10^5$.

IMPORTANT: READ THESE LINES BEFORE RUNNING THE CODE FOR THE FIRST TIME.

*The results will be plotted on a separate window.

**The input file can be used to run the code locally, for which a copy of the code is needed. This can be obtained from [F. Javier García de Abajo](#). An online version of the input-file manual is also available [here](#).

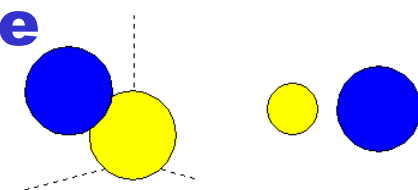
***Reset all input values (including cluster specification) to the original settings.

For comments/questions/suggestions, please contact F. Javier García de Abajo at jga@sw.ehu.es

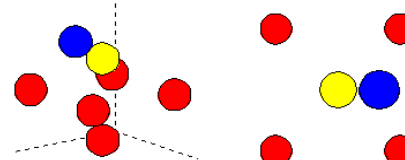
CO/Fe(001)—Effect of CO height z above first Fe plane

2 atoms: $z =$

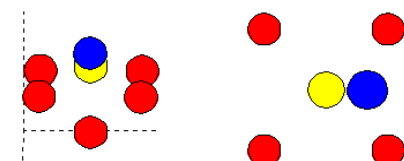
∞



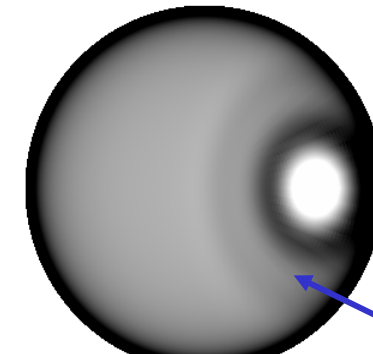
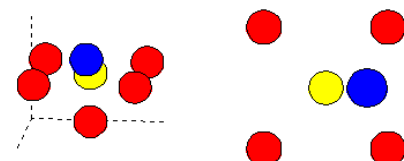
7 atoms: 1.0 \AA



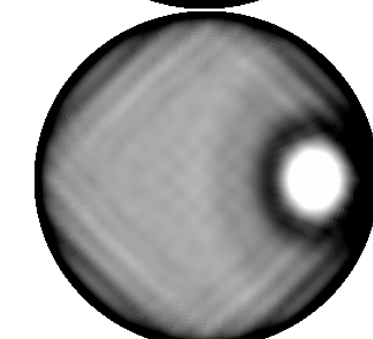
0.5 \AA



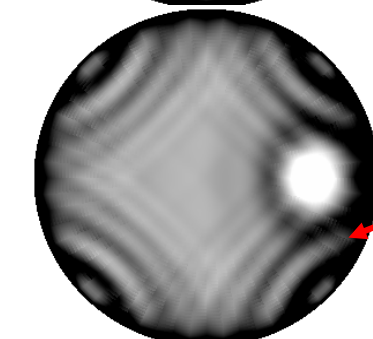
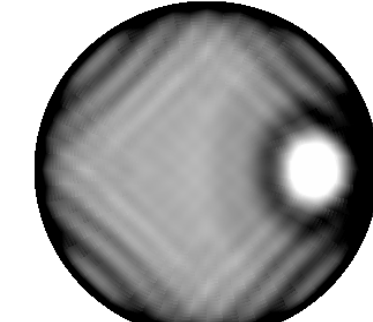
0.0 \AA



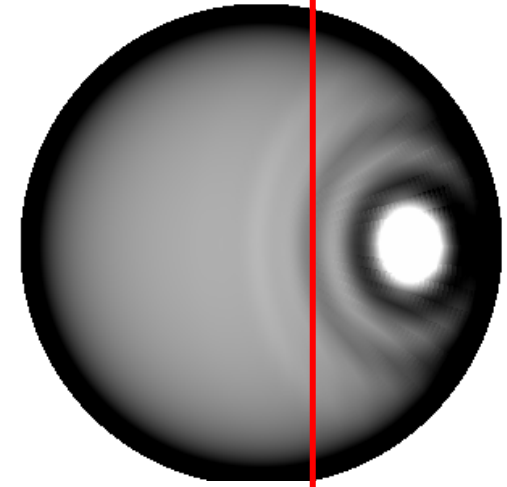
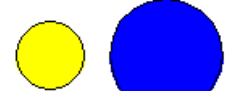
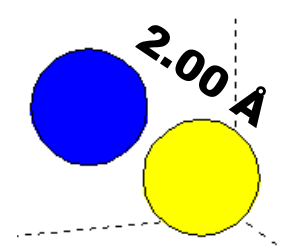
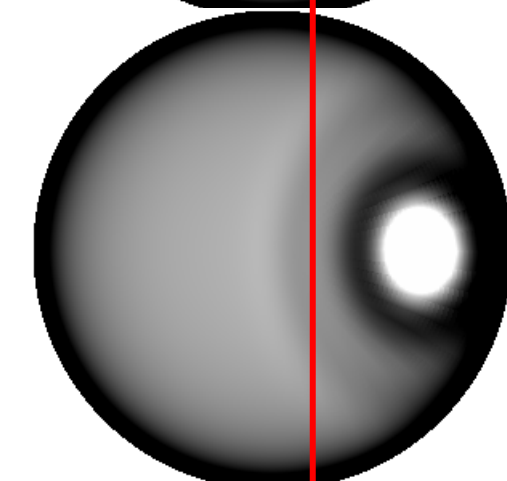
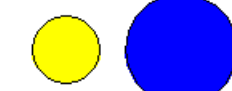
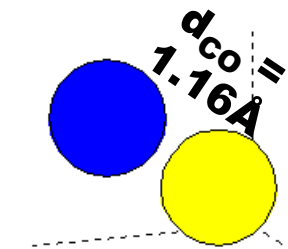
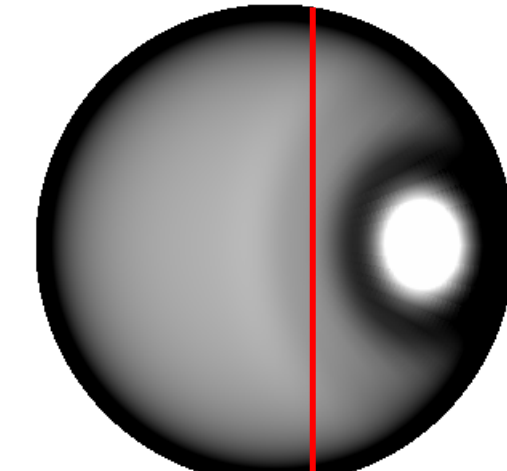
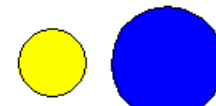
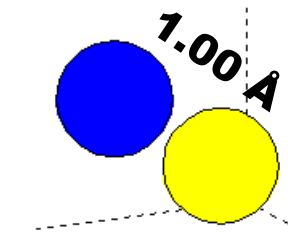
Oxygen-
1st order
diff. ring



Iron-
1st order
diff. ring

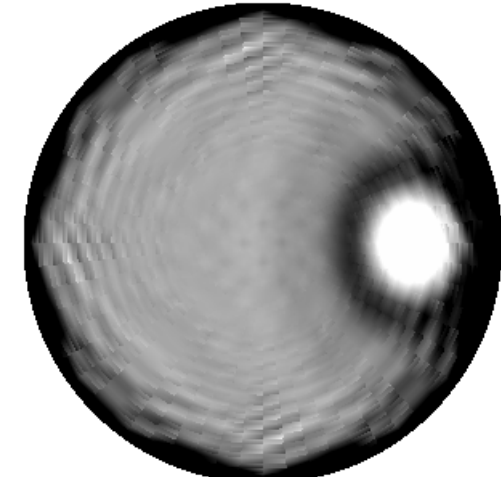
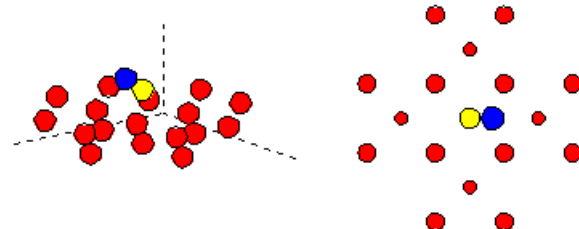


CO/Fe(001)—Effect of CO bond dist.

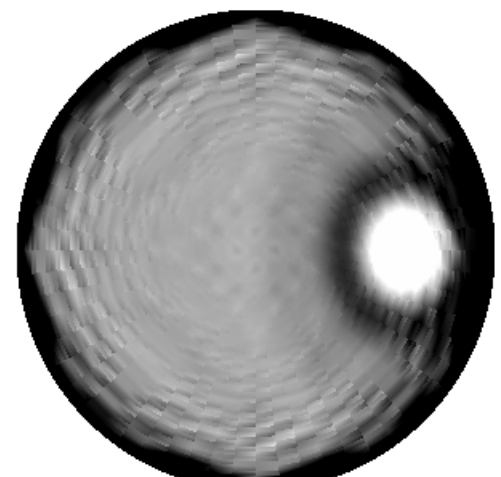
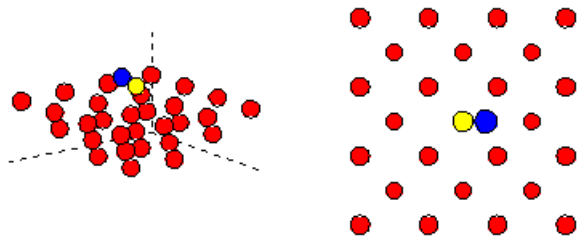


CO/Fe(001)—Effect of cluster size

19 atoms:



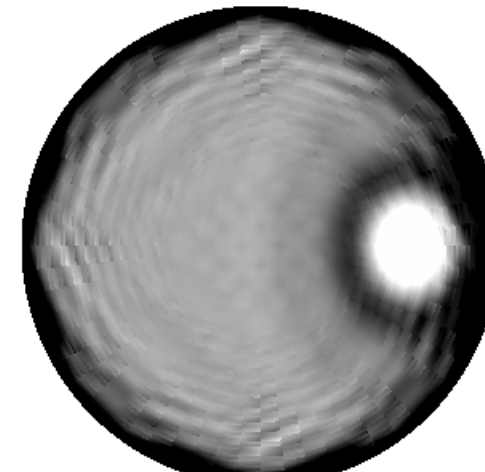
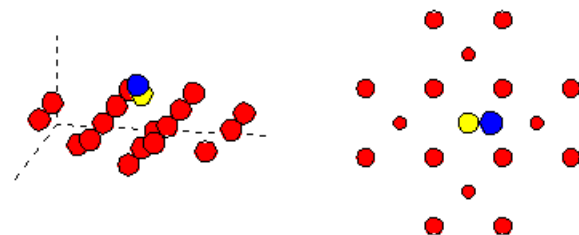
31 atoms:



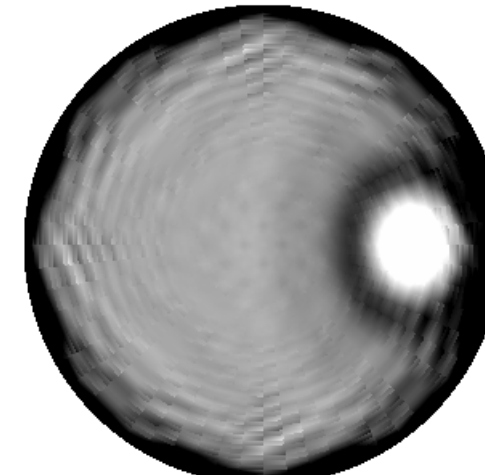
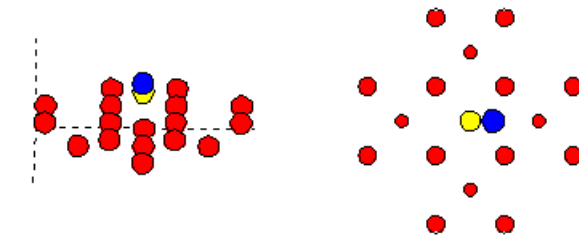
19 ≈ 31, AND SO “CONVERGED” AT 19 OR LESS

CO/Fe(001)—Effect of scattering order

Single scattering:



Fourth order scattering:

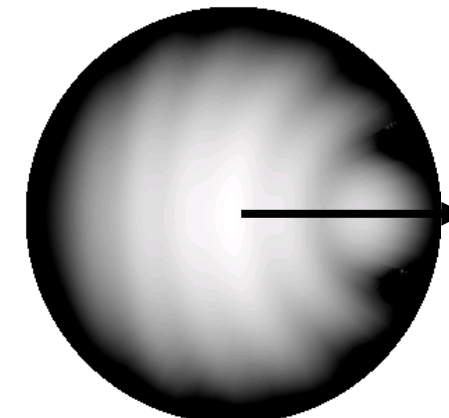
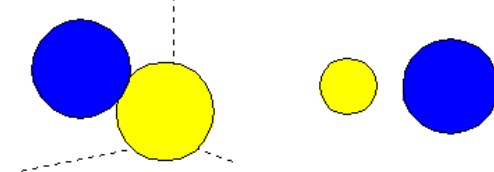


APPROX. CONVERGED AT SINGLE—FOR THIS PARTICULAR PROBLEM ONLY!

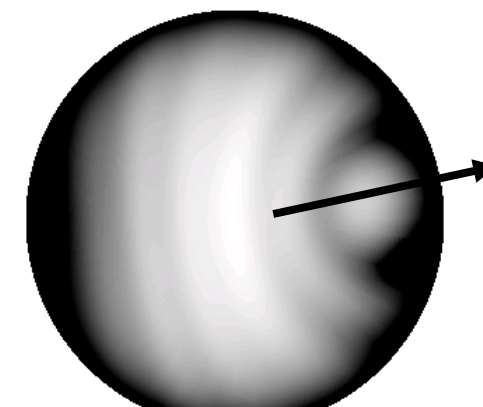
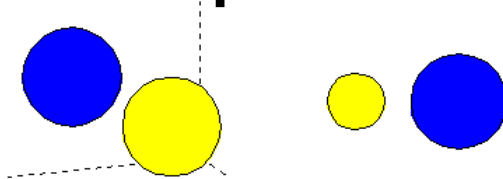
Effect of varying the polarization?: C 1s emission from CO

$E_{\text{kin}} = 200 \text{ eV}$

Linear p polarization:

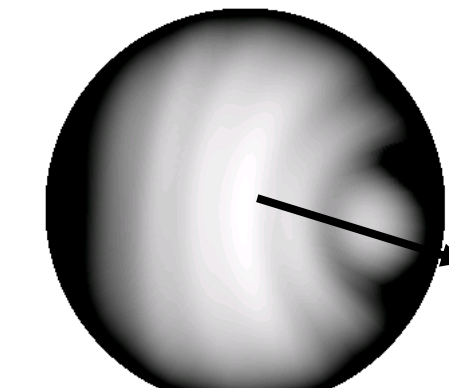
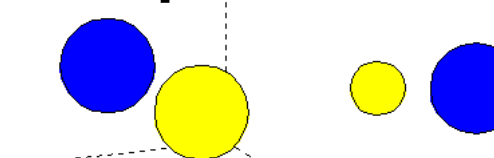


Right circular polarization:

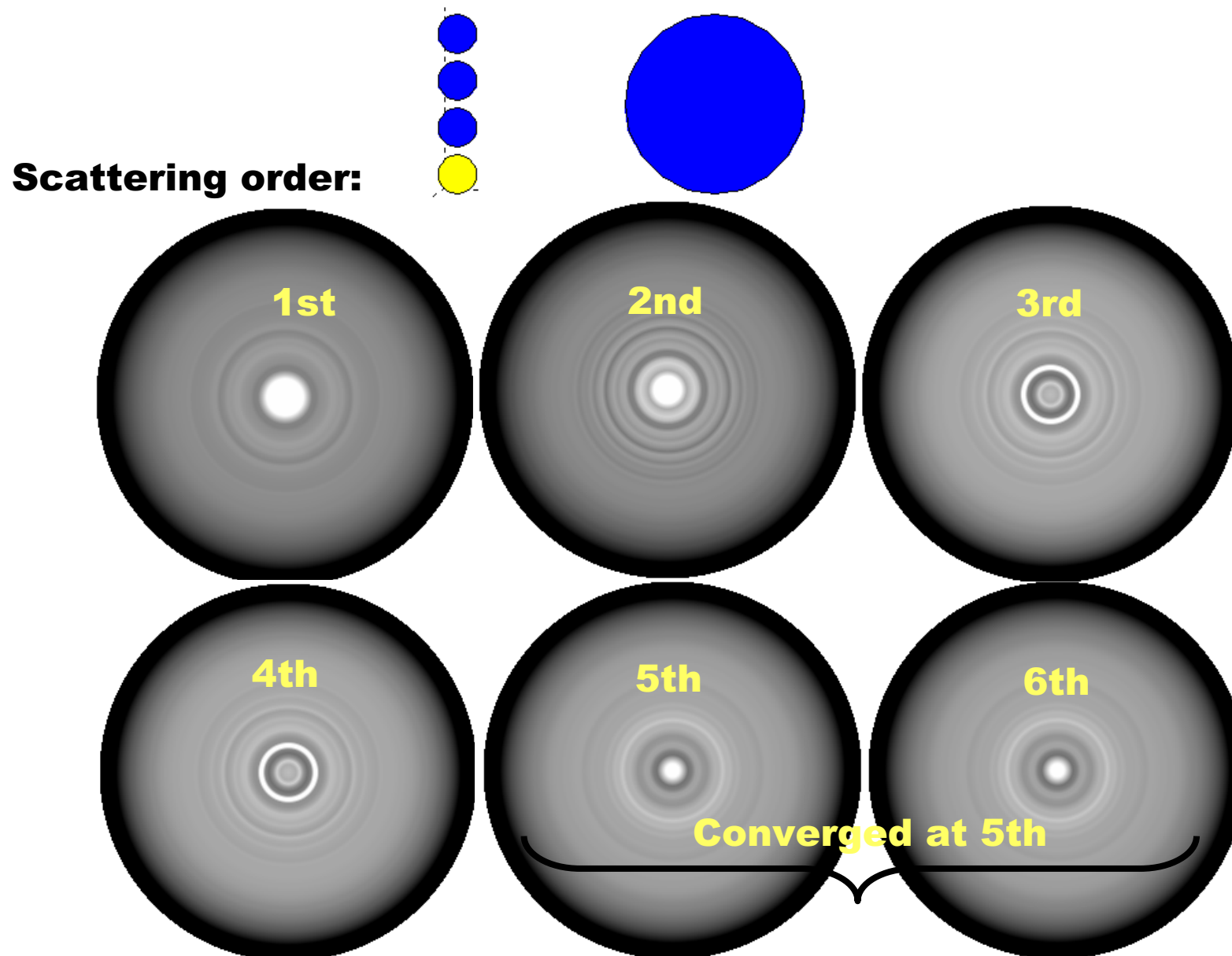


Circular dichroism
in angular
distributions
(CDAD)—more
later

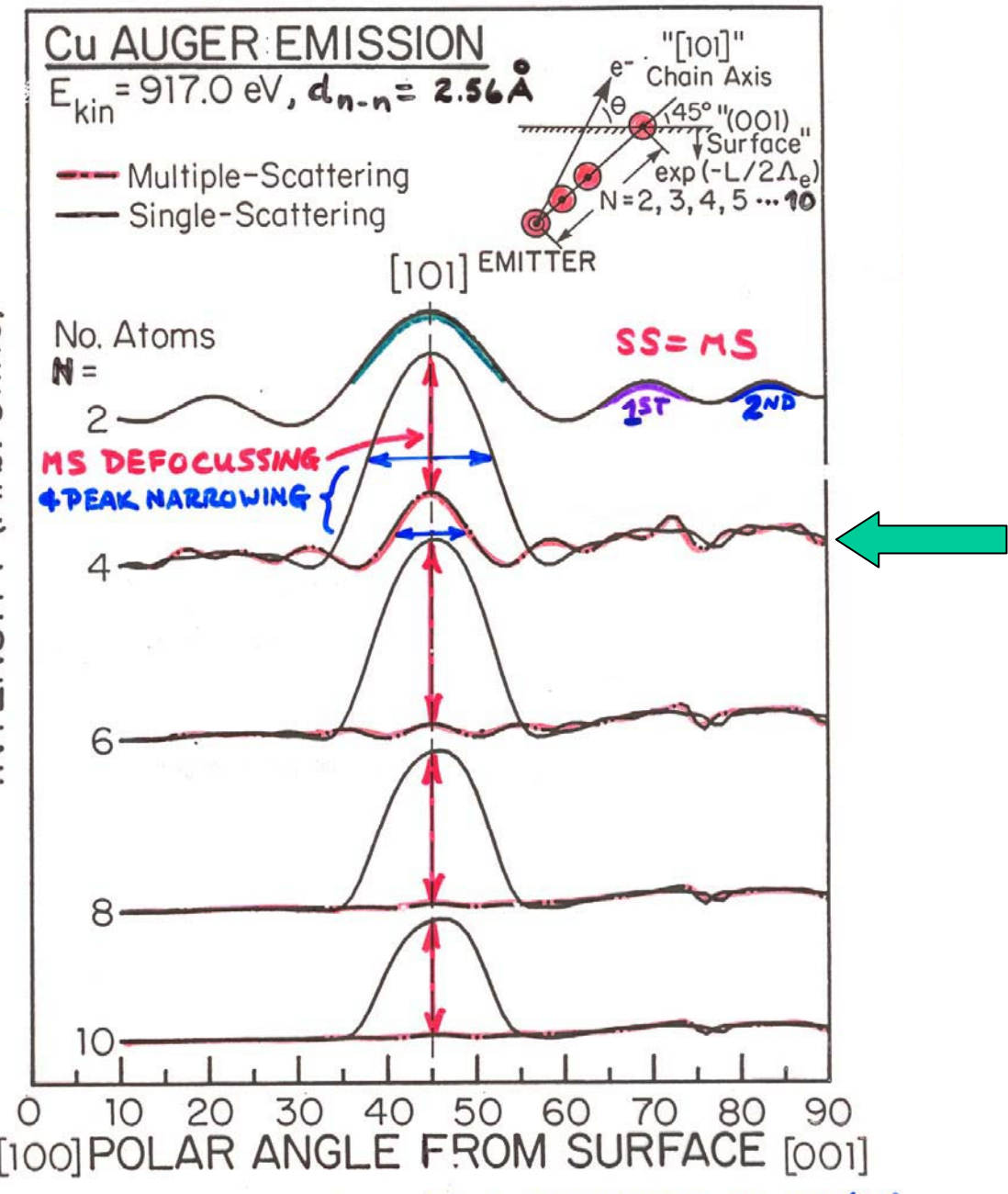
Left circular polarization:



4-atom Fe nearest-neighbor chain along [110]— Effect of scattering order



Cu nearest-neighbor chains along [110]—Effect of scattering order

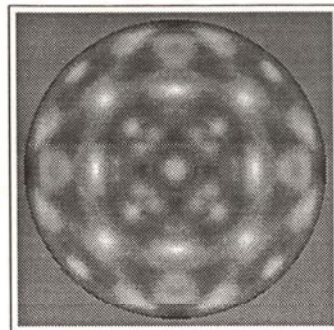


Plus cf. Figs. 6 and 7 in C.F., "The Study of Surface Structures by Photoelectron Diffraction and Auger Electron Diffraction"

Photoelectron Intensities From Different Surfaces
(Stereographic Projection)

Ni(001):Ni 2p at 636 eV

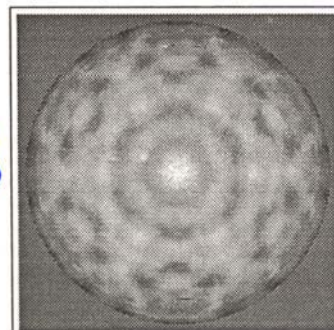
fcc
(001)



THEVUTHASAN
ET AL.

Ru(0001):Ru 3d at 1206 eV

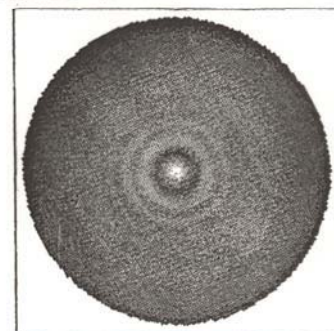
hcp
(0001)



THEVUTHASAN
ET AL.

HOPG: Graphite (0001): C 1s at 946 eV

textured

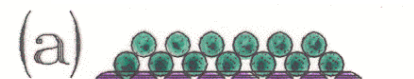


OSTERWALDER
ET AL.



Fingerprint
identification
of short-range
atomic
structure
and symmetry

- Some growth modes:



LAYER-BY-LAYER (FvdM)
EX. Fe/W(110)
Gd/W(110)



INTERDIFFUSION
Fe/Cu(001)



SURFACE ALLOY
Co/Pt



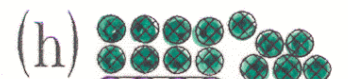
FLOATING
SURFACTANT
Au/Si(111)-Ag



MIXED (SK)
Cu/Ru(001)
Gd/Ru(001)



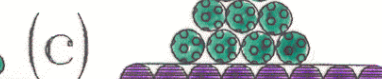
MIXED-PHASE
EPITAXY/**METASTABILITY**
fcc & bcc Fe/Cu(001)



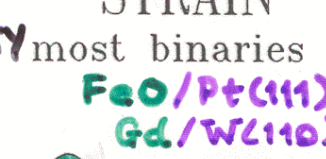
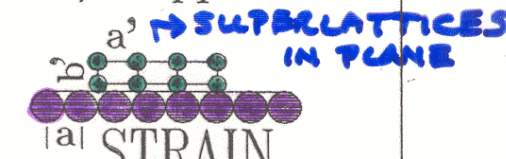
DEFECTS/STEPS
Fe/Cu
Cr/Fe



ALLOYING
SURFACTANT
Ga/Si(111)-Sn



ISLAND/CLUSTER (VW)
3D → 2D → 1D
Fe/Stepped W

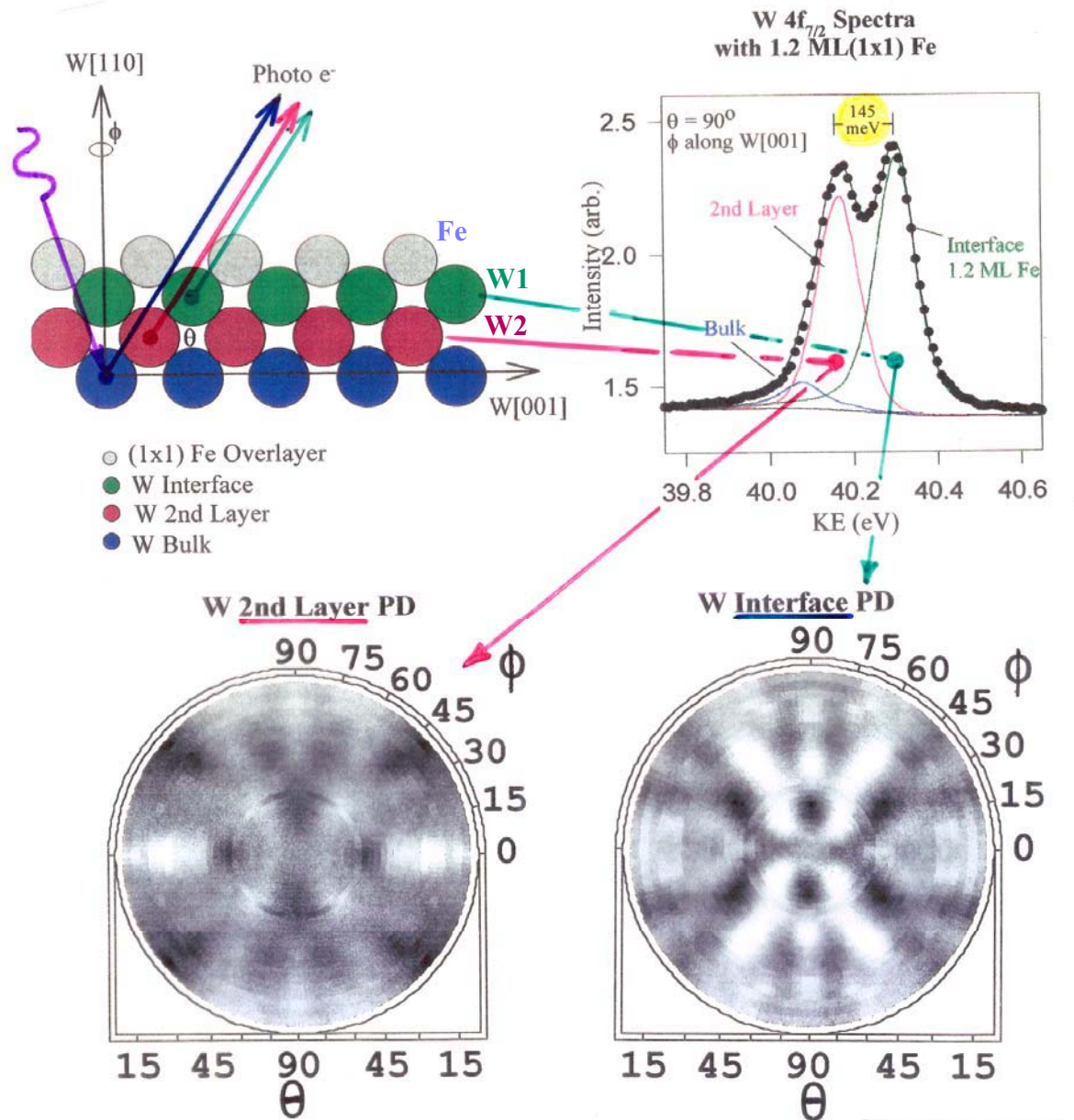


ROUGHNESS
Co/Cu
Cr/Fe



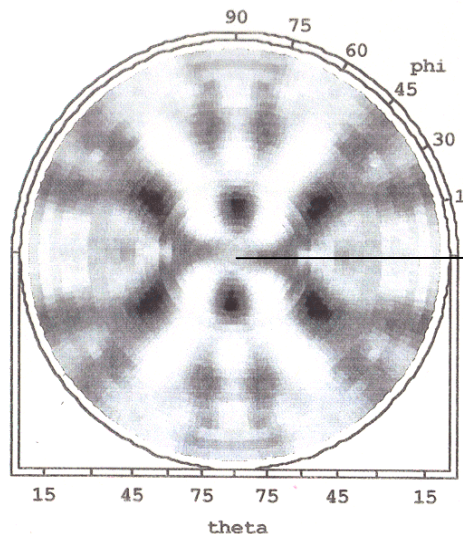
TEXTURING
Tb-Fe
(Amorphous?)
HOPG graphite

Photoelectron diffraction from W(110) interface atoms beneath an Fe overlayer



TOBER ET AL.
P.R.L.,
79, 2085 ('93)

Fe on W(110): Determination of structure by expt./theory comparison

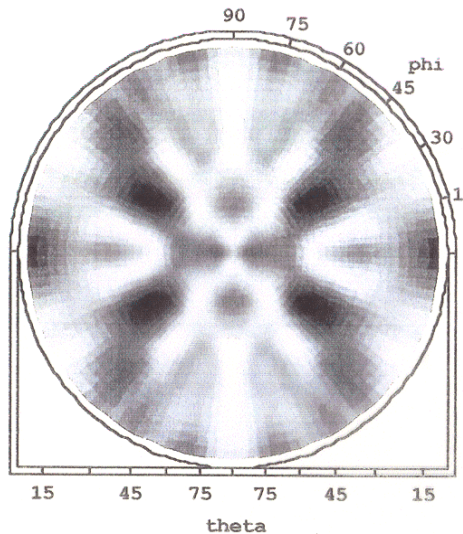


W 4f_{7/2}
Interface Diffraction

Experiment

$$h\nu = 70 \text{ eV}$$

$$E_{\text{kin}} = 40 \text{ eV}$$



W 4f_{7/2}
Interface Diffraction

Multiple Scattering
Theory
(110 atom cluster)

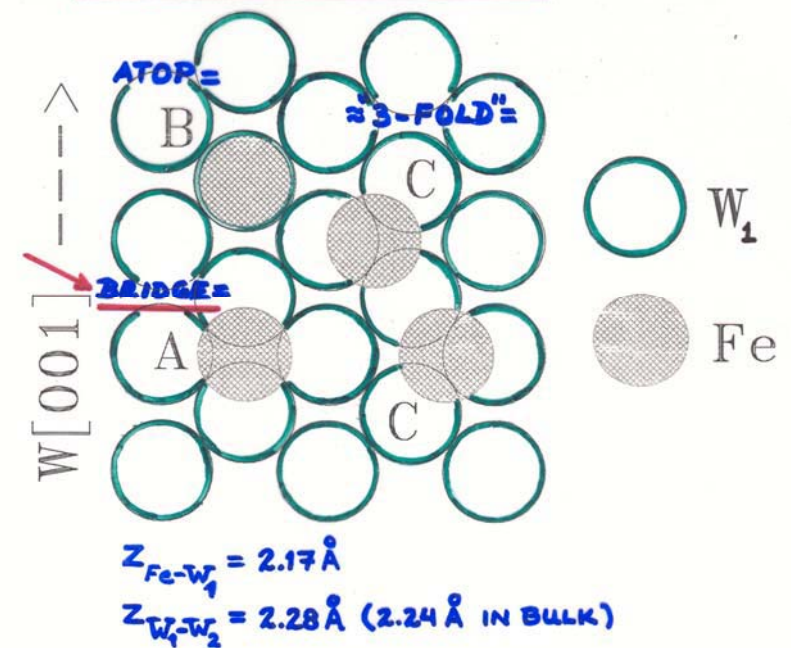
$$E_{\text{kin}} = 40 \text{ eV}$$

$$Z_{\text{Fe}} = 2.165 \text{ \AA}$$

(Bridge Site)

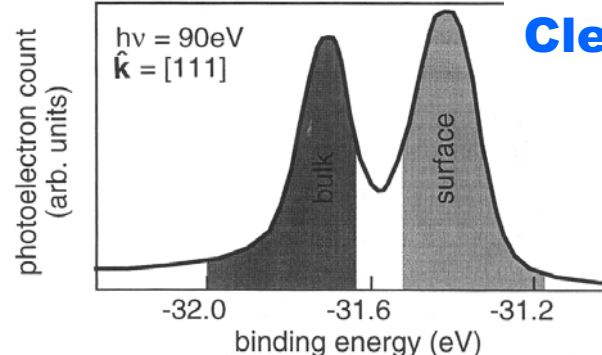
↳ ~CONTINUES BULK
W STRUCTURE

STRUCTURE DETERMINATION:



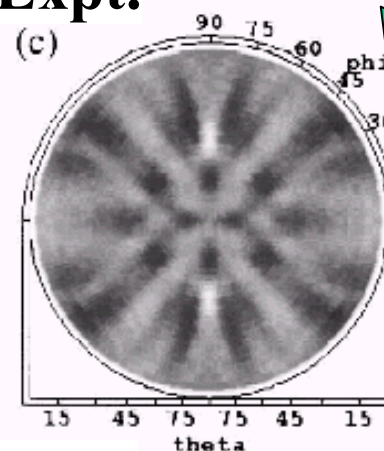
$$Z_{\text{Fe}-W_1} = 2.17 \text{ \AA}$$

$$Z_{W_1-W_2} = 2.28 \text{ \AA} \text{ (2.24 \AA IN BULK)}$$

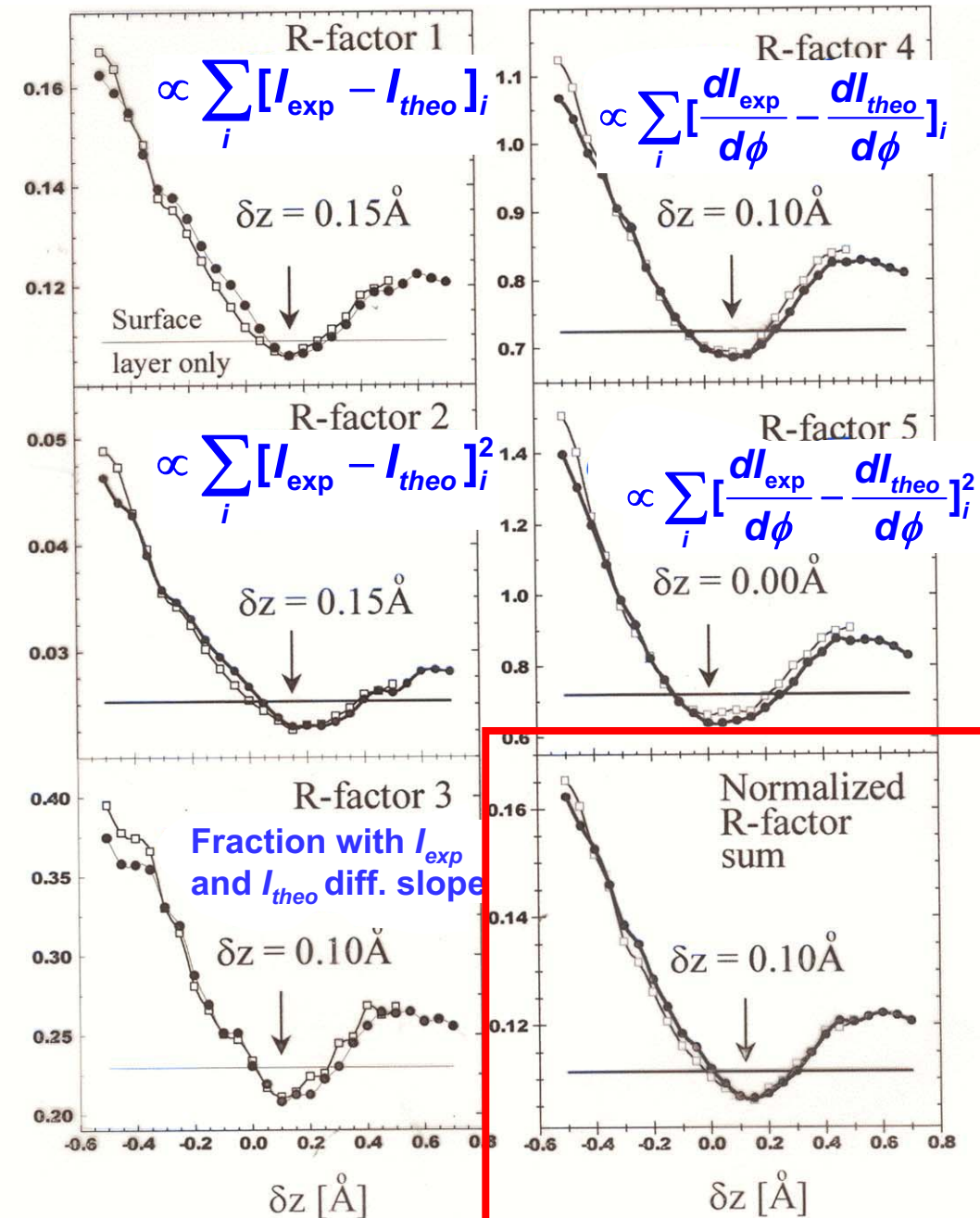
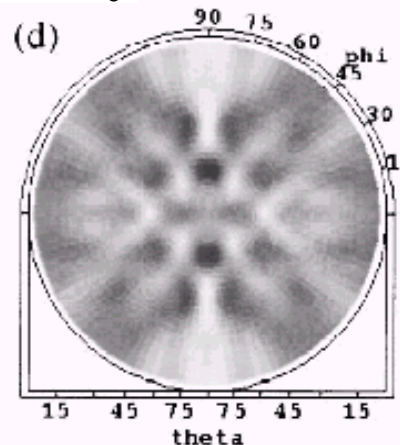


Clean W(110) 4f Surface Peak: R-Factor Analysis

Expt.



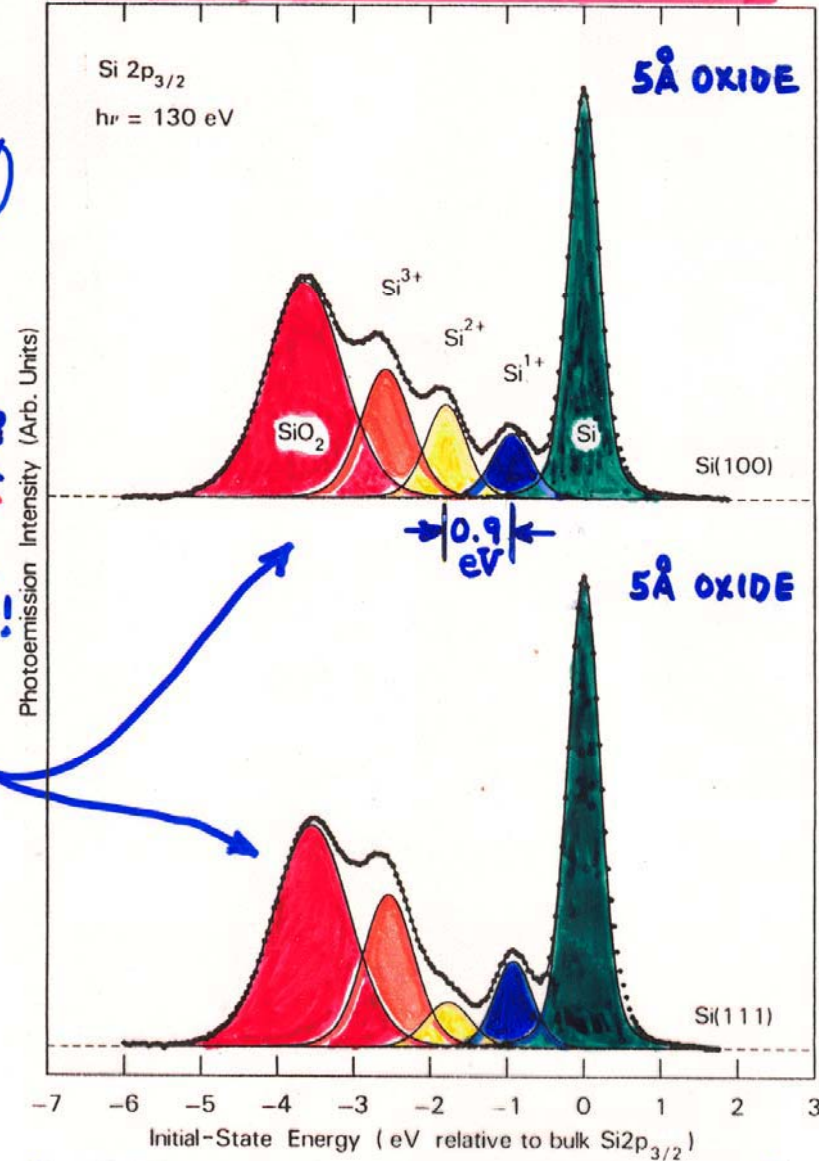
Theory



PHOTOELECTRON SPECTRA
OXIDIZED SILICON
CHEMICAL SHIFTS OF CORE LEVELS

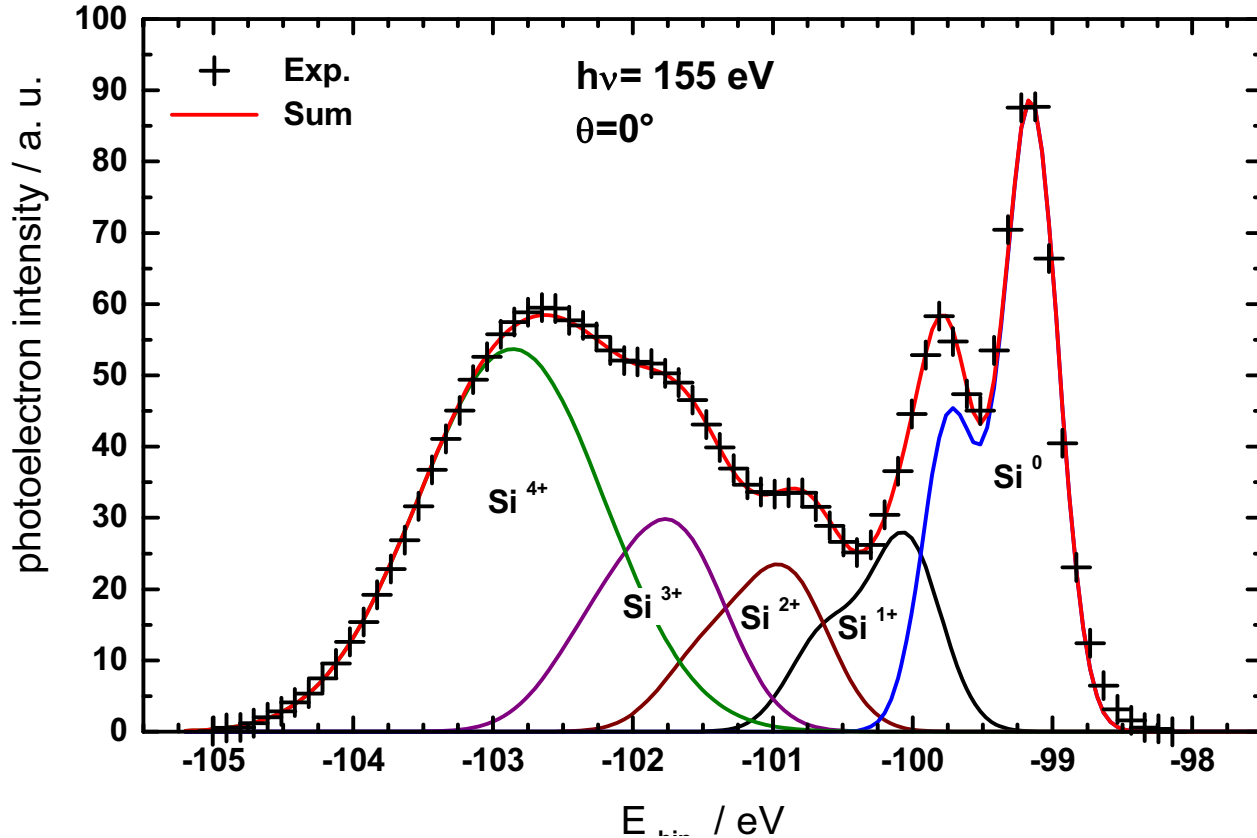


EXACTLY
WHAT IS
STRUCTURE
OF INTERFACE?
NEED STATE-
SPECIFIC
STRUCTURAL
INFORMATION!



HIMPEL ET AL., PHYS. REV. B, 39, 6084 ('90)

Case study: Interface structure of $\text{SiO}_x/\text{SiO}_2$ (Westphal et al.)

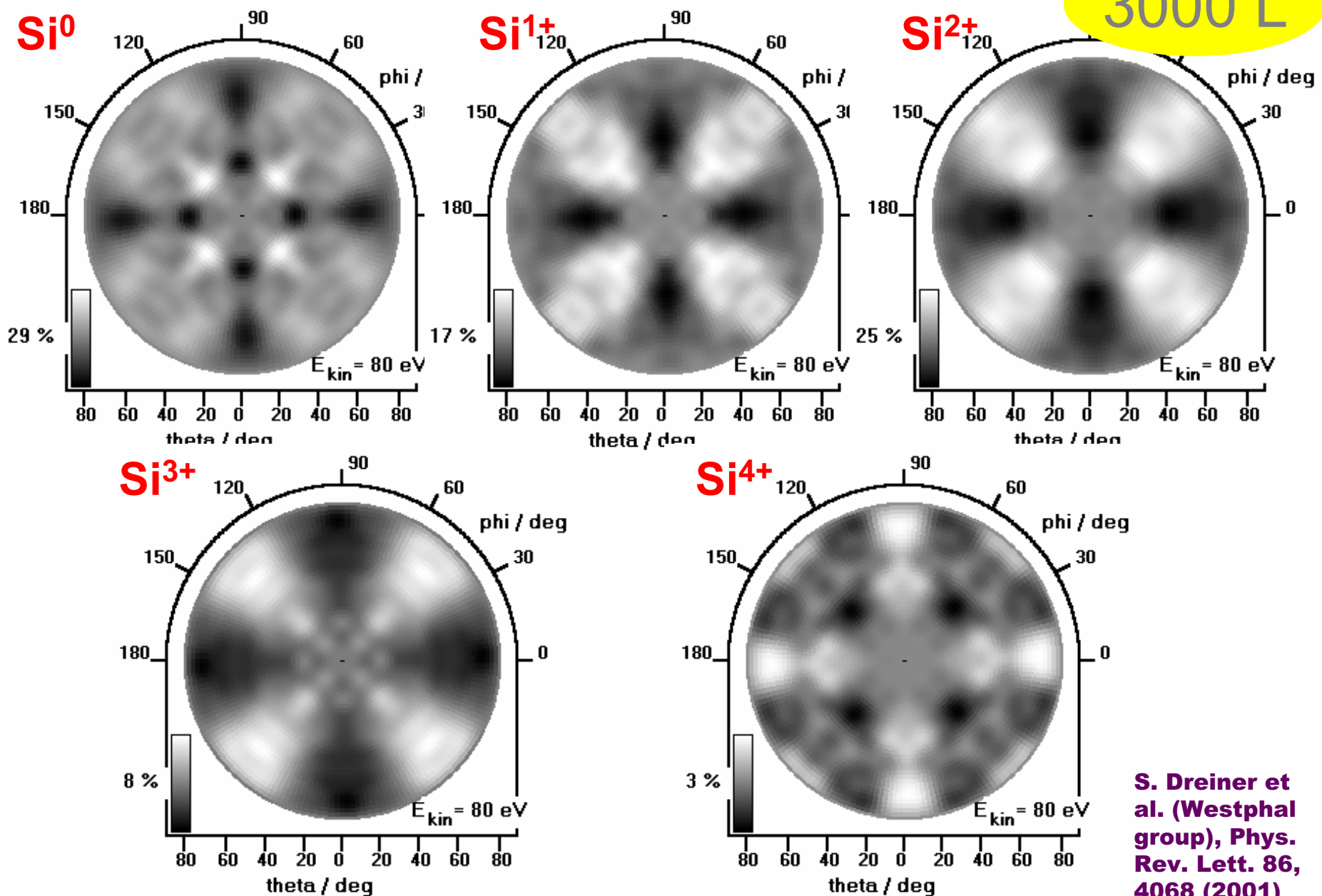


Spin-orbit-splitting	0.58 eV
Si^0 width	0.48 eV
Si^{1+} shift / width	0.9 / 0.59 eV
Si^{2+} shift / width	1.74 / 0.72 eV
Si^{3+} shift / width	2.46 / 0.84 eV
Si^{4+} shift / width	3.54 / 1.42 eV

F.J. Himpsel et al, Phys. Rev. B 38 (1988) 6084

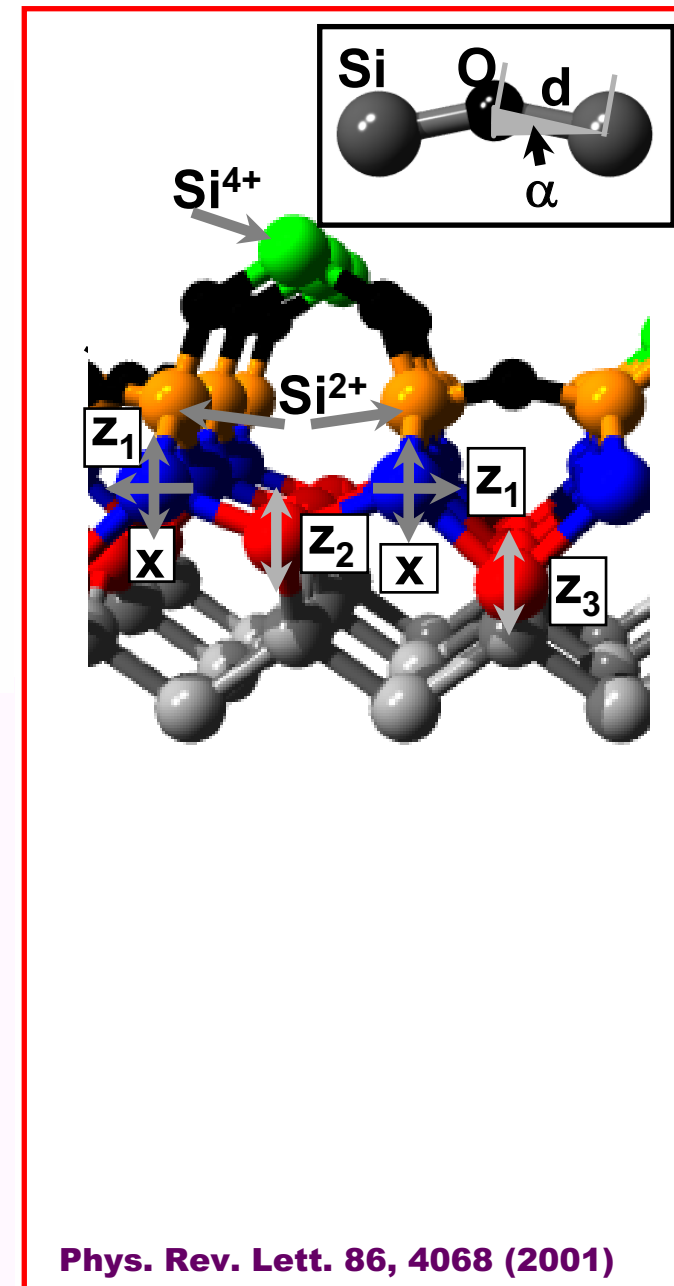
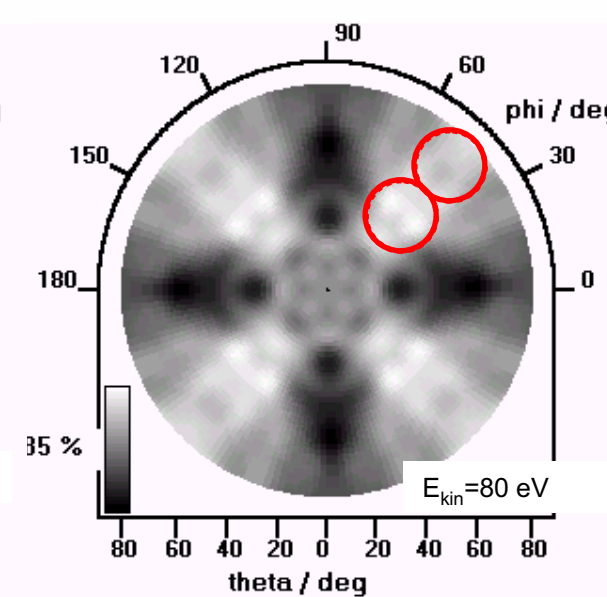
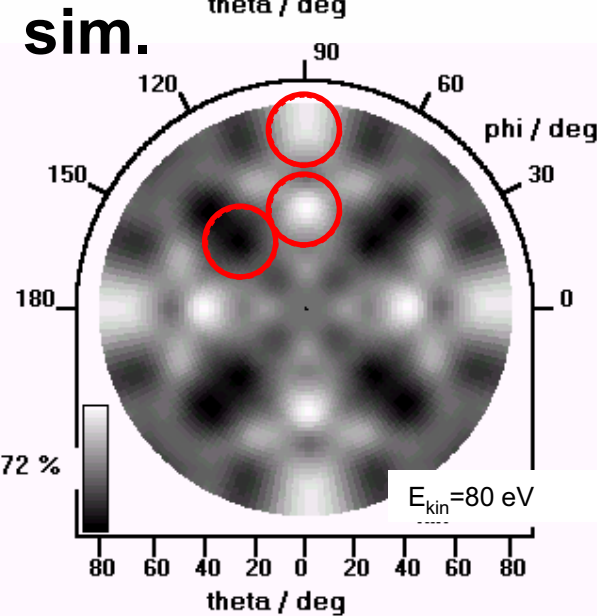
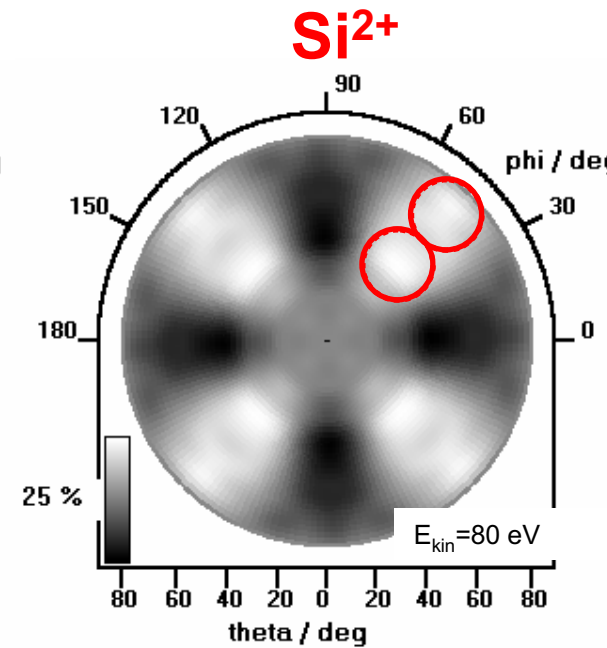
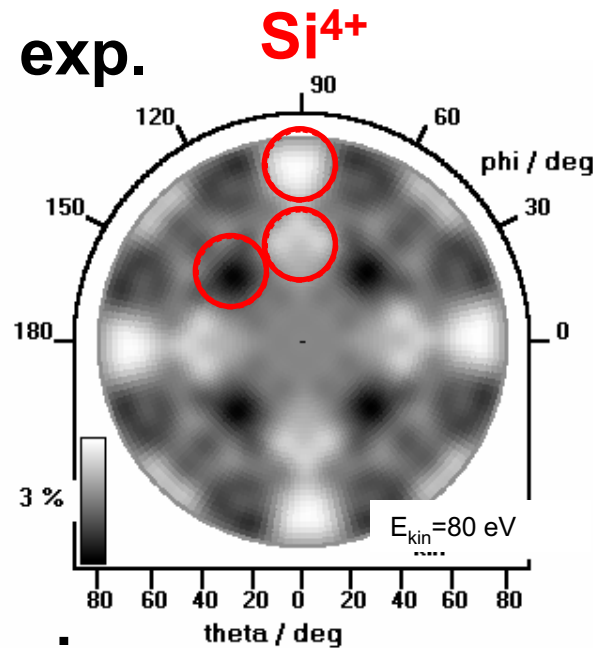
S. Dreiner et al. (Westphal group), Phys. Rev. Lett. 86, 4068 (2001)

Experimental diffraction patterns for $\text{SiO}_2/\text{Si}(100)$

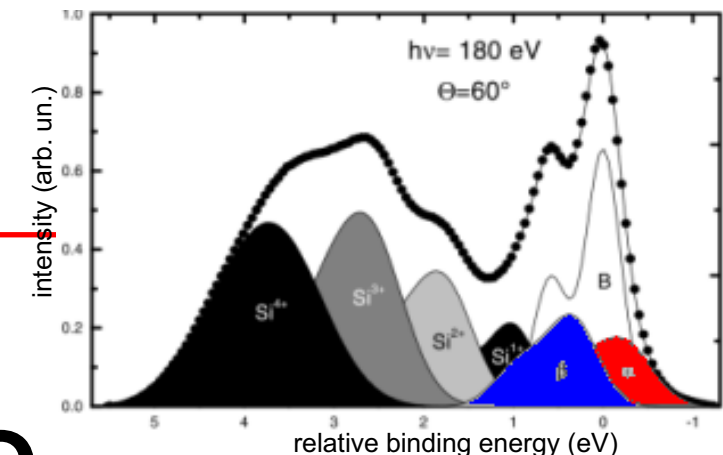
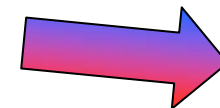


S. Dreiner et al. (Westphal group), Phys. Rev. Lett. 86, 4068 (2001)

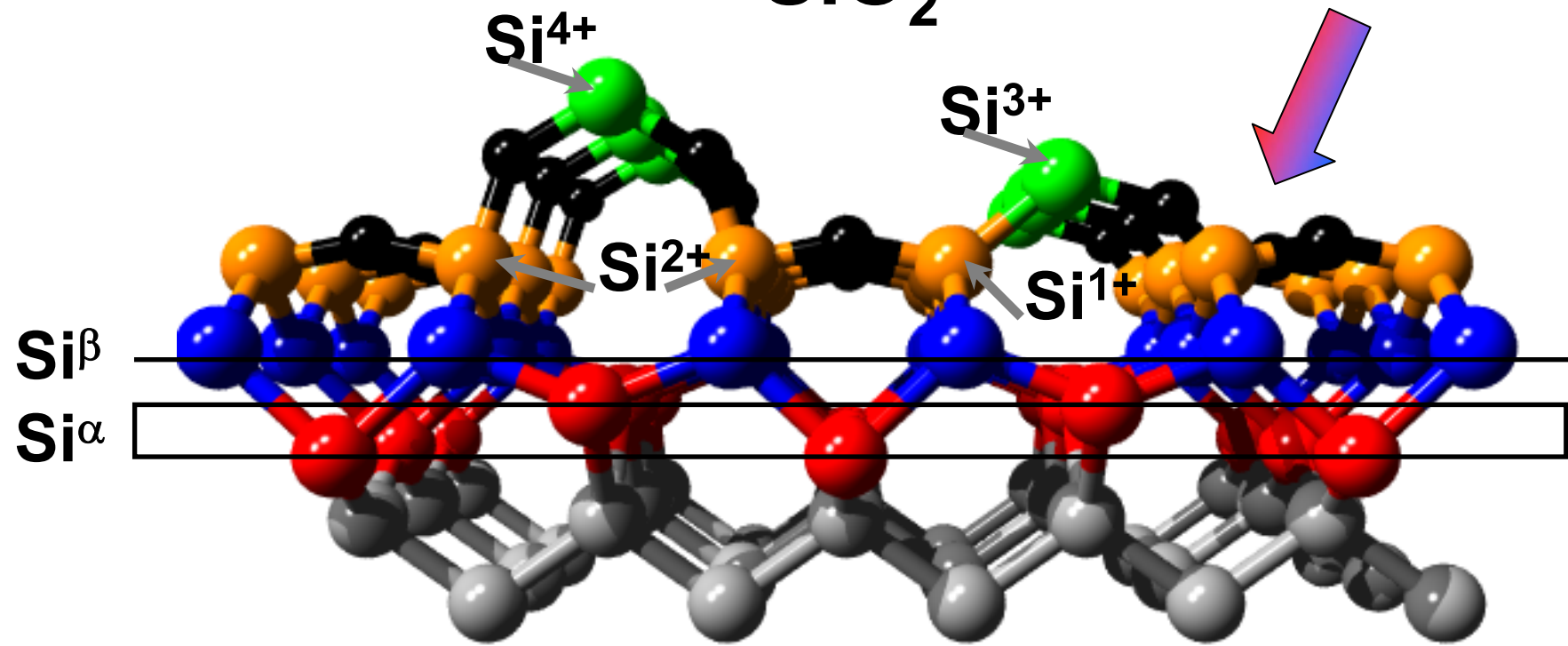
Structure determination by R-factor analysis: $\text{SiO}_x/\text{Si}(100)$



+ Assignment of additional
 Si^α - and Si^β -components



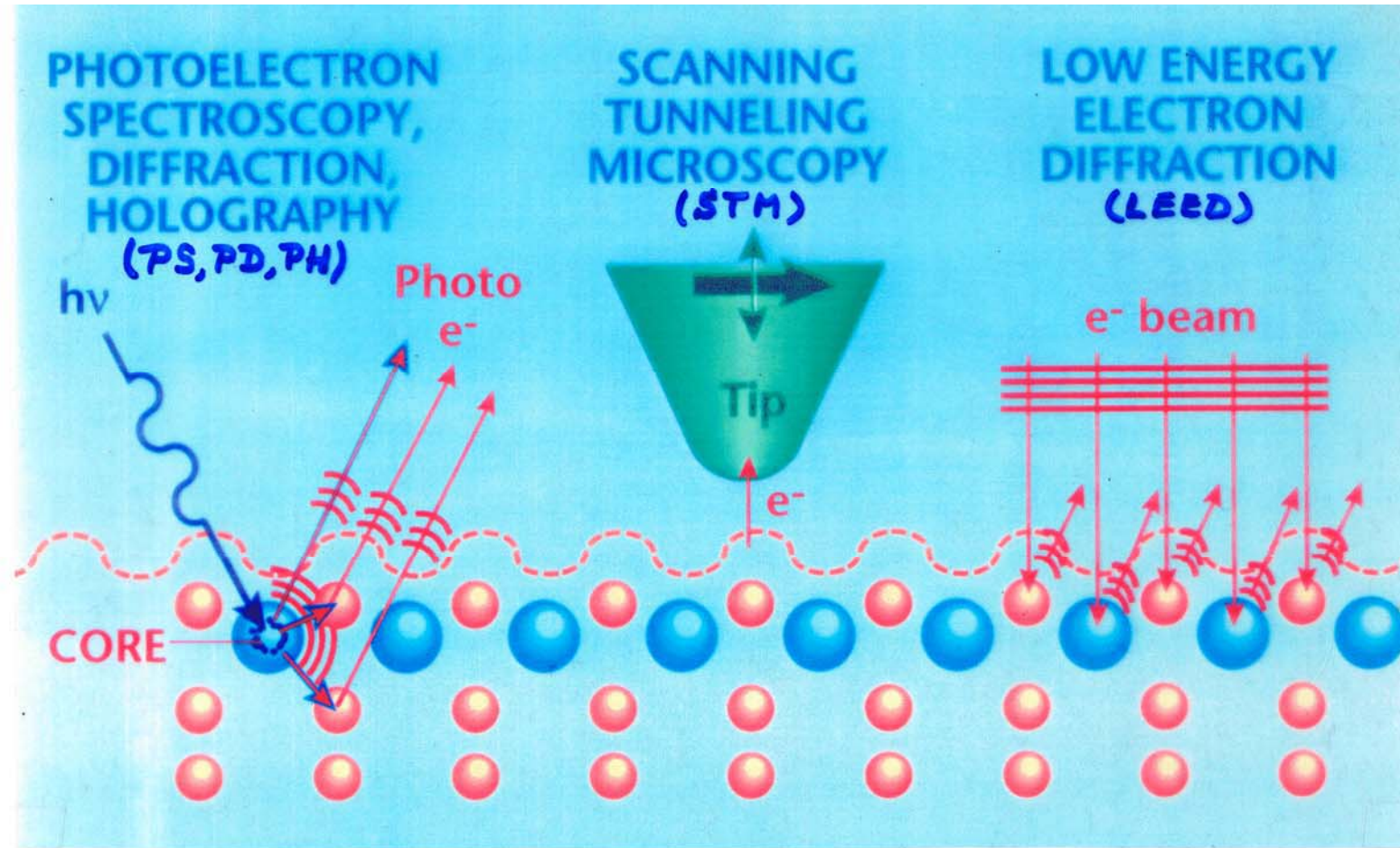
SiO_2



Si-bulk

S. Dreiner et al. (Westphal group)

Some Comple- mentary Surface Structure Probes

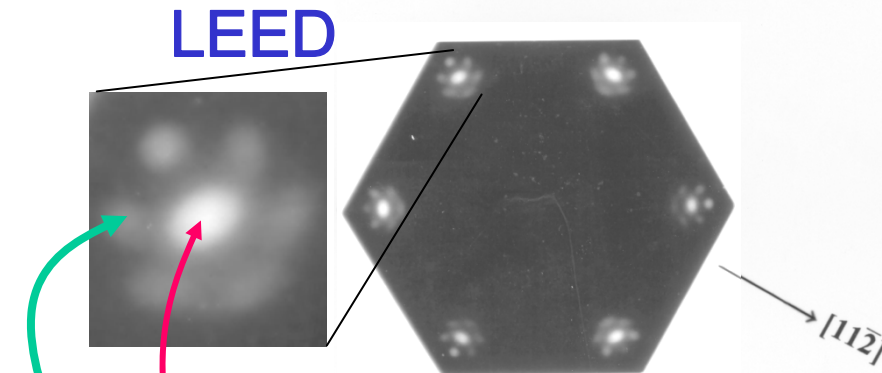


<u>Type of order:</u>	Short (< 10 \AA)	Short, long and disorder	Long (> 100 \AA)
<u>Atom & site specific:</u>	Yes	No	No
<u>Sensing depth:</u>	5-40 \AA	Mostly surface D.O.S.	5-20 \AA
<u>Lateral resolution:</u>	1 mm ² to (300 \AA) ²	Single atom	1 mm ² to 1 micron ²

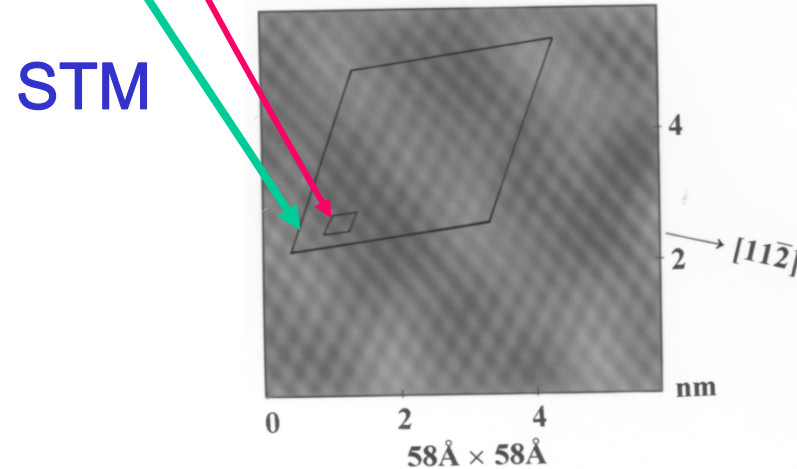
Case study: 1 ML of FeO on Pt(111): A combined LEED, STM, XPD study

Galloway et al., Surf. Sci. 198, 127 ('93);
J. Vac. Sci. Tech. A12, 2302 ('94).
Y.J. Kim et al.,
Phys. Rev. B 55, R 13448 ('97);
Surf. Sci. 416, 68 ('98)

(a) Low energy electron diffraction



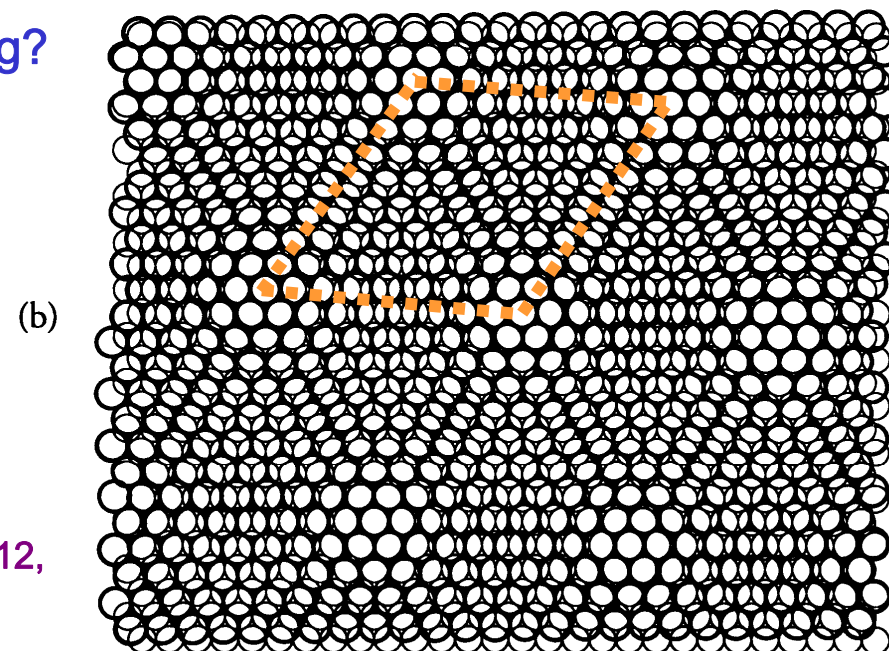
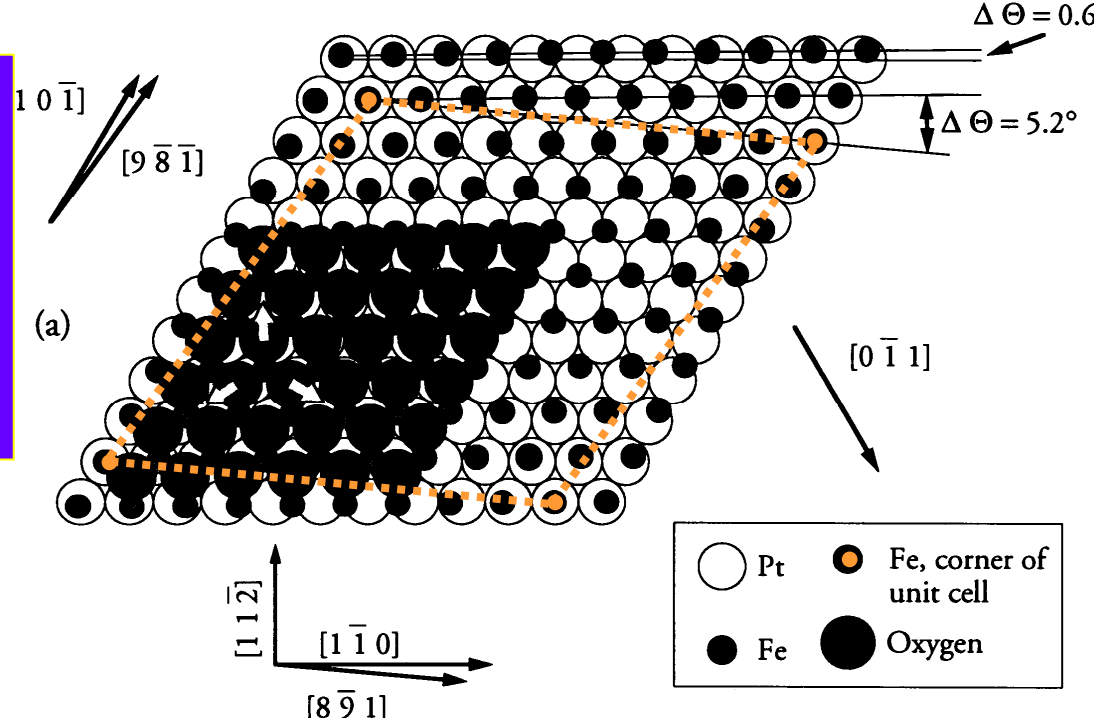
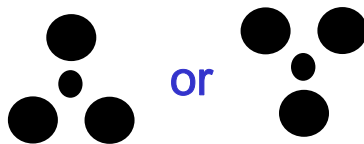
(b) Scanning tunneling microscopy



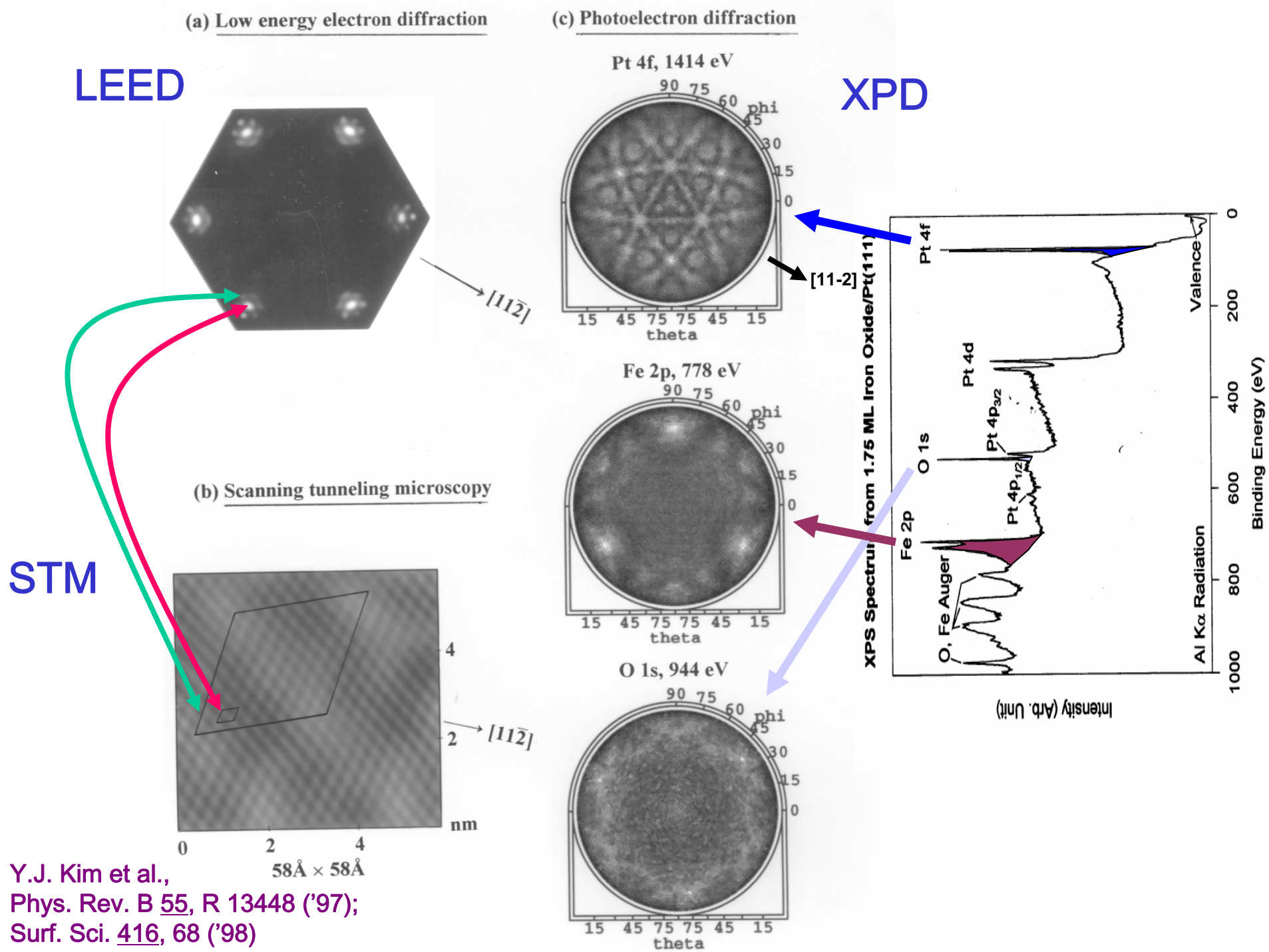
1 ML of FeO
on Pt(111):
Structural model
from
LEED and STM

Remaining
Questions:

- Is Fe or O on top?
- Fe-O interlayer spacing?
- Fe-O orientation?

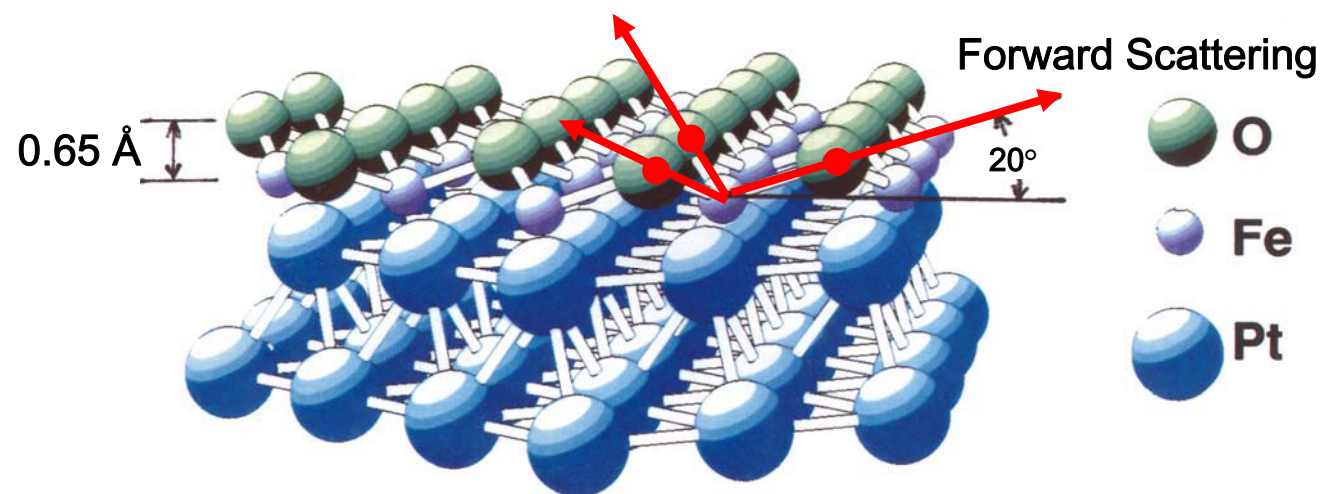
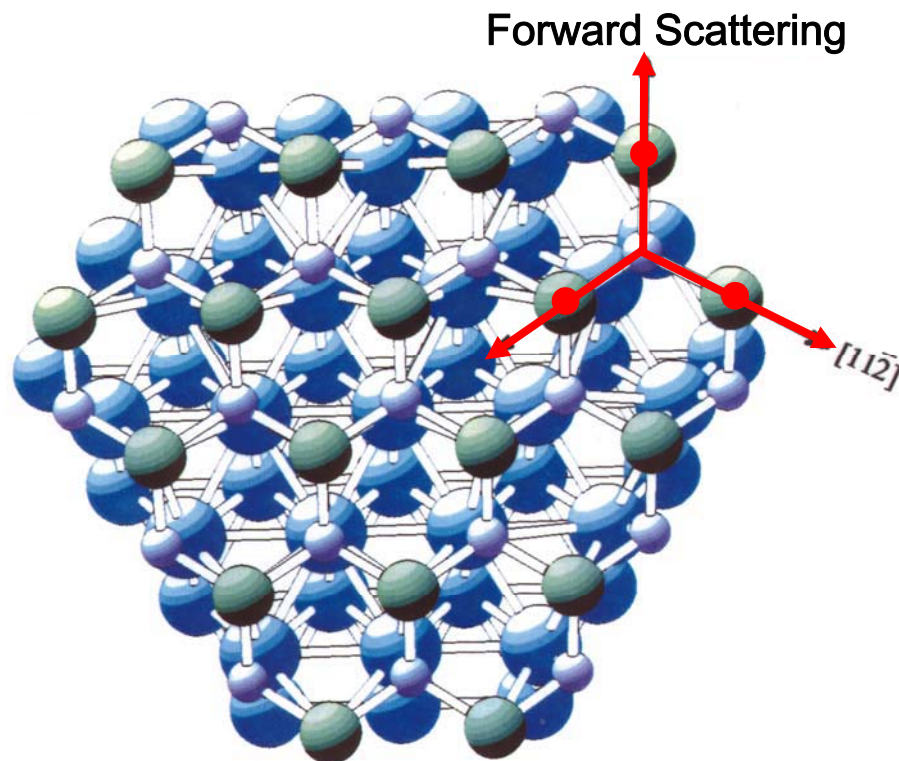


Galloway et al., Surf. Sci. 198,
127 ('93); J. Vac. Sci. Tech. A12,
2302 ('94).



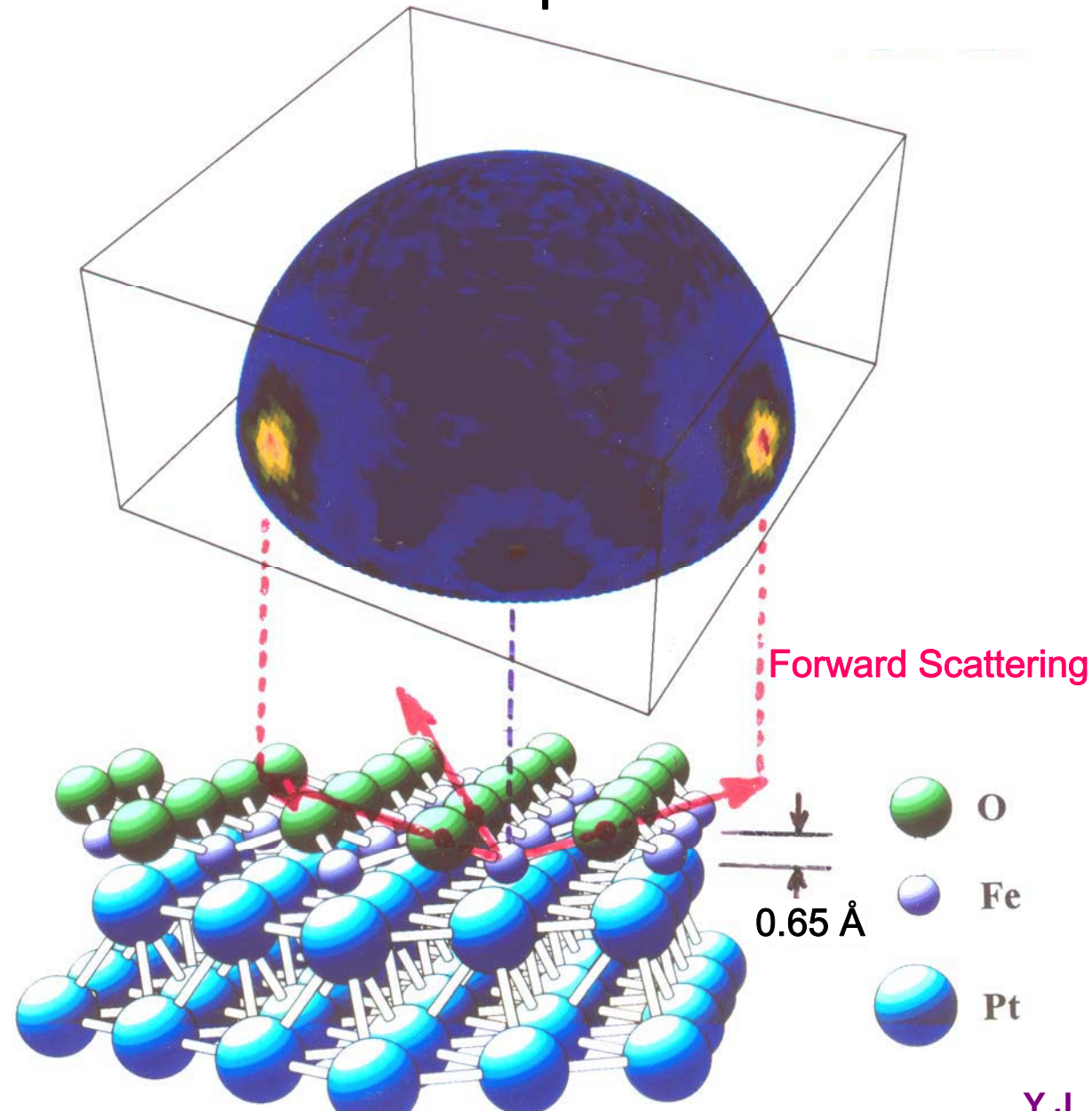
Y.J. Kim et al.,
 Phys. Rev. B 55, R 13448 ('97);
 Surf. Sci. 416, 68 ('98)

FeO/Pt(111)



- O
- Fe
- Pt

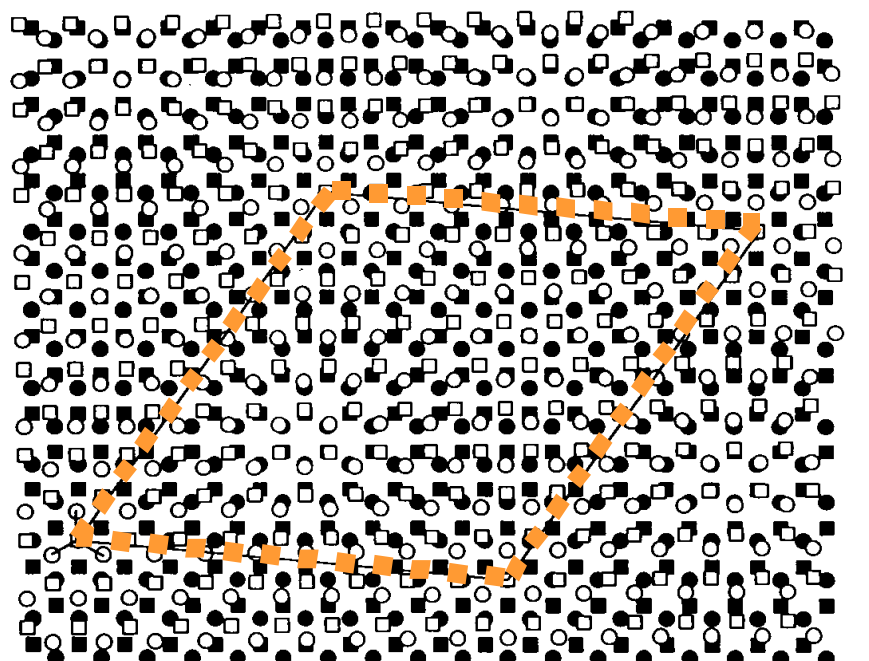
X-ray Photoelectron Diffraction: Fe 2p from 1ML FeO on Pt(111)



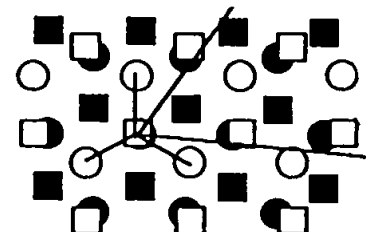
Y.J. Kim et al.
Phys. Rev. B 55, R 13448 ('97)

Permits selecting favored domain of growth—2nd layer Pt effect

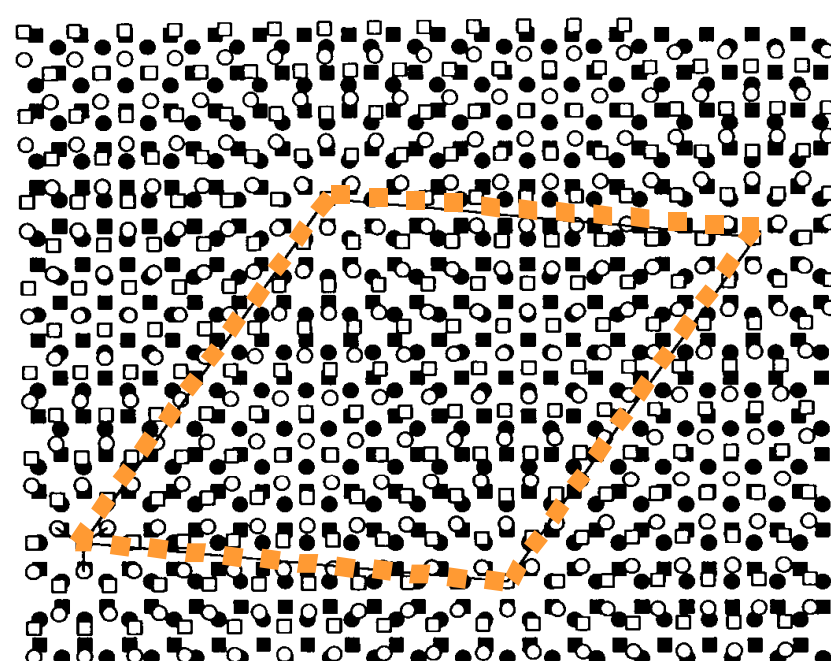
(a) FeO/Pt(111) - Favored



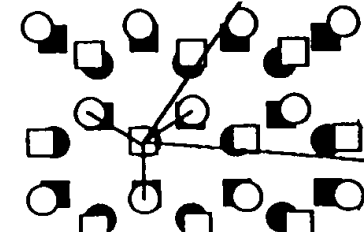
● Top Pt ○ O
■ 2nd Pt □ Fe
→ [112̄]



(b) FeO/Pt(111) - Unfavored

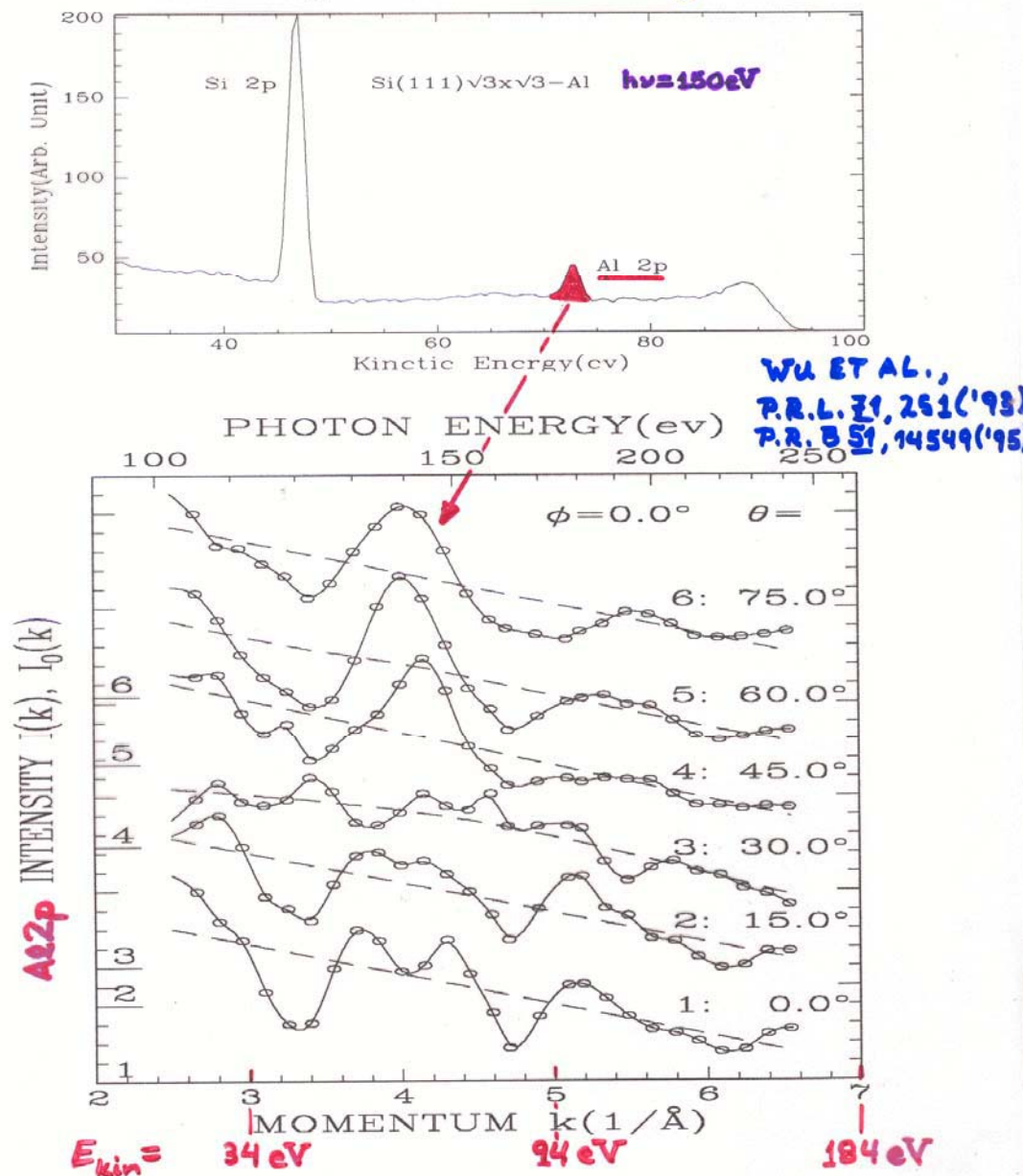


● Top Pt ○ O
■ 2nd Pt □ Fe
→ [112̄]



SCANNED-ENERGY PHOTOELECTRON DIFF.
 $(\sqrt{3} \times \sqrt{3})$ Al on Si(111)

* 41 diffraction curves χ taken from Al 2p } ~1100 DATA POINTS
 * $\theta = 0 \sim 70^\circ, \varphi = 0 \sim 60^\circ$



Outline

Surface, interface, and nanoscience—short introduction

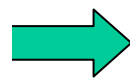
Some surface concepts and techniques→photoemission

Synchrotron radiation: experimental aspects

Electronic structure—a brief review

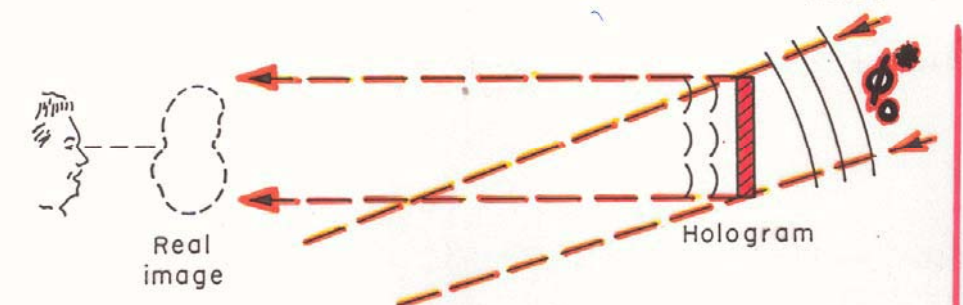
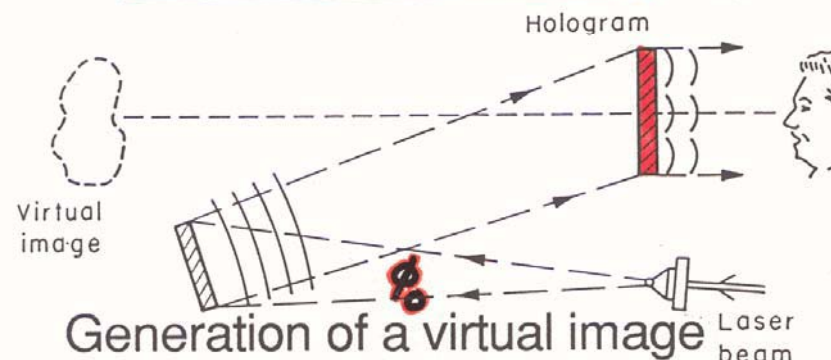
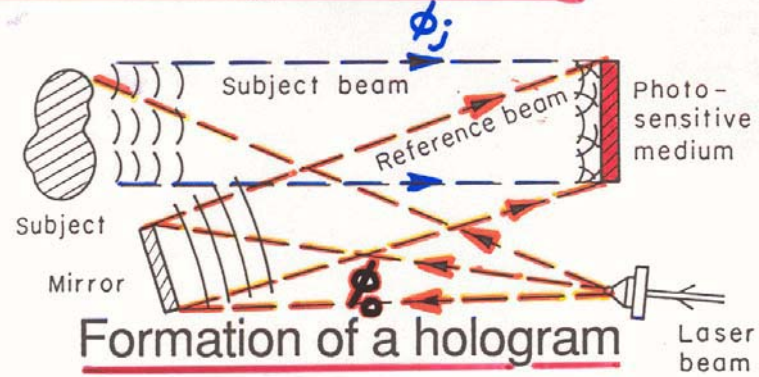
**The basic synchrotron radiation techniques:
more experimental and theoretical details**

Valence-level photoemission

 **Core-level photoemission:
Photoelectron diffraction → Photoelectron holography**

**Photoemission with high ambient pressure
around the sample**

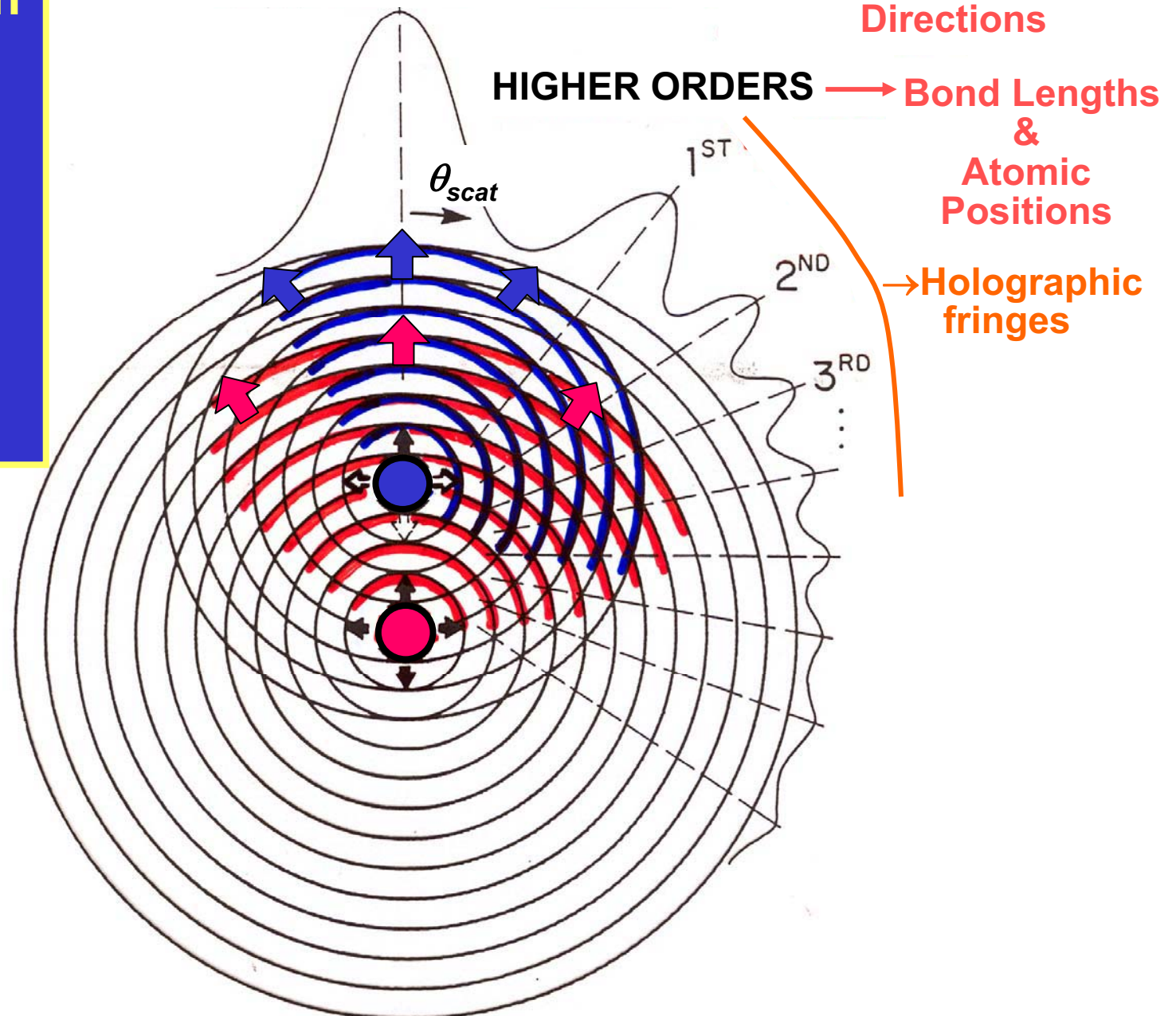
CLASSIC OPTICAL HOLOGRAPHY:



In electron emission holography,
reference is outgoing spherical &
conjugate is incoming spherical

Photoelectron
diffraction →
holography:
Element-
specific
short-range
atomic
structure

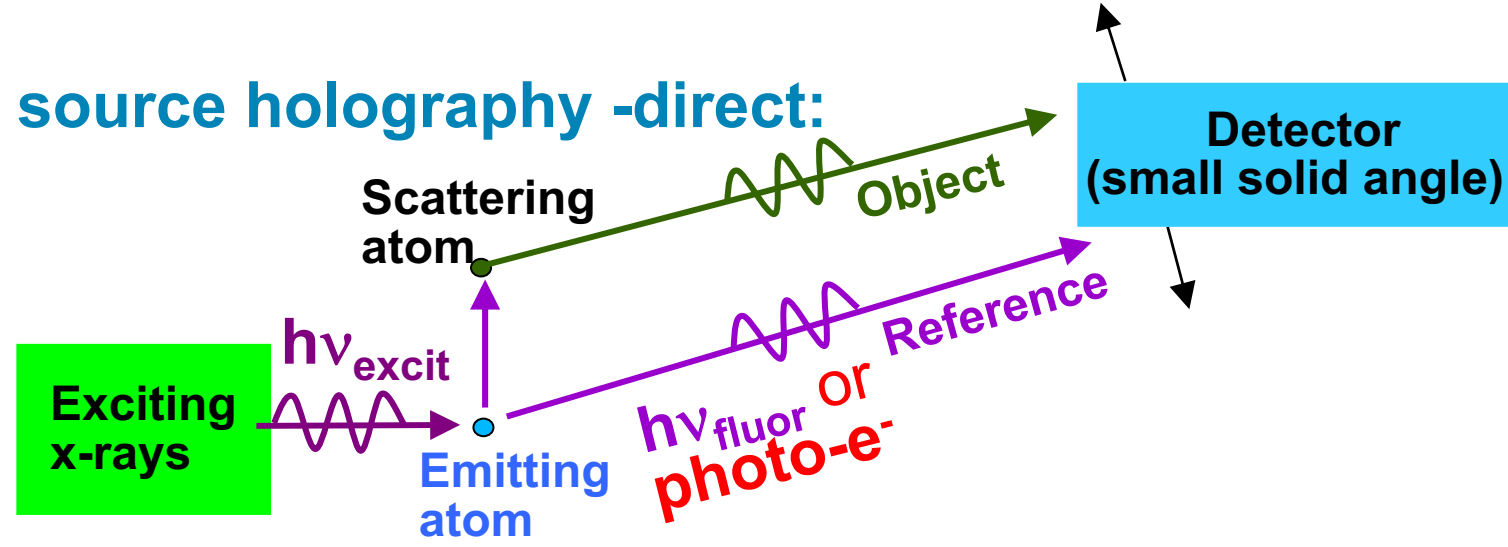
FORWARD SCATT. = “0TH ORDER” → Bond & Low-Index Directions



Principles of photoelectron and x-ray fluorescence holography:

(a) Inner source holography -direct:

ALS
undulator
beamlines
7.0.2, 4.0.2



Recent overviews:

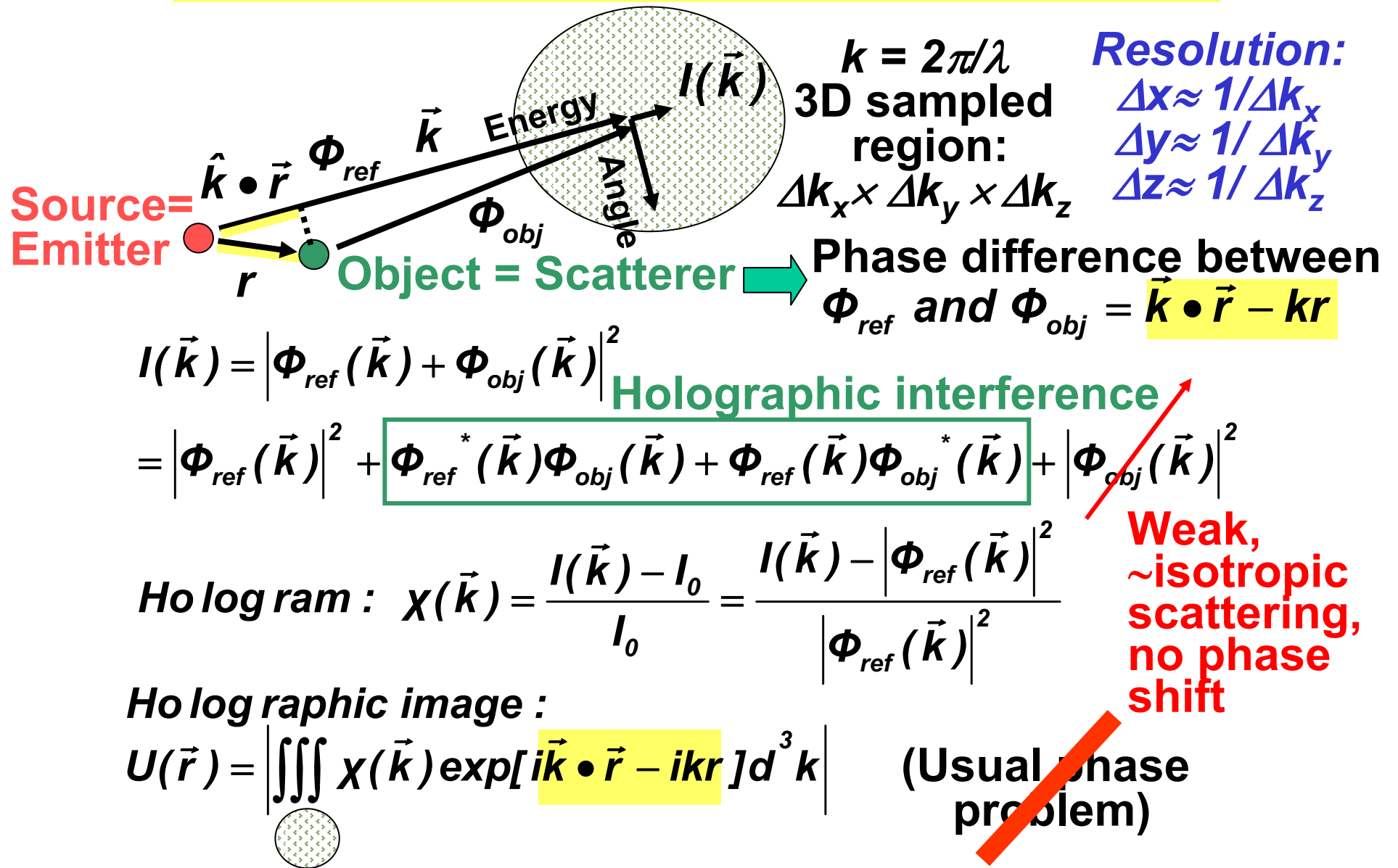
G. Faigel and M. Tegze, Rep. Prog. Phys. 62, 355 (1999)

Adams et al., Phys. Stat. Sol. (b) 215, 757 (1999)

C.S.F., M.A Van Hove, et al., J. Phys. B Cond. Matt. 13, 10517 (2001)

The basic imaging ideas

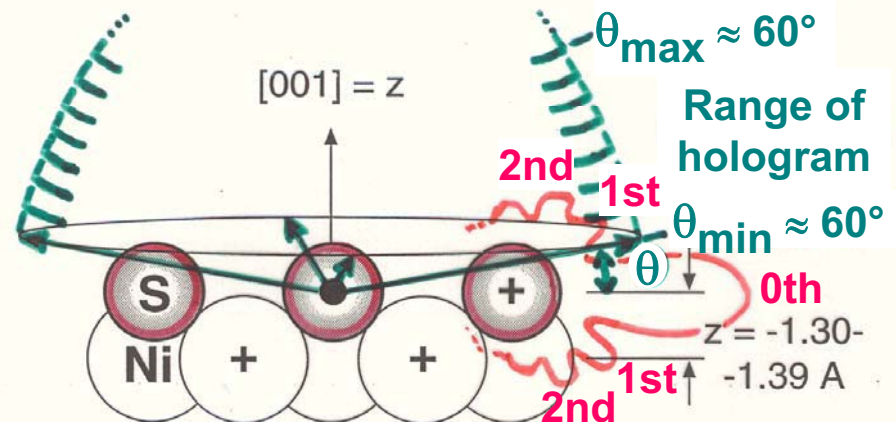
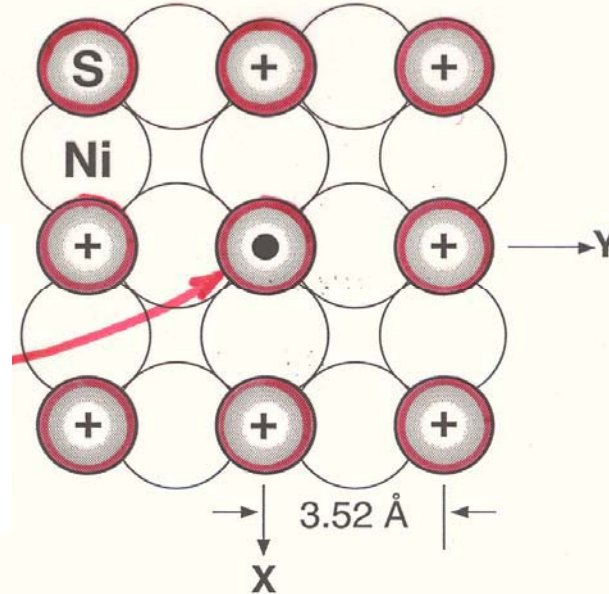
(Gabor; Helmholtz-Kirchoff; Wolf; Szöke; Barton-Tong)



Inside-source PH- first adsorbate: $\text{S}/\text{Ni}(100)$

Typical S emitter
 $h\nu = 1486.6 \text{ eV} \rightarrow$
 $E_{\text{kin}} = 1327 \text{ eV}$

c(2x2)S on Ni(001) A Well-Defined Test Case

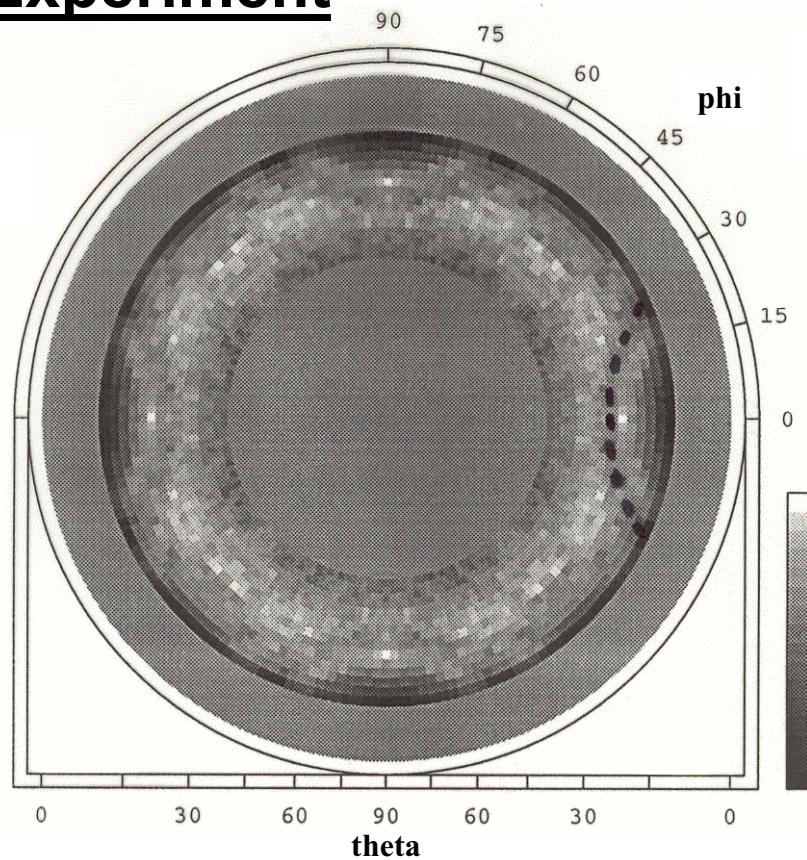


Thevuthasan et al.,
Phys. Rev. Lett. 70, 595 ('93)

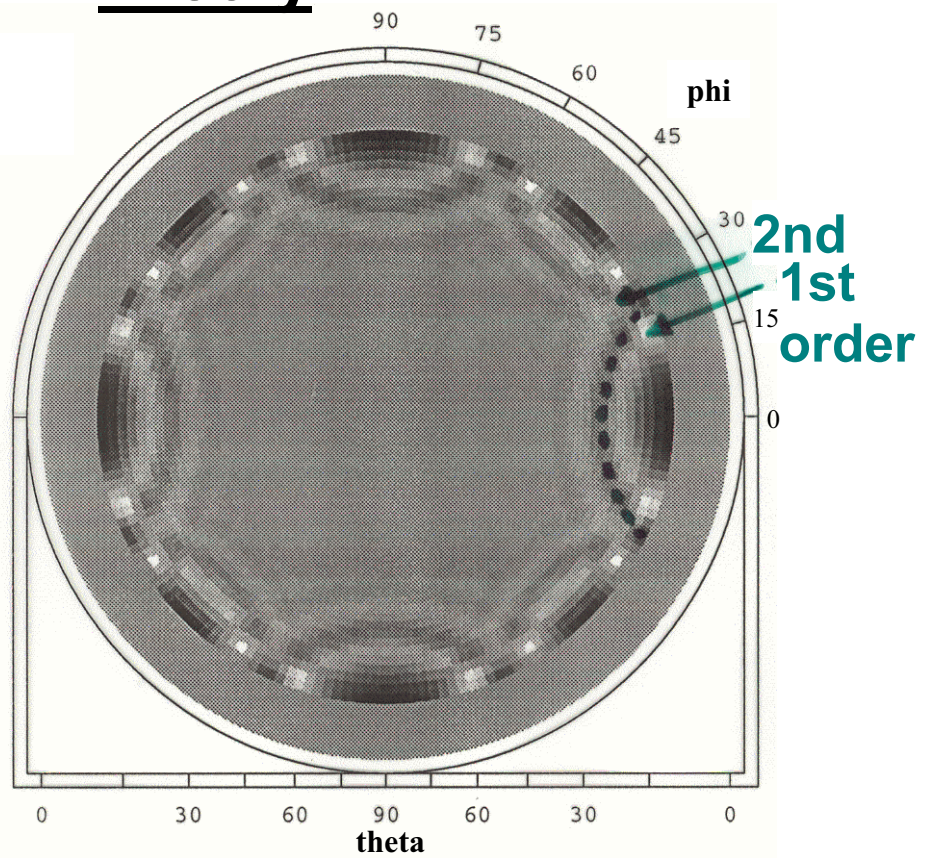
XBL 925-5252

Holograms: S/Ni(001)

Experiment

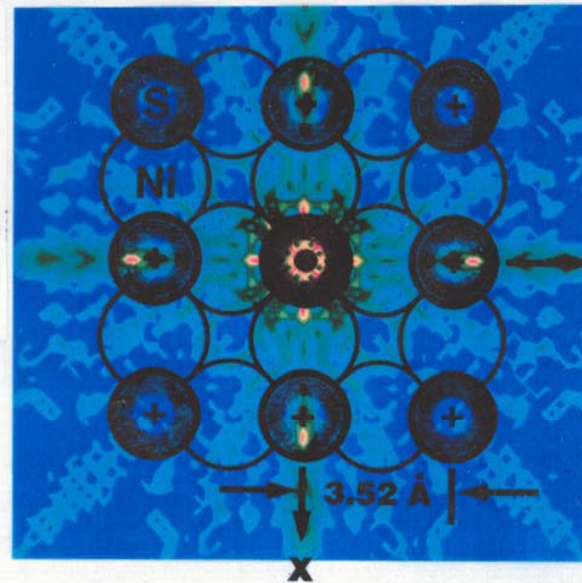


Theory

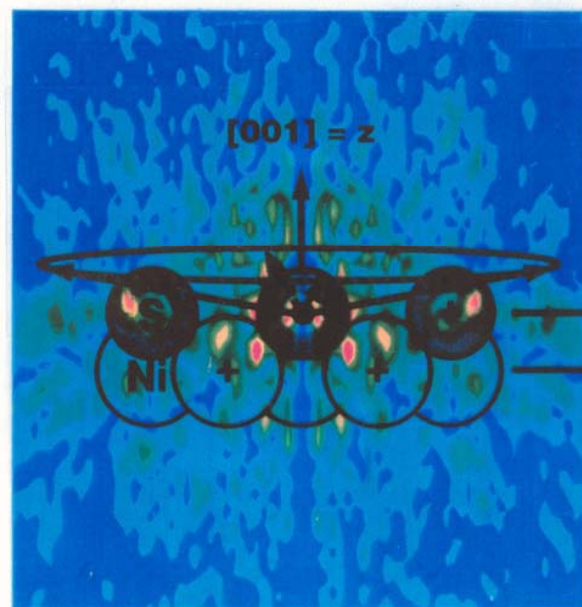


Holographic Images: S/Ni(001)

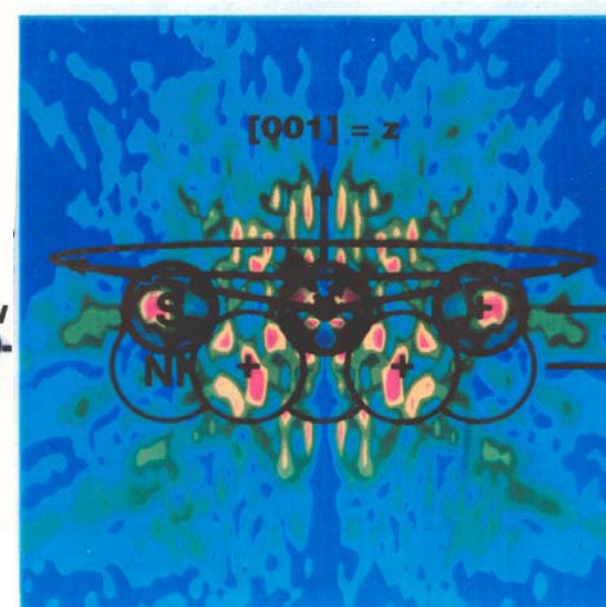
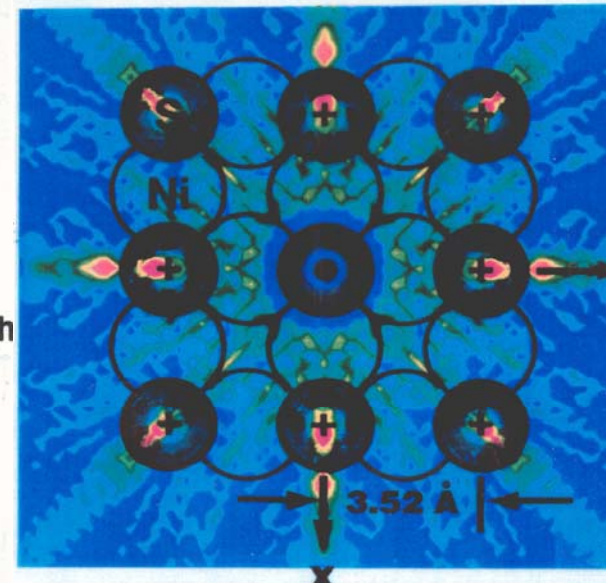
Fourier transform with scatt. wave correc. in sulfur(xy) plane



Fourier transform with scatt. wave correc. in yz plane



EXPT.



Thevuthasan et al., Phys. Rev. Lett. 70, 595 ('93)

Derivative photoelectron holography: As and Si emission from As/Si(111):

$$U(\vec{r}) = \left| \iiint \chi(\vec{k}) \exp[i\vec{k} \cdot \vec{r} - ikr] d^3k \right|$$

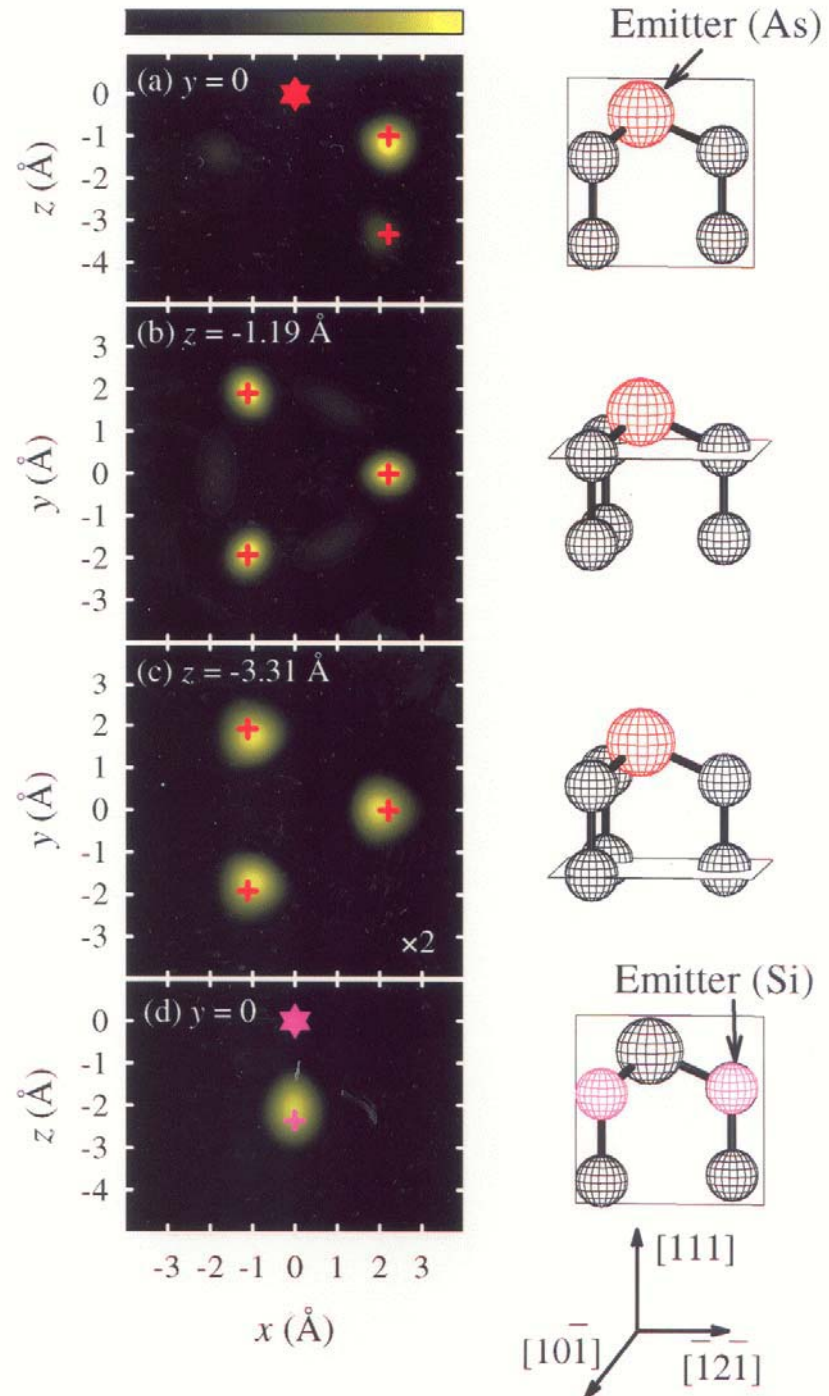
$$\text{with } \chi = \frac{I(\vec{k}) - I_0}{I_0}$$

and $I(\vec{k})$ from integration of logarithmic derivative

$$L(hv, \hat{k}) = \frac{I(hv + \delta, \hat{k}) - I(hv - \delta, \hat{k})}{[I(hv + \delta, \hat{k}) + I(hv - \delta, \hat{k})]\delta}$$

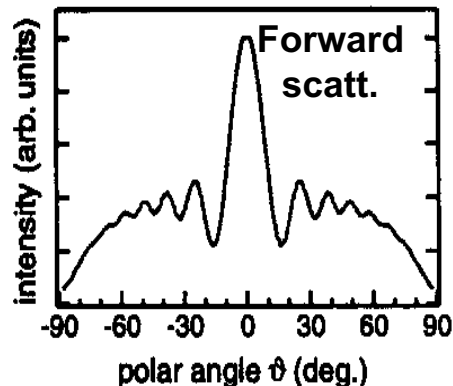
$$I(\vec{k}) \equiv I(k, \hat{k}) = A \int L(hv, \hat{k}) d^3k$$

Luh, Miller, Chiang, PRL
81, 4160 (1998)

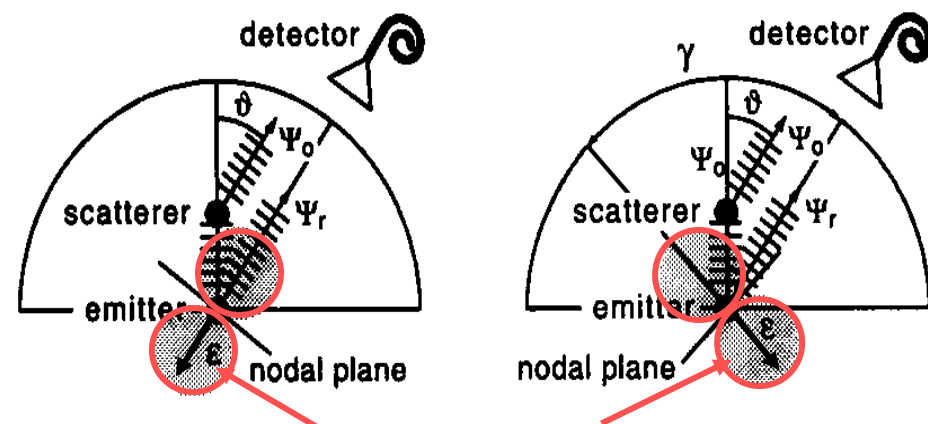
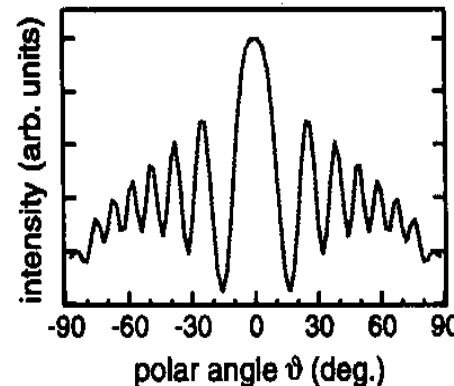


Single-atom holograms

a) far node geometry ($\gamma = 0^\circ$)



b) near node geometry ($\gamma = 80^\circ$)

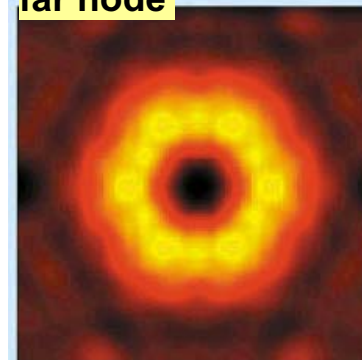


$$M(\vec{k}, \vec{r}) \propto \sqrt{\text{photoe}^- \text{ cross sec.}} = \hat{\epsilon} \cdot \hat{k}$$

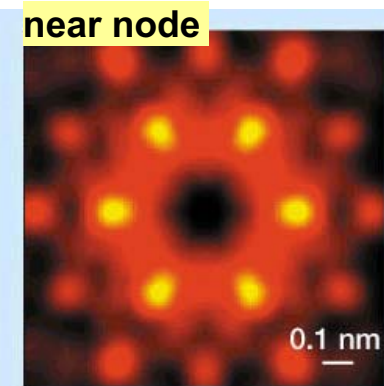
Wider et al. PRL
86, 2337 (2001)

Near-node photoelectron holography: Al 2s emission from Al(111)

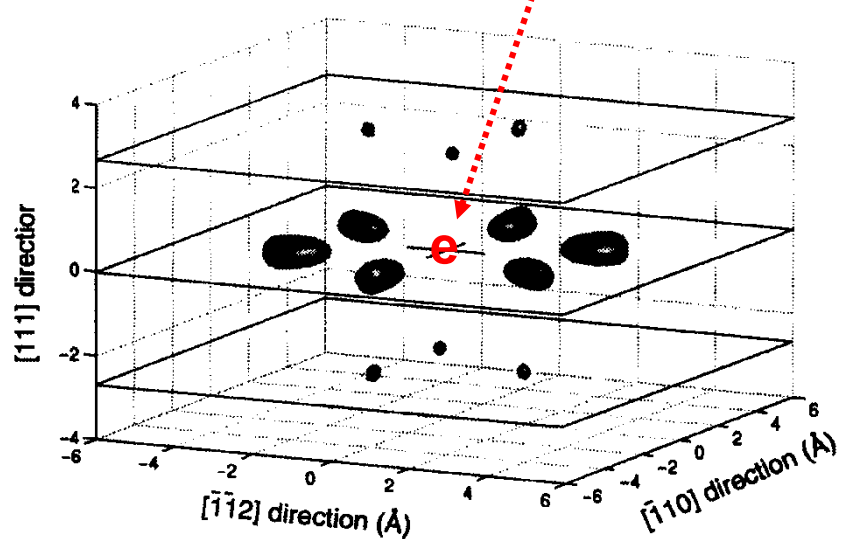
far node



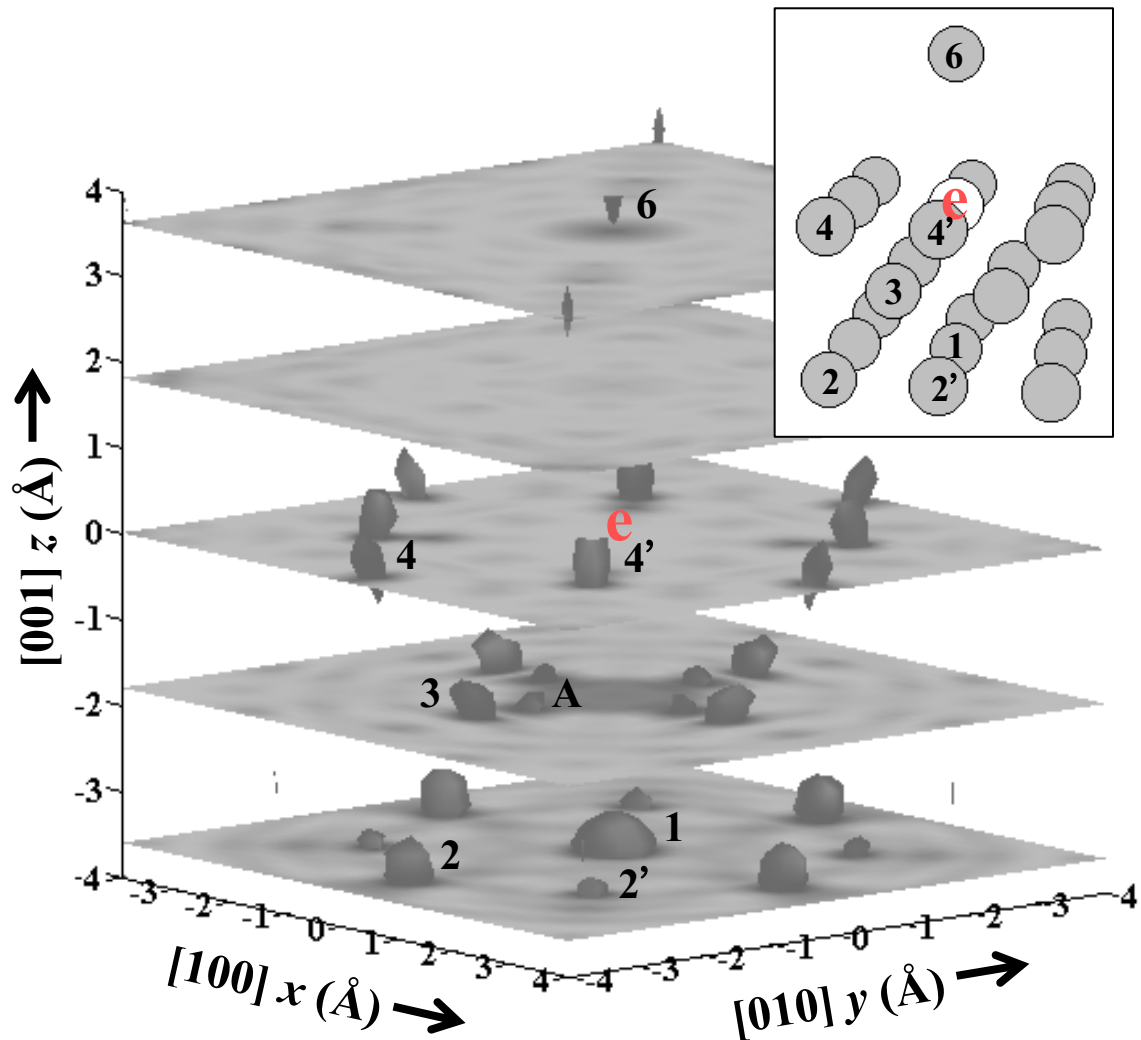
near node



Images around
typical Al emitter



Cu 3p-Cu(001)-- differential photoelectron holography



Imaging of back, side, (and fwd.) scattering atoms
(Omori et al., PRL 88, 055504 ('02) and
animations at <http://electron.lbl.gov/marchesini/dph>)

Outline

Surface, interface, and nanoscience—short introduction

Some surface concepts and techniques→photoemission

Synchrotron radiation: experimental aspects

Electronic structure—a brief review

**The basic synchrotron radiation techniques:
more experimental and theoretical details**

Valence-level photoemission

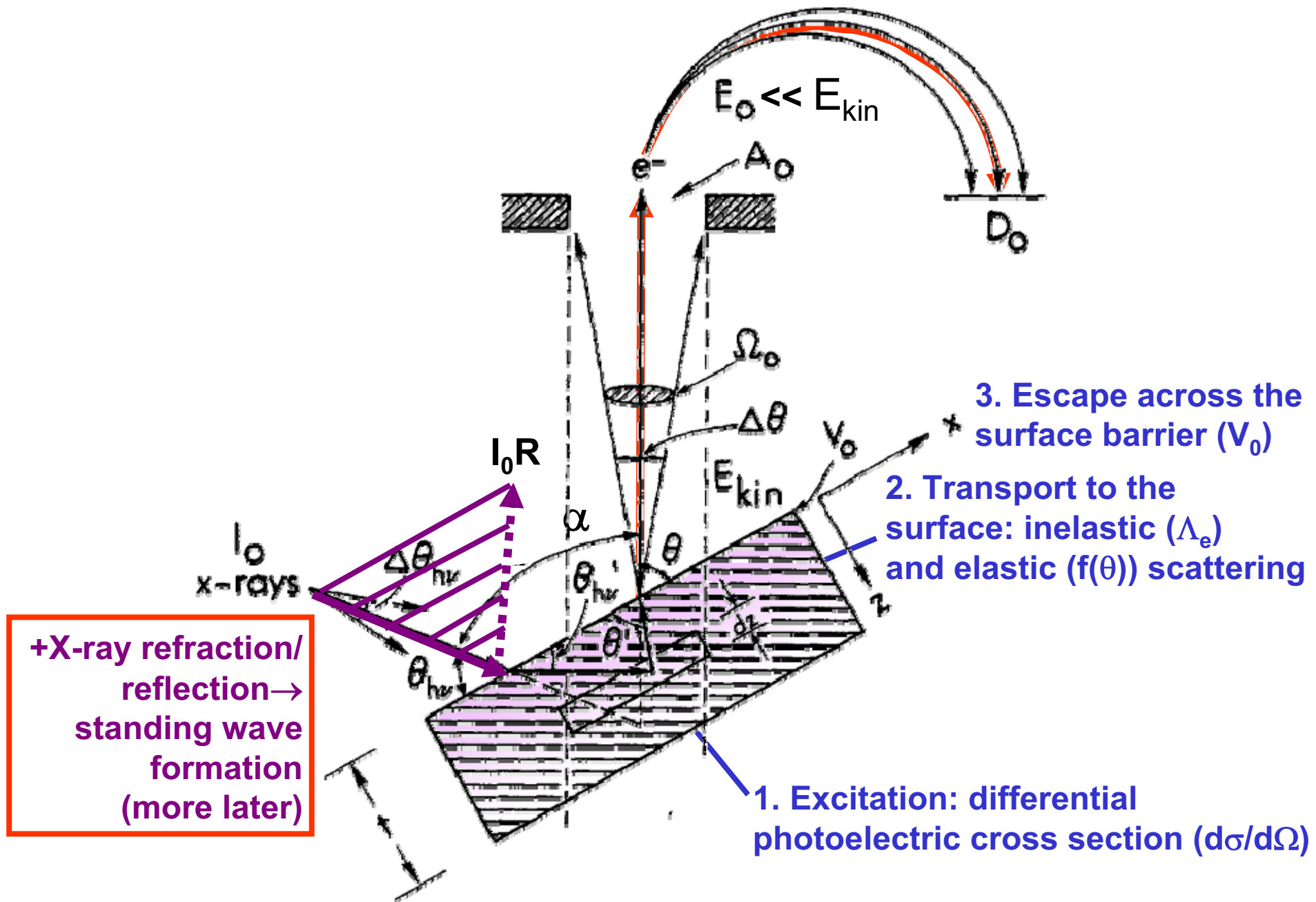


Core-level photoemission:

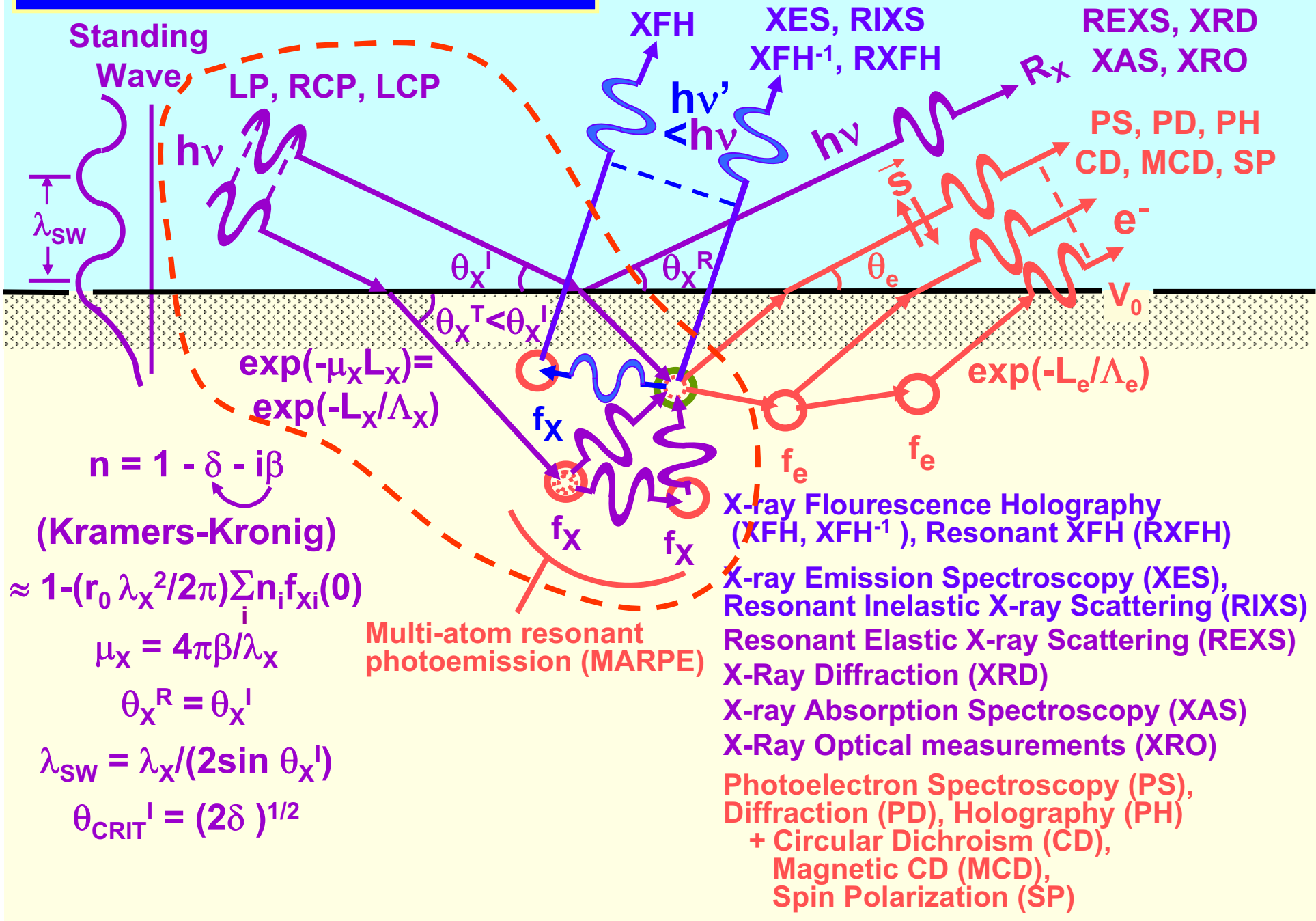
X-ray optical and standing-wave effects on intensities

**Photoemission with high ambient pressure
around the sample**

PHOTOELECTRON INTENSITIES—THE 3-STEP MODEL



Some basic measurements:



A LITTLE X-RAY OPTICS

(E.G. See pp. 1-38, 1-44, 5-18-5-19 in X-Ray Data Booklet)

Index of refraction = $n = 1 - \delta - i\beta$

$\delta = +$ no. = refractive decrement $\ll 1$ (**Sometimes negative through absorption resonances**)

$\beta = +$ no. = absorptive decrement $\ll 1$

δ and β linked by Kramers-Kronig transform

n also = $1 - (r_e/2\pi)\lambda_{hv}^2 \sum n_i f_i (0 = \text{fwd. scatt.})$

$$r_e = \text{classical electron radius} \\ = e^2/4\pi\epsilon_0 m_e e^2 = 2.817 \times 10^{-15} \text{ m}$$

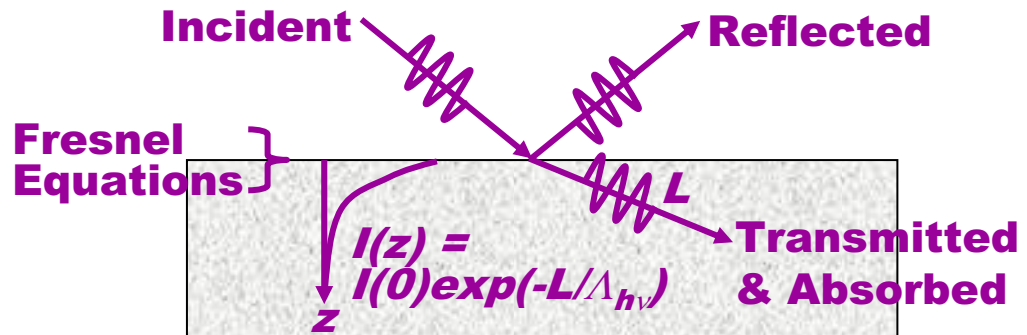
λ_{hv} = x-ray wavelength

n_i = no. i atoms per unit volume

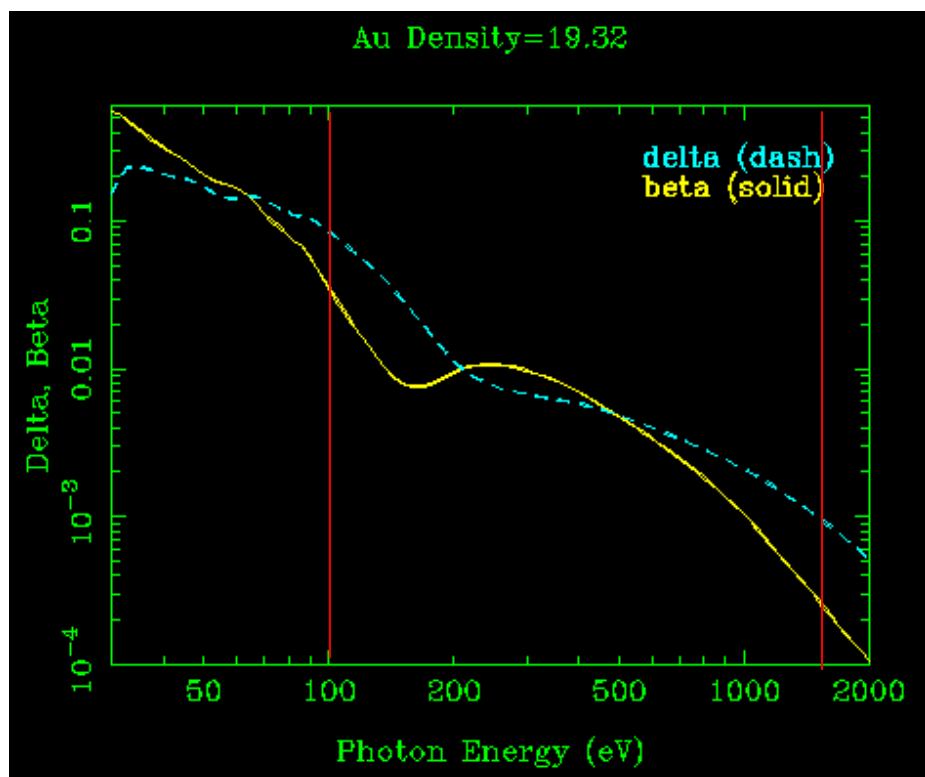
f_i = x-ray scattering factor for ith type of atom, in forward direction

Exponential absorption length = $l_{abs} = \lambda_{hv}/(4\pi\beta) = \Lambda_{hv}$

θ_{CRIT} = critical grazing angle at which reflectivity begins ($R \approx 0.20$)
 $= [2\delta]^{0.5}$



Online data and calculations at:
http://www-cxro.lbl.gov/optical_constants/



X-ray scattering factor:
 $f_i = \text{Ref}_i + i(\text{Imf}_i)$

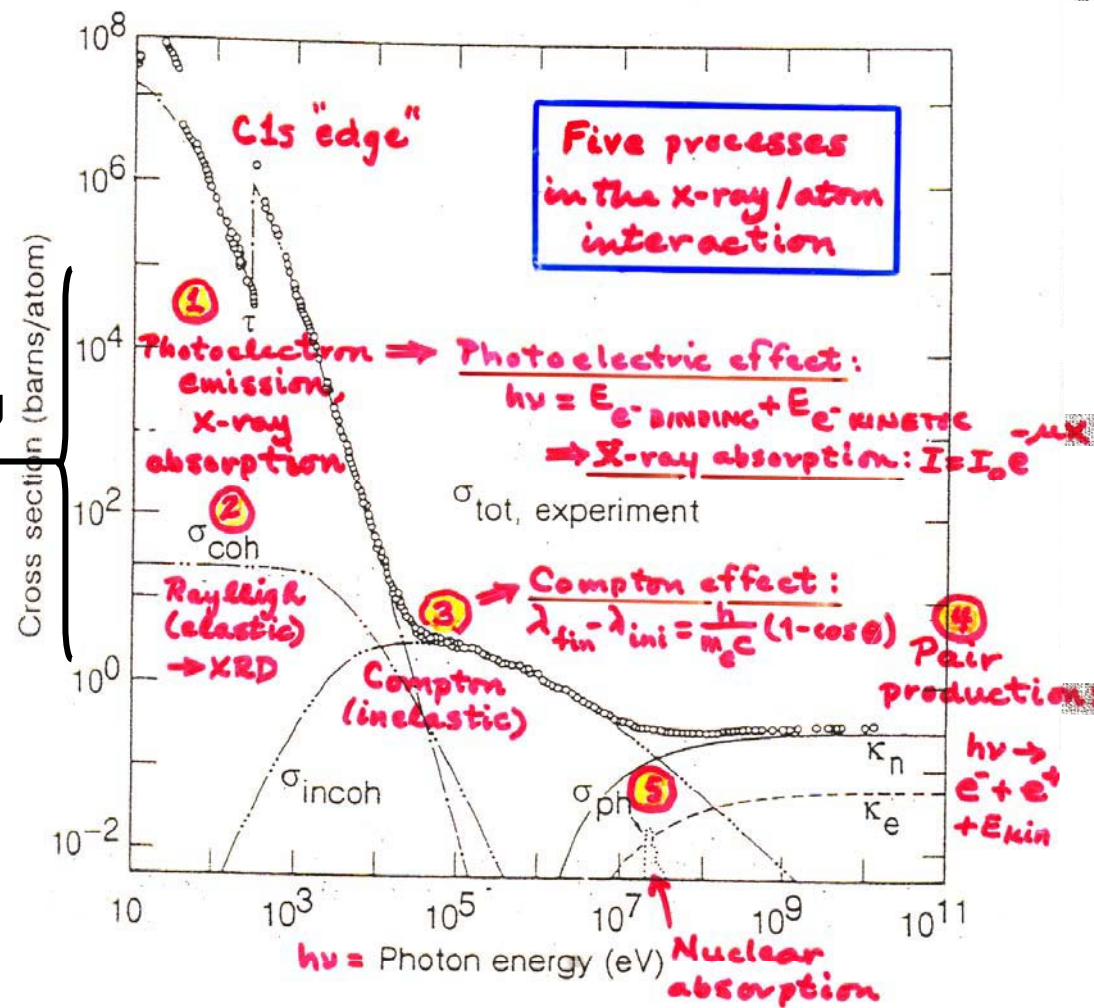


Fig. 3-1. Total photon cross section σ_{tot} in carbon, as a function of energy, showing the contributions of different processes: τ , atomic photo-effect (electron ejection, photon absorption); σ_{coh} , coherent scattering (Rayleigh scattering—atom neither ionized nor excited); σ_{incoh} , incoherent scattering (Compton scattering off an electron); κ_n , pair production, nuclear field; κ_e , pair production, electric field; σ_{ph} , photonuclear absorption (nuclear absorption, usually followed by emission of a neutron or other particle). (From Ref. 3; figure courtesy of J. H. Hubbell.)



Website

X-Ray Interactions with Matter

Contents

- [Introduction](#)
- Access the [atomic scattering factor](#) files.
- Look up [x-ray properties of the elements](#).
- The [index of refraction](#) for a compound material.
- The x-ray [attenuation length](#) of a solid.
- X-ray transmission
 - Of a [solid](#).
 - Of a [gas](#).
- X-ray reflectivity
 - Of a [thick mirror](#).
 - Of a [single layer](#).
 - Of a [bilayer](#).
 - Of a [multilayer](#).
- The diffraction efficiency of a [transmission grating](#).
- Related calculations:
 - Synchrotron [bend magnet radiation](#).

NEW! [What's New?](#)

[Other x-ray web resources](#)

These pages utilize *JavaScript*, but the [decaffeinated versions](#) are still available.

Reference

B.L. Henke, E.M. Gullikson, and J.C. Davis. *X-ray interactions: photoabsorption, scattering, transmission, and reflection at E=50-30000 eV, Z=1-92*, Atomic Data and Nuclear Data Tables Vol. **54** (no.2), 181-342 (July 1993).

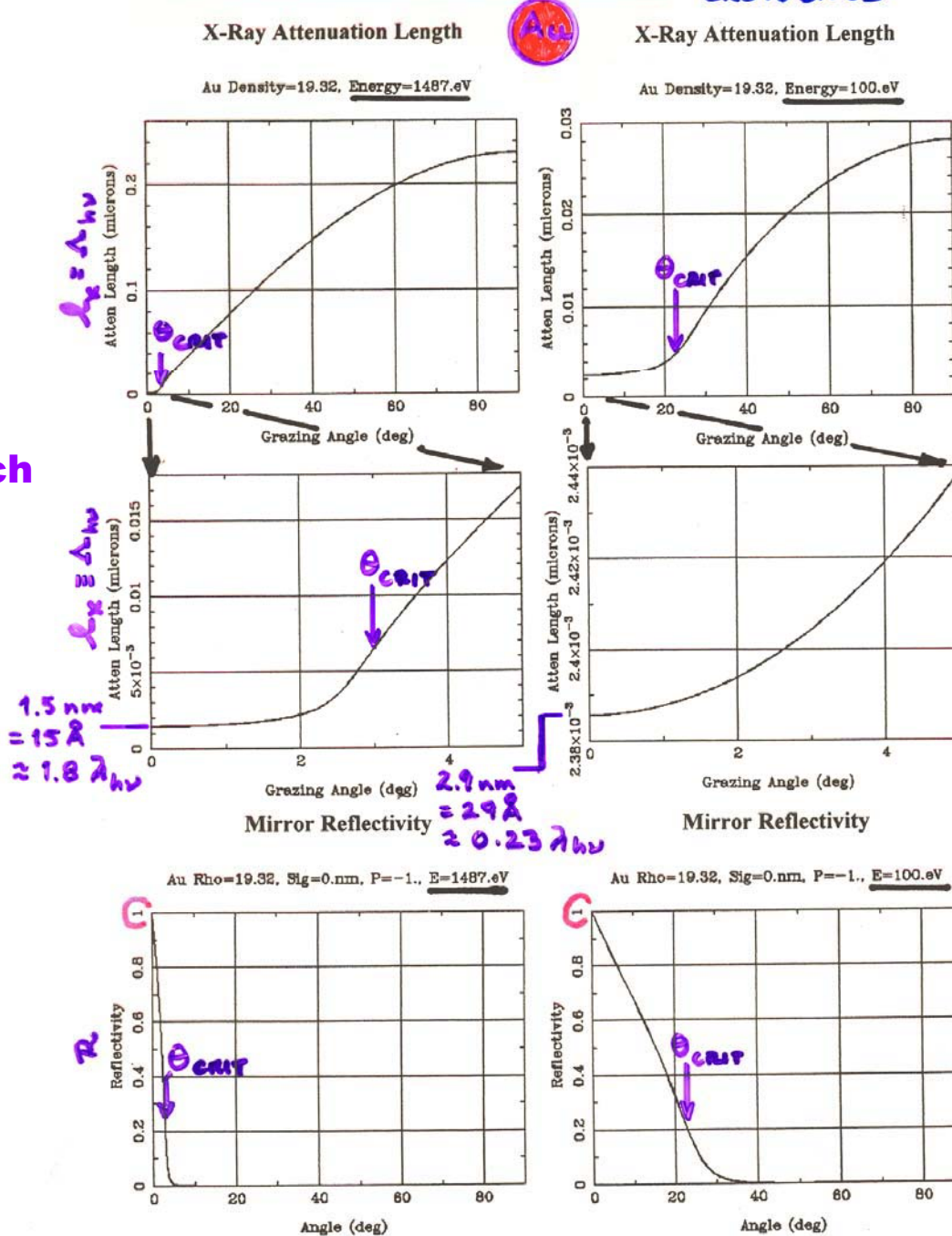
| [CXRO](#) | [ALS](#) |

By Eric Gullikson. Please direct any comments to EMGullikson@lbl.gov
[Server Statistics](#) © 1995-2001

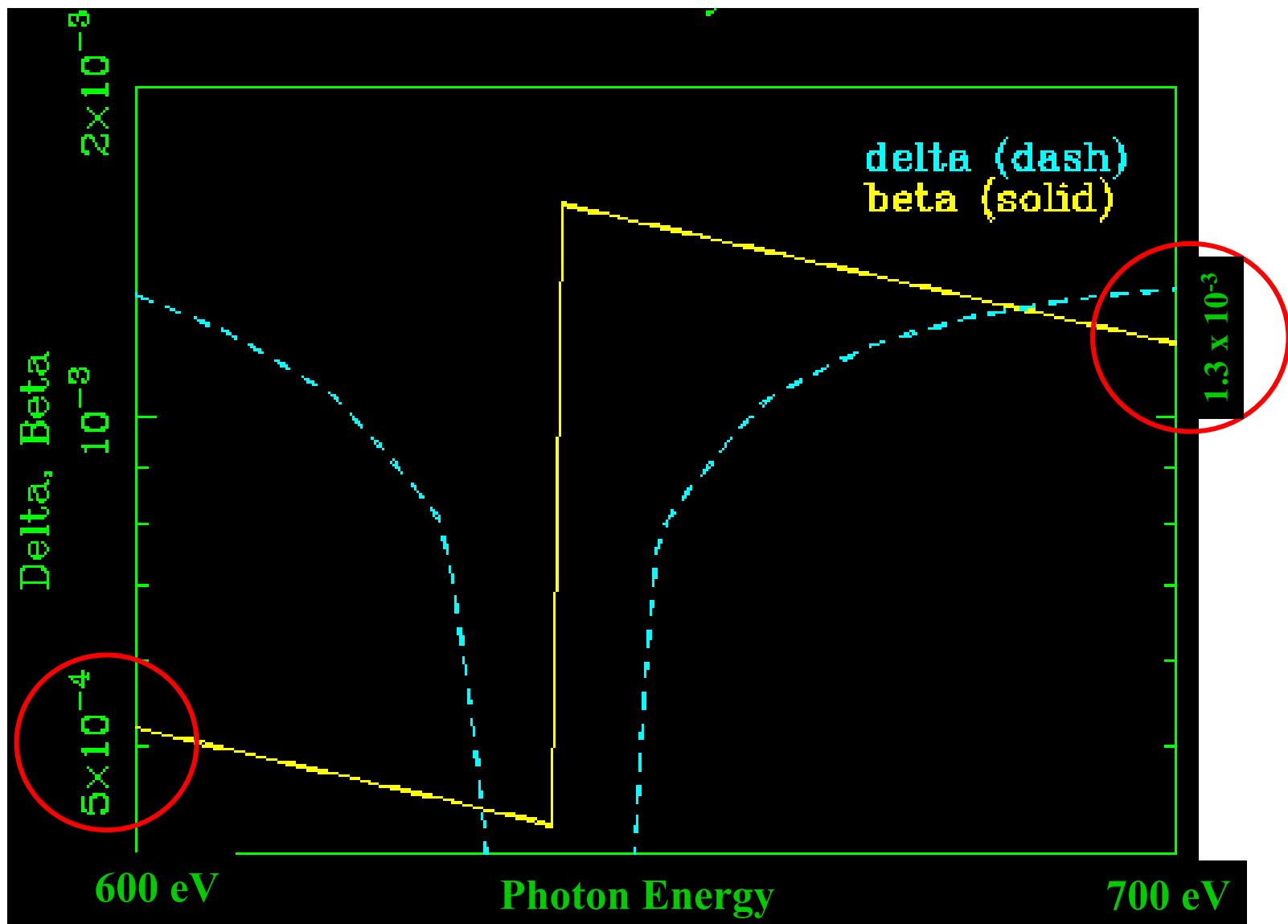
SOME X-RAY OPTICAL EFFECTS: REDUCED PENETRATION DEPTHS AND INCREASED REFLECTIVITY AT GRAZING INCIDENCE ANGLES

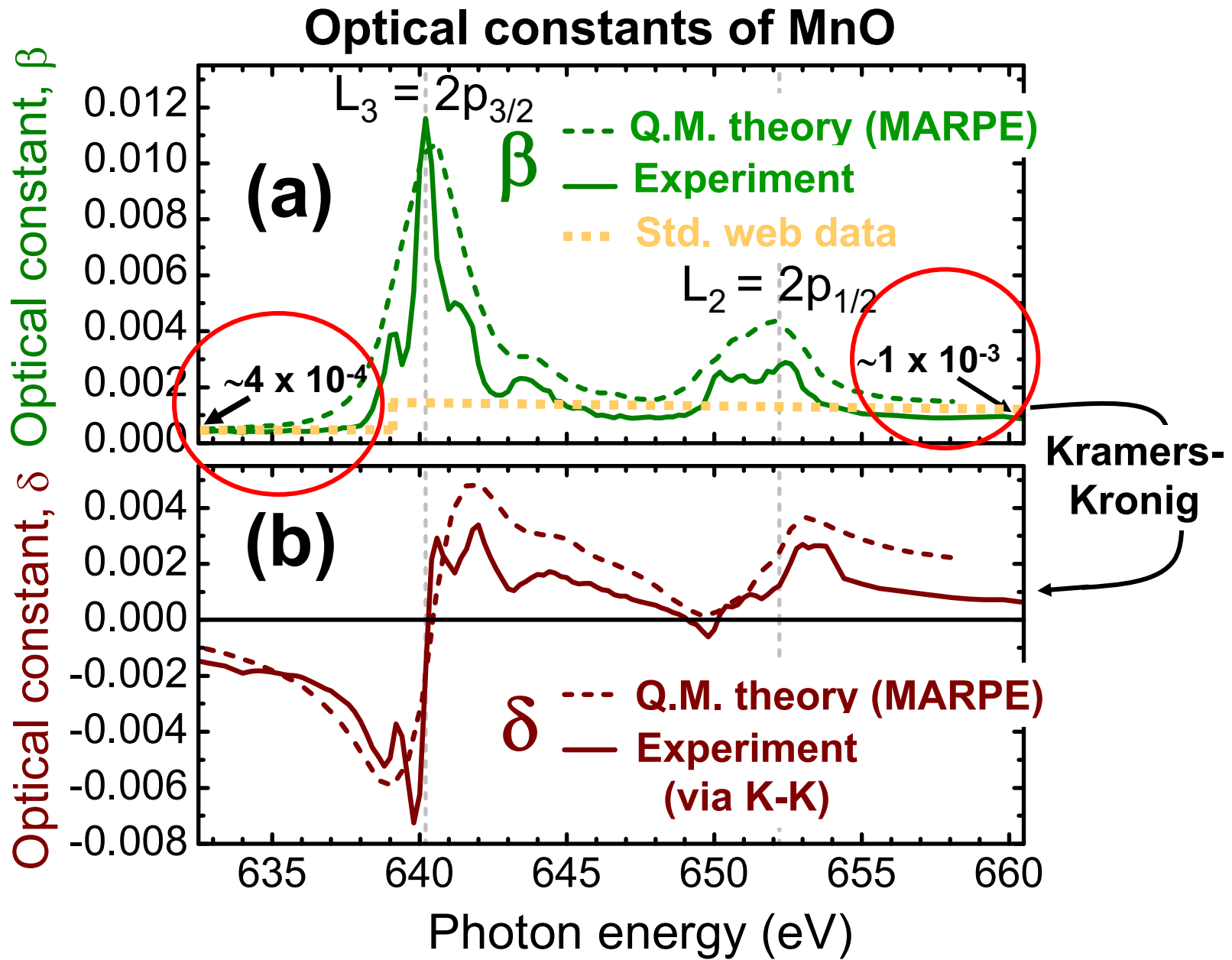
θ_{CRIT} = Grazing angle at which reflectivity begins ($R \approx 0.20$)
 $= [2\delta]^{0.5}$

ENHANCED SURFACE SENSITIVITY @ GRAZING INCIDENCE

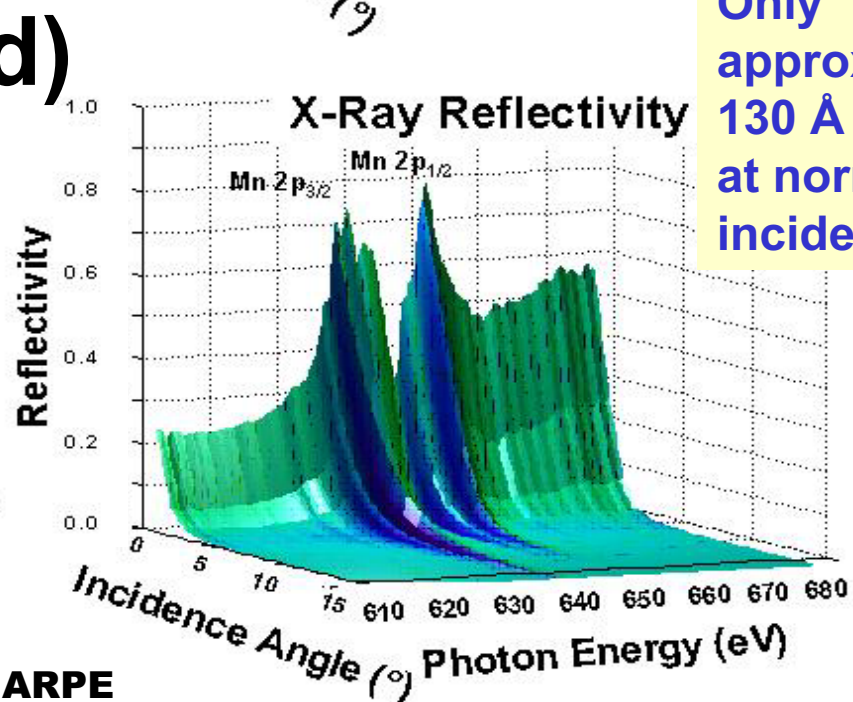
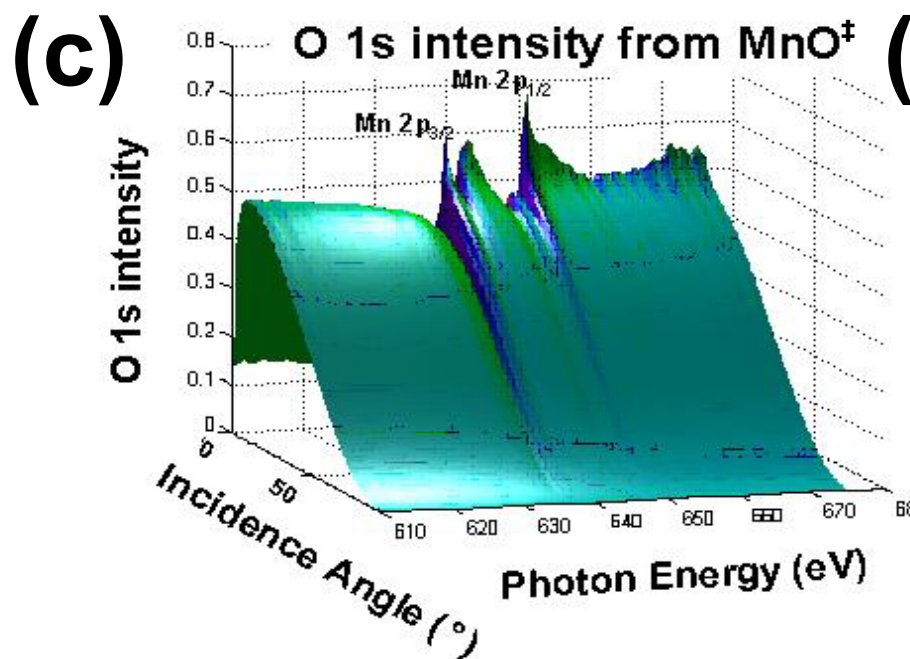
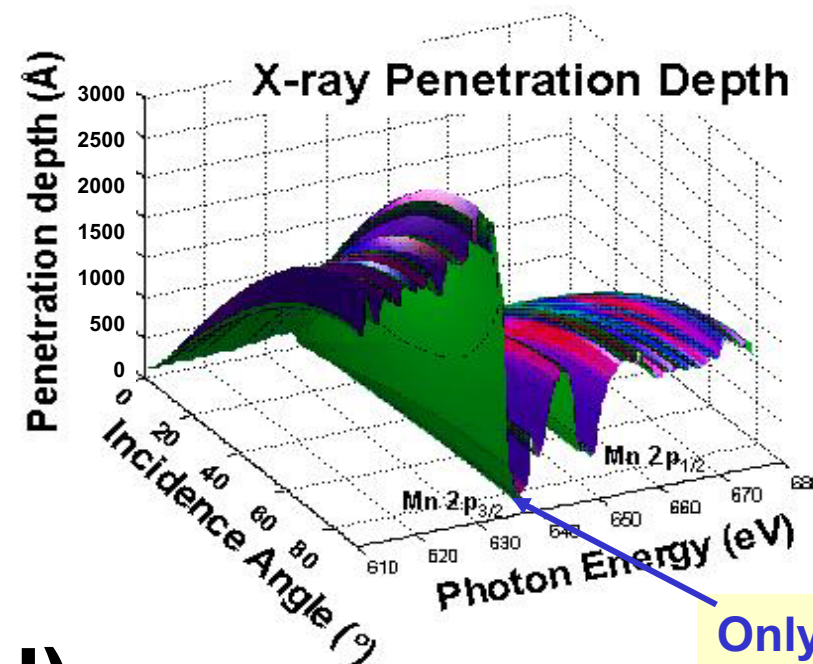
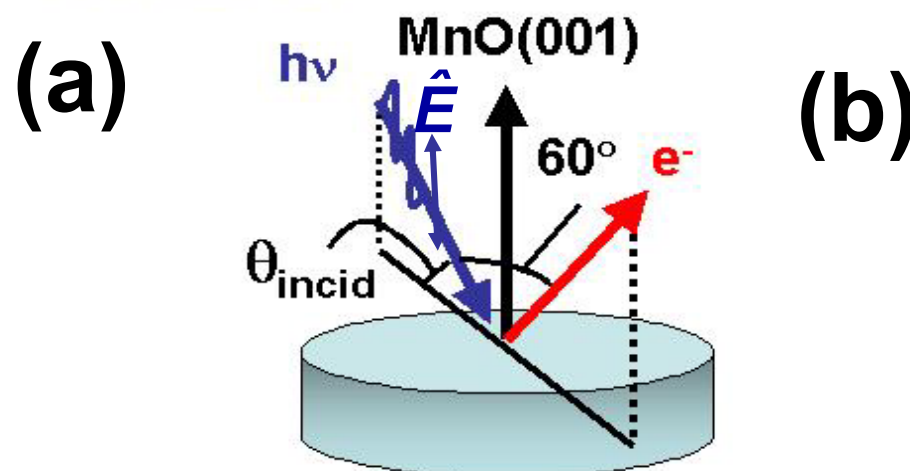


Optical constants through Mn 2p edges of MnO— Web data without absorption peaks





X-ray optical effects through core resonances:



[‡]Aka Multi-Atom Resonant Photoemission = MARPE

Outline

Surface, interface, and nanoscience—short introduction

Some surface concepts and techniques→photoemission

Synchrotron radiation: experimental aspects

Electronic structure—a brief review

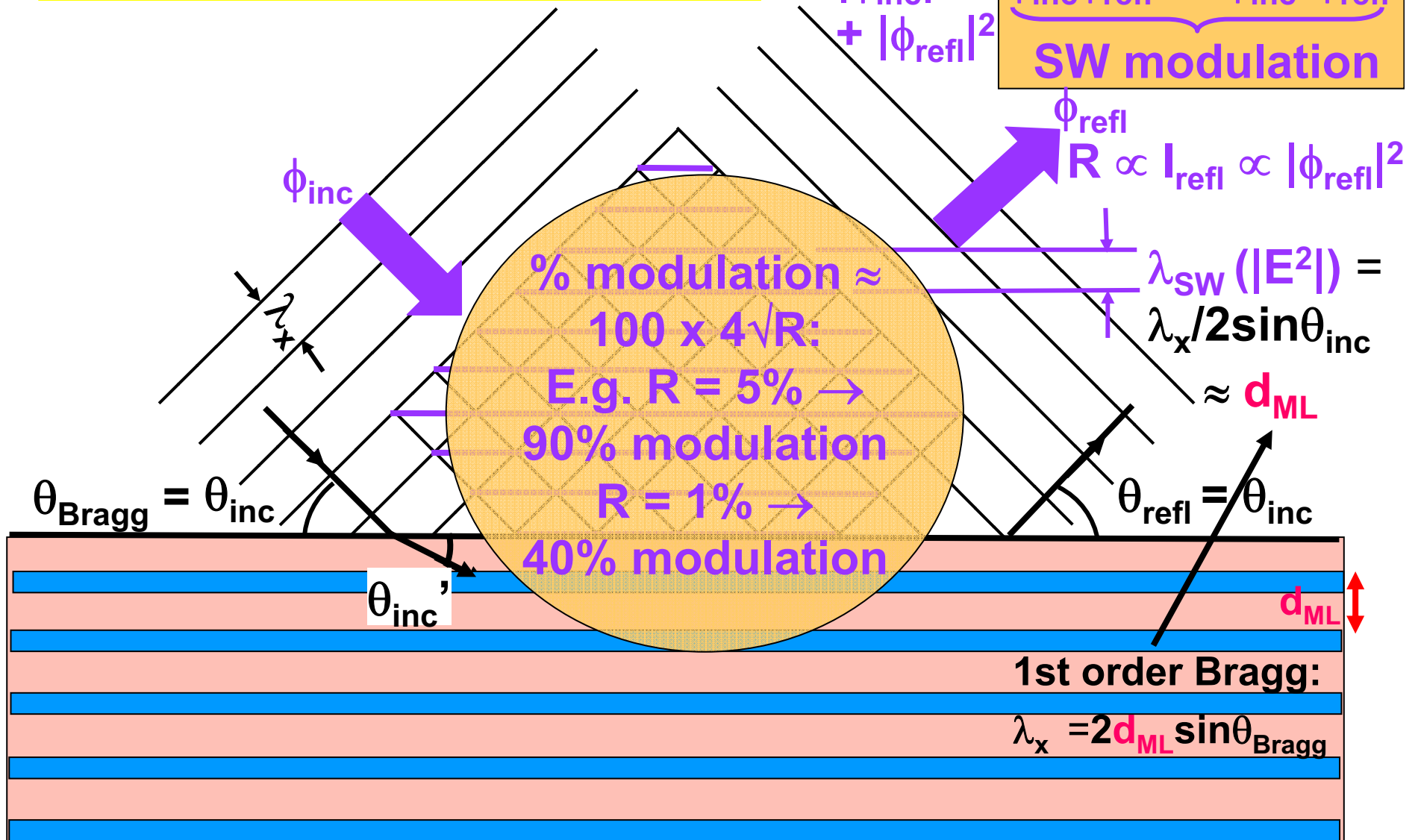
**The basic synchrotron radiation techniques:
more experimental and theoretical details**

Valence-level photoemission

 **Core-level photoemission:
X-ray optical effects on emission→
Use of standing waves to probe buried interfaces**

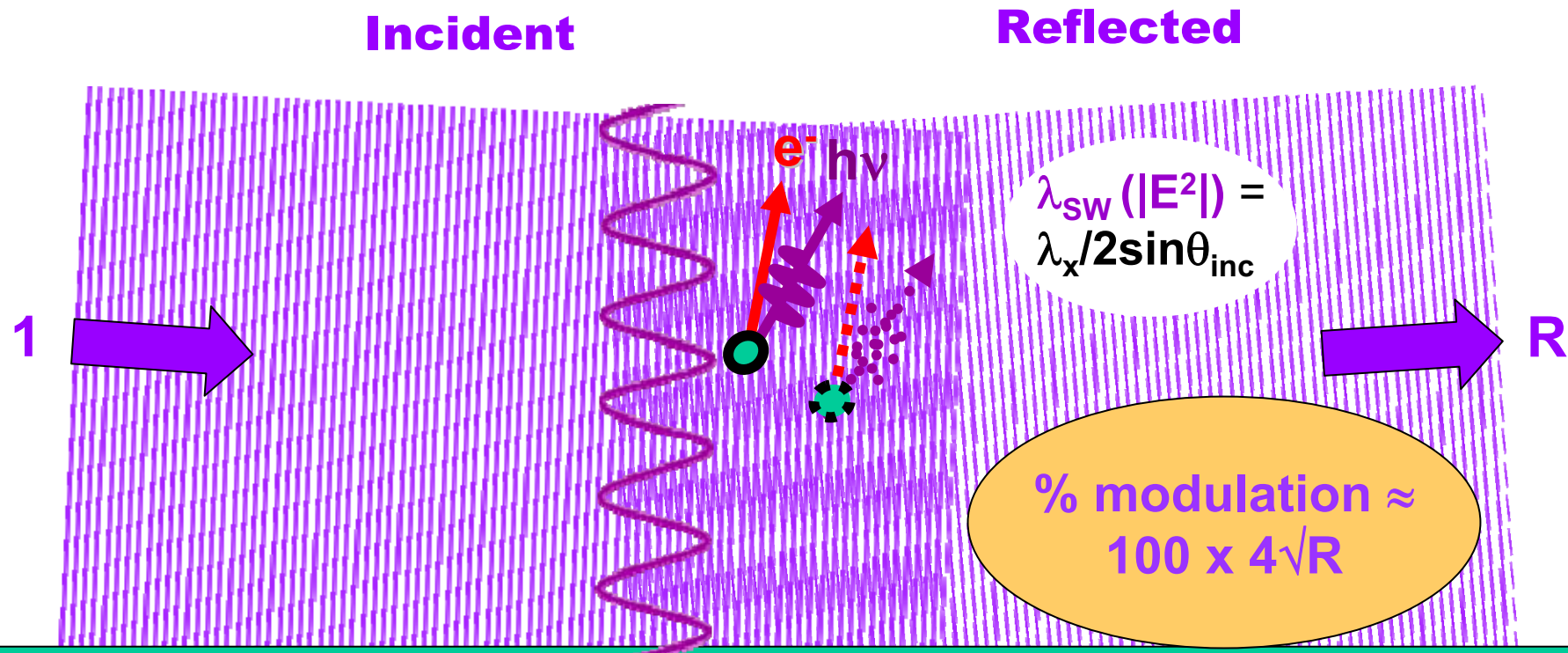
**Photoemission with high ambient pressure
around the sample**

Standing wave formation:



Periodic atomic planes: $d_{\text{ML}} \leq \sim 5 \text{ \AA}$ —Si(111)— $\leq 3.74 \text{ \AA}$, LaB₆(001) — $\leq 23.52 \text{ \AA} \rightarrow 5.88 \text{ \AA}$, mica— 10.0 \AA ; or Synthetic multilayers: $d_{\text{ML}} \approx \sim 20-40 \text{ \AA}$

Standing wave formation in reflection from a surface, or single-crystal Bragg planes⁺, or a multilayer mirror



- Rocking curve:

$$I(\theta_{inc}) \propto 1 + R(\theta_{inc}) + 2\sqrt{R(\theta_{inc})} f \cos[\varphi(\theta_{inc}) - 2\pi P]$$

XMCD—Kim, Kortright,
PRL 86, 1347 (2001)

- Energy scan:

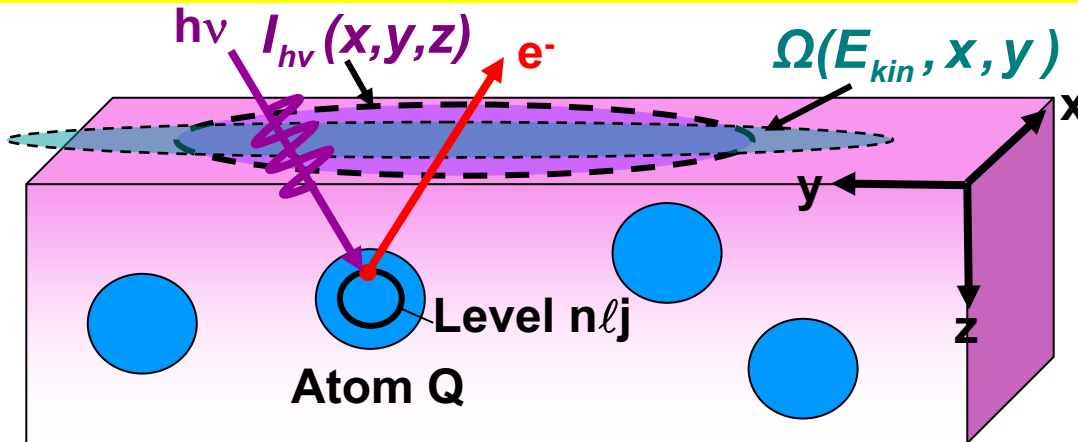
$$I(hv) \propto 1 + R(hv) + 2\sqrt{R(hv)} f \cos[\varphi(hv) - 2\pi P]$$

with: f = coherent fraction of atoms, P = phase of coherent-atom position

- Phase scan with wedge-shaped sample (“Swedge” method):

⁺Standing waves via Bragg reflection of hard x-rays: Batterman, Phys. Rev A 133, 759 (1964)

CORE PHOTOELECTRON INTENSITIES AND COMPOSITION



$$I(Qn\ell j) =$$

$$C \int_0^{\infty} I_{hv}(x,y,z) \rho_Q(x,y,z) \frac{d\sigma_{Qn\ell j}(hv)}{d\Omega} \exp\left[-\frac{z}{\Lambda_e(E_{kin}) \sin \theta}\right] \Omega(E_{kin}, x, y) dx dy dz$$

$I_{hv}(x,y,z)$ = x-ray flux

$\rho_Q(x,y,z)$ = density of atoms Q → quantitative analysis

$\frac{d\sigma_{Qn\ell j}(hv)}{d\Omega}$ = energy-dependent differential photoelectric cross section for subshell $Qn\ell j$

$\Lambda_e(E_{kin})$ = energy-dependent inelastic attenuation length

→ Effective Attenuation Length (EAD) → Mean Emission Depth (MED)

$\Omega(E_{kin}, x, y)$ = energy-dependent spectrometer acceptance solid angle

Calculating XRO effects on spectroscopy--Yang

- $n(h\nu) = 1 - \delta(h\nu) + i\beta(h\nu)$
- variable polarization
- multiple reflection/refraction
- exact treatment of interlayer intermixing a/o roughness
- electric field at i -th layer:

$$|E_{sw,i}(z)|^2 = |E_i^+(z) + E_i^-(z)|^2$$

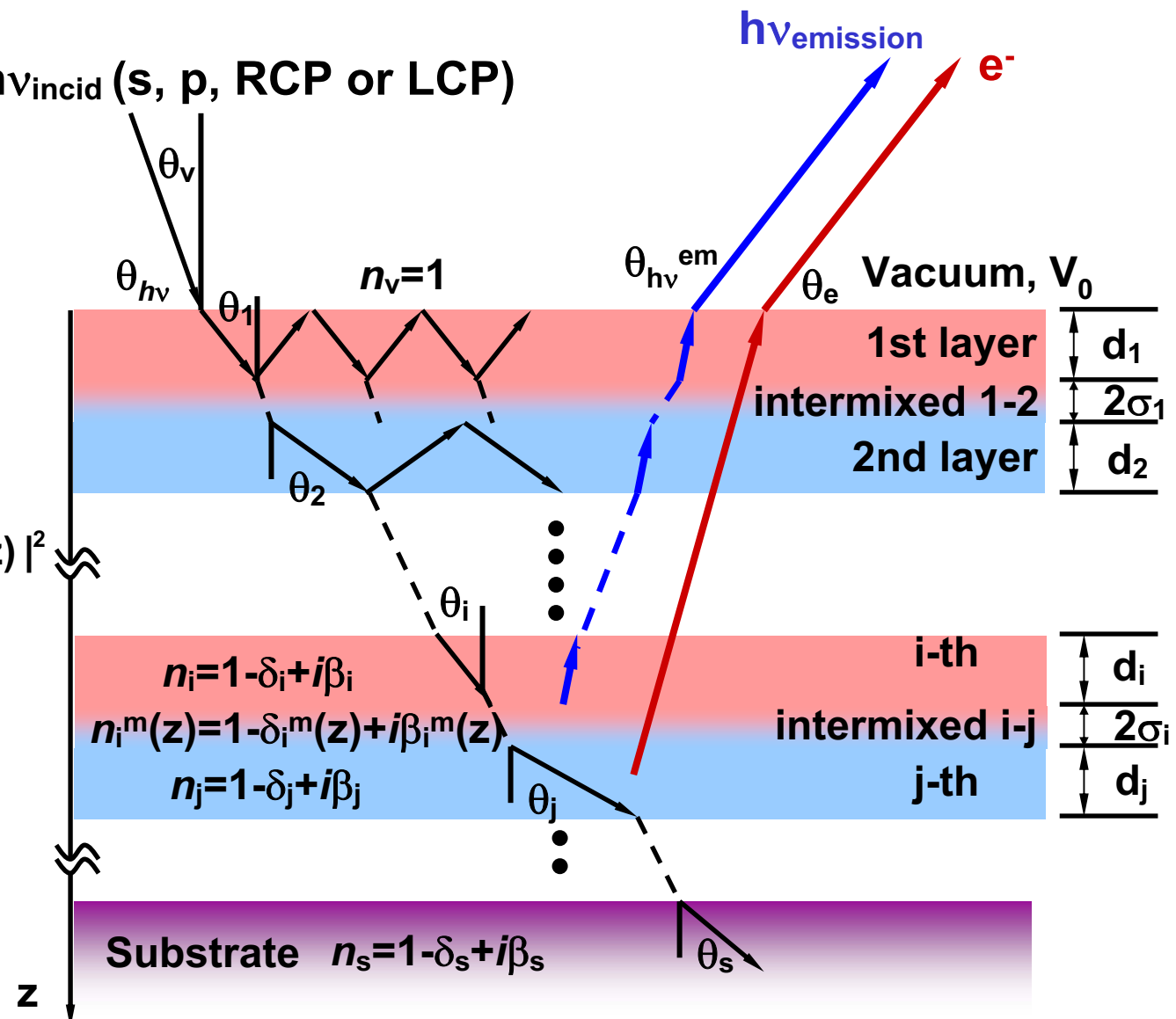
Photoemission:

- differential cross section
- inelastic attenuation
- surface refraction

X-ray emission:

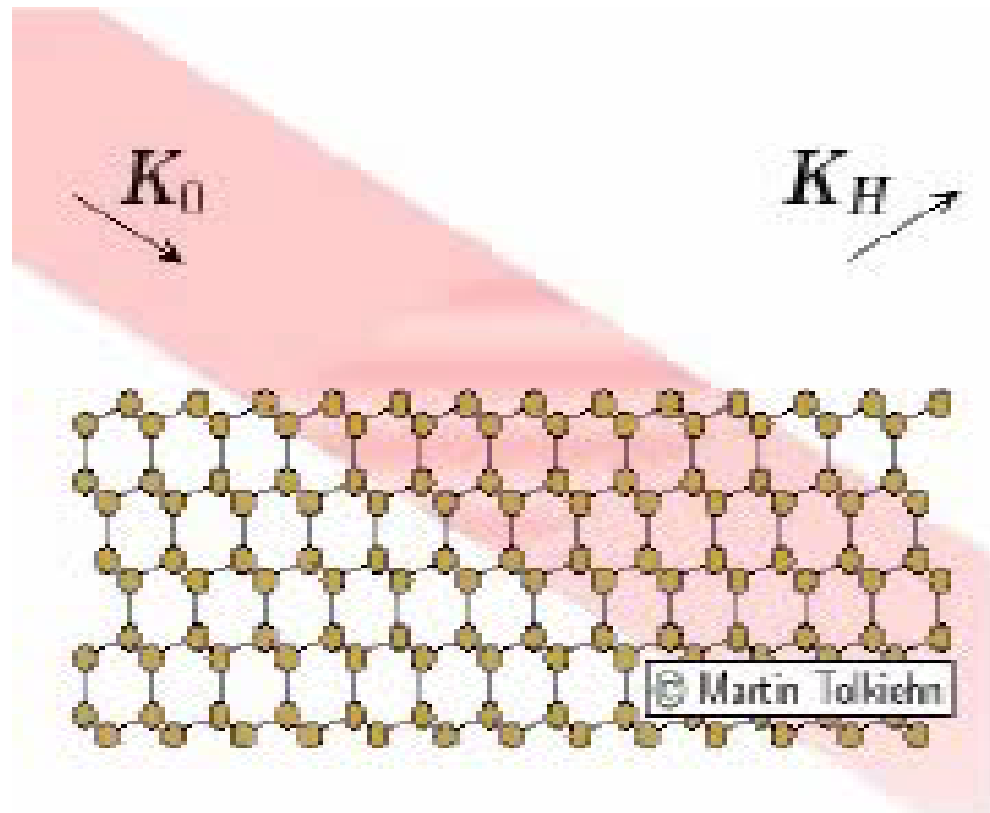
- fluorescence yield

$h\nu_{incid}$ (s, p, RCP or LCP)

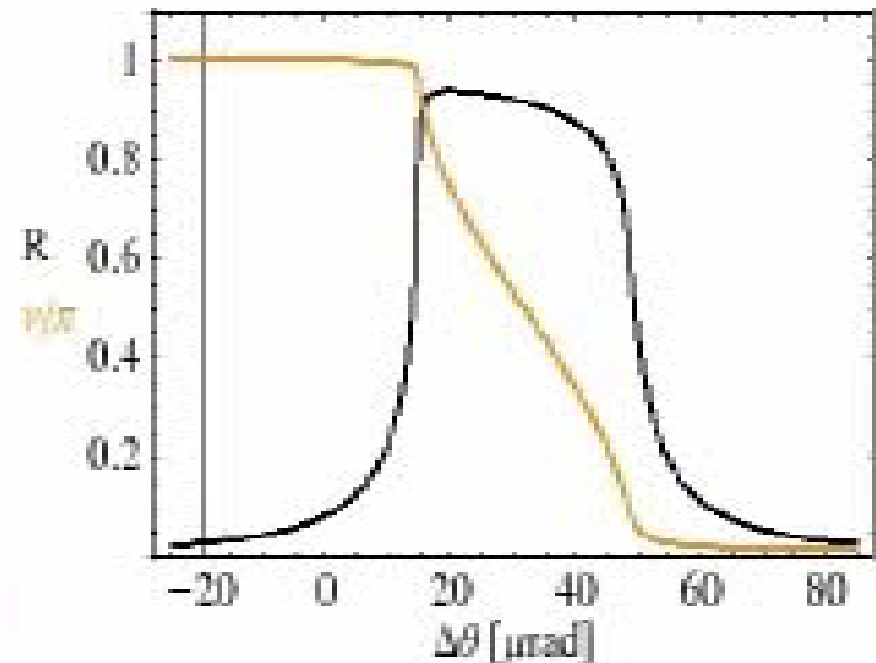


Standing Wave Behavior During a Rocking Curve Scan

+Same general forms if photon energy is scanned

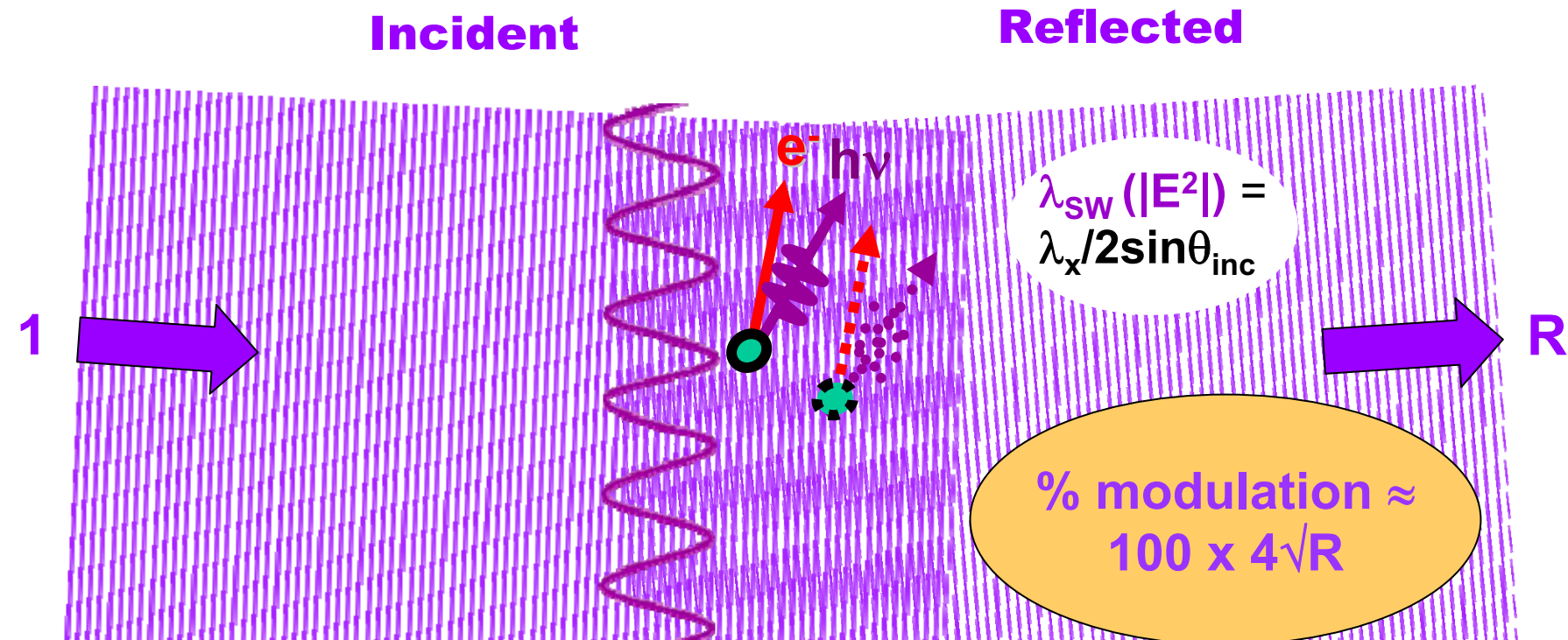


— Reflectivity
— Relative phase



With thanks to Martin Tolkiehn, Dimitri Novikov, Hasylab

Standing wave formation in reflection from a surface, or single-crystal Bragg planes⁺, or a multilayer mirror



- Rocking curve:

$$I(\theta_{inc}) \propto \frac{1 + R(\theta_{inc}) + 2\sqrt{R(\theta_{inc})} f \cos[\varphi(\theta_{inc}) - 2\pi P]}{f}$$

XMCD—Kim, Kortright,
PRL 86, 1347 (2001)

- Energy scan:

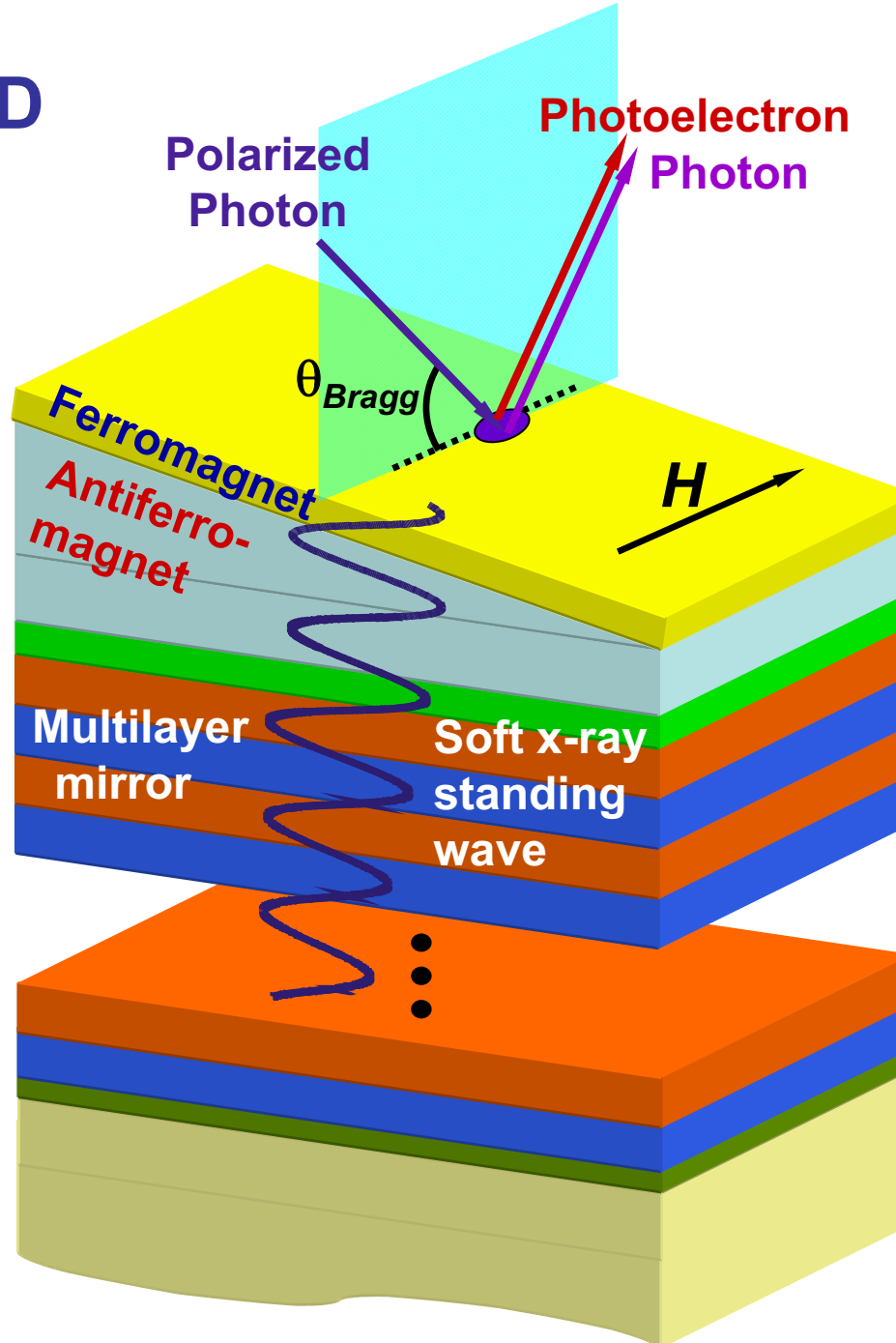
$$I(hv) \propto \frac{1 + R(hv) + 2\sqrt{R(hv)} f \cos[\varphi(hv) - 2\pi P]}{f}$$

with: f = coherent fraction of atoms, P = phase of coherent-atom position

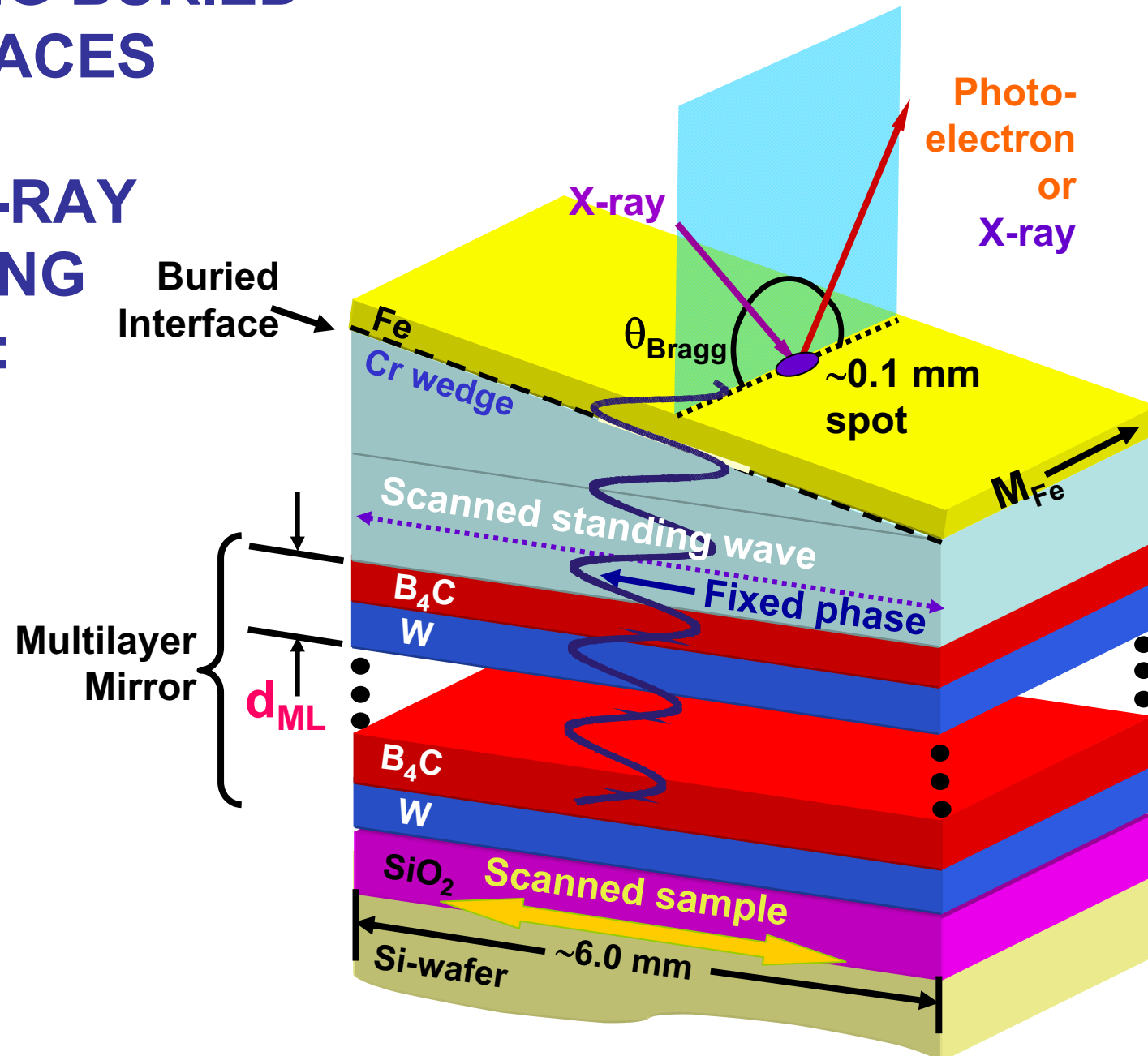
- • Phase scan with wedge-shaped sample (“Swedge” method):

⁺Standing waves via Bragg reflection of hard x-rays: Batterman, Phys. Rev A 133, 759 (1964)

PROBING BURIED INTERFACES WITH SOFT X-RAY STANDING WAVES:

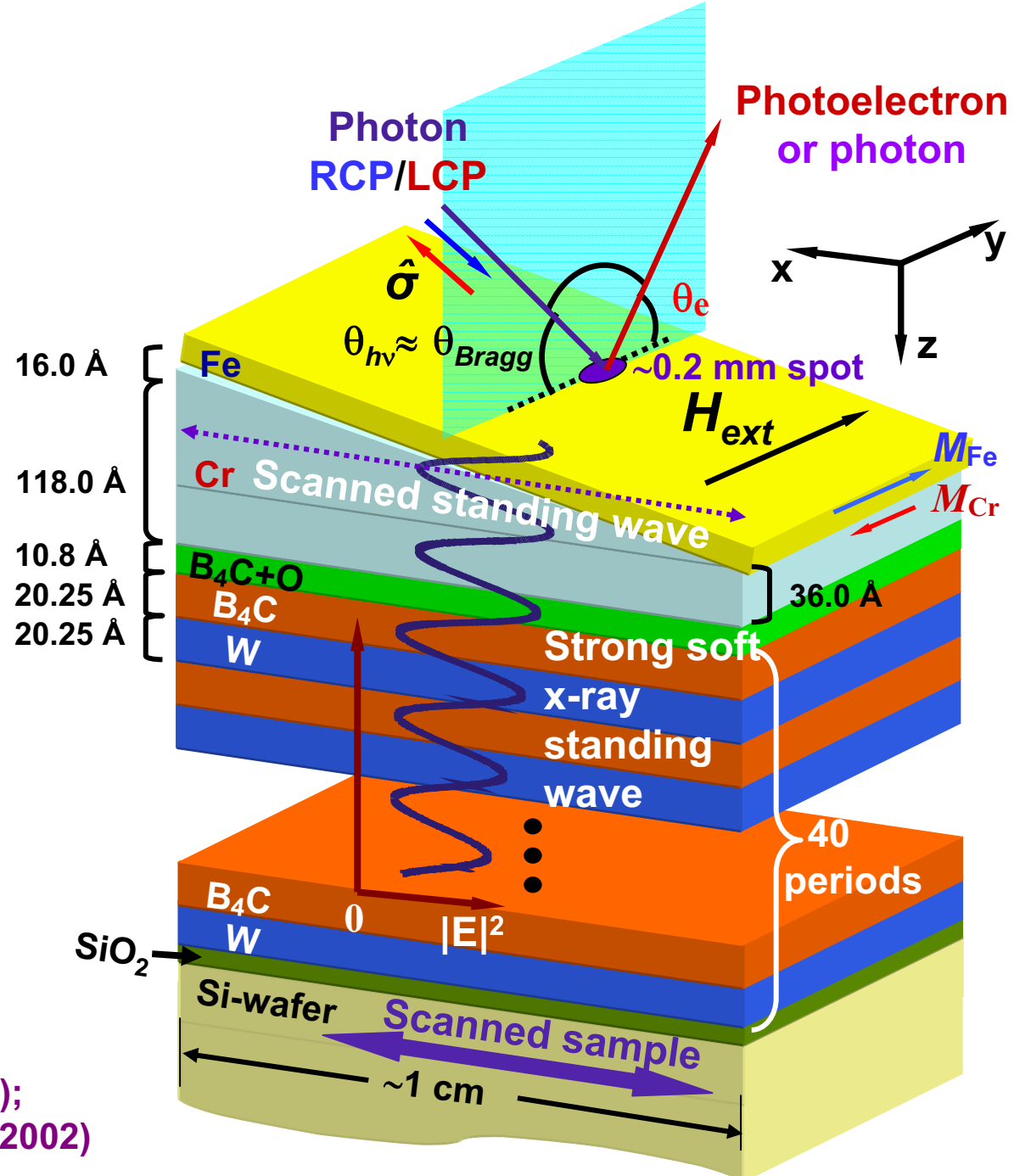


PROBING BURIED INTERFACES WITH SOFT X-RAY STANDING WAVES:



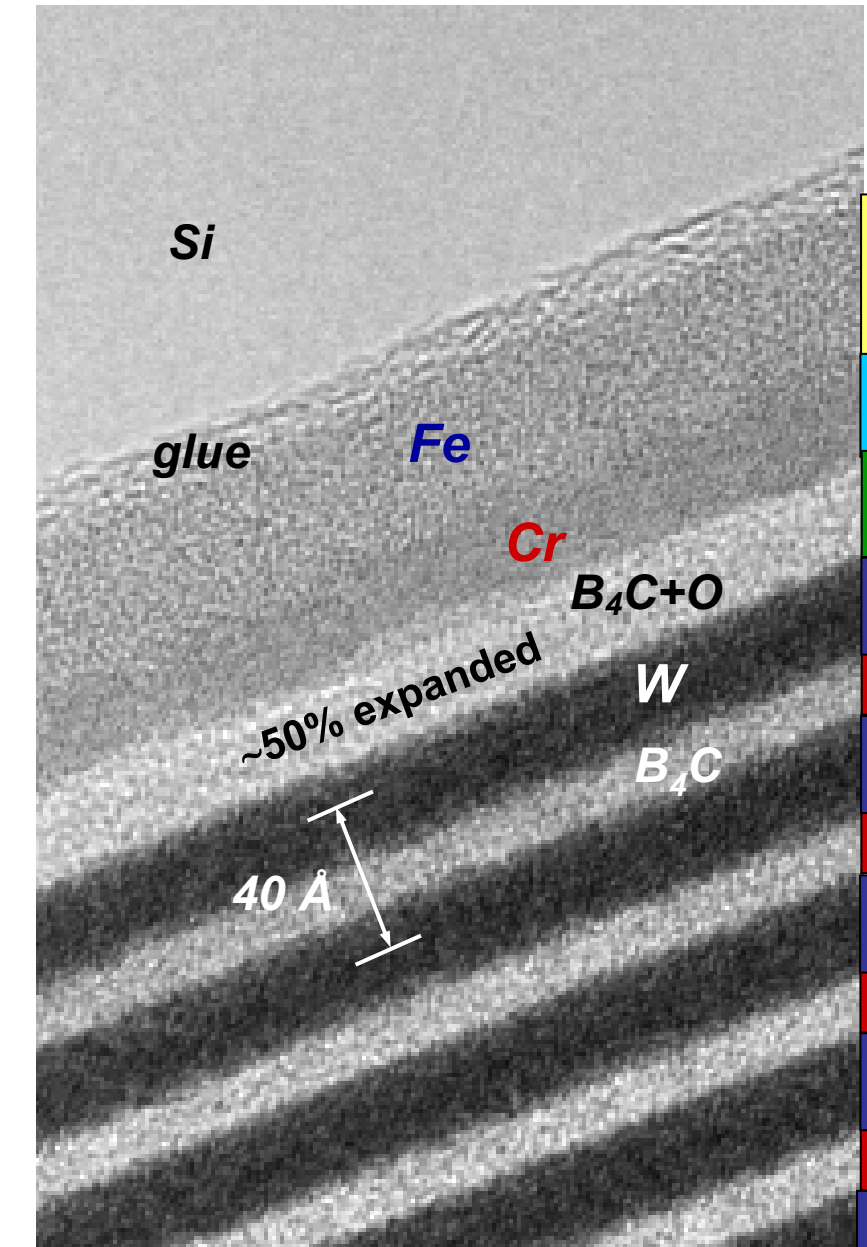
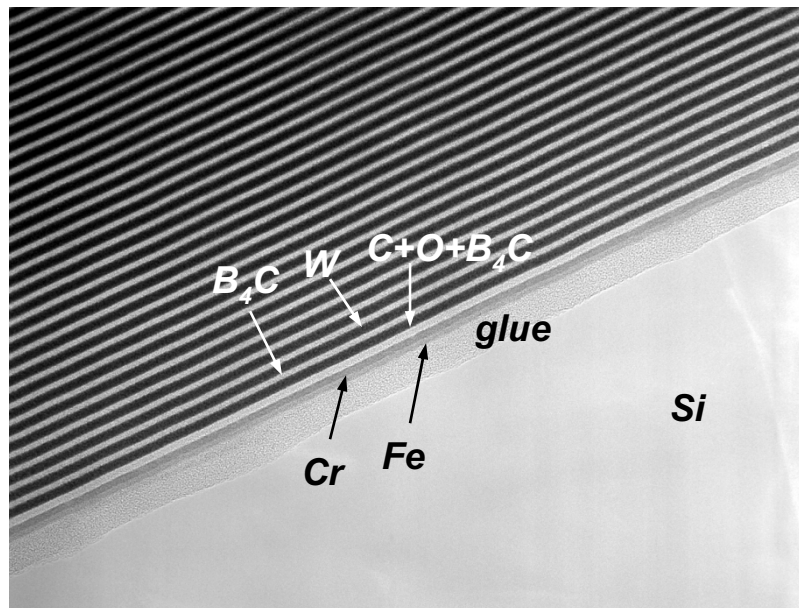
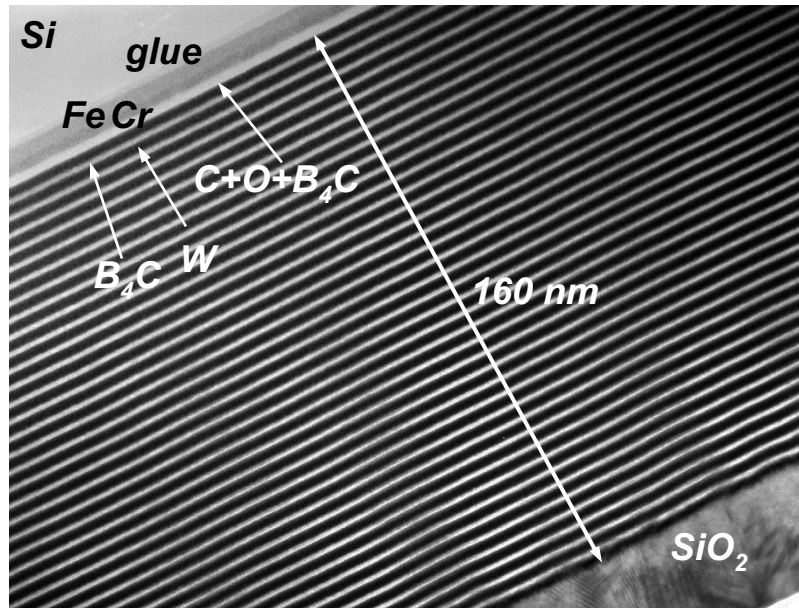
PROBING BURIED INTERFACES WITH SOFT X-RAY STANDING WAVES:

40.50 Å
period =
standing
wave
period

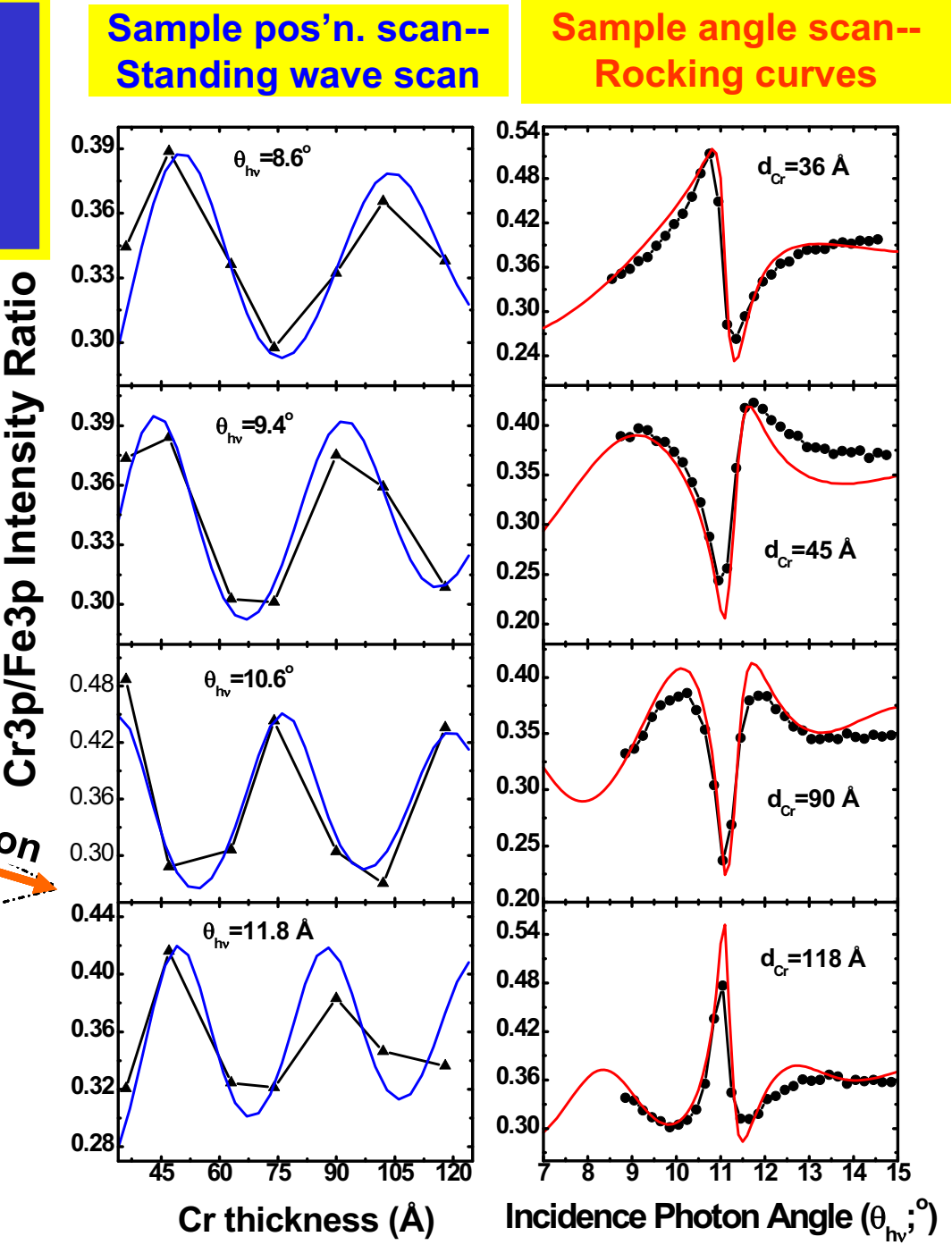
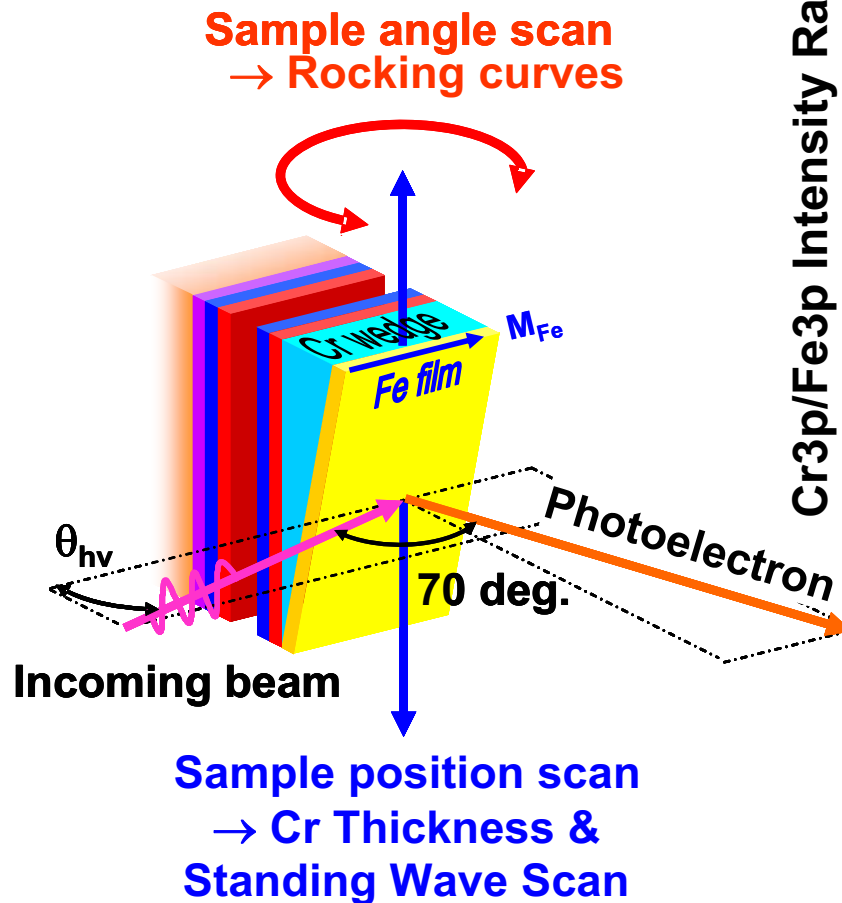


S.-H. Yang, B.S. Mun et al.,
Surf. Sci. Lett. 461, L557 (2000);
J. Phys. Cond. Matt. 14, L406 (2002)

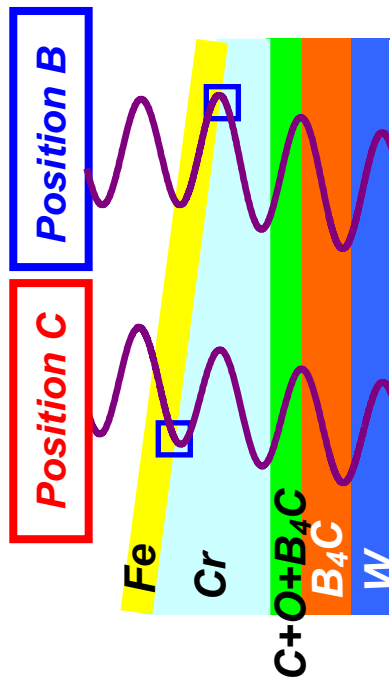
**TRANSMISSION ELECTRON MICROSCOPY IMAGE FOR Fe/Cr/MULTILAYER SWG
(Synthesis-CXRO, and Imaging-NCEM, LBNL)**



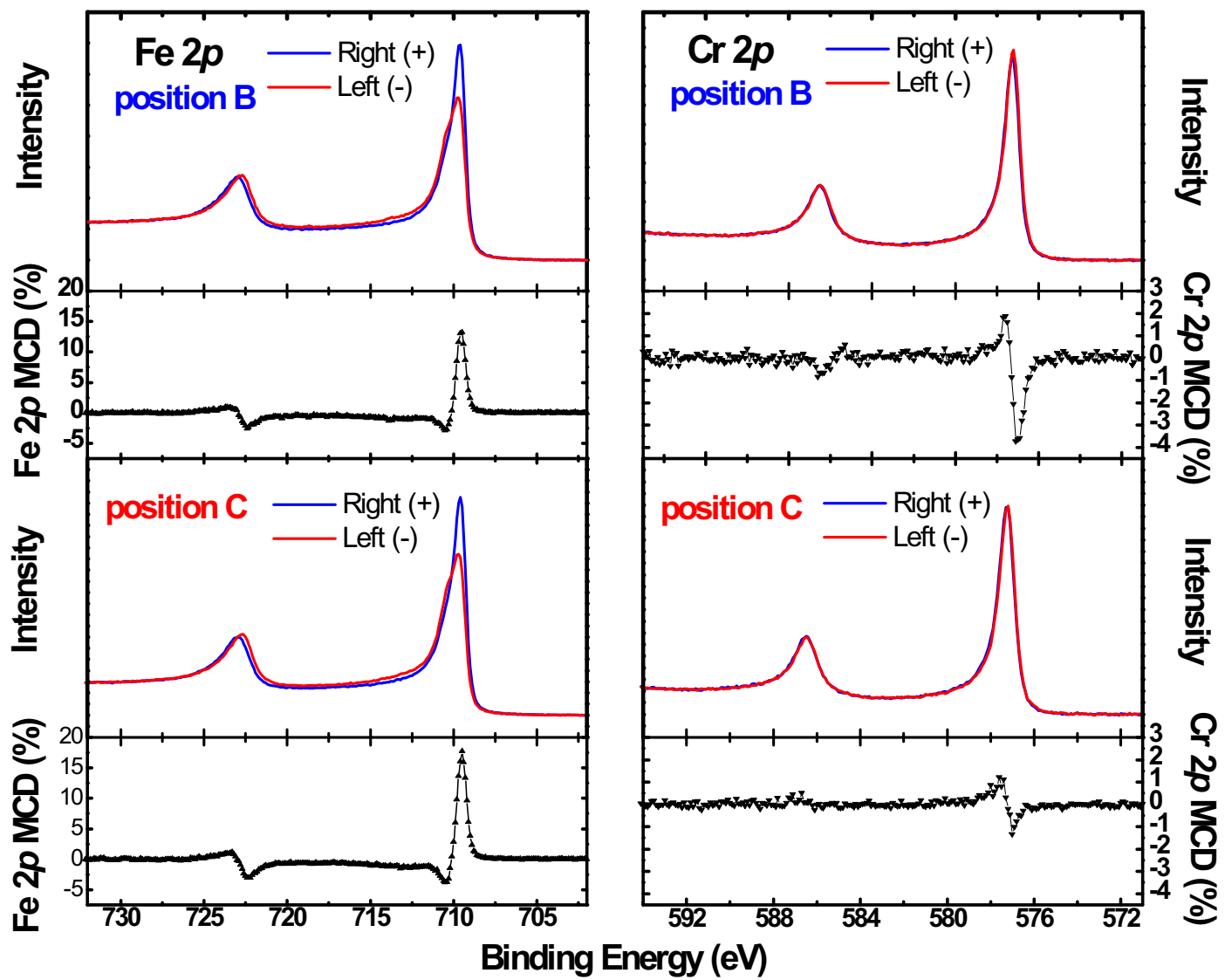
*Experimental + Calculated
Photoemission Yield Ratio
 $I(\text{Fe } 3p)/I(\text{Cr } 3p)$ from Fe/Cr wedge
on standing-wave multilayer*

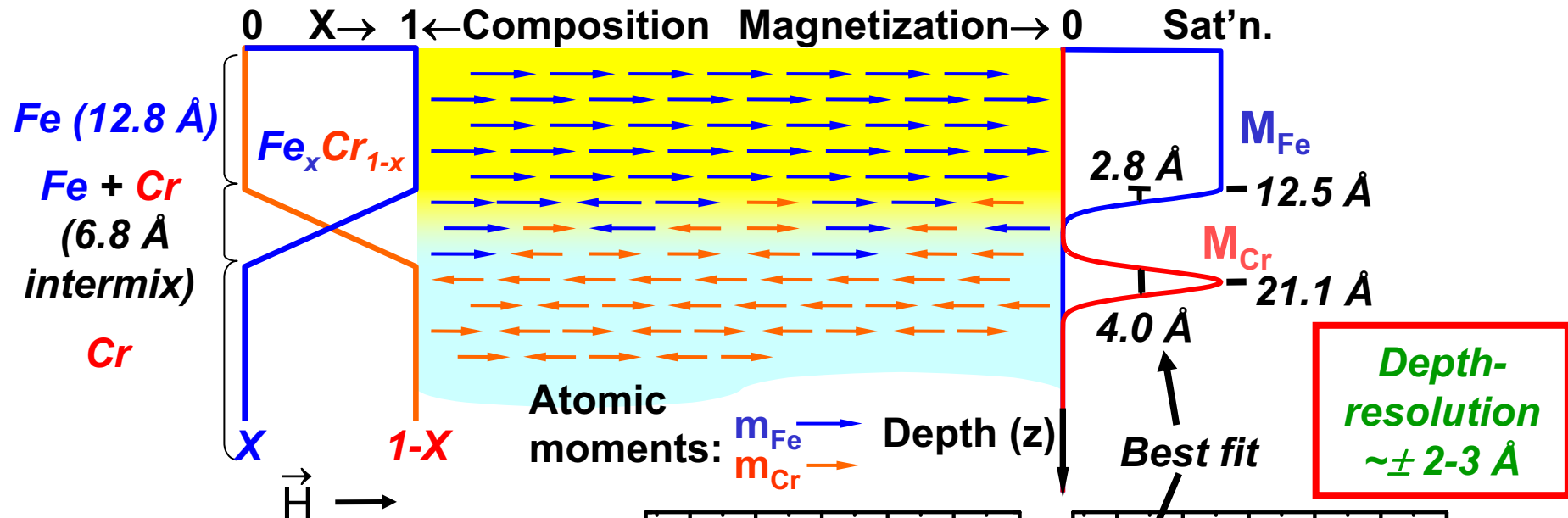


**Cr magnetization
Is antiparallel to
Fe; systematic
variation of MCD
strengths vs d_{cr}**

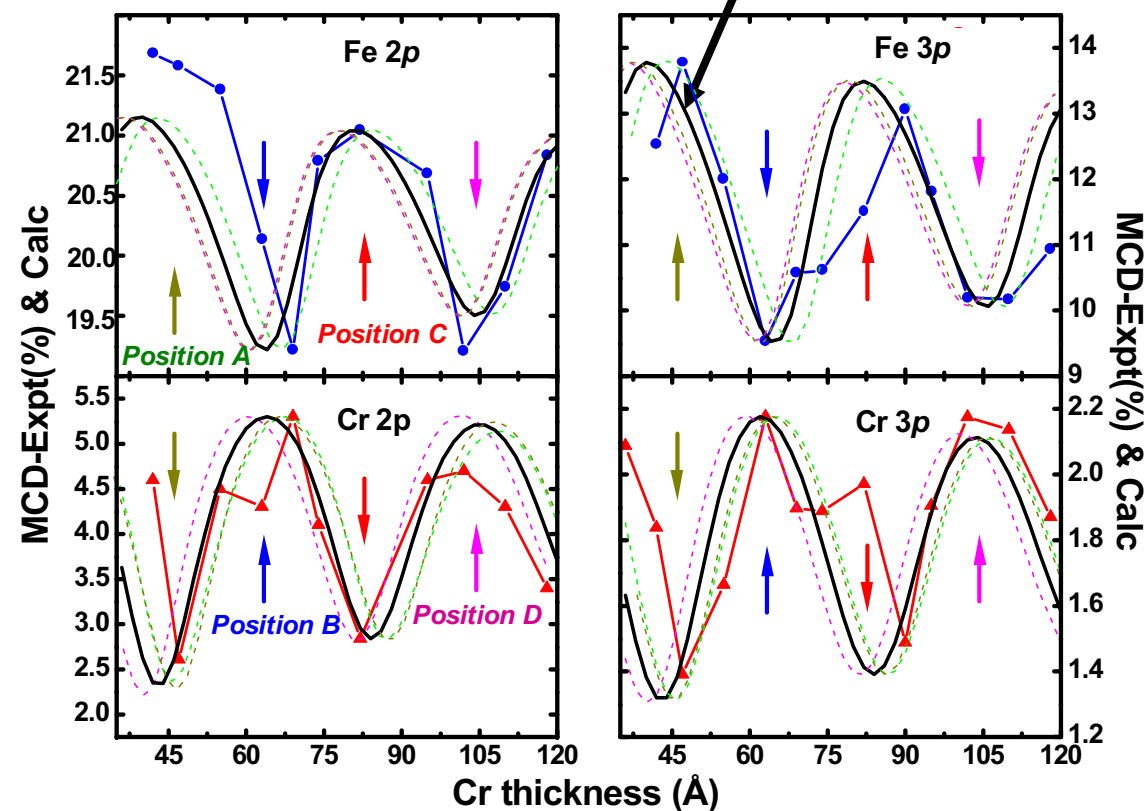


Fe & Cr 2p MCD Data from wedge (Fe/Cr)+SWG



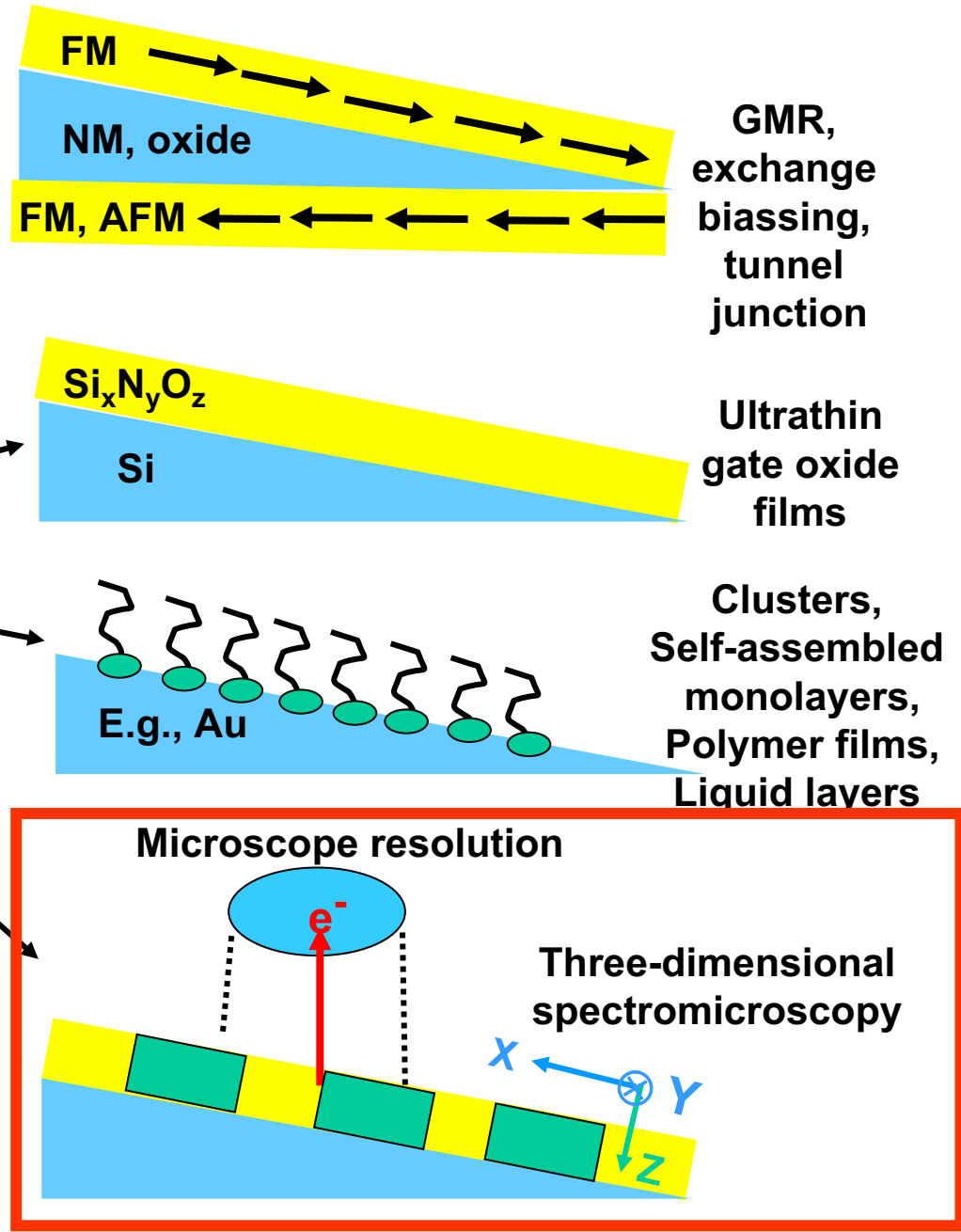
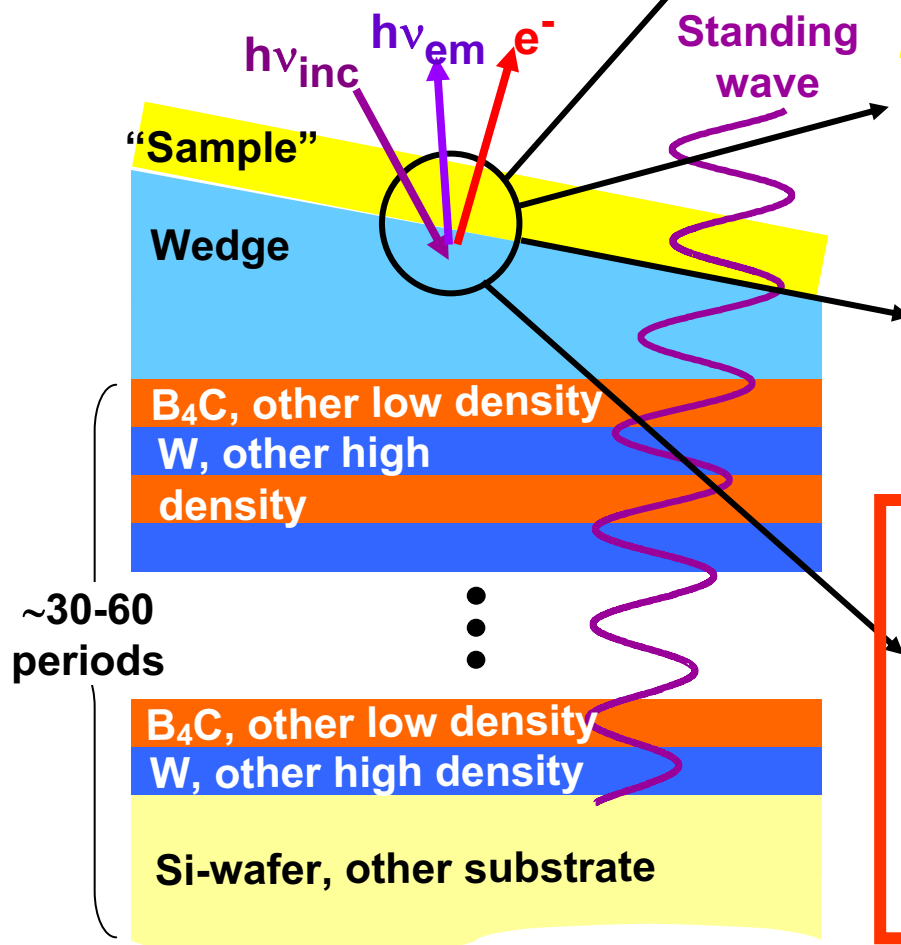


**Non-destructive,
depth-resolved
det'n. of
composition and
magnetization
profiles from
standing-wave
excited
photoemission**



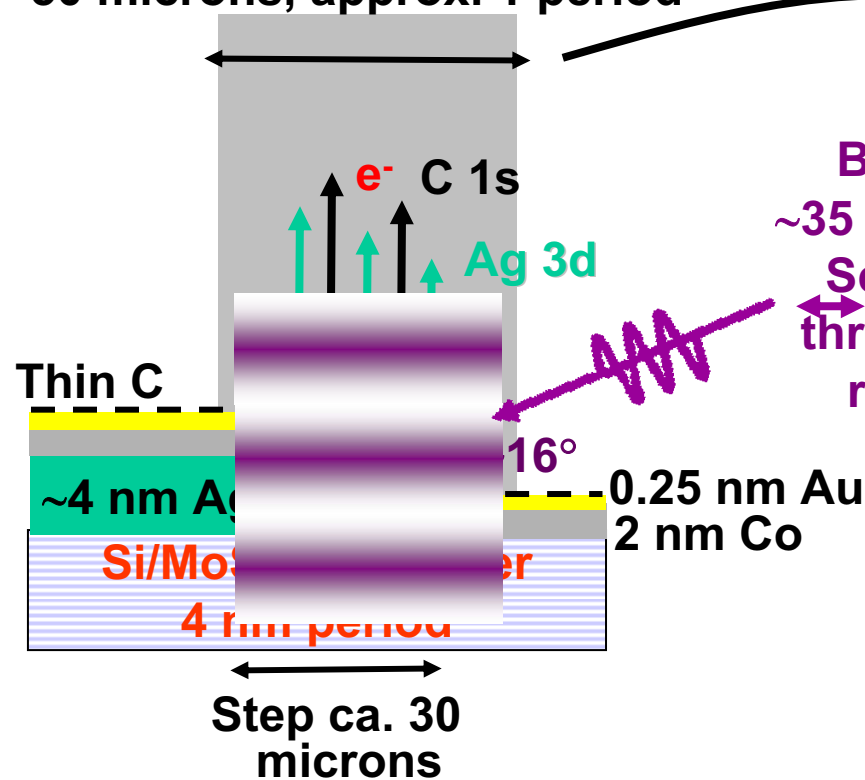
Standing-Wave Excited Spectroscopy--Future Possibilities

- Other material pairs in multilayer (B_4C/W , Al_2O_3/Pt , ...) + epitaxial multilayers → epitaxial samples
- Smaller periods (to ~25-30 Å) → smaller SW period, better resolution
- Lower $h\nu_{inc}$ → higher Bragg angles → perpend. component of M
- X-ray emission → deeper layers, more sensitivity to SW position



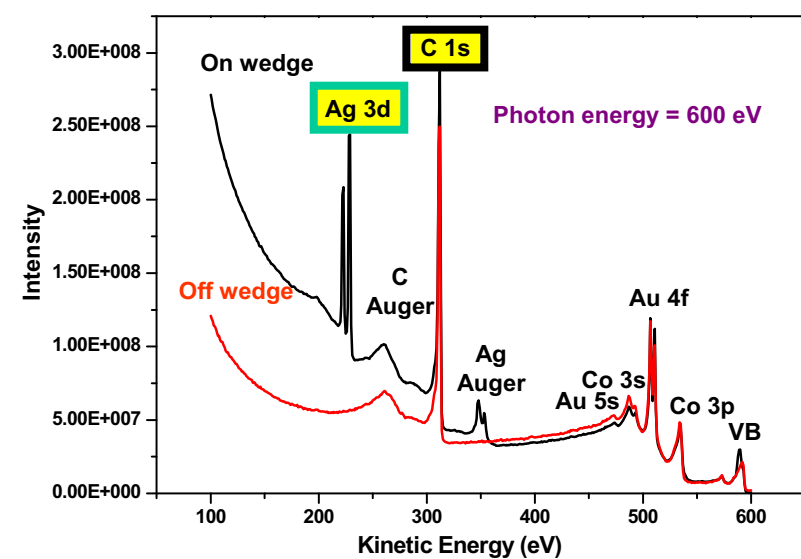
Adding depth resolution to the photoelectron microscope via standing wave excitation

Spin-Polarized Photoelectron Microscope—BESSY, Berlin
Microscope field of view
~50 microns, approx. 1 period



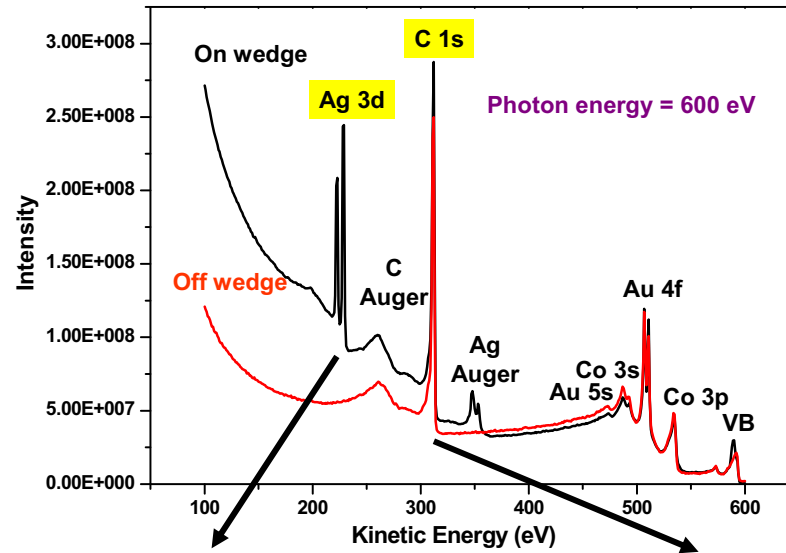
Beam spot:
~35 x 10 microns
Scanning $h\nu$
through Bragg
resonance

Imaging with
element-specific
photoelectron peaks



F. Kronast et al., Appl. Phys. Lett. 93, 243116 (2008)

Standing wave effects in a photoelectron microscope



Ag 3d

C 1s



F. Kronast, H. Dürr,
BESSY
D. Buerger, R.
Scheiber, C.
Schneider, Jülich
Yang, IBM, CF,
Appl. Phys. Lett.
93, 243116 (2008)

